INTERNATIONAL DOCTORAL
SCHOOL OF THE USC

Alfonso
Bayón Fernández

PhD Thesis

Hierarchical Assembly of D,L-Cyclic Peptides for the Construction of New Materials

Santiago de Compostela, 2023

Doctoral Programme in Chemical Science and Technology

ESCOLA DE DOUTORAMENTO
INTERNACIONAL DA USC

DOCTORAL THESIS

HIERARCHICAL ASSEMBLY OF *D,L*-CYCLIC PEPTIDES FOR THE CONSTRUCTION OF NEW MATERIALS

Alfonso Bayón Fernández

Supervisors: Juan Ramón Granja Guillán and Javier Montenegro García

Tutor: Juan Ramón Granja Guillán

PHD PROGRAMME IN CHEMICAL SCIENCE AND TECHNOLOGY

SANTIAGO DE COMPOSTELA

A mis abuelos y mi madrina,

You'll never walk alone.

AGRADECIMIENTOS

"*God gave you a gift of 86,400 seconds today. Have you used one to say, 'thank you?'*." – William Arthur Ward. Hoy, siguiendo el consejo de William, me gustaría agradecerles a todas aquellas personas que me han ayudado durante todos estos años.

Javier Montenegro y Juan R. Granja, me gustaría empezar con vosotros, mis dos directores oficiales. Sin vosotros nada de lo que viene a continuación sería posible. Javi, si hoy estoy aquí es gracias a un correo que me mandaste en el año 2016 después de dos años de darme prácticas en la Facultad de Farmacia. En aquel momento, como ahora, estabas en la búsqueda de estudiantes motivados para ingresar en el grupo. Hoy recurro al Tito Floren para comparar vuestros dones de gestión y fichajes. Gracias de corazón por acordarte de mí y rodearme de gente extraordinaria todos estos años.

Juan, gracias por estar siempre dispuesto a escucharme y guiarme a lo largo de esta etapa. Yo sé que para un químico como tú ha sido difícil mantener la paciencia cuando un farmacéutico emplea durante cinco años mal el término "puentes de hidrógeno". Aun así, siempre has tenido la puerta del despacho abierta para recibir todas mis dudas. Además, me gustaría resaltar que durante estos años te he perdido el miedo, pero nunca el respeto como te gusta comentar a ti en el laboratorio.

Alejandro Méndez, si hoy me encuentro escribiendo este libro es gracias a ti. Aunque los papeles digan lo contrario eres un director más en esta tesis doctoral. En el laboratorio has sido el mejor profesor que un alumno pueda desear. De todas formas, no puedo solo agradecerte lo que has hecho por mí a nivel académico, sino que también necesito agradecerte tu implicación en mi vida a nivel personal. Fuera del laboratorio has sido un amigo con el que he compartido cenas, digestivos, "botellas para cocinar", rescates de gorros y un sinfín de etcéteras. No tengo palabras suficientes para describir lo significó tenerte a mi lado durante esta etapa, pero te garantizo que si me tocase la lotería seguiría siendo menos afortunado de lo que soy ahora por haberte conocido.

Luis Castedo, Manuel Amorín, Ángel Piñeiro y Rebeca Fandiño, tanto vuestra presencia en el grupo como vuestra ayuda y motivación en los seminarios han sido fundamentales tanto para mi formación como para que esta tesis saliese adelante.

Sebastien Ulrich y Carmen Álvarez, vuestra colaboración ha sido fundamental para el desarrollo de esta tesis. Gracias por vuestra ayuda y consejos.

A la Xunta de Galicia me gustaría darle las gracias por mi beca predoctoral (ED481A-2019/085) que me ha permitido disfrutar de una de las etapas más bonitas de mi vida. Además, también me gustaría dar las gracias a todas las instituciones que han financiado la investigación del grupo durante estos años, como la agencia estatal de investigación (SAF2017-89890-R, CTQ2016-78423-R, PCI2019-103400, PID2019-111126RB-100, PID2020-117143RB-I00, PID 2020-113881RB-I00) y Xunta de Galicia (ED431G/09, ED431C 2019/03, 2017/25, 2021/21 and 2016-AD031) por financiar los proyectos dirigidos por los profesores Juan R. Granja Y Javier Montenegro, sin la cual estos trabajos no habrían podido realizarse.

A la RIAIDT de la Universidad de Santiago de Compostela por poner a nuestra disposición vuestros medios técnicos para el desarrollo de la actividad investigadora del grupo. Me gustaría destacar especialmente a Raquel Antón por todas las fotos de STEM, tanto las que se han plasmado en esta Tesis como las que no.

A mi familia los Bayón, los Fernández, los Prieto, los Losada-Márquez y los Graham. Papá y mamá, no hay palabras ni gestos suficientes que puedan agradeceros todas las oportunidades que me habéis brindado en la vida. También me habéis enseñado que los momentos difíciles pasan y que se solucionan juntos. Nieves y Elena, la relación entre hermanos es una relación de amor-odio en la que con los años siempre acaba ganando el amor. Paco, Mar, Javi y Carliños cada vez que os veo es una alegría para mi corazón. Edu, Mariam, Yago, Javi e Inés, teneros como familia es el mejor regalo que una persona puede pedir. Los Prieto, solo voy a nombrar a la matriarca Noemi, porque si no llenaría 3 páginas de nombres. No hay sensación comparable a llegar a un pueblo y que la mitad sea familia, dan ganas de llorar de felicidad. Josela, Manolo, Carmen, Manuel y Alejandro, se ve que el registro miente porque dice que no estamos emparentados, pero ninguno de los mencionados lo siente así. Se dice que los amigos son la familia que se escoge y quiero dar las gracias a mis dos padres Manolo y Alfonso por conocerse hace 40 años y permitirme disfrutar de esta gran familia. Jean, Art, Mariah, Sarah y Levi, aunque fueron mis padres los que me obligaron a estudiar en los EEUU vosotros hicisteis que mereciese la pena. Me fui aterrorizado y sin saber inglés y volví habiendo vivido la mejor experiencia de mi vida. Que después de 10 años sin vernos Mariah me invitase a su boda habla por sí solo. Gracias a toda mi familia por siempre estar a mi lado.

Finalmente, gracias a las personas a las que va dedicada esta tesis. Ninguno de vosotros se encuentra ya físicamente entre nosotros, pero eso no significa que no estéis presentes. Como dicen los aficionados del Liverpool “nunca caminarás solo”. Gracias a vosotros esté donde esté siempre estaré acompañado de vuestras enseñanzas. Ser la mitad de persona que cada uno de vosotros, significa ser un 10. Abuela Neli, gracias por confiar en mí y darme siempre tanto amor. Abuelo Manolo, fuiste, eres y serás siempre mi ídolo y referente. Abuela Pacita, gracias por tratarme siempre como un nieto más. Madrina, gracias por quererme como soy y sentirte siempre orgullosa de mí. Abuelo Alfonso, siempre me quedará la espinita de no haber conocido a la persona de la que heredé destellos de la mejor personalidad conocida por el hombre. Gracias a los cinco de todo corazón.

INDEX

ABBREVIATIONS

1D	One Dimensional
^{1}HRMN	Proton Nuclear Magnetic Resonance
2-CTC	2-Chlorotrytil chloride resin
2D	Two Dimensional
3D	Three Dimensional
δ	Chemical shift
λ_{exc}	Excitation wavelength
λ_{max}	Maximum emission wavelength
Aa	Amino acid
Abs	Absorbance
ACQ	Aggregation-Caused Quenching
AFM	Atomic Force Microscopy
AIE	Aggregation Induced Emission
Ala	Alanine
Arg	Arginine
Asp	Aspartic acid
Boc	*tert*-Butoxycarbonyl
BTA	Benzene-1,3,5-tricarboxamide
CAC	Critical Aggregation Concentration
CB	Cucurbituril
CD	Circular Dichroism
CDs	Cyclodextrins
CP	Cyclic Peptide
D	Doublet
DCM	Dichloromethane
DIEA	*N,N*-Diisopropylethylamine
DMAP	4-Dimethylaminopyridine
DMF	Dimethylformamide
DMSO	Dimethyl sulfoxide
DNA	Deoxyribonucleic acid
Equiv	Equivalent

Fmoc	Fluorenylmethoxycarbonyl
FRET	Förster Resonance Energy Transfer
FTIR	Fourier Transform Infrared Spectroscopy
G’	Storage moduli
G’’	Loss moduli
Glu	Glutamic acid
Gly	Glycine
HATU	1-[*Bis*(dimethylamino)methylene]-1H-1,2,3-triazolo[4,5-b]pyridinium 3-oxide hexafluorophosphate
HBC	Hexa-peri-hexabenzocoronene
HBTU	3-[*Bis*(dimethylamino)methyliumyl]-3H-benzotriazol-1-oxide hexafluorophosphate
HEPES	2-[4-(2-hydroxyethyl)piperazin-1-yl]ethane-1-sulfonic acid
His	Histidine
HOBt	1-Hydroxybenzotriazole
HPLC	High Performance Liquid Chromatography
HRMS	High Resolution Mass Spectrometry
Ile	Isoleucine
J	Coupling constant
LBL	Layer by Layer
Leu	Leucine
Lys	Lysine
M	Multiplet
M/z	Mass-to-charge ratio
MeOH	Methanol
MES	2-(*N*-morpholino)ethanesulfonic acid
MOF	Metal organic framework
MS	Mass Spectrometry
Mtt	*m*-methyltrityl
NDI	Naphtalenediimide
NMM	*N*-Methylmorpholine

OFN	Octafluoronaphthalene
Orn	Ornithine
PA	Peptide amphiphiles
PDB	Protein Data Bank
PDMS	Poly(dimethylsiloxane)
PEG	Polyethylene glycol
Phe	Phenylalanine
Ppm	Part per million
PyAOP	(7-Azabenzotriazol-1-yloxy)tripyrrolidinophosphonium hexafluorophosphate
RNA	Ribonucleic acid
Rt	Room temperature
S	Singlet
SA	Supramolecular amphiphile
SANS	Small-Angle Neutron Scattering
SCPN	Self-assembling Cyclic Peptide Nanotube
SDS	Sodium dodecyl sulfate
SEM	Scanning Electron Microscopy
Ser	Serine
STEM	Scanning Transmission Electron Microscopy
T	Triplet
^{t}Bu	*tert*-Butyl
TEM	Transmission Electron Microscopy
TFA	Trifluoroacetic Acid
ThT	Thioflavin-t
Thr	Threonine
TIS	Triisopropylsilane
TMV	Tobacco Mosaic Virus
TPE	Tetraphenylethylene
Trp	Tryptophan
Tyr	Tyrosine

UPy	2-Ureidopyrimidone
UT	Ureidotriazine
UV-Vis	Ultraviolet-visible spectroscopy
Val	Valine

SUMMARY

Since the beginning of humankind chemistry has been involved in our life. At the beginning it was an unconscious use exemplified by the use of fire to cook with all the chemical transformations that are involved in the process. As society improved its knowledge, the use of chemistry switched towards a more rational use of this powerful tool. This new tendency triggered a need to obtain more and more complex structures specifically designed to overcome social deficiencies. In the first moment, synthetic chemistry played a key role in the development of new strategies for the obtention covalent bonds and the introduction of functional groups in the chemical structures. However, the knowledge gathered in other fields such as biochemistry and molecular biology enhanced the need for the development of larger molecules with higher complexity, like the DNA doble helix. These new chemical entities were inaccessible by using covalent organic synthesis. In this context, a new discipline in organic chemistry started to emerge, supramolecular chemistry, which can be defined as the "*chemistry beyond the molecule*".

This new field is devoted to the study of the weak interactions that hold together different molecules like hydrogen bonding, π-π and Van der Walls interactions, among others. The combination of these forces provides a way for simple molecules to interact with each other giving rise to very complex tridimensional structures. Moreover, the non-covalent nature of such bonds provides these structures with special properties such as reversibility, stimuli responsiveness and self-healing. Among the huge diversity of structures that can be generated by molecular design, supramolecular polymers have arisen as very interesting materials with promising applications in catalysis, drug delivery or sensors, among others. Interestingly, these new polymeric materials can combine the properties of their covalent counterparts with the advantages of supramolecular systems paving the way to wide variety of morphologies suited for the desired applications.

Over the years many different building blocks have been used to design supramolecular polymers, among which cyclic peptides (CP), composed by an even number of amino acids with alternated chirality, stand out. This peptide family is characterized by its planar conformation in which carbonyl and amino groups are oriented perpendicular to the plane allowing the CP-CP interaction though hydrogen bonding, giving rise to β-sheet like tubular structures. These designs offer great control over critical parameters. In this way the tubular diameter depends directly the number of amino acids included in the sequence while the properties of the inner and outer layers are related with the nature of the selected amino acids. More recently, the presence of reactive groups in the amino acids side chains has been exploited to functionalized CPs with carbon tails, aromatic moieties or polymers giving rise to a variety of supramolecular structures with potential application in biology, material science or electronics.

With all this knowledge in mind, in this Thesis we want to explore deeper the relationship between the aromatic functionalization of D,L-α-CPs and their self-assembling properties. The presence of these moieties can affect the aggregation process of the cyclic peptides thus regulating the hierarchical assembly. To achieve such a goal it was necessary to generate cyclic peptides libraries bearing different aromatic units to unmask those key parameters that govern these peptide assemblies.

In the first chapter of this memory, we design, synthesize and characterize a new family of hydrogelators based on cyclic peptides. For this reason, the peptide structure was specifically designed to bear pH responsive amino acids that allowed us to control the aggregate state on demand, one or two alkoxyamines to further functionalize the peptides with different aromatic

residues and to segregate the hydrophobic and hydrophilic phases to induce a hierarchical self-assembling process. In a first step, infrared spectroscopy confirmed that the CPs were stacked following an antiparallel β-sheet pattern. Moreover, monitoring the absorbance and fluorescence upon alkalinization of an acidic solution of CP demonstrated that the aromatic units were in close proximity confirming this way the pH responsiveness of the system. To unveil the hierarchical process samples of these cyclic peptide derivatives were visualize under different microscopy techniques unveiling the presence of nanotubes that could further interact with each other to form fibers which persistent length was directly related with the number and nature of the aromatic pendants. Lastly, rheological studies were carried out once we confirmed the gel formation by the inverted vial test. As expected, the viscoelastic properties were related with the length of the fibers as well as with the number and nature of aromatic moieties, introducing this way the main principles for the design of gels with controlled properties.

In the second chapter, inspired by the behavior of the cytoskeleton in living cells, which has been regarded as a natural gel, we decided to investigate the behavior of the most promising hydrogelator in confined spaces. The selected peptide was the one bearing one pyrene residue (**1TP**) which, as demonstrated before, presented a pH responsive behavior. However, the presence of charges should also respond to an increase in ionic strength. For this reason, the first studies were done to confirm the possibility to induce aggregation through ionic force and compare the properties of the assemblies with the pH obtained ones. From these experiments we could conclude that the **1TP** presents ionic force responsiveness highly dependent on the nature of the anions and the aggregates present a lower packing degree and higher hydrophilicity than the ones obtained through alkalinization. In the next step we studied the behavior of the peptide in confined conditions taking advantage of the control offered by microfluidics to create homogeneous water droplets in size and content. These studies unveiled the high tendency of the **1TP** to assemble in the external surface of the droplet when triggered by pH and in the core of the sphere when using ionic force. These differences arise from the different nature of the aggregates depending on the trigger employed. Additionally, the use of increasing amounts of ionic force could displace the assemblies from the water-oil interface towards the core of the droplets. These results confirm that it is possibility to have spatiotemporal control over the CPs polymerization in confined spaces and also highlight the importance that has chemical environment in the fibers positioning.

In the third chapter, we wanted to come a step closer towards finding a synthetic way to mimic the cytoskeleton. In order to do that, we need to reduce the length and diameter variability of our CP fibers. For this reason, we search for an aromatic scaffold that could bear multiple aromatic units and that could be synthesized with low synthetic effort. Our hunt brought tetraphenylethylene (TPE), a known compound with aggregation induced emission (AIE) properties that allow many chemical modifications on the main scaffold. This way we were able to obtain a tetrasubstituted TPE with aldehyde groups on the para position of the phenyl rings and endow our final system with AIE properties that should facilitate the monitorization of the assembling process and the visualization of the final aggregates. We hypothesize that the synthesis of the tetrasubstituted TPE core with four cyclic peptides pendants (**4CP$_{1k}$-U-TPE**) would give rise to fibers with a homogeneous diameter and with lower dispersion lengths. In this way, we first characterize the system by spectroscopic techniques confirming the pH responsiveness, the AIE behavior and the simultaneous assembling process of TPE and CPs. However, when the images obtained by different microscopy techniques showed a 2D system instead of the 1D fibers we predicted with our design.

Specifically, atomic force microscopy clearly showed sheet like structures which height was the same one we expected for the fibers. In this sense, we hypothesize that the fibers are actually form, but the spatial disposition of the CPs around the TPE enhances the lateral growth by interactions though amino acids side chains, specifically, hydrogen bonding His-His. To corroborate this hypothesis multiple derivatives of the cyclic peptide and TPE were synthesized. Generally speaking, the derivatives exhibit a similar spectroscopic behavior giving rise to similar morphologies. Anyway, this modifications allowed us to gather some relevant structural information: i) a charged residue is key to maintain water stability al high pH values; ii) at least one histidine is necessary to maintain the water solubility at low pH and maintain the pH responsiveness, iii) the position of the histidines do not influence the 2D growth of the system, iv) TPE substituted in meta shows the same tendency towards the lateral growth; v) monosubstituted TPE assembles into a mix of nanotubes and sheets suggesting that the tetrasubstitution is important to stabilize the 2D system. Finally, preliminary studies suggest that this robust scaffold to build 2D systems can be useful as catalyst.

In conclusion, we have reported though the lines of this Theses robust knowledge about aromatically functionalized cyclic peptides assemblies that can guide scientist in the design of new supramolecular materials based on CPs that are suitable for the desired applications.

RESUMO

Dende o inicio da nosa existencia a química é parte fundamental de moitos dos avances humanos, xa fose mediante o uso experimental ou unha aproximación máis racional. O primeiro uso humano da química, independentemente do seu descoñecemento sobre a materia, considérase o emprego do lume na manipulación da comida. Dende ese momento e durante moitos anos, o uso da química pasou inadvertido á vez que proporcionaba distintos materiais de uso común como os perfumes, os metais ou a pintura. O uso racional da química comezaría coa chegada da alquimia, pero non sería ata o século XVII cando tería lugar o nacemento desta disciplina.

A evolución exponencial da sociedade dende os seu primitivos inicios vese reflexada no avance da química. O paso dos anos e a ganancia de coñecementos, permitiu pouco a pouco xerar metodoloxías sintéticas que permitían a obtención de moléculas máis grandes e complexas. Non obstante, co nacemento e avances noutras disciplinas científicas como por exemplo a bioquímica e a bioloxía molecular viron a luz estruturas moito máis grandes e complexas (como a dobre hélice do ADN) das que se podían sintetizar mediante a química orgánica tradicional. A falta de metodoloxías sintéticas apropiadas e o esforzo e tempo requiridos, fixeron que a obtención destas estruturas fose inabordable dende a síntese orgánica covalente. Neste contexto, nos anos sesenta, apareceu unha nova disciplina dentro da química orgánica denominada química supramolecular que se definiu como "a química máis alá da molécula".

Esta nova rama da química encárgase do estudo das interaccións entre diferentes entidades químicas mediante forzas non covalentes entre as que se atopan os enlaces de hidróxeno, as forzas de Van der Walls ou as interaccións tipo π-π e dipolo-dipolo, entre outras. A combinación destas interaccións permite que moléculas sinteticamente sinxelas se asocien entre elas para dar lugar a estruturas dunhas dimensións e complexidade moito máis grandes. Ademais, a natureza non covalente e reversible destas forzas que organizan a tódalas moléculas para forma arquitecturas complexas trasládase tamén ao comportamento final destes materiais supramoleculares. En xeral encóntranse certas características moi comúns entre este tipo de estruturas como poden ser a reversibilidade, a resposta a estímulos externos ou a capacidade de autoreparación, que de forma esperada, son similares as observadas en materiais naturais.

Da mesma maneira que fixo no seu momento a química orgánica covalente, a química supramolecular busca a cada paso crear novas estruturas cunha maior complexidade tendo como referencia en moitos casos procesos naturais. Para conseguir este obxectivo, a química supramolecular basease en dous procesos claves, o recoñecemento e o autoensamblaxe molecular. O recoñecemento molecular, refírese a unión específica entre dúas moléculas complementarias, un anfitrión e un hospede, xerando un novo complexo de forma similar ao proceso de recoñecemento dun substrato polo seu encima. Por outro lado, o autoensamblaxe é o proceso mediante o cal moléculas desorganizadas adoptan unha disposición específica a través de enlaces non covalentes. Este proceso pode ser intramolecular, onde unha sola molécula adquire unha conformación espacial determinada como é o caso da estrutura secundaria das proteínas; ou intermolecular, onde moitas moléculas asócianse entre si para xerar estruturas definidas como é o caso do virus do mosaico do tabaco.

Concretamente, o autoensamblaxe intermolecular, da man do deseño molecular permitiu a obtención dun novo tipo de estruturas, os polímeros supramoleculares. Estes novos polímeros manteñen as propiedades dos seus homólogos covalentes e, adicionalmente, conservan tódalas vantaxes dos sistemas supramoleculares. Durante os últimos anos, os estudos de polímeros

supramoleculares baseados tanto en moléculas sintéticas como naturais intensificouse debido as súas potenciais aplicacións. A posibilidade de facer pequenas modificacións sintéticas nas moléculas que causen cambios morfolóxicos no polímero final, ou que lle confiran unha funcionalidade especial, son as razóns que permitiron o seu uso como sensores, catalizadores, sistemas de liberación de fármacos, biomímeticos, etc.

Dentro da multitude de posibles compoñentes coñecidos para o deseño de novos polímeros supramoleculares, un dos máis prometedores son os péptidos cíclicos (CPs) compostos dun número par de alfa aminoácidos con quiralidade alterna. Esta familia de péptidos, caracterízase por ter unha conformación plana onde os grupos carbonilo e amino adoptan unha disposición perpendicular ao plano que permite a formación de enlaces de hidróxeno entre as subunidades peptídicas dando lugar a estruturas tubulares tipo lámina beta. A maiores, o emprego deste tipo de estruturas presenta a vantaxe principal de que mediante o control da secuencia de aminoácidos, poden modularse as propiedades do nanotubo. Neste sentido, variacións no número de residuos permiten o control do diámetro do tubo, mentres que a natureza dos aminoácidos e as súas cadeas laterais modulan as propiedades da cavidade interna ou da zona externa respectivamente. De forma mais recente, a existencia de aminoácidos con grupos reactivos explotouse para funcionalizar os péptidos cíclicos con cadeas hidrocarbonadas, residuos aromáticos ou polímeros dando lugar a unha extensa variedade de estruturas onde atopamos entre outras as cápsulas, os tubisomas, as láminas ou as fibras. De forma análoga a outros polímeros supramoleculares, estas estruturas amosan potenciais aplicacións en bioloxía, ciencia de materiais ou electrónica.

Coa idea de ampliar o coñecemento existente entre a funcionalización dos ciclopéptidos e as súas propiedades de autoensamblaxe, o obxectivo desta tese doutoral é o deseño e síntese de novos polímeros supramoleculares baseados en D,L-α-CPs funcionalizados con residuos aromáticos. A incorporación deste tipo de grupos pode afectar ao empillamento das distintas subunidades peptídicas e polo tanto regular o ensamblaxe xerárquico. A xeración de librerías de CPs con distintas funcionalizacións pode desenmascarar os parámetros críticos que gobernan as ensamblaxes peptídicas permitindo o deseño de materiais para aplicacións específicas.

No primeiro capítulo desta tese abórdase o deseño, a síntese e a caracterización dunha nova familia de hidroxeladores baseados en péptidos cíclicos con capacidade de resposta a estímulos. Para dito fin, empregáronse dous esqueletos peptídicos que incluían na súa estrutura un ou dous residuos alcoxiamina, dúas histidinas e que segregaban a parte hidrófila da hidrófoba. O grupo alcoxiamina é coñecido polo seu alto rendemento en reaccións de condensación con aldehidos. Desta maneira, cun mínimo esforzo sintético, logrouse funcionalizar os péptidos cíclicos con aldehidos aromáticos e obter unha batería de CPs con capacidades xelificantes. Por outro lado, as histidinas son aminoácidos susceptibles de protonarse ou desprotonarse de forma reversible en función do pH, proporcionando un estímulo para controlar o ensamblaxe. Desta forma, o sistema atoparíase desensamblado a pH ácido onde as cadeas laterais presentarían cargas positivas e polo tanto os CPs repeleríanse uns os outros, mentres que a neutralización do pH e da carga permitiríanos desprazar o equilibrio cara o estado ensamblado. Por último, a orde escollida para os aminoácidos na secuencia propiciou a separación dos dominios hidrófobo e hidrófilo, e desta forma favorecer un ensamblaxe xerárquico en dous pasos. No primeiro paso, as distintas subunidades peptídicas empíllanse para dar lugar a nanotubos onde os residuos hidrófobos sitúanse nunha cara do agregado mentres que os hidrófilos sitúanse na oposta. Esta disposición permite que nun segundo paso, co

obxectivo de ocultar os dominios hidrófobos da auga, os nanotubos interaccionen entre si dando lugar a agregados dunha maior lonxitude e grosor (fibras). Estes ensamblados de gran tamaño son capaces de formar unha rede tridimensional que limita o fluxo da auga, sistema que se coñece como hidroxel.

Para demostrar a veracidade deste deseño, usáronse diferentes técnicas espectroscópicas, microscópicas e reolóxicas. Confirmando o deseño inicial, a caracterización mediante espectroscopía infravermella revelou que os CPs empillábanse formando estructuras de tipo lámina beta antiparalela. Ademais, a monitorización da absorbancia e fluorescencia dunha disolución acuosa ácida de péptido lentamente alcalinizada, amosou as transicións esperadas entre os estados desensamblado e ensamblado. Un maior análise dos datos mostrou unha coincidencia entre o pH de transición do noso sistema e o pH de desprotonación das histidinas, dando veracidade ao deseño. Por outro lado, empregáronse distintas técnicas de microscopía para visualizar os nanotubos e o seu ensamblaxe en fibras de maior tamaño. A maiores, unha análise exhaustiva destas imaxes, demostraron unha relación directa entre as lonxitudes que podían acadar os nanotubos e o número e natureza dos residuos aromáticos empregados na edición dos CPs. Por último, a formación do xel foi confirmada pola técnica do vial invertido e as súas propiedades avaliadas mediante reoloxía. A análise conxunta de tódolos datos evidenciou unha relación entre o carácter hidrófobo dos derivados CPs, a lonxitude dos nanotubos resultantes do seu ensamblaxe e as propiedades viscoelásticas dos xeis. Desta maneira introducíronse os principios necesarios para o deseño e síntese de hidroxeladores baseados en CPs.

Como pode observarse na natureza, os hidroxeis son sistemas cunha alta versatilidade que forman parte de estruturas moi importantes a nivel biolóxico como son as matrices extracelulares ou o citoesqueleto celular. Concretamente o citoesqueleto é un sistema de alta complexidade que forma parte de procesos fundamentais para a vida como son a mobilidade e a división celular. Neste sentido é necesario destacar que o citoesqueleto está formado fundamentalmente por tres polímeros supramoleculares (microtúbulos, microfilamentos e filamentos intermedios) e mailas súas proteínas reguladoras. Estes compoñentes son capaces de traballar de forma conxunta para adaptar a resposta celular ante determinados estímulos extra- ou intracelulares. Unha das actuacións conxuntas mais destacadas é a que ocorre durante a división celular. Durante este proceso os microtúbulos reorganízanse na célula para xerar o fuso mitótico encargado da separación dos cromosomas, mentres de forma simultánea a actina forma un anel de contracción no medio da membrana plasmática que separa as dúas células fillas ao final do proceso. Neste sentido, calquera sistema sintético que pretenda imitar as características e funcións do citoesqueleto precisa atopar restricións de espazo igual que o citoesqueleto está limitado pola membrana plasmática, e ten que presentar un minucioso control espacial e temporal sobre a polimerización dos seus compoñentes.

No segundo capítulo desta memoria, inspirados polo comportamento do citoesqueleto, estudouse o comportamento do ciclo péptido funcionalizado cun residuo de pireno (**1TP**) en espazos confinados, concretamente gotas de auga en aceite. Como xa se mencionou anteriormente, este CP presenta na súa secuencia aminoácidos sensibles ao pH e mediante a funcionalización dótaselle coa capacidade de formar fibras. Como se comentou previamente, a pH ácido esta molécula atópase de forma individualizada pola presenza de cargas positivas nas cadeas laterais da histidina, o cal facilita as repulsións CP-CP. Polo tanto, en principio, unha redución na repulsión mediante un aumento da forza iónica pode, igual que o pH, dar lugar a arquitecturas fibrilares

similares. De todas formas, atendendo a natureza do estímulo pódese presupoñer que as estruturas obtidas mediante un aumento na concentración de sales presentarán un carácter máis hidrófilo así como un menor grado de empaquetamento se as comparamos coas obtidas por alcalinización.

Para levar a cabo este estudo, o primeiro que se fixo neste capítulo foi comprobar a resposta do **1TP** á forza iónica en solución, en condicións similares as estudadas previamente co pH. Os resultados obtidos en dicroísmo circular e fluorescencia amosaron un empillamento gradual dos pirenos a medida que aumentaba a concentración de sales no medio. O uso de diferentes catións e anións demostrou que os anións xogan o papel predominante no ensamblaxe deste tipo de CPs, ocultando as cargas positivas unhas doutras. A maiores, a comparación entre os obtidos trala polimerización por forza iónica e por pH suxerían un empaquetamento máis compacto no caso do pH, probablemente relacionado coa ausencia de cargas.

Unha vez coñecida a resposta ao dous estímulos, pasamos a estudar o seu comportamento en espazos confinados. Para levar a cabo este estudo empregamos unha técnica novidosa coñecida como microfluídica. Esta metodoloxía permite un maior control sobre diversos parámetros clave na formación das gotas que reducen o error experimental, entre os que se atopan a forma, o tamaño e a concentración. A polimerización do **1TP** mediante pH no interior das gotas deu lugar a unha acumulación dos agregados na superficie externa da gota; mentres que a forza iónica deu lugar a ensamblados con tendencia a localizarse no núcleo da gota. Esta diferenza débese á natureza dos agregados, onde a forza iónica xera ensamblados cun carácter máis hidrófilos debido a unha maior presenza de cargas e un menor grado de empillamento. A maiores, o uso de catións multivalentes (SO_4^{2-}) baixo distintos réximes de fluxo, que permitían modular a concentración de ións no medio, desprazou a presenza de agregados da parte externa á parte interna. Estes estudos en espazos confinados demostraron a posibilidade de ter un control espaciotemporal sobre a polimerización de sistemas baseados en CPs e ao mesmo tempo, resaltouse a importancia que pode ter o ambiente químico na distribución espacial das fibras en sistemas naturais como o citoesqueleto.

Nestas comparacións con citoesqueleto, démonos de conta que o minucioso control sobre parámetros como diámetro e lonxitude que existe nestas fibras naturais contrasta coa variabilidade das fibras obtidas mediante a polimerización de CPs. Co obxectivo de reducir esta dispersión sen alterar as bases da ensamblaxe buscouse un dominio aromático que permitise a incorporación de forma sinxela de varios grupos aldehidos para así obter fibras cun núcleo hidrófobo rodeado dun número limitado de nanotubos peptídicos. Neste contexto, encontrouse o tetrafeniletileno (TPE) un dominio aromático facilmente accesible e modificable con catro grupos aldehido nas posicións para de cada anel de fenilo. Desta maneira a fibra xerada nesta caso estaría constituída por catro nanotubos unidos de forma covalente a ese núcleo de TPE. Ademais, o TPE pertence a un grupo especial de fluoróforos onde a emisión é inducida pola agregación (AIE). Estes fluoróforos caracterízanse por presentar unha baixa ou nula emisión cando están separados que se volve forte cando o sistema está ensamblado. Polo tanto, esta molécula ademais de permitir a xeración fibras controladas, serviría para realizar un seguimento do de ensamblaxe dos CPs mediante fluorescencia e caracterizar a morfoloxía dos agregados finais por microscopía de fluorescencia.

Por mor das devanditas razóns, no terceiro capítulo desta tese doutoral abordouse o deseño e síntese de distintos derivados de CPs unidos de forma covalente a un núcleo central de TPE.

En primeiro lugar, empregouse o mesmo esqueleto peptídico que no caso do **1TP** pero condensando catro unidades de CPs nun só residuo de TEP dando lugar ao derivado **4CP$_{1k}$-U-TPE**. Este composto presenta un núcleo central hidrófobo de TPE rodeado de catro péptidos cíclicos. En segundo lugar, os estudos de fluorescencia confirmaron as propiedades AIE do novo sistema onde o pH controla o estado da agregación como pasaba nos anteriores derivados CPs. Ademais, o uso de tioflavina-t demostrou que a ensamblaxe do TPE ocorría de forma simultánea co empillamento dos péptidos cíclicos. Mencionar que a tioflavina-t é unha sonda empregada especificamente para detectar estruturas tipo lámina beta. Para confirmar a morfoloxía destes agregados recorreuse as mesmas técnicas de imaxe empregadas no primeiro capítulo. De forma moi interesante e inesperada, estes novos agregados non tiñan forma de fibras, se non que constituían láminas de gran tamaño. A análise das imaxes tomadas por microscopía de forza atómica amosou láminas con alturas que coincidían coa altura esperada para unha fibra formada polo ensamblaxe do **4CP$_{1k}$-U-TPE**. A primeira hipótese foi que o noso composto nun primeiro lugar ensamblábase en fibras mediante o empillamento dos CPs e do TPE, na cal a disposición espacial das distintas cadeas laterais dos aminoácidos, especialmente as histidinas mediante a formación de enlaces de hidróxeno, favorecían o crecemento lateral deste novo sistema. Para coñecer as limitacións e criterios de ensamblaxe deste novo tipo de sistemas bidimensionais baseados en CPs unidos ao TPE, deseñáronse minuciosamente diferentes derivados do CP e do TPE coa intención de desestabilizar esta estrutura. En xeral tanto a caracterización espectroscópica e microscópica amosou resultados similares aos obtidos no caso do **4CP$_{1k}$-U-TPE**, indicando que a arquitectura baseado nun TPE rodeado de catro péptidos cíclicos é óptima para realizar novos deseños funcionais de sistemas 2D. Ademais, as modificacións estruturais permitíronnos deducir a importancia de certo parámetros estruturais: i) a lisina é clave para manter a estabilidade a pH superiores a 6, ii) a presenza de polo menos unha histidina é importante para manter a solubilidade en auga a pH ácidos e para poder controlar o ensamblaxe mediante pH; iii) a posición das histidinas e os posibles enlaces de hidróxeno entre elas non son imprescindibles para o crecemento lateral do sistema; iv) a substitución en para do TPE non é fundamental para manter o empaquetamento en dous dimensións do sistema, v) o derivado monosubstituído do TPE é capaz de ensamblarse en nanotubos ou láminas sinalando a importancia da tetrasubstitución para desprazar o equilibrio cara a formación de sistemas totalmente bidimensionais. Por último, testouse a capacidade catalítica destas láminas xa que a gran área da que dispoñen permitiría a exposición de moitos sitos activos, no noso caso representados polas histidinas que participan en reaccións hidrolíticas. Os resultados preliminares obtidos na hidrólisis do acetato de para-nitrofenol, inda que non son concluíntes, indican que este tipo de sistemas poderíanse empregar como catalizadores químicos.

En resumidas contas, ao longo desta tese doutoral estudáronse os principios que dirixen o ensamblaxe de péptidos cíclicos funcionalizados con residuos aromáticos que modulan a morfoloxía e propiedades finais dos agregados supramoleculares. Para elo foi necesario realizar múltiples estudos con distintos residuos aromáticos, distintos estímulos e condicións de ensamblaxe. En primeiro lugar, a funcionalización con diferentes residuos aromáticos dos péptidos cíclicos revelou a importancia do control do pH, das interaccións tipo π e do balance hidrofilia-lipofilia na xeración de hidroxeis con capacidade de autoreparación. A súa vez, permitiu relacionar a morfoloxía dos agregados microscópicos coas propiedades macroscópicas dos xeis confirmando que mediante o deseño molecular pódense preparar moléculas que dean materias con propiedades adaptadas para aplicacións específicas. En segundo lugar, inspirados polo citoesqueleto celular e

polas diferenzas existentes entre a conducta adoptada polas moléculas en disolución e en espazos confinados, caracterizouse o comportamento deste tipo de polímeros supramoleculares en espazos confinados. O emprego do pH e da forza iónica que da lugar a ensamblados similares, permite controlar a localización destes agregados dentro das gotas de auga en aceite. O pH provoca a polimerización mediante a desprotonación das histidinas dando lugar a estruturas cun carácter amfipático que propicia a súa localización maioritaria no límite entre a auga e o aceite. Polo outro lado, a natureza mais hidrófila dos polímeros xerados mediante un aumento da forza iónica despraza a localización dos agregados cara ó interior da gota. Desta maneira conseguiuse simular unha das claves do comportamento do citoesqueleto cun modelo sintético simple. Sen embargo, a dispersión existente nos polímeros supramoleculares sintéticos en comparación coas fibras naturais, dirixiunos cara o deseño de estruturas que puidesen dar lugar a ensamblados mais homoxéneos. Polo que en terceiro lugar, deseñouse unha nova arquitectura na que o centro está ocupado por unha molécula aromática de TPE decorada na parte externa con catro péptidos cíclicos que dirixiran a ensamblaxe para a formación de fibras homoxéneas en diámetro e lonxitude. Contrariamente ás fibras unidimensionais esperadas, os estudos morfolóxicos revelaron a presenza de grandes agregados bidimensionais como consecuencia da interacción lateral destas fibras. A vista destes resultados, deseñáronse diferentes modificacións tanto do núcleo aromático como da secuencia do péptido cíclico para coñecer o tipo de forzas que favorecían esta ensamblaxe lateral. A constante formación de estruturas laminares revelou o potencial uso desde tipo de arquitecturas aromáticas tetrafuncionalizadas con CPs para a formación de sistemas 2D estables en medios acuosos alcalinos. A maiores, ensaios preliminares amosaron o seu potencial uso como deste sistema como catalizador. Como reflexión final, consideramos importantes tódolos coñecementos recompilados nesta tese doutoral xa que poderán guiar nun futuro a outros científicos para o deseño de novos materiais supramoleculares baseados en octapéptidos cíclicos de quiralidade alternada.

INTRODUCTION

1. SUPRAMOLECULAR CHEMISTRY

"*Ignorantia juris non excusat*". Even though someone is unaware of the contents of the law but breaks it, this act is still a crime, and therefore he is a criminal. Following the same argument, we could consider the first living organism as the first chemist because it unconsciously performed chemical reactions.

However, humans did not start to employ "intended" chemical transformations until they started to master fire about 1.9 million years ago and employed it to improve food intake.[1] From that point, the unconscious use of chemistry starts to form part of human life in things, such as paintings,[2] perfumes[3] or metallurgy[4,5] among others; leading society to a more "rational" use of this tool exemplified with the appearance of alchemy, which the oldest known sources date the third century.[6] Subsequently, the publication of "*The Sceptical Chymist*" in 1661 by R. Boyle is noted as the birth date of modern chemistry. However, chemistry as we know it today did not really appear until the 18th century with the work developed by A. Lavoisier among others.[7] From that time on, the main efforts of the chemistry community were dedicated to the synthesis of complex molecules from simple reactants through covalent bonds such as the synthesis of urea.[8] Its main limitation was the construction of molecules with high functional complexity and composed of an enormous number of atoms covalently linked. This deficiency became apparent with the progress in biochemistry and molecular biology. From this point, the understanding of living systems and the possibility of mimicking them caught the chemists' attention. To achieve such goal, the synthesis of much complex chemical entities not achievable by conventional synthesis, was the main requirement.[9]

Many chemists have focused their efforts on developing tools based on supramolecular chemistry over the last decades. Supramolecular chemistry was defined by J.-M. Lehn as "*chemistry beyond the molecule*"[10] and its aim is to study and control the weak and reversible non-covalent interactions between molecules.[11] Even though the actual name is relatively recent, it started back in 1873 when the existence of intermolecular forces was first reported by J. D. van der Waals.[12] Right after, E. Fisher compared the interaction of an enzyme and its substrate as the lock with its key (Figure 1a), that will later become the principles for molecular recognition and host-

---

[1] D. M. J. S. Bowman, J. K. Balch, P. Artaxo, W. J. Bond, J. M. Carlson, M. A. Cochrane, C. M. D'Antonio, R. S. DeFries, J. C. Doyle, S. P. Harrison, F. H. Johnston, J. E. Keeley, M. A. Krawchuk, C. A. Kull, J. B. Marston, M. A. Moritz, I. C. Prentice, C. I. Roos, A. C. Scott, T. W. Swetnam, G. R. Van Der Werf and S. J. Pyne, *Science*, **2009**, *324*, 481–484.
[2] C. S. Henshilwood, F. D'errico, K. L. Van Niekerk, Y. Coquinot, Z. Jacobs, S.-E. Lauritzen, M. Menu and R. García-Moreno, *Science*, **2011**, *334*, 219–222.
[3] N. Balasubramanian, in *Chemical Technology in Antiquity*, American Chemical Society, Washington DC, **2015**, vol. 1211, pp. 219–244.
[4] M. Radivojević and B. W. Roberts, *J. World Prehist*., **2021**, *34*, 195–278.
[5] M. Radivojević, T. Rehren, E. Pernicka, D. Šljivar, M. Brauns and D. Borić, *J. Archaeol. Sci*., **2010**, *37*, 2775–2787.
[6] T. Bock, *History of Alchemy from Early to Middle Ages*, GRIN Verlag, Munich, **1997**.
[7] A. Lavoisier, *Traité élémentaire de chimie, présenté dans un ordre nouveau et d'apres les découvertes modernes*, Cuchet, Paris, **1798**.
[8] K. C. Nicolaou, *Isr. J. Chem.*, **2018**, *58*, 104–113.
[9] J.-M. Lehn, *Angew. Chem. Int. Ed*., **2013**, *52*, 2836–2850.
[10] J.-M. Lehn, *Science*, ***1993***, *260*, 1762–1763.
[11] H. J. Schneider, *Angew. Chem. Int. Ed*., **2009**, *48*, 3924–3977.
[12] J. D. van der Waals, *On the Continuity of the Gaseous and Liquid States*, University of Leiden, Leiden, **1873**.

guest chemistry.[13] Later on, in the 20s with the introduction of hydrogen bonds by M. L. Huggins the understanding and the spotlight on non-covalent bonds got dramatically increased.[14,15] This knowledge paved the way to some of the biggest breakthroughs in biological chemistry such as the elucidation of the double helical structure of DNA[16-18] and the secondary structure of proteins.[19] Moreover, it also boosted the discovery of other intermolecular forces such as π-π, ion-dipole, dipole-dipole or halogen bond among others.[20]

The concept of supermolecule (Übermoleküle) was introduced in 1937 by K.L. Wolf,[21] but it is not until the 60s when this field really claims the attention of the scientific community with the works of D.J. Cram,[22] C.J. Pedersen[23], and J.-M. Lehn[24] on macrocycles with the ability to selectively bind ions or small organic molecules by non-covalent interactions. Their discoveries were awarded with the Nobel Prize in 1987. More recently, in 2016, J-P. Sauvage, J.F. Stoddart and B.L. Feringa were also awarded with the Nobel Prize for the design and synthesis of molecular machines highlighting the importance of supramolecular chemistry nowadays.[25] Over the years, the use of intermolecular forces allowed the design and synthesis of a wide variety of supramolecular structures which complexity couldn't be achieved by covalent chemistry.[26,27] Furthermore, the possibility to modify the building blocks at the molecular level gave rise to a new methodology for the design of architectures with the desired size, shape, and functionality; the "bottom-up" approach.[28] Additionally, since these arrangements are the result of weak interactions, they tend to be reversible and stimuli responsive materials.[29] Despite being a recent discipline, supramolecular chemistry has shown a huge growth, increasing knowledge and mimicking of biological processes,[30] and displaying promising applications in modern society.[31]

2. SELF-ASSEMBLY AND MOLECULAR RECOGNITION

Molecular recognition and self-assembly are the cornerstones of the recent development of supramolecular chemistry.[32] In order to get a supramolecular entity from two molecules, they have to bear complementary groups correctly arranged in space to achieve the precise interactions that hold both species together. All essential information to carry out this process such as shape, surface,

---

[13] E. Fischer, *Ber. Dtsch. Chem. Ges.*, **1894**, *27*, 2985–2993.
[14] W. M. Latimer and W. H. Rodebush, *J. Am. Chem. Soc.*, **1920**, *42*, 1419–1433.
[15] T. S. Moore and T. F. Winmill, *J. Chem. Soc.*, **1912**, *101*, 1635–1676.
[16] J. D. Watson and F. H. C. Crick, *Nature*, **1953**, *171*, 737–738. R. E.
[17] M. H. F. Wilkins, A. R. Stokes and H. R. Wilson, *Nature*, **1953**, *171*, 738–740.
[18] Franklin and R. G. Gosling, *Nature*, **1953**, *171*, 740–741.
[19] L. Pauling, R. B. Corey and H. R. Branson, *Proc. Natl. Acad. Sci. U. S. A.*, **1951**, *37*, 205–211.
[20] F. Biedermann and H. J. Schneider, *Chem. Rev*., **2016**, *116*, 5216–5300.
[21] K. L. Wolf, H. Prahm and H. Harms, *Z. Phys. Chem*., **1937**, *36B*, 237–287.
[22] D. J. Cram, *Angew. Chem. Int. Ed. Engl.*, **1988**, *27*, 1009–1020.
[23] C. J. Pedersen, *Angew. Chem. Int. Ed. Engl.*, **1988**, *27*, 1021–1027.
[24] J.-M. Lehn, *Angew. Chem. Int. Ed. Engl.*, **1988**, *27*, 89–112.
[25] J. C. Barnes and C. A. Mirkin, *Proc. Natl. Acad. Sci. U. S. A*., **2017**, *114*, 620–625.
[26] D. N. Reinhoudt and M. Crego-Calama, *Science*, **2002**, *295*, 2403–2407.
[27] I. V. Kolesnichenko and E. V. Anslyn, *Chem. Soc. Rev.*, **2017**, *46*, 2385–2390.
[28] V. Balzani, A. Credi and M. Venturi, *Chem. Eur. J*., **2002**, *8*, 5524–5532.
[29] K. Liu, Y. Kang, Z. Wang and X. Zhang, *Adv. Mater*., **2013**, *25*, 5530–5548.
[30] S. Yang, Y. Geiger, M. Geerts, M. J. Eleveld, A. Kiani and S. Otto, *J. Am. Chem. Soc*., **2023**, *145*, 16889–16898.
[31] G. T. Williams, C. J. E. Haynes, M. Fares, C. Caltagirone, J. R. Hiscock and P. A. Gale, *Chem. Soc. Rev*., **2021**, *50*, 2737–2763.
[32] H. Wang and X. Zheng, *Phys. Chem. Chem. Phys*., **2022**, *24*, 19011–19028.

and functional groups is encoded on the chemical structure.[33] Although molecular recognition and self-assembly are closely related concepts separated by a very thin line, generally speaking, the main difference between the two is related to the number of molecules that form the supramolecular entity. On the one hand, molecular recognition refers to the specific binding between at least two entities through non-covalent interactions to generate a supramolecular aggregate called host-guest complex.[34] The binding pocket of the host possesses distinctive characteristics such as size, geometry and functional groups that make the interaction with the guest highly specific.[35] Great examples of this process are the biotin recognition by streptavidin (Figure 1b),[36] the binding of vancomycin to terminal D-Ala-D-Ala peptides (Figure 1c),[37] the binding between an antibody and the antigen or the binding of an enzyme and its substrate.

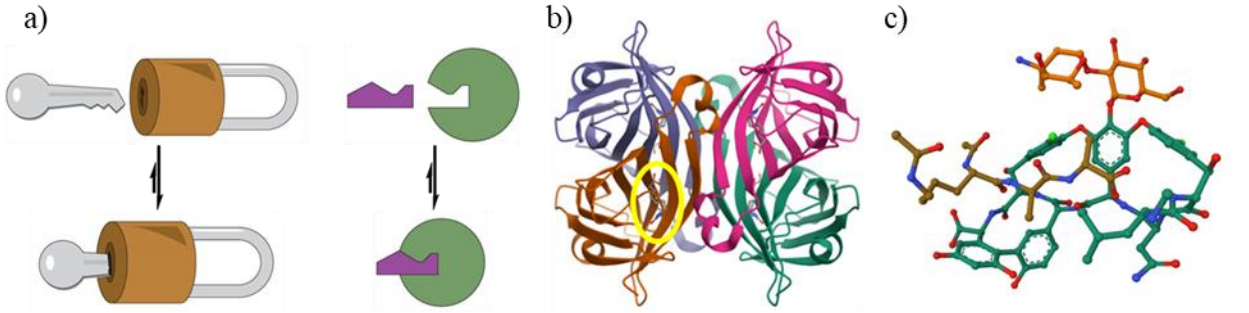

Figure 1. a) Schematic representation of the key-lock model; b) streptavidin-biotin complex (biotin recognition site in yellow). PDB: 1STP. From Patricia C. Weber et al., Structural Origins of High-Affinity Biotin Binding to Streptavidin. *Science* **243**, 85-88 (1989). Reprinted with permission from AAAS; and c) vancomycin cell wall precursor analog complex. PDB: 1FVM. Reprinted with permission from Ref.37. Copyright © 2008 Elsevier Ltd.

On the other hand, molecular self-assembly is the process that guides molecules to adopt a specific arrangement through non-covalent interactions to form larger aggregates. It takes place without intervention from an outside source, since all the information needed is encoded in the molecular structure.[38] Even though the process can be intra- or intermolecular, the first is usually known as folding while the second is commonly referred as self-assembly. Folding is a phenomenon widely observed in nature, exemplified by proteins and the acquisition of specific conformations, known as secondary structures, such as α-helix or β-sheet through the formation of H-bonds or hydrophobic effects (Figure 2a).[39,40] This process can be observed in artificial

[33] J. Rebek, *Proc. Natl. Acad. Sci. U. S. A.*, **2009**, *106*, 10423–10424.
[34] J. W. Steed, D. R. Turner and K. J. Wallace, *Core Concepts in Supramolecular Chemistry and Nanochemistry*, John Wiley & Sons, Chichester, **2007**.
[35] J. Pleiss, *ChemCatChem*, **2014**, *6*, 944–950.
[36] P. C. Weber, D. H. Ohlendorf, J. J. Wendoloski and F. R. Salemme, *Science*, **1989**, *243*, 85–88.
[37] Y. Nitanai, T. Kikuchi, K. Kakoi, S. Hanamaki, I. Fujisawa and K. Aoki, *J. Mol. Biol.*, **2009**, *385*, 1422–1432.
[38] G. M. Whitesides and M. Boncheva, *Proc. Natl. Acad. Sci. U. S. A.*, **2002**, *99*, 4769–4774.
[39] P. D. Sun, C. E. Foster and J. C. Boyington, *Curr. Protoc. Protein Sci.*, **2004**, *35*, 17.1.1-17.1.189.
[40] E. Marcos, B. Basanta, T. M. Chidyausiku, Y. Tang, G. Oberdorfer, G. Liu, G. V. T. Swapna, R. Guan, D.-A. Silva, J. Dou, J. H. Pereira, R. Xiao, B. Sankaran, P. H. Zwart, G. T. Montelione and D. Baker, *Science*, **2017**, *355*, 201–206.

molecules, known as foldamers, in which non-natural oligomers designed by chemists fold in particular conformations (Figure 2b).[41,42]

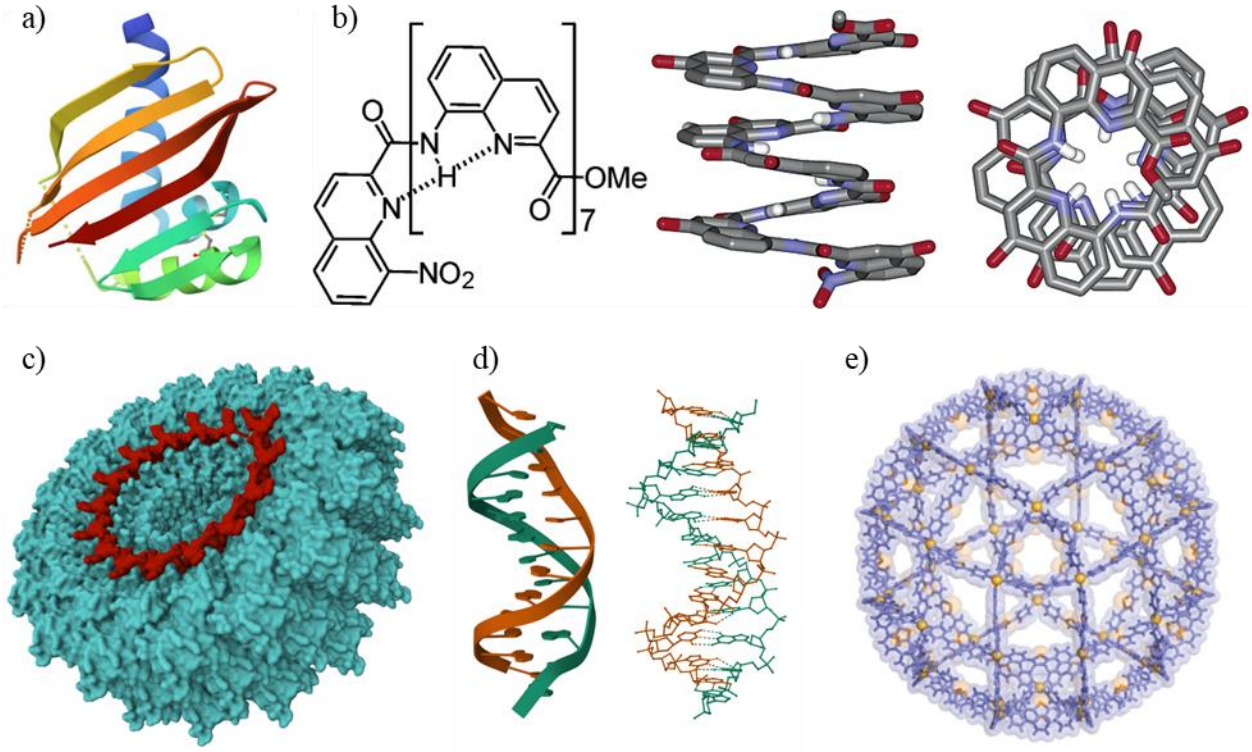

Figure 2. Examples of self-assembly. Intramolecular: a) folded protein with alpha-helix and beta-sheet domains. PDB: 5TS4;[40] and b) foldamer based on aromatic gamma-peptides – chemical structure, side and zenithal views of the folded molecule (from left to right). Adapted with permission from Ref. 42. Copyright © 2003 American Chemical Society. Intermolecular: c) TMV where an RNA chain (red) guides the arrangement of the surrounding proteins (blue) – PDB: 2TMV. Reprinted with permission from Ref.45. Copyright © 1989 Elsevier Ltd.; d) DNA double helix; schematic (left) and atomistic (right) representation – PDB: 1BNA; and e) Fujita 144-member Goldberg polyhedral capsule. Adapted with permission from Ref.49. Copyright © 2016, Macmillan Publishers Limited, part of Springer Nature.

In the case of molecular self-assembly, it involves a larger number of molecules interacting simultaneously and is intrinsically more complex than molecular recognition or folding. Strictly speaking self-assembly involves a finite number of molecules and is perfectly exemplified by the formation of the Tobacco Mosaic Virus (TMV).[43] It consists of a helical virus particle composed by an RNA core of 6340 bases shielded by 2130 identical protein subunits, containing 158 aa residues each. The final particle is 300 nm x 18 nm where the protein shell provides high stability to the RNA (Figure 2c).[44,45] Another natural example is the structure of DNA, which spontaneously forms a double helix promoted by H-bonds between the complementary nucleobase pairs, guanine-

[41] D. J. Hill, M. J. Mio, R. B. Prince, T. S. Hughes and J. S. Moore, *Chem. Rev.*, **2001**, *101*, 3893–4012.
[42] H. Jiang, J. M. Léger and I. Huc, *J. Am. Chem. Soc.*, **2003**, *125*, 3448–3449.
[43] J. W. Steed and J. L. Atwood, *Supramolecular Chemistry*, John Wiley & Sons Ltd, Chichester, 3rd edn., **2022**.
[44] D. L. D. Caspar, in *Advances in Protein Chemistry*, **2008**, vol. 18, pp. 37–121.
[45] K. Namba, R. Pattanayek and G. Stubbs, *J. Mol. Biol.*, **1989**, *208*, 307–325.

cytosine and adenine-thymine (Figure 2d).[46] Over the years chemist have also developed synthetic systems that can self-assembly into finite structures that mimic the behavior of viral capsids[47] or DNA complementarity.[48] Interestingly, Fujita *et al* were able to design a Goldberg polyhedral compose of 144-members of which 96 are ligands and 48 are Pd^{2+} ions (Figure 2e).[49] Despite this fact, the concept of self-assembly is also commonly used to describe supramolecular polymers built with an infinite number of molecules. This concept will be further explained in the next section.

3. Supramolecular Polymers and Hierarchical Assembly

Going again back in time to the early days of humankind, polymers (wool, cotton, linen…) have been fundamental components of different commodities. However, it wasn't until 1920 when Hermann Staudinger define polymers as long chains built from repeating molecular subunits (monomers) linked by covalent bonds.[50] Since that moment the field of polymer has grown exponentially with huge impact in commercial applications. For these contributions, H. Staudinger received the Nobel Prize in 1953.[51]

The later development of supramolecular chemistry showed that molecules did not need to be covalently bonded to achieve long chains, leading to the birth of supramolecular polymers.[52] They were defined by W. Meijer as "*polymeric arrays of monomeric units that are held together by highly directional and reversible non-covalent interactions, resulting in polymeric properties in solution and bulk*".[53]

The supramolecular polymerization can take place typically by four different mechanisms (Figure 3a):[54,55] i) isodesmic, where all intermolecular interactions are considered to be identical, thus all the species present the same reactivity; ii) ring-chain mediated, where the monomers have two functional ends giving rise to an equilibrium between linear polymer chains and cyclic oligomers; iii) cooperative, where a less favorable activation step (nucleation) initially takes place followed by a more favorable polymer growth (elongation); or iv) anti-cooperative, where a more favorable dimerization step is followed by a less favorable elongation process. Usually, the resulting supramolecular polymers are classified attending to three different aspects: the physical nature of the interaction, the molecular component, or the Gibbs free energy.[56] However, in this section we will classify them attending to the nature of the different building blocks.

Supramolecularly assembled polymers can often undergo complex morphological transitions to life-like resembling structures due to hierarchical assembly processes. The latter can be defined

---

[46] H. R. Drew, R. M. Wingt, T. Takano, C. Broka, S. Tanaka, K. Itakura and R. E. Dickerson, *Proc. Natl. Acad. Sci. U. S. A*., **1981**, *78*, 2179–2183.
[47] Y. S. Chen, E. Solel, Y. F. Huang, C. L. Wang, T. H. Tu, E. Keinan and Y. T. Chan, *Nat. Commun*., **2019**, *10*, 3443.
[48] J. Saarbach, P. M. Sabale and N. Winssinger, *Curr. Opin. Chem. Biol.*, **2019**, *52*, 112–124.
[49] D. Fujita, Y. Ueda, S. Sato, N. Mizuno, T. Kumasaka and M. Fujita, *Nature*, **2016**, *540*, 563–566.
[50] H. Staudinger, *Ber. Dtsch. Chem. Ges*., **1920**, *53*, 1073–1085.
[51] H. Staudinger, *Macromolecular chemistry*, **1953**.
[52] C. Fouquey, J.-M. Lehn and A.-M. Levelut, *Adv. Mat*., **1990**, *2*, 254–257.
[53] L. Brunsveld, B. J. B. Folmer, E. W. Meijer and R. P. Sijbesma, *Chem. Rev*., **2001**, *101*, 4071–4097.
[54] U. S. Schubert, G. R. Newkome and A. Winter, *Supramolecular Polymers and Assemblies: From Synthesis to Properties and Applications*, John Wiley & Sons, **2021**.
[55] J. Gershberg, F. Fennel, T. H. Rehm, S. Lochbrunner and F. Würthner, *Chem. Sci*., **2016**, *7*, 1729–1737.
[56] T. F. A. De Greef, M. M. J. Smulders, M. Wolffs, A. P. H. J. Schenning, R. P. Sijbesma and E. W. Meijer, *Chem. Rev*., **2009**, *109*, 5687–5754.

as the process of achieving multilevel organization from simple molecular units that initially are compiled through non-covalent interactions into ordered secondary structures. These act as the building blocks of subsequent assembly processes to form more complex multifunctional structures. This action can take place more than once, achieving multiple levels of structural complexity (Figure 3b).[57,58] These self-assembled structures have shown that the bottom-up approach has great potential in the fabrication of new functional materials and nano-devices.[59]

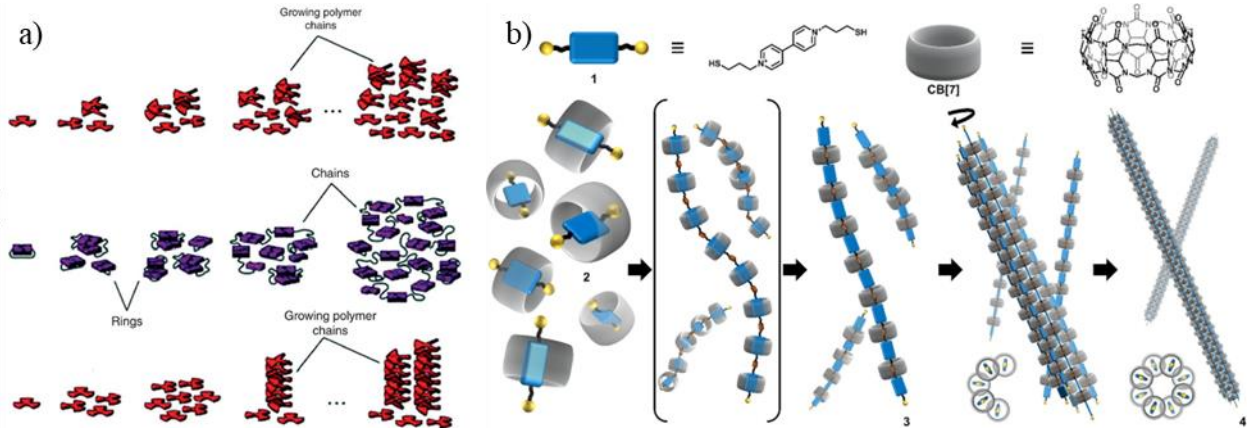

Figure 3. a) Schematic representation of the different supramolecular polymerization mechanisms (from top to bottom): isodesmic, ring-chain and cooperative. Reprinted with permission from Ref.56. Copyright © 2009 American Chemical Society; and b) schematic representation of the hierarchical self-assembly of artificial microtubules (numbers indicate the different steps/complexity levels in the hierarchical assembly). Reprinted with permission from Ref.58. Copyright © 2020 Wiley-VCH Verlag GmbH & Co. KGaA, Weinheim.

As usual, nature provides us with magnificent examples of these types of systems that have paved the way for chemists to develop increasingly complex systems. Among those, we can find fundamental cell components like the cytoskeleton (actin filaments, microtubules and intermediate filaments)[60] or other protein aggregates involved in cell damage such as amyloids in Alzheimer's disease.[61] For instance, microtubules are the result of the self-assembly of two globular subunits, α- and β-tubulin. Both proteins form a heterodimer that can undergo the nucleation step to form linear oligomers, called protofilaments. When these protofilaments reach a critical length, they begin to interact laterally, forming a curved sheet that eventually closes to form a microtubule.[62,63] Figure 3b shows a synthetic approach that attempts to simulate the hierarchical assembly of microtubules using simpler components, such as cucurbiturils and dimercaptoviologens.[58] In a first step, the bipyridinium derivative is internalized in the cucurbituril cavity which subsequently polymerizes linearly in an oxidation process leading to the formation of disulfide bonds. These

[57] S. Datta, M. L. Saha and P. J. Stang, *Acc. Chem. Res*., **2018**, *51*, 2047–2063.
[58] W. Hwang, J. Yoo, I. Hwang, J. Lee, Y. H. Ko, H. W. Kim, Y. Kim, Y. Lee, M. Y. Hur, K. M. Park, J. Seo, K. Baek and K. Kim, *Angew. Chem. Int. Ed*., **2020**, *59*, 3460–3464.
[59] A. Wang, J. Huang and Y. Yan, *Soft Matter*, **2014**, *10*, 3362–3373.
[60] A. Sharko, D. Livitz, S. De Piccoli, K. J. M. Bishop and T. M. Hermans, *Chem. Rev.*, **2022**, *122*, 11759–11777.
[61] A. W. P. Fitzpatrick, G. T. Debelouchina, M. J. Bayro, D. K. Clare, M. A. Caporini, V. S. Bajaj, C. P. Jaroniec, L. Wang, V. Ladizhansky, S. A. Müller, C. E. MacPhee, C. A. Waudby, H. R. Mott, A. De Simone, T. P. J. Knowles, H. R. Saibil, M. Vendruscolo, E. V. Orlova, R. G. Griffin and C. M. Dobson, Proc. *Natl. Acad. Sci. U. S. A*., **2013**, *110*, 5468–5473.
[62] F. Pampaloni and E. L. Florin, *Trends Biotechnol.*, **2008**, *26*, 302–310.
[63] J. Roostalu and T. Surrey, *Nat. Rev. Mol. Cell Biol*., **2017**, *18*, 702–710.

covalently bonded linear aggregates are laterally assembled by van der Walls interactions to generate the final tubular structure. As in this example, chemists do not limit themselves to the use of natural products. This issue, together with the large number of scientific publications on this subject, makes it almost impossible to cover all of them in this introduction.[64,65] For this reason, only some of the most relevant synthetic supramolecular polymers will be mentioned.

3.1. Synthetic building blocks

3.1.1. Coordination supramolecular polymers

Coordination chemistry is widely used to construct hierarchical polymeric self-assemblies. The constructuion of the main chain of coordination polymers requires only the design of low molecular weight polytopic ligands and transition metal ions that act as connectors between these ligands.[66,67] The presence of net-charged coordination centers allows the introduction of oppositely charged components to achieve a hierarchical level of self-assembly.[59]

In this sense Kurth *et al*. reported a layer-by-layer (LBL) assembly with a positively charged coordination polymer and negatively charged polyelectrolytes[68] that could further be employed to prepare capsules.[69] Careful control of the stoichiometry of the components is key for the formation of these coordination polymers, since excess in one of the components could act as a stopper. However, Lan and coworkers were able to develop LBL assemblies regardless of the initial metal/bisligand ratio in solution.[70] This is possible with reversible supramolecular polymers that, under appropriate conditions, undergo phase separation into a dense and a dilute phase, in which the concentrated phase drives out the species that act like chain stoppers.

Subsequently, Yan *et al*. demonstrated the formation of more complex structures, such as micelles based on coordination supramolecular polymers, by mixing them with diblock polyelectrolytes that allowed the micellar core size to be controlled.[71] This self-assembly strategy was further developed in order to build micelles with concentration responsive properties that were evaluated following the Eu^{3+} complex fluorescence emission.[72] Moreover, by replacing the metal ion with a redox active ion (Fe^{3+}), the micelles undergo shape transitions[73] and content delivery[74] upon redox changes in the media (Figure 4a).

All the knowledge gathered paved the way for designing more complex structures, such as ladders, which are really difficult to achieve in both polymer and supramolecular sciences. To this end, a rigid bisligand based on tetraphenylethylene (TPE) was synthesized. Their metal

---

[64] P. K. Hashim, J. Bergueiro, E. W. Meijer and T. Aida, *Prog. Polym. Sci*., **2020**, *105*, 101250.
[65] H. Q. Peng, W. Zhu, W. J. Guo, Q. Li, S. Ma, C. Bucher, B. Liu, X. Ji, F. Huang and J. L. Sessler, *Prog. Polym. Sci*., **2023**, *137*, 101635.
[66] Y. Yan and J. Huang, *Coord. Chem. Rev.*, **2010**, *254*, 1072–1080.
[67] N. Bäumer, J. Matern and G. Fernández, *Chem. Sci.*, **2021**, *12*, 12248–12265.
[68] M. Schütte, D. G. Kurth, M. R. Linford, H. Cölfen and H. Möhwald, *Angew. Chem. Int. Ed*., **1998**, *37*, 2891–2893.
[69] D. G. Kurth, F. Caruso, C. Schüler and S. Schüler, *Chem. Comm*., **1999**, 1579–1580.
[70] Y. Lan, L. Xu, Y. Yan, J. Huang, A. De Keizer, N. A. M. Besseling and M. A. C. Stuart, *Soft Matter*, **2011**, *7*, 3565–3570.
[71] Y. Yan, A. De Keizer, M. A. C. Stuart and N. A. M. Besseling, *Soft Matter*, **2009**, *5*, 790–796.
[72] L. Yang, Y. Ding, Y. Yang, Y. Yan, J. Huang, A. De Keizer and M. A. C. Stuart, *Soft Matter*, **2011**, *7*, 2720–2724.
[73] Y. Ding, Y. Yang, L. Yang, Y. Yan, J. Huang and M. A. C. Stuart, *ACS Nano*, **2012**, *6*, 1004–1010.
[74] L. Zhao, Y. Yan and J. Huang, *Langmuir*, **2012**, *28*, 5548–5554.

coordination complexes self-assemble into cocoon-like particles, which with the addition of a charge balancing block copolymer, evolve into ultra-long ladders (Figure 4b).[75]

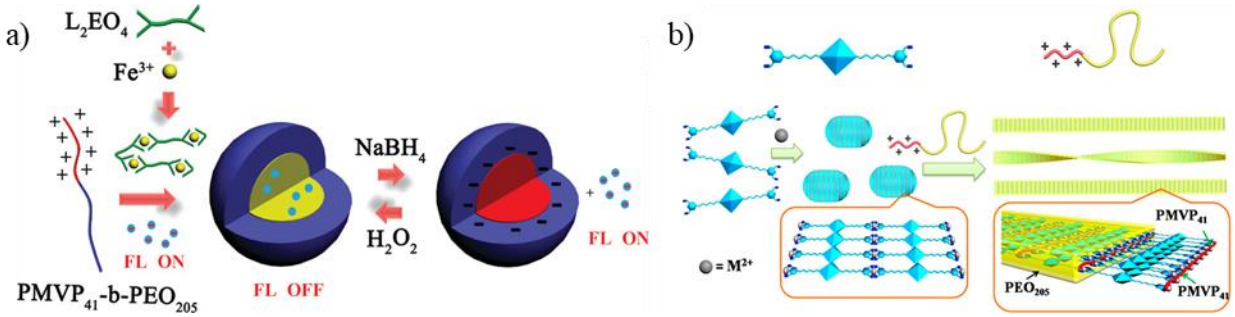

Figure 4. a) Schematic representation of formation of a redox responsive micelle delivery complex. Reprinted with permission from Ref.74. Copyright © 2012 American Chemical Society; and b) schematic representation of the ladder formation. Reprinted with permission from Ref.75. Copyright © 2014 American Chemical Society.

3.1.2. Cyclodextrins

Cyclodextrins (CDs) are a family of cyclic oligosaccharides composed of α-(1,4) linked D-glucopyranose subunits. Depending on the number of glycosyl units (6-8) CDs are classified as α, β or γ. They form host-guest complexes with non-polar molecules and present high biocompatibility that make them very suitable for biological applications as drug delivery carriers or cosmetics among other industrial applications.[76] Their ability to form host-guest complexes have been exploited in the design the basic components of different types of supramolecular polymerization.[77]

For example, A. Harada's group has exploited this feature to design an α-CD functionalized with one[78] or two[79] cinnamoyl derivative that self-assembles into a linear or hyperbranched supramolecular polymer in aqueous solution. Furthermore, these authors employed β-CD competitive guest strategy to build a supramolecular copolymer in which alternating α and β-CD were present. To achieve this goal, they synthesized α-CD-adamantane and β-CD-cinnamoyl derivatives. Upon mixing adamantane expels the cinnamoyl group from the β-CD and this group exposed to water now interacts with the α-CD forming a polymer (Figure 5a).[80] Similar strategies, but using β-CD-cinnamoyl-trinitrophenol derivatives, were used to form a [2]Rotaxane supramolecular polymer[81] and chemical responsive supramolecular hydrogels (Figure 5b).[82]

Also, the known ability of CDs to form inclusion complex with fatty acids[83] was exploited by J. Huang group to build supramolecular polymers with different morphologies. The inclusion

[75] L. Xu, L. Jiang, M. Drechsler, Y. Sun, Z. Liu, J. Huang, B. Z. Tang, Z. Li, M. A. C. Stuart and Y. Yan, *J. Am. Chem. Soc*., **2014**, *136*, 1942–1947.
[76] E. M. M. Del Valle, *Process Biochem.*, **2004**, *39*, 1033–1046.
[77] A. Harada, Y. Takashima and H. Yamaguchi, *Chem. Soc. Rev*., **2009**, *38*, 875–882.
[78] M. Miyauchi, Y. Takashima, H. Yamaguchi and A. Harada, *J. Am. Chem. Soc*, **2005**, *127*, 2984–2989.
[79] A. Miyawaki, Y. Takashima, H. Yamaguchi and A. Harada, *Tetrahedron*, **2008**, *64*, 8355–8361.
[80] M. Miyauchi and A. Harada, , *J. Am. Chem. Soc.*, **2004**, *126*, 11418–11419.
[81] M. Miyauchi, T. Hoshino, H. Yamaguchi, S. Kamitori and A. Harada, *J. Am. Chem. Soc.*, **2005**, *127*, 2034–2035.
[82] W. Deng, H. Yamaguchi, Y. Takashima and A. Harada, *Angew. Chem. Int. Ed.*, **2007**, *46*, 5144–5147.
[83] H. Schlenk and D. M. Sand, *J. Am. Chem. Soc.*, **1961**, *83*, 2312–2320.

complex formed between sodium dodecyl sulfate (SDS) and two β-CDs can self-assemble through H-bonds to form lamellae, multilayered microtubes, vesicles or rhombic dodecahedra in water (Figure 5c).[84,85] Their morphology can be controlled by the component concentrations or temperature.[86,87] Moreover, when the inclusion complex is formed with a zwitterionic surfactant (tetradecyl dimethylammonium propane sulfonate) the microtubes can form multi-stimuli responsive hydrogels.[88] All these characteristics together with the possibility of achieving supramolecular structures using non-ionic surfactants,[89] alkyl amines[90] or alkyl chains[91] inclusion complexes make them particular suitable for the development of materials applications.

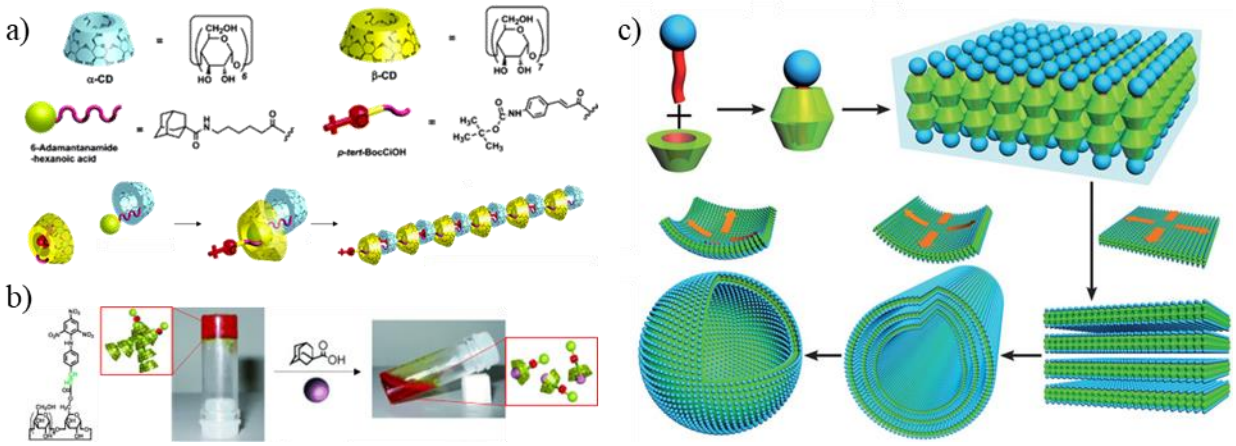

Figure 5. a) Chemical structures and supramolecular polymerization of functionalized α- and ß-CDs. Reprinted with permission from Ref.80. Copyright © 2004 American Chemical Society; b) gel-sol transition of a CD based supramolecular polymer upon addition of a chemical stimuli. Adapted with permission from Ref.82. Copyright © 2007 WILEY-VCH Verlag GmbH & Co. KGaA, Weinheim; and c) schematic morphology transition of SDS@2 ß-CD supramolecular polymer upon dilution. Reproduced from Ref. 86 with permission from the Royal Society of Chemistry.

3.1.3. Cucurbit[n]urils

Cucurbit[n]urils (CB[n]) are macrocyclic receptors composed of a variable number of glycouril units (n = 5–8, 10, 13–15) with cavities of different sizes that show promising guest binding properties (Figure 6). They are also biocompatible and, mostly, water soluble.[92] All these reasons make them very suitable for material[93] and biomedical applications.[92] The host-guest binding properties have also been used to build supramolecular polymers.[94]

---

[84] L. Jiang, Y. Peng, Y. Yan, M. Deng, Y. Wang and J. Huang, *Soft Matter*, **2010**, *6*, 1731–1736.
[85] S. Yang, Y. Yan, J. Huang, A. V. Petukhov, L. M. J. Kroon-Batenburg, M. Drechsler, C. Zhou, M. Tu, S. Granick and L. Jiang, *Nat. Commun.*, **2017**, *8*, 15856.
[86] L. Jiang, Y. Peng, Y. Yan and J. Huang, *Soft Matter*, **2011**, *7*, 1726–1731.
[87] C. Zhou, X. Cheng, Y. Yan, J. Wang and J. Huang, *Langmuir*, **2014**, *30*, 3381–3386.
[88] L. Jiang, Y. Yan and J. Huang, *Soft Matter*, **2011**, *7*, 10417–10423.
[89] C. Zhou, X. Cheng, Q. Zhao, Y. Yan, J. Wang and J. Huang, *Langmuir*, **2013**, *29*, 13175–13182.
[90] X. Wang, M. Li, P. Song, X. Lv, Z. Liu, J. Huang and Y. Yan, *Chem. Eur. J.*, **2018**, *24*, 13734–13739.
[91] C. Zhou, J. Huang and Y. Yan, *Soft Matter*, **2016**, *12*, 1579–1585.
[92] Z. Wang, C. Sun, K. Yang, X. Chen and R. Wang, *Angew. Chem. Int. Ed.*, **2022**, *61*, e202206763.
[93] H. Zou, J. Liu, Y. Li, X. Li and X. Wang, *Small*, **2018**, *14*, 1802234.
[94] Y. Liu, H. Yang, Z. Wang and X. Zhang, *Chem. Asian J.*, **2013**, *8*, 1626–1632.

In this field, O. A. Sherman group employed CB[8] to achieve supramolecular polymerization. Taking advantage of the ability of CB[8] to co-encapsulate azobenzene and bipyridinium, they designed a monomer capable of undergoing supramolecular polymerization in a photoresponsive manner.[95] Moreover, by using these functional motifs on other monomers, they were able to obtain higher order architectures, such as gels. The resulting supramolecular polymerization was reversible by photo and chemical stimuli (Figure 6a).[96] In addition, other types of molecules have been exploited to bind to CB[8], such as imidazolium salts, to achieve a two-step supramolecular polymerization in which semi-flexible polymeric chains are formed and subsequently evolve into two-dimensional fibers.[97] Finally, it is important to mention that CBs can be also used to crosslink polymers in order to achieve different morphologies, such as vesicles,[98] microcapsules[99] or stimuli responsive hydrogels[100] with applications in biology,[101] catalysis[102] and surface functionalization.[103]

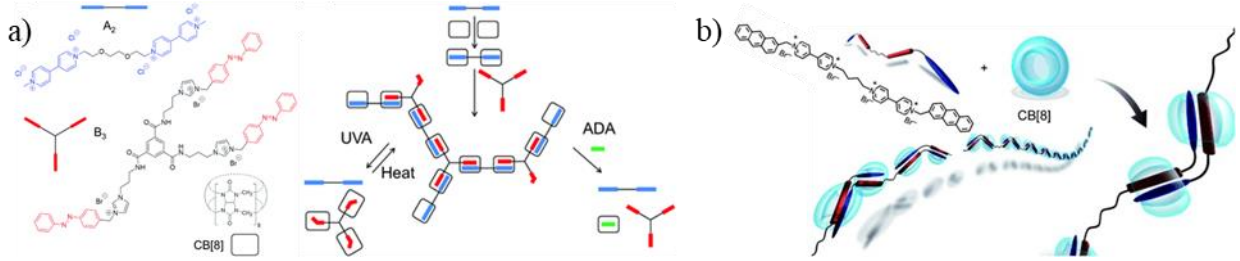

Figure 6. a) Chemical structures for the formation of a CB[8] based supramolecular polymer that exhibits stimuli responsiveness. Adapted from Ref. 96 with permission from the Royal Society of Chemistry; and b) self-assembly scheme of a CB based supramolecular polymer with gelation capabilities. Adapted with permission from Ref.104. Copyright © 2010 WILEY-VCH Verlag GmbH & Co. KGaA, Weinheim.

X. Zhang group has also made contributions to this field. They exploited the host stabilization of charge-transfer interactions between bipyridinium and anthracene moieties to build a tetrafunctional monomer (two of each) that polymerizes upon CB addition. Their high degree of polymerization and interchain interactions lead to a hydrogel formation (Figure 6b).[104] Moreover, they have employed bifunctional ligands to control supramolecular polymerization with different driving forces[105] or self-sorting properties,[106] which were then used in the design of materials, especially for biomedical applications.[93]

---

[95] J. Del Barrio, P. N. Horton, D. Lairez, G. O. Lloyd, C. Toprakcioglu and O. A. Scherman, *J. Am. Chem. Soc.*, **2013**, *135*, 11760–11763.
[96] A. S. Groombridge, A. Palma, R. M. Parker, C. Abell and O. A. Scherman, *Chem. Sci*., **2017**, *8*, 1350–1355.
[97] J. Del Barrio, J. Liu, R. A. Brady, C. S. Y. Tan, S. Chiodini, M. Ricci, R. Fernández-Leiro, C. J. Tsai, P. Vasileiadi, L. Di Michele, D. Lairez, C. Toprakcioglu and O. A. Scherman, *J. Am. Chem. Soc.*, **2019**, *141*, 14021–14025.
[98] D. Jiao, J. Geng, X. J. Loh, D. Das, T. C. Lee and O. A. Scherman, *Angew. Chem. Int. Ed.*, **2012**, *51*, 9633–9637.
[99] Z. Yu, Y. Lan, R. M. Parker, W. Zhang, X. Deng, O. A. Scherman and C. Abell, *Polym. Chem.*, **2016**, *7*, 5996–6002.
[100] J. Liu, C. S. Y. Tan and O. A. Scherman, *Angew. Chem. Int. Ed.*, **2018**, *57*, 8854–8858.
[101] H. Qiao, J. Jia, W. Chen, B. Di, O. A. Scherman and C. Hu, *Adv. Healthc. Mater*., **2019**, *8*, 1801458.
[102] A. Wagner, K. H. Ly, N. Heidary, I. Szabó, T. Földes, K. I. Assaf, S. J. Barrow, K. Sokołowski, M. Al-Hada, N. Kornienko, M. F. Kuehnel, E. Rosta, I. Zebger, W. M. Nau, O. A. Scherman and E. Reisner, *ACS Catal.*, **2020**, *10*, 751–761.
[103] C. Hu, F. Tian, Y. Zheng, C. S. Y. Tan, K. R. West and O. A. Scherman, *Chem. Sci*., **2015**, *6*, 5303–5310.
[104] Y. Liu, Y. Yu, J. Gao, Z. Wang and X. Zhang, *Angew. Chem. Int. Ed.*, **2010**, *49*, 6576–6579.
[105] Y. Liu, Z. Huang, X. Tan, Z. Wang and X. Zhang, *Chem. Comm*., **2013**, *49*, 5766–5768.
[106] Z. Huang, L. Yang, Y. Liu, Z. Wang, O. A. Scherman and X. Zhang, *Angew. Chem. Int. Ed.*, **2014**, *53*, 5351–5355.

3.1.4. 2-Ureido-4-Pyrimidone and Ureidotriazine

The known propensity of 2-Ureido-4-Pyrimidone (UPy) and Ureidotriazine (UT) to form dimers through four cooperative hydrogen bonds, was exploited by Meijer group to design one of the first supramolecular polymers. UPy was used to form a reversible self-assembled polymer with exquisite control of its properties, such as viscosity or chain length.[107] On the other hand, UT was functionalized with solubilizing size chains to form helical supramolecular structures (Figure 7a).[108] Additionally, functionalization with oligo(*p*-phenylene vinylene)s allows the hierarchical assembly into dimers through H bonding that further polymerizes in chiral stacks by π–π stacking (Figure 7b).[109] The stability and helicity of the polymers could be controlled by molecular design[110] or by external stimuli.[111] This versatile H-bonded moieties were used in new responsive materials,[112,113] electronic devices,[114] bioactive scaffolds[115] and drug delivery systems.[116]

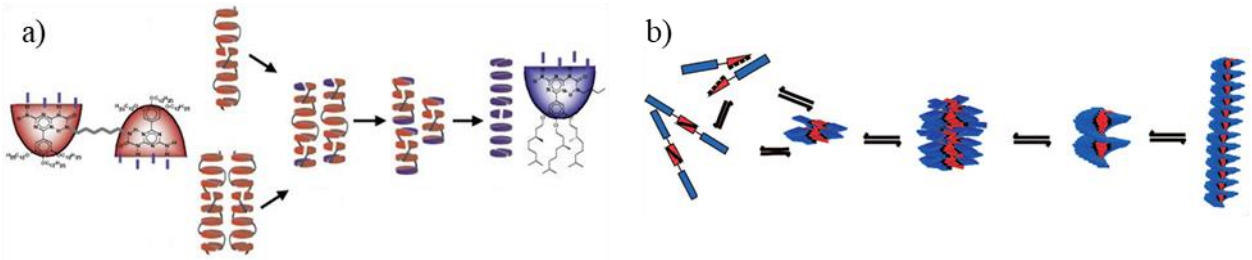

Figure 7. a) Mono- and bi-UT forming helical supramolecular structures. Adapted with permission from Ref.108. Copyright © 2000 Macmillan Magazines Ltd.; and b) schematic representation of the dimer formation and the corresponding helical aggregate. From Pascal Jonkheijm *et al.*,Probing the Solvent-Assisted Nucleation Pathway in Chemical Self-Assembly. *Science* **313**, 80-83 (2006). Reprinted with permission from AAAS.

3.1.5. Benzene-1,3,5-tricarboxamide

Meijer's group has also employed benzene-1,3,5-tricarboxamide (BTA) as a central core to form disk-like molecules that self-assemble into dynamic helical columnar aggregates taking

---

[107] R. P. Sijbesma, F. H. Beijer, L. Brunsveld, B. J. B Folmer, J. H. K Ky Hirschberg, R. F. M Lange, J. K. L Lowe and E. W. Meijer, *Science*, **1997**, *278*, 1601–1604.
[108] J. H. K. Ky Hischberg, L. Brunsveld, A. Ramzi, J. A. J. M. Vekemans, R. P. Sijbesma and E. W. Meijer, *Nature*, **2000**, *407*, 167–170.
[109] P. Jonkheijm, P. van der Schoot, A. P. H. J. Schenning and E. W. Meijer, *Science*, **2006**, *313*, 80–83.
[110] P. Jonkheijm, F. J. M. Hoeben, R. Kleppinger, J. Van Herrikhuyzen, A. P. H. J. Schenning and E. W. Meijer, *J. Am. Chem. Soc.*, **2003**, *125*, 15941–15949.
[111] S. J. George, Ž. Tomović, M. M. J. Smulders, T. F. A. De Greef, P. E. L. G. Leclère, E. W. Meijer and A. P. H. J. Schenning, *Angew.Chem. Int. Ed.*, **2007**, *46*, 8206–8211.
[112] R. E. Kieltyka, A. C. H. Pape, L. Albertazzi, Y. Nakano, M. M. C. Bastings, I. K. Voets, P. Y. W. Dankers and E. W. Meijer, *J. Am. Chem. Soc.*, **2013**, *135*, 11159–11164.
[113] B. J. B. Folmer, R. P. Sijbesma, R. M. Versteegen, J. A. J. Van Der Rijt and E. W. Meijer, *Adv. Mater.*, **2000**, *12*, 874–878.
[114] A. El-ghayoury, A. P. H. J. Schenning, P. A. Van Hal, J. K. J. Van Duren, R. A. J. Janssen and E. W. Meijer, *Angew. Chem. Int. Ed.*, **2001**, *40*, 3660–3663.
[115] P. Y. W. Dankers, M. C. Harmsen, L. A. Brouwer, M. J. A. Van Luyn and E. W. Meijer, *Nat. Mater.*, **2005**, *4*, 568–574.
[116] P. Y. W. Dankers, T. M. Hermans, T. W. Baughman, Y. Kamikawa, R. E. Kieltyka, M. M. C. Bastings, H. M. Janssen, N. A. J. M. Sommerdijk, A. Larsen, M. J. A. Van Luyn, A. W. Bosman, E. R. Popa, G. Fytas and E. W. Meijer, *Adv. Mater.*, **2012**, *24*, 2703–2709.

advantage of the π–π stacking and H-bonds formation.[117] These assemblies are usually guided by the majority rules[118] and sergeant-soldier principles.[119] In addition, the chirality of the supramolecular polymer can also be controlled with chiral solvents[120] or chemical transformations.[121] Moreover, functionalization of the pendants with reactive groups allows covalent polymerization on the periphery with the desired helical structure (Figure 8a).[122] Interestingly, the resulting covalent polymer is capable of storing the helical supramolecular information (chiral memory) upon polymer refolding. Furthermore, amphiphilic[123] and fluorinated[124] derivatives can also self-assemble hierarchically into columnar stacks that evolve into fibers (Figure 8b). The great versatility of the system has allowed its use as a drug delivery vehicle,[125] photo-responsive hydrogel[126] (Figure 8c) and protein recruitment platform[127] among others.

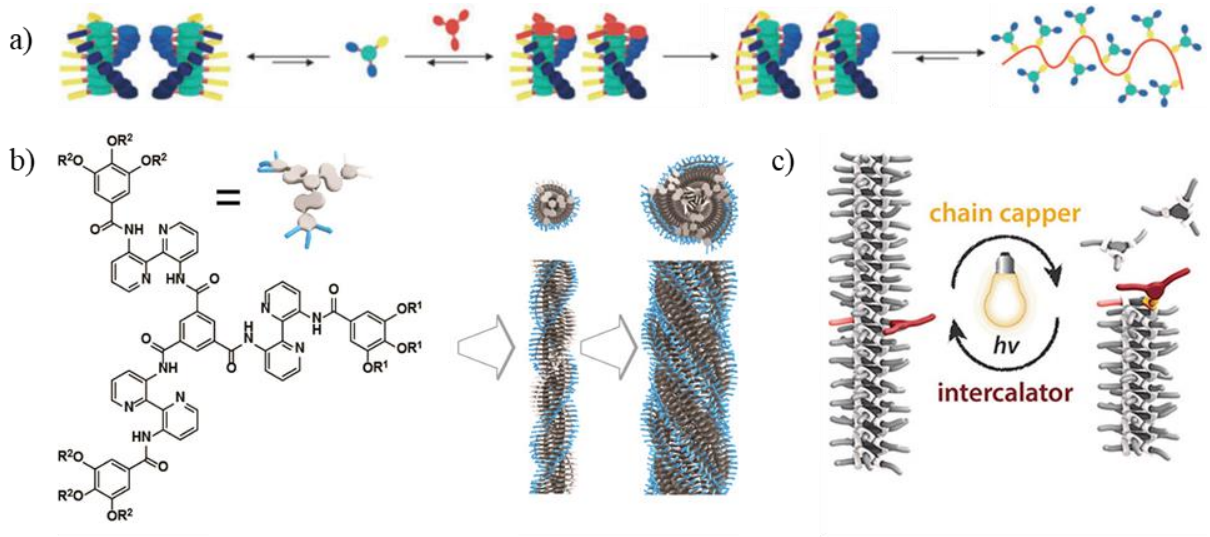

Figure 8. a) Covalent polymerization of a chiral columnar aggregate. Adapted with permission from Ref.122. Copyright © 2005 WILEY-VCH Verlag GmbH & Co. KGaA, Weinheim; b) hierarchical supramolecular self-assembly of a BTA derivative. Adapted with permission from Ref.123. Copyright © 2014 American Chemical Society; and c) schematic representation of the disassembly process upon irradiation of a BTA stack. Adapted with permission from Ref.126. Copyright © 2020 American Chemical Society.

[117] L. Albertazzi, D. Van Der Zwaag, C. M. A. Leenders, R. Fitzner, † Remco, W. Van Der Hofstad and E. W. Meijer, *Science*, **2014**, *344*, 491–495.
[118] J. Van Gestel, A. R. A. Palmans, B. Titulaer, J. A. J. M. Vekemans and E. W. Meijer, *J. Am. Chem. Soc.*, **2005**, *127*, 5490–5494.
[119] A. R. A. Palmans, J. A. J. M. Vekemans, E. E. Havinga and E. W. Meijer *Angew. Chem. Int. Ed.*, **1997**, *36*, 2648–2651.
[120] A. K. Mondal, M. D. Preuss, M. L. Ślęczkowski, T. K. Das, G. Vantomme, E. W. Meijer and R. Naaman, *J. Am. Chem. Soc.*, **2021**, *143*, 7189–7195.
[121] F. V. de Graaf, S. A. H. Jansen, T. Schnitzer, E. W. Meijer and G. Vantomme, *J. Am. Chem. Soc.*, **2023**, *145*, 14379–14386.
[122] A. J. Wilson, M. Masuda, R. P. Sijbesma and E. W. Meijer, *Angew. Chem. Int. Ed.*, **2005**, *44*, 2275–2279.
[123] M. A. J. Gillissen, M. M. E. Koenigs, J. J. H. Spiering, J. A. J. M. Vekemans, A. R. A. Palmans, I. K. Voets and E. W. Meijer, *J. Am. Chem. Soc.*, **2014**, *136*, 336–343.
[124] P. J. M. Stals, P. A. Korevaar, M. A. J. Gillissen, T. F. A. De Greef, C. F. C. Fitié, R. P. Sijbesma, A. R. A. Palmans and E. W. Meijer, *Angew. Chem. Int. Ed.*, **2012**, *51*, 11297–11301.
[125] M. H. Bakker, C. C. Lee, E. W. Meijer, P. Y. W. Dankers and L. Albertazzi, *ACS Nano*, **2016**, *10*, 1845–1852.
[126] E. Weyandt, G. M. Ter Huurne, G. Vantomme, A. J. Markvoort, A. R. A. Palmans and E. W. Meijer, *J. Am. Chem. Soc.*, **2020**, *142*, 6295–6303.
[127] S. P. W. Wijnands, W. Engelen, R. P. M. Lafleur, E. W. Meijer and M. Merkx, *Nat. Commun.*, **2018**, *9*, 65.

3.1.6. Supramolecular amphiphiles

Conventional amphiphiles are molecules that contain a hydrophilic and a hydrophobic part covalently linked by a covalent bond. Their applications in many fields such as nanodevices or drug delivery vehicles make them chemically attractive. For this reason, new methodologies were developed to build more complex systems using simple non-covalent analogues, the supramolecular amphiphiles (SAs).[128]

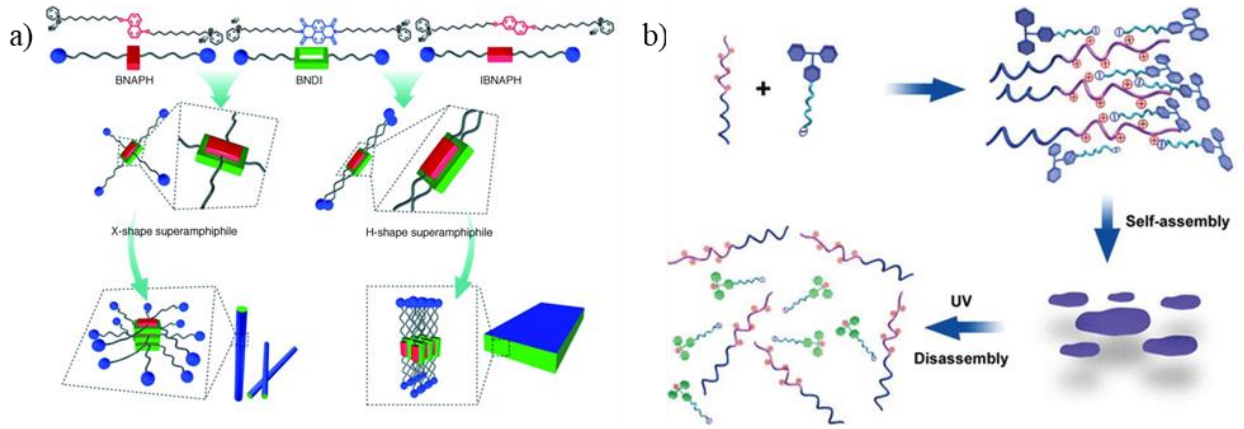

Figure 9. a) Schematic representation of the X- and H-shape SAs and their assembly into 1D or 2D nanostructures. Reprinted with permission from Ref.130. Copyright © 2011 WILEY-VCH Verlag GmbH & Co. KGaA, Weinheim; and b) photoresponsive sheets formed by the co-assembly of a SA with a block copolymer. Reprinted with permission from Ref.131. Copyright © 2009 American Chemical Society.

Significant examples of the use of this strategy are illustrated in the works of X. Zhang and collaborators in which they are able to control the self-assembly process thought the use of charge-transfer interactions. For example, using pyrene and dinitrobenzoate derivatives they were able to switch from tube to vesicles morphology.[129-131] They were also able to generate new X- or H-shaped supramolecular amphiphiles morphologies that undergo different self-assembling pathways leading to nanorods or nanosheets, respectively (Figure 9a).[130] Additionally, photo-responsiveness can also be achieved by a malachite green based supramolecular amphiphiles. Its co-assembly with a block copolymer triggered the formation of sheet-like assemblies through electrostatic interactions. Upon UV irradiation the solubility of the malachite green derivative increases that leads to the disassembly of the aggregates (Figure 9b).[131]

3.1.7.Hexa-peri-hexabenzocoronene

Hexa-peri-hexabenzocoronene (HBC) is a planar polycyclic aromatic hydrocarbon that consists of 13 fused benzene rings with strong π-π stacking, high intrinsic charge mobility and good self-assembly properties. T. Aida's group have taken advantage of this molecule to build supramolecular polymers with a wide range of properties and applications.[132-143] In 2004 they

[128] X. Zhang and C. Wang, *Chem. Soc. Rev*., **2011**, *40*, 94–101.
[129] C. Wang, S. Yin, S. Chen, H. Xu, Z. Wang and X. Zhang, *Angew. Chem. Int. Ed.*, **2008**, *47*, 9049–9052.
[130] K. Liu, C. Wang, Z. Li and X. Zhang, *Angew. Chem. Int. Ed.*, **2011**, *50*, 4952–4956.
[131] P. Han, S. Li, C. Wang, H. Xu, Z. Wang, X. Zhang, J. Thomas and M. Smet, *Langmuir*, **2011**, *27*, 14108–14111.

reported a modified HBC with two alkyl and two ethylene glycol chains capable of self-assembling into hollow nanotubes (NTs) with high redox activity and conductivity (Figure 10a).[132] Further systematic studies revealed the importance of having two phenyls and two long alkyl groups on opposite sides of the core to obtain the desired NTs.[133] Moreover, modifications on the ethylene derivative have allowed the control over the NT chirality,[134] stability,[135] wall layers (Figure 10b),[136] and photoconductivity properties (Figure 10c).[137] The system also offers the possibility to control the outer and inner functionalization of the NTs[138] and the construction of segmented NTs with unique properties (Figure 10d).[139] The versatility and design control has allowed to build different materials such as macroscopic conductive fibers,[140] conductive nanocoils,[141] photoresponsive NTs[142] or water compatible NTs.[143]

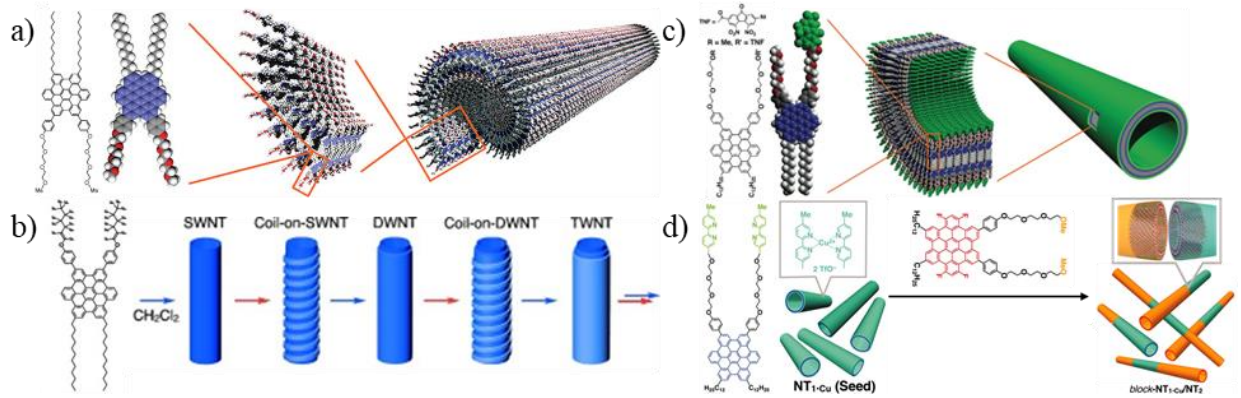

Figure 10. a) Hexa-peri-hexabenzocoronene self-assembly into nanotubes. From Jonathan P. Hill *et al.*, Self-Assembled Hexa-peri-hexabenzocoronene Graphitic Nanotube. *Science* **304**, 1481-1483 (2004). Reprinted with permission from AAAS; b) multiwalled NT assembly based on fluorinated hexa-peri-hexabenzocoronene. Adapted with permission from Ref.136. Copyright © 2015 WILEY-VCH Verlag GmbH & Co. KGaA, Weinheim; c) photoconductive NT based on a trinitrofluorenone derivative. From Yohei Yamamoto *et al.*, Photoconductive Coaxial Nanotubes of Molecularly Connected Electron Donor and Acceptor Layers. *Science* **314**, 1761-1764 (2006). Reprinted with permission from AAAS; and d) construction of segmented NTs based on hexa-peri-hexabenzocoronene with different properties. From Wei Zhang *et al.*, Supramolecular Linear Heterojunction Composed of Graphite-Like Semiconducting Nanotubular Segments. *Science* **334**, 340-343 (2011). Reprinted with permission from AAAS.

[132] J. P. Hill, W. Jin, A. Kosaka, T. Fukushima, H. Ichihara, T. Shimomura, K. Ito, T. Hashizume, N. Ishii and T. Aida, *Science*, **2004**, *304*, 1481–1483.
[133] W. Jin, Y. Yamamoto, T. Fukushima, N. Ishii, J. Kim, K. Kato, M. Takata and T. Aida*, J. Am. Chem. Soc*., **2008**, *130*, 9434–9440.
[134] W. Jin, T. Fukushima, M. Niki, A. Kosaka, N. Ishii and T. Aida, *Proc. Natl. Acad. Sci. U. S. A*., **2005**, *102*, 10801–10806.
[135] W. Jin, T. Fukushima, A. Kosaka, M. Niki, N. Ishii and T. Aida, *J. Am. Chem. Soc.*, **2005**, *127*, 8284–8285.
[136] S. Prasanthkumar, W. Zhang, W. Jin, T. Fukushima and T. Aida, *Angew. Chem. Int. Ed.*, **2015**, *54*, 11168–11172.
[137] Y. Yamamoto, T. Fukushima, Y. Suna, N. Ishii, A. Saeki, S. Seki, S. Tagawa, M. Taniguchi, T. Kawai and T. Aida, *Science*, **2006**, *314*, 1761–1764.
[138] J. L. Mynar, T. Yamamoto, A. Kosaka, T. Fukushima, N. Ishii and T. Aida, *J. Am. Chem. Soc.*, **2008**, *130*, 1530–1531.
[139] W. Zhang, W. Jin, T. Fukushima, A. Saeki, S. Seki and T. Aida, *Science*, **2011**, *334*, 340–343.
[140] Y. Yamamoto, T. Fukushima, W. Jin, A. Kosaka, T. Hara, T. Nakamura, A. Saeki, S. Seki, S. Tagawa and T. Aida, *Adv. Mater*., **2006**, *18*, 1297–1300.
[141] T. Yamamoto, T. Fukushima, Y. Yamamoto, A. Kosaka, W. Jin, N. Ishii and T. Aida, *J. Am. Chem. Soc.*, **2006**, *128*, 14337–14340.
[142] Y. He, Y. Yamamoto, W. Jin, T. Fukushima, A. Saeki, S. Seki, N. Lshii and T. Aida, *Adv. Mater*, **2010**, *22*, 829–832.
[143] G. Zhang, W. Jin, T. Fukushima, A. Kosaka, N. Ishii and T. Aida, *J. Am. Chem. Soc.*, **2007**, *129*, 719–722.

In addition, T. Aida has also contributed to the field of supramolecular polymerization with other components, such as porphyrins,[144] proteins,[145] and corannulene[146] among others; some of which have found applications in water desalination,[147] security inks[148] and drug delivery.[145]

3.1.8. Block copolymers

Block copolymers consist of two or more chemically different polymer segments, or blocks, connected by a covalent linkage with an extraordinary structural and compositional versatility. The specific design of the blocks allows the self-assembly in different morphologies with application in material sciences or drug delivery systems.[149]

I. Manners and M. A. Winnik have contributed to this field by using block copolymers based on ferrocene derivatives that can undergo crystallization driven self-assembly. They reported the spontaneous formation of cylindrical micelles upon cooling the polymer solution. The subsequent addition of more polymer, the same or a different one, induced the epitaxial growth of the seeds forming longer cylindrical micelles or co-micelles respectively.[150] Interestingly, the system showed great versatility, as it could be selectively functionalized[151] and stabilized[152] allowing its dispersion length and size to be fine-tuned (Figure 11a,b).[153] In addition, the growth of the cylindrical micelle could be further adjusted to form 1D[154] or 2D[155] structures, leading to more complex structures (Figure 11e,f). Further experiments also showed that the selection of the polymeric materials was important in developing hierarchical systems in which cylindrical micelles acted as building blocks in the preparation of more complex structures (Figure 11c).[156] The highly accurate design of these systems paved the way to applications of these block copolymers in sensing,[157] photocatalysis[158] (Figure 11d) and surface functionalization[159] among others.

Another interesting example described in the literature is based on the use of triblock co-polymers with three immiscible segments, one hydrophilic and two hydrophobic, one with hydrocarbon

---

[144] K. V. Rao, D. Miyajima, A. Nihonyanagi and T. Aida, *Nat. Chem*., **2017**, *9*, 1133–1139.
[145] S. Biswas, K. Kinbara, T. Niwa, H. Taguchi, N. Ishii, S. Watanabe, K. Miyata, K. Kataoka and T. Aida, *Nat. Chem*., **2013**, *5*, 613–620.
[146] J. Kang, D. Miyajima, T. Mori, Y. Inoue, Y. Itoh and T. Aida, *Science*, **2015**, *347*, 646–651.
[147] Y. Itoh, S. Chen, R. Hirahara, T. Konda, T. Aoki, T. Ueda, I. Shimada, J. J. Cannon, C. Shao, J. Shiomi, K. V Tabata, H. Noji, K. Sato and T. Aida, *Science*, **2022**, *376*, 738–743.
[148] A. Kishimura, T. Yamashita, K. Yamaguchi and T. Aida, *Nat. Mater*., **2005**, *4*, 546–549.
[149] H. Feng, X. Lu, W. Wang, N. G. Kang and J. W. Mays, *Polymers*, **2017**, *9*, 494.
[150] X. Wang, G. Guerin, H. Wang, Y. Wang, I. Manners and M. A. Winnik, *Science*, **2007**, *317*, 644–647.
[151] H. Wang, W. Lin, K. P. Fritz, G. D. Scholes, M. A. Winnik and I. Manners, *J. Am. Chem. Soc*., **2007**, *129*, 12924–12925.
[152] X. Wang, K. Liu, A. C. Arsenault, D. A. Rider, G. A. Ozin, M. A. Winnik and I. Manners, *J. Am. Chem. Soc.*, **2007**, *129*, 5630–5639.
[153] J. B. Gilroy, T. Gädt, G. R. Whittell, L. Chabanne, J. M. Mitchels, R. M. Richardson, M. A. Winnik and I. Manners, *Nat. Chem*., **2010**, *2*, 566–570.
[154] P. A. Rupar, L. Chabanne, M. A. Winnik and I. Manners, *Science*, **2012**, *337*, 559–562.
[155] H. Qiu, Y. Gao, C. E. Boott, O. E. C. Gould, RobertL. Harniman, M. J. Miles, S. E. D. Webb, M. A. Winnik and I. Manners, *Science*, **2016**, *352*, 697–701.
[156] H. Qiu, Z. M. Hudson, M. A. Winnik and I. Manners, *Science*, **2015**, *347*, 1329–1332.
[157] Y. Zhang, S. Pearce, J. C. Eloi, R. L. Harniman, J. Tian, C. Cordoba, Y. Kang, T. Fukui, H. Qiu, A. Blackburn, R. M. Richardson and I. Manners, *J. Am. Chem. Soc*., **2021**, *143*, 5805–5814.
[158] J. Tian, Y. Zhang, L. Du, Y. He, X. H. Jin, S. Pearce, J. C. Eloi, R. L. Harniman, D. Alibhai, R. Ye, D. L. Phillips and I. Manners, *Nat. Chem*., **2020**, *12*, 1150–1156.
[159] J. Cai, C. Li, N. Kong, Y. Lu, G. Lin, X. Wang, Y. Yao, I. Manners and H. Qiu, *Science*, **2019**, *366*, 1095–1098.

segments and another with fluorocarbons chains. Z. Li *et al*. reported terpolymer that can form different morphologies from multicompartment micelles to wormlike structures by varying the relative length of the main components.[160] Further experiments demonstrated the versatility of this strategy in obtaining a range of different morphologies such as polygonal bilayers[161] or burger-like micelles.[162] Moreover, the different nature of the polymeric chains allowed the storage of molecules in different compartments of the micelles, showing their suitability for the developments of drug delivery applications.[163]

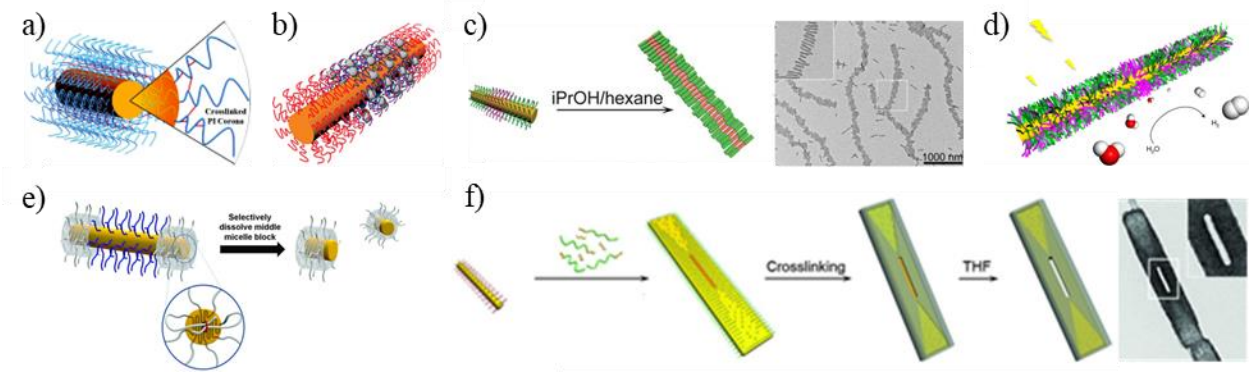

Figure 11. a) Stabilization of the supramolecular structure upon polymer crosslinking. Adapted with permission from Ref.152. Copyright © 2007 American Chemical Society; b) cylindrical micelle functionalization with Ag nanoparticles. Adapted with permission from Ref.151. Copyright © 2007 American Chemical Society; c) hierarchical assembly of a cylindrical micelle. From Huibin Qiu *et al.*, Multidimensional hierarchical self-assembly of amphiphilic cylindrical block comicelles. *Science* **347**, 1329-1332 (2015). Reprinted with permission from AAAS.; d) photocatalytic cylindrical micelle. Reprinted with permission from Ref.158. Copyright © 2020 Springer Nature Limited; and e) 1D[154] and f) 2D[155] growth of cylindrical micelles. From Paul A. Rupar *et al.*, Non-Centrosymmetric Cylindrical Micelles by Unidirectional Growth. *Science* **337**, 559-562 (2012) and Huibin Qiu *et al.*, Uniform patchy and hollow rectangular platelet micelles from crystallizable polymer blends. *Science* **352**, 697-701 (2016), respectively. Reprinted with permission from AAAS.

3.1.9. Peptoids

Peptoids are a promising class of bioinspired polymers based on an N-derivatized glycine backbone, in which side chains of the residues are incorporated into the substituents of the amide groups. Thanks to this, they combine the sequence specificity of biopolymers with the intra/intermolecular interactions and robustness of synthetic polymers. They present certain advantages over the natural counterparts such as physicochemical structure tunability, higher stability, and better processability.[164] Their assembly capabilities have been exploited to obtain different architectures with applications in different fields.[165]

Zukerman *et al*. have invested many years on the structural characterization; and folding and assembling properties of peptoid-like polymers. Initial studies explored the structural similarity

[160] Z. Li, E. Kesselman, Y. Talmon, M. A. Hillmyer and T. P. Lodge, *Science*, **2004**, *306*, 98–101.
[161] Z. Li, M. A. Hillmyer and T. P. Lodge, *Nano Lett*., **2006**, *6*, 1245–1249.
[162] Z. Li, M. A. Hillmyer and T. P. Lodge, *Macromolecules*, **2006**, *39*, 765–771.
[163] T. P. Lodge, A. Rasdal, Z. Li and M. A. Hillmyer, *J. Am. Chem. Soc.*, **2005**, *127*, 17608–17609.
[164] J. Sun and R. N. Zuckermann, *ACS Nano*, **2013**, 7, 4715–4732.
[165] Z. Li, B. Cai, W. Yang and C. L. Chen, *Chem. Rev*., **2021**, *121*, 14031–14087.

between peptoids and peptides as mimics of protein secondary[166] and tertiary structures (Figure 12a).[167] In the same way the known capability of peptides and proteins to self-assembly into higher order structures was also explored with peptoids. The supramolecular polymerization of these derivatives resulted, in many cases, in hierarchical assemblies that form a wide variety of architectures, such as 2D-nanosheets (Figure 12b),[168] superhelices (Figure 12c),[169] nanotubes,[170] nanoribbons[171] or nanobrushes.[172] The controlled behavior has been exploited in the development of applications, such as antibody-mimetic analogues,[173] templated mineralization[174] or sensing.[175]

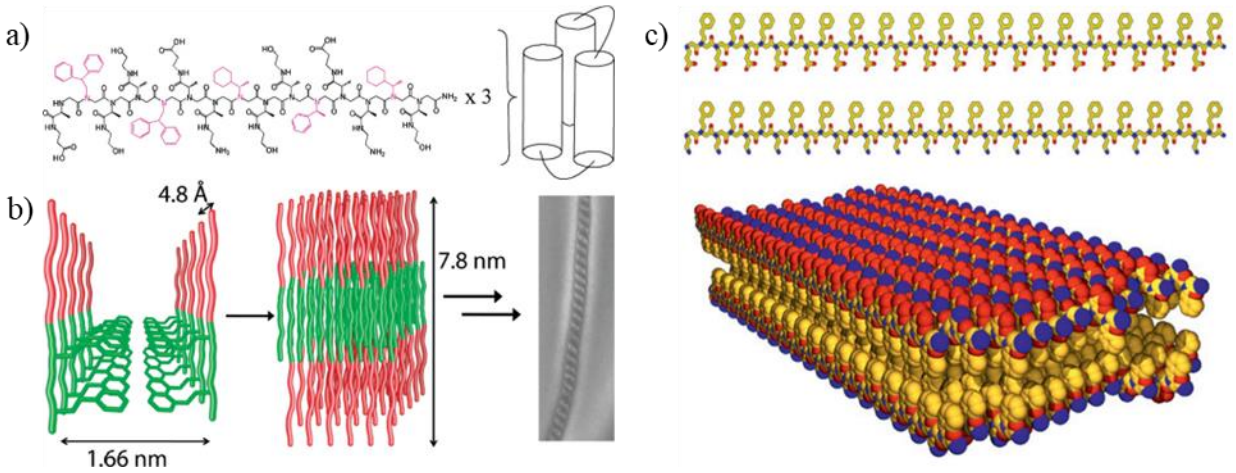

Figure 12. a) Structure and representation of a peptoid tertiary structure. Reprinted with permission from Ref.167. Copyright © 2005 American Chemical Society; b) schematic representation of peptoid superhelices. Reprinted with permission from Ref.169. Copyright © 2010 American Chemical Society; and c) peptide based nanosheet assembly. Reprinted with permission from Ref.168. Copyright © 2010 Springer Nature Limited.

Peptoid chemistry has captured the attention of many scientists who have contributed to increasing the type of morphologies that can be prepared, such as microspheres,[176] fibers,[177] or structures similar to MOFs (Figure 13a).[178] These studies have shed light on the design principles since small modifications on the sequence and length can affect dramatically to the size,[176]

---

[166] C. W. Wu, T. J. Sanborn, K. Huang, R. N. Zuckermann and A. E. Barron, *J. Am. Chem. Soc.*, **2001**, *123*, 6778–6784.
[167] B. C. Lee, R. N. Zuckermann and K. A. Dill, *J. Am. Chem. Soc.*, **2005**, *127*, 10999–11009.
[168] K. T. Nam, S. A. Shelby, P. H. Choi, A. B. Marciel, R. Chen, L. Tan, T. K. Chu, R. A. Mesch, B. C. Lee, M. D. Connolly, C. Kisielowski and R. N. Zuckermann, *Nat. Mater.*, **2010**, *9*, 454–460.
[169] H. K. Murnen, A. M. Rosales, J. N. Jaworski, R. A. Segalman and R. N. Zuckermann, *J. Am. Chem. Soc.*, **2010**, *132*, 16112–16119.
[170] J. Sun, X. Jiang, R. Lund, K. H. Downing, N. P. Balsara and R. N. Zuckermann, *Proc. Natl. Acad. Sci. U. S. A.*, **2016**, *113*, 3954–3959.
[171] C. L. Chen, R. N. Zuckermann and J. J. Deyoreo, *ACS Nano*, **2016**, *10*, 5314–5320.
[172] J. Sun, Z. Wang, C. Zhu, M. Wang, Z. Shi, Y. Wei, X. Fu, X. Chen and R. N. Zuckermann, *Proc. Natl. Acad. Sci. U. S. A.*, **2020**, *117*, 31639–31647.
[173] G. K. Olivier, A. Cho, B. Sanii, M. D. Connolly, H. Tran and R. N. Zuckermann, *ACS Nano*, **2013**, *7*, 9276–9286.
[174] J. M. V. Jun, M. V. P. Altoe, S. Aloni and R. N. Zuckermann, *Chem. Comm.*, **2015**, *51*, 10218–10221.
[175] D. J. Murray, J. H. Kim, E. M. Grzincic, S. C. Kim, A. R. Abate and R. N. Zuckermann, *Langmuir*, **2019**, *35*, 13671–13680.
[176] M. L. Hebert, D. S. Shah, P. Blake, J. P. Turner and S. L. Servoss, *Org. Biomol. Chem.*, **2013**, *11*, 4459–4464.
[177] N. Jiang, T. Yu, O. A. Darvish, S. Qian, I. K. Mkam Tsengam, V. John and D. Zhang, *Macromolecules*, **2019**, *52*, 8867–8877.
[178] I. Izzo, G. Ianniello, C. De Cola, B. Nardone, L. Erra, G. Vaughan, C. Tedesco and F. De Riccardis, *Org. Lett.*, **2013**, *15*, 598–601.

morphology[177] or coordination capabilities[178] of the final assemblies. This knowledge has been used to design more complex assemblies, such as the nanotubes described by Jin *et al.*[179] that undergo contraction-relaxation motion upon pH changes (Figure 13c) or the oxidation-sensitive vesicles described by Deng *et al.* (Figure 13b).[180]

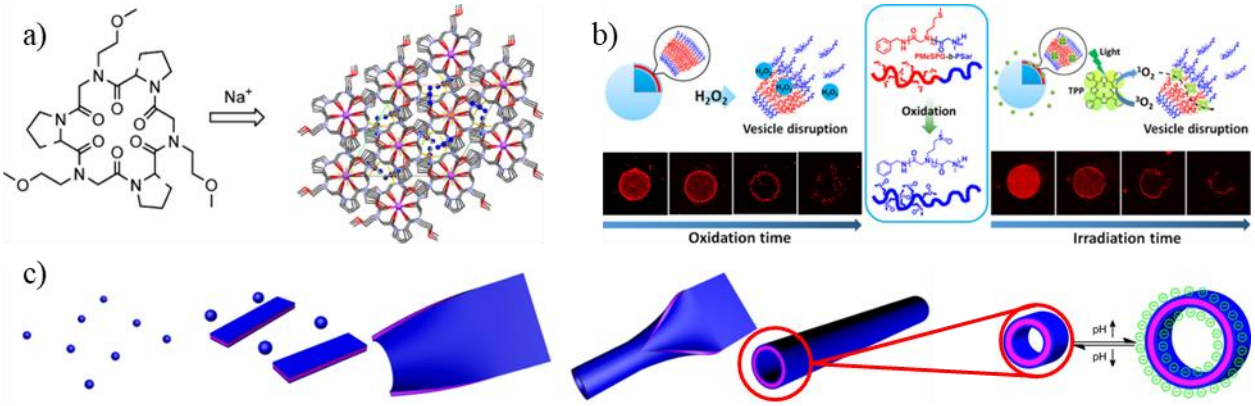

Figure 13. a) Model of MOF like structure derived from a cyclic hexapeptoid. Reprinted with permission from Ref.178. Copyright © 2013 American Chemical Society; b) peptoid based vesicle disassembly upon oxidation. Reprinted with permission from Ref.180. Copyright © 2019 American Chemical Society; and c) assembly mechanism of a peptoid nanotube and its contraction-relaxation dependency with pH. Reprinted with permission from Ref.179. Copyright © 2018 Springer Nature Limited.

3.2. Natural Building Blocks

3.2.1. DNA

The specific recognition and binding of DNA base pairs is a powerful tool used in nanotechnology to direct the assembly of highly structured materials with specific features on demand.[181] Moreover, DNA offers the possibility of creating more complex systems by incorporating specific structures such as G-quadruplexes or i-motifs, enzymatic responsiveness, interactions with metal ions or other functionalizations.[182,183] Even though not discussed in this introduction, there are several examples of nanomaterials, guided by similar principles to DNA, based on RNAs with application in nanotechnology.[184,185]

Over the years, DNA has been employed to prepare various supramolecular architectures by polymerizing small DNA building blocks. For example, 2D crystals were reported by Winfree *et al*. in 1998 taking advantage of sticky ends in DNA double-crossover derivatives.[186] Moreover, Yan *et al.* designed a 4x4 DNA tile that can undergo self-assembly into 2D nano-grids or nanoribbons

[179] H. Jin, Y. H. Ding, M. Wang, Y. Song, Z. Liao, C. J. Newcomb, X. Wu, X. Q. Tang, Z. Li, Y. Lin, F. Yan, T. Jian, P. Mu and C. L. Chen, *Nat. Commun.*, **2018**, *9*, 270.
[180] Y. Deng, H. Chen, X. Tao, F. Cao, S. Trépout, J. Ling and M. H. Li, *Biomacromolecules*, **2019**, *20*, 3435–3444.
[181] N. C. Seeman, *Nature*, **2003**, *421*, 427–431.
[182] A. Krissanaprasit, C. M. Key, S. Pontula and T. H. Labean, *Chem. Rev.*, **2021**, *121*, 13797–13868.
[183] O. I. Wilner and I. Willner, *Chem. Rev.*, **2012**, *112*, 2528–2556.
[184] H. Ohno, S. Akamine and H. Saito, *Curr. Opin. Biotechnol.*, **2019**, *58*, 53–61.
[185] W. W. Grabow and L. Jaeger, *Acc. Chem. Res.*, **2014**, *47*, 1871–1880.
[186] E. Winfree, F. Liu, L. A. Wenzler and N. C. Seeman, *Nature*, **1998**, *394*, 539–544.

(Figure 14a). Further functionalization of these structures allowed the preparation of protein arrays and the production of highly conductive nanowires.[187]

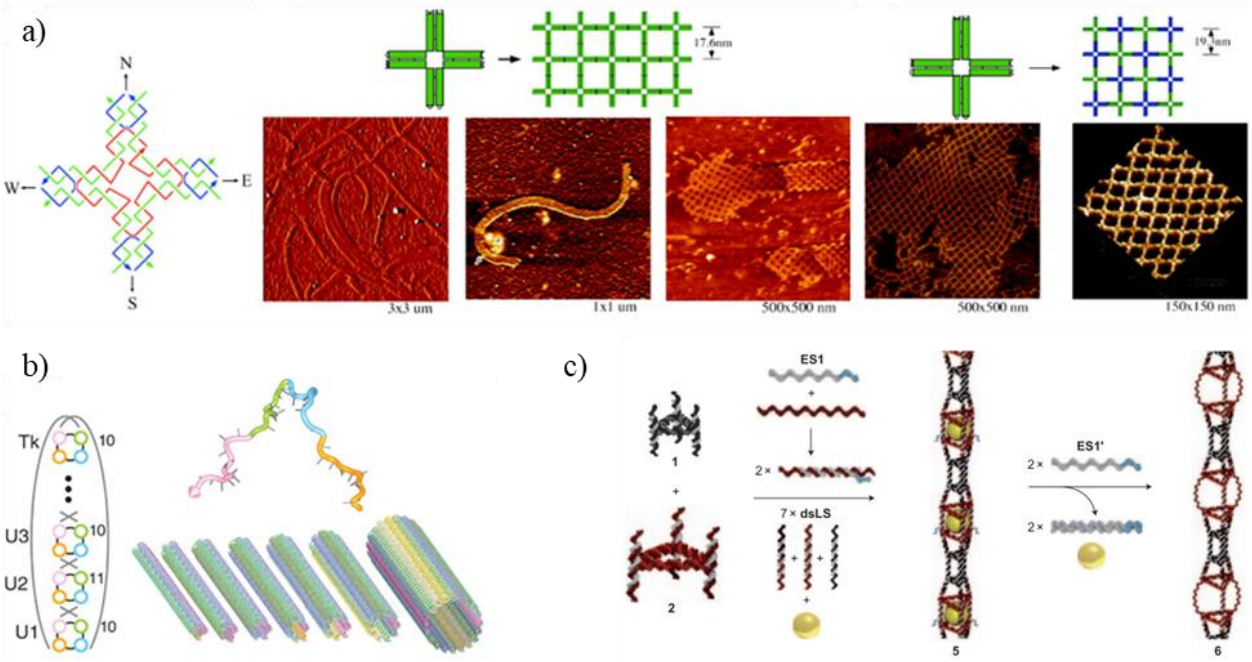

Figure 14. a) DNA polymerization into nanoribbons and 2D-nanogrids. From Hao Yan *et al.*, DNA-Templated Self-Assembly of Protein Arrays and Highly Conductive Nanowires. *Science* **301**, 1882-1884 (2003). Reprinted with permission from AAAS; b) DNA nanotubes with tunable diameter. From Peng Yin *et al.*, Programming DNA Tube Circumferences. *Science* **321**, 824-826 (2008). Reprinted with permission from AAAS; and c) DNA nanotubes with selective cargo encapsulation and release. Reprinted with permission from Ref.189. Copyright © 2010 Springer Nature Limited.

This technology was also exploited to accomplish different morphologies such as nanotubes. P. Yin *et al.* described a 42-base ssDNA motif with specific complementarity between four modular domains.[188] Annealing of the sample results in DNA tubes with tunable monodisperse diameters (Figure 14b). Furthermore, a DNA-based nanotube with longitudinal variations and alternating larger and smaller zones along the tube was also described.[189] The cavities allowed the size-selective encapsulation and controlled release of model cargos (Figure 14c). Interestingly, DNA has also been used to direct and control the hierarchical assembly of DNA-protein hybrid structures. Functionalization of the protein surface with small DNA fragments encodes the information to assemble hierarchically into bundles of tubes or sheets.[190]

In addition, DNA hybridization has been exploited to functionalize polymers, peptides and others to produce hydrogels, many of which present stimuli responsiveness, making them suitable for a variety of applications, e.g., sensing devices and shape memory materials.[191] However,

[187] H. Yan, S. Ha Park, G. Finkelstein, J. H. Reif and T. H. LaBean, *Science*, **2003**, *301*, 1882–1884.
[188] P. Yin, R. F. Hariadi, S. Sahu, H. M. T. Choi, H. P. Sung, T. H. LaBean and J. H. Reif, *Science*, **2008**, *321*, 824–826.
[189] P. K. Lo, P. Karam, F. A. Aldaye, C. K. McLaughlin, G. D. Hamblin, G. Cosa and H. F. Sleiman, *Nat. Chem.*, **2010**, *2*, 319–328.
[190] O. G. Hayes, B. E. Partridge and C. A. Mirkin, *Proc. Natl. Acad. Sci. U. S. A.*, **2021**, *118*, 1–8.
[191] J. Shi, Z. Shi, Y. Dong, F. Wu and D. Liu, *ACS Appl. Bio. Mater.*, **2020**, *3*, 2827–2837.

polymerization of pure DNA has also been described. To achieve this goal. Liu *et al*. employed a three-stranded DNA nanostructure that self-assembles by forming intermolecular i-motif structures (Figure 15a). The sensibility and fast response of i-motifs to pH changes makes them particularly suitable for cargo encapsulation and release.[192] Further studies also demonstrated the possibility of using DNA sticky ends to prepare hydrogels with thermal and enzyme responsiveness (Figure 15b).[193]

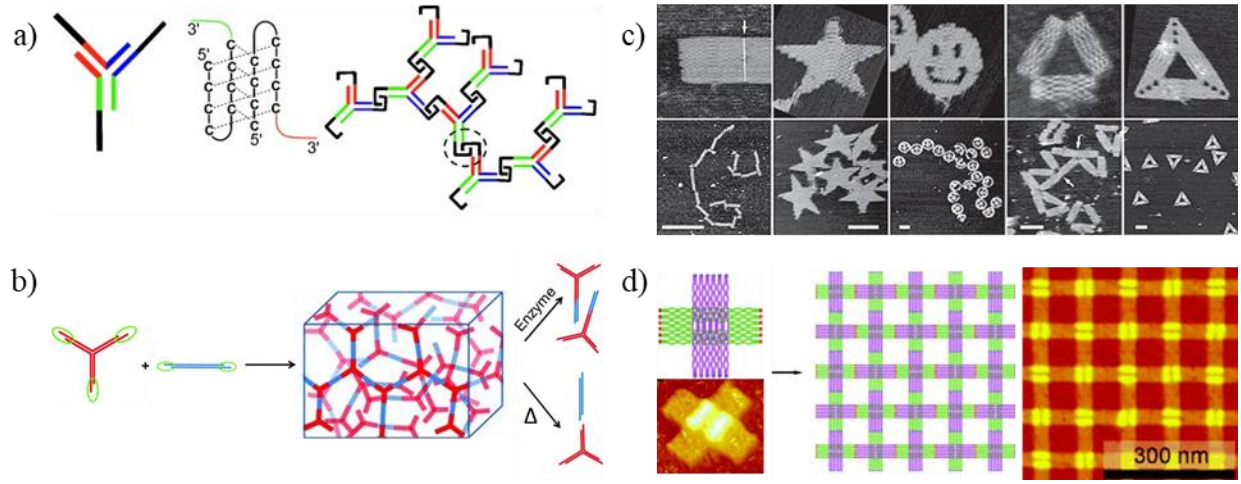

Figure 15. a) Scheme of the i-motif formation with the consequent hydrogelation. Adapted with permission from Ref.192. Copyright © 2009 WILEY-VCH Verlag GmbH & Co. KGaA, Weinheim; b) DNA based hydrogel exhibiting enzyme and thermal responsiveness. Adapted with permission from Ref.193. Copyright © 2011 WILEY-VCH Verlag GmbH & Co. KGaA, Weinheim; c) DNA origami structures. Adapted with permission from Ref.194. Copyright © 2006 Springer Nature Limited; and d) DNA origami based 2D-nanogrids. Adapted with permission from Ref.196. Copyright © 2011 WILEY-VCH Verlag GmbH & Co. KGaA, Weinheim.

Finally, it is worth mentioning the DNA origami and their applications as building block for supramolecular polymers. This technology consists of a long single strand of DNA (scaffold) that is folded into precise shapes by hundreds of short complementary synthetic oligonucleotides (staple strands) (Figure 15c).[194] Over the years, many structures have been developed with various applications in chemistry, biology, physics or computer science that generally require programmed spatial control of the components (molecules or atoms) in 3D arrangements.[195] However, it wasn't until recently that their modification with sticky ends gave rise to supramolecular polymers of DNA origami. A remarkable example of this is the 2D structure reported by Liu *et al*. in which a double-layered DNA-origami tile with two orthogonal sticky ends self-assembled into well-ordered two-dimensional DNA arrays (Figure 15d).[196] Another interesting example was described by Li *et al*. in which they manage to control the morphology of the molecular assembly by modulating the

[192] E. Cheng, Y. Xing, P. Chen, Yang, Y. Sun, D. Zhou, T. Xu, Q. Fan and D. Liu, *Angew. Chem. Int. Ed.*, **2009**, *48*, 7660–7663.
[193] Y. Xing, E. Cheng, Y. Yang, P. Chen, T. Zhang, Y. Sun, Z. Yang and D. Liu, *Adv. Mater*., **2011**, *23*, 1117–1121.
[194] P. W. K. Rothemund, *Nature*, **2006**, *440*, 297–302.
[195] F. Hong, F. Zhang, Y. Liu and H. Yan, *Chem. Rev*., **2017**, *117*, 12584–12640.
[196] W. Liu, H. Zhong, R. Wang and N. C. Seeman, *Angew. Chem. Int. Ed.*, **2011**, *50*, 264–267.

dimensions of the DNA tiles and the linker strands.[197] This shows the great potential of DNA and DNA origami-based polymerization for the synthesis of nano-materials.

3.2.2. Peptides

Peptides and their derivatives are excellent supramolecular building blocks due to their versatility, molecular diversity, and easy large-scale synthesis. Their supramolecular assemblies are dynamic and flexible, consequently opening up new horizons for sophisticated biomaterials and other nanotechnological applications.[198]

Natural peptides have the ability to self-assemble into different types of aggregates. As commented before, the β-amyloid peptide forms insoluble fibrils through β-sheet structures. These fibrils are the main component of brain plaques in patients with Alzheimer's disease.[199] D. Lynn have devoted great effort to discover and exploit the self-assembling properties of this peptide. Structural studies establish the formation of a parallel β-sheet structure in register of the central core of the β-amyloid[200] that subsequently laminates to form fibrils.[201] This fibrillation could be favored by the presence of metals[202] or nucleic acids.[203] In addition, the reduction in peptide length leads to an increase in the size of the sheets, creating peptide bilayers[204] that are further supercoiled into robust nanotubes.[205] This transition takes places as a consequence of the change in the internal order of the laminates in which the peptide-peptide interactions evolve from out-of-register antiparallel to in register parallel beta-sheet.[206] Further studies revealed the kinetics of a two-step nucleation mechanism in which systems move from liquid-liquid phase separation to fibers,[207] which can become twisted/helical ribbons and nanotubes (Figure 16a).[208] Interestingly, the final morphology can be easily controlled by modifying the metal ion concentration.[209] All these experimental learnings enabled the synthesis of nucleic acid (Figure 16b)[210] and lipids-peptide hybrids,[211] asymmetric (Figure 16c),[212] and catalytic materials.[213]

---

[197] Z. Li, M. Liu, L. Wang, J. Nangreave, H. Yan and Y. Liu, *J. Am. Chem. Soc*., **2010**, *132*, 13545–13552.
[198] Y. Chen, K. Tao, W. Ji, V. B. Kumar, S. Rencus-Lazar and E. Gazit, *Mater. Today*, **2022**, *60*, 106–127.
[199] J. Dong, K. Lu, A. Lakdawala, A. K. Mehta and D. G. Lynn, *Amyloid*, **2006**, *13*, 206–215.
[200] T. L. S. Benzinger, D. M. Gregory, T. S. Burkoth, H. Hélène Miller-Auer, D. G. Lynn, R. E. Botto and S. C. Meredith, *Proc. Natl. Acad. Sci. U. S. A*., **1998**, *95*, 13407–13412.
[201] T. S. Burkoth, T. L. S. Benzinger, V. Urban, D. M. Morgan, D. M. Gregory, P. Thiyagarajan, R. E. Botto, S. C. Meredith and D. G. Lynn, *J. Am. Chem. Soc*., **2000**, *122*, 7883–7889.
[202] D. M. Morgan, J. Dong, J. Jacob, K. Lu, R. P. Apkarian, P. Thiyagarajan and D. G. Lynn, *J. Am. Chem. Soc*., **2002**, *124*, 12644–12645.
[203] C. Gordon-Kim, A. Rha, G. A. Poppitz, J. Smith-Carpenter, R. Luu, A. B. Roberson, R. Conklin, A. Blake and D. G. Lynn, *Front Mol Biosci*., **2022**, *9*.
[204] W. S. Childers, A. K. Mehta, R. Ni, J. V. Taylor and D. G. Lynn, *Angew. Chem. Int. Ed.*, **2010**, *49*, 4104–4107.
[205] K. Lu, J. Jacob, P. Thiyagarajan, V. P. Conticello and D. G. Lynn, *J. Am. Chem. Soc.*, **2003**, *125*, 6391–6393.
[206] C. Liang, R. Ni, J. E. Smith, W. S. Childers, A. K. Mehta and D. G. Lynn, *J. Am. Chem. Soc*., **2014**, *136*, 15146–15149.
[207] M. C. Hsieh, D. G. Lynn and M. A. Grover, *J. Phys. Chem. B*., **2017**, *121*, 7401–7411.
[208] W. S. Childers, N. R. Anthony, A. K. Mehta, K. M. Berland and D. G. Lynn, *Langmuir*, **2012**, *28*, 6386–6395.
[209] J. Dong, J. E. Shokes, R. A. Scott and D. G. Lynn, *J. Am. Chem. Soc*., **2006**, *128*, 3540–3542.
[210] A. K. Rha, D. Das, O. Taran, Y. Ke, A. K. Mehta and D. G. Lynn, *Angew. Chem. Int. Ed.*, **2020**, *59*, 358–363.
[211] R. Ni, W. S. Childers, K. I. Hardcastle, A. K. Mehta and D. G. Lynn, *Angew. Chem. Int. Ed.*, **2012**, *51*, 6635–6638.
[212] S. Li, A. K. Mehta, A. N. Sidorov, T. M. Orlando, Z. Jiang, N. R. Anthony and D. G. Lynn, *J. Am. Chem. Soc*., **2016**, *138*, 3579–3586.
[213] T. O. Omosun, M. C. Hsieh, W. S. Childers, D. Das, A. K. Mehta, N. R. Anthony, T. Pan, M. A. Grover, K. M. Berland and D. G. Lynn, *Nat. Chem*., **2017**, *9*, 805–809.

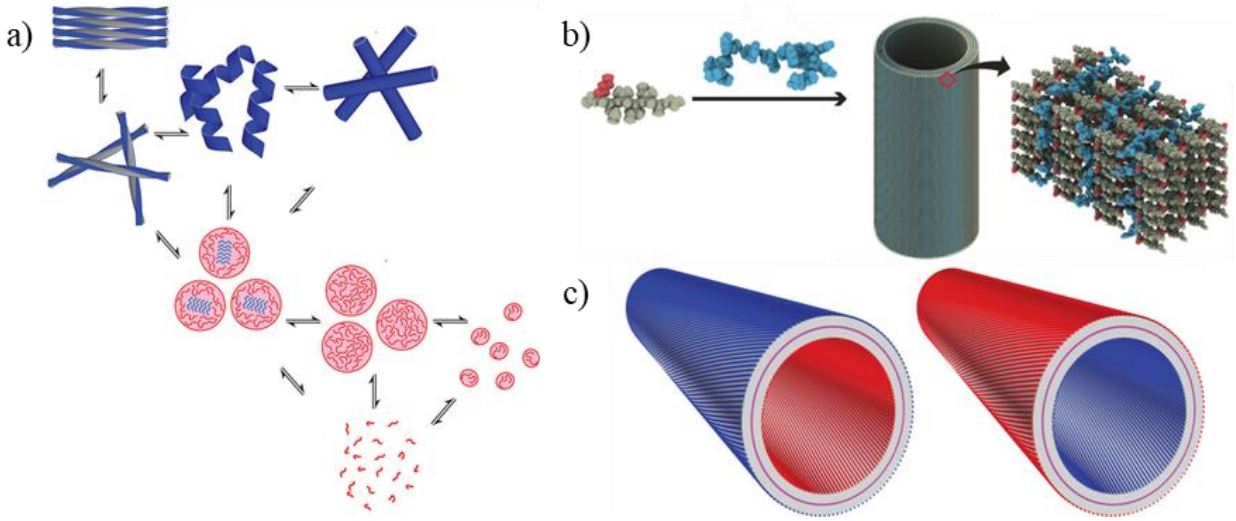

Figure 16. a) Schematic representations of the different phase transition of the amyloid beta peptides. Adapted with permission from Ref.208. Copyright © 2012 American Chemical Society; b) amyloid beta peptide (grey) assembly templated by DNA (blue). Adapted with permission from Ref.210. Copyright © 2020 WILEY-VCH Verlag GmbH & Co. KGaA, Weinheim; and c) representation of asymmetric materials based on amyloid derivatives. Adapted with permission from Ref.212. Copyright © 2016 American Chemical Society.

In the same direction but using different proteins, V. P. Conticello has also exploited natural peptides to build supramolecular systems using collagen mimetic peptides (CMPs). These peptides first self-assemble into a collagen like triple helix that can further agglomerate to form fibers,[214] nanotubes[215] or nanosheets (Figure 17a).[216] Interestingly, the authors claim that CMPs could form sheet monolayers in which the peptide length defines the height of the sheets.[217] This height could be also modified by co-assembling oppositely charged CMPs to form a triple layer[218] (Figure 17b) or CMPs with DNA origami to form nanowires.[219] Moreover, as already mentioned for the previous model,[217] the length of the peptide again has a direct impact on the height, but it also can modulate the size of the obtained nanosheets,[220] allowing the molecular design of multifunctional sheets under thermodynamic control (Figure 17c).[221] Furthermore, the use of heteromeric CMPs possessing complementarity charge pairs provided a pH responsive 2D material that under certain conditions coils to form NTs (Figure 17a).[215] Over the years, Conticello's group has also taken

[214] S. Rele, Y. Song, R. P. Apkarian, Z. Qu, V. P. Conticello and E. L. Chaikof, *J. Am. Chem. Soc*., **2007**, *129*, 14780–14787.
[215] A. D. Merg, G. Touponse, E. Van Genderen, T. B. Blum, X. Zuo, A. Bazrafshan, H. M. H. Siaw, A. McCanna, R. Brian Dyer, K. Salaita, J. P. Abrahams and V. P. Conticello, *J. Am. Chem. Soc.*, **2020**, *142*, 19956–19968.
[216] T. Jiang, C. Xu, Y. Liu, Z. Liu, J. S. Wall, X. Zuo, T. Lian, K. Salaita, C. Ni, D. Pochan and V. P. Conticello, *J. Am. Chem. Soc.*, **2014**, *136*, 4300–4308.
[217] T. Jiang, C. Xu, X. Zuo and V. P. Conticello, *Angew. Chem. Int. Ed.*, **2014**, *53*, 8367–8371.
[218] T. Jiang, O. A. Vail, Z. Jiang, X. Zuo and V. P. Conticello, *J. Am. Chem. Soc.*, **2015**, *137*, 7793–7802.
[219] T. Jiang, T. A. Meyer, C. Modlin, X. Zuo, V. P. Conticello and Y. Ke, *J. Am. Chem. Soc.*, **2017**, *139*, 14025–14028.
[220] A. D. Merg, G. Touponse, E. van Genderen, X. Zuo, A. Bazrafshan, T. Blum, S. Hughes, K. Salaita, J. P. Abrahams and V. P. Conticello, *Angew. Chem. Int. Ed.*, **2019**, *58*, 13507–13512.
[221] A. D. Merg, E. Van Genderen, A. Bazrafshan, H. Su, X. Zuo, G. Touponse, T. B. Blum, K. Salaita, J. P. Abrahams and V. P. Conticello, *J. Am. Chem. Soc*, **2019**, *141*, 20107–20117.

advantage of other proteins such as elastin[222] or Ile zipper GCN4-pII[223] to design supramolecular materials with pH,[224] metal[225] or thermo-responsive properties.[226]

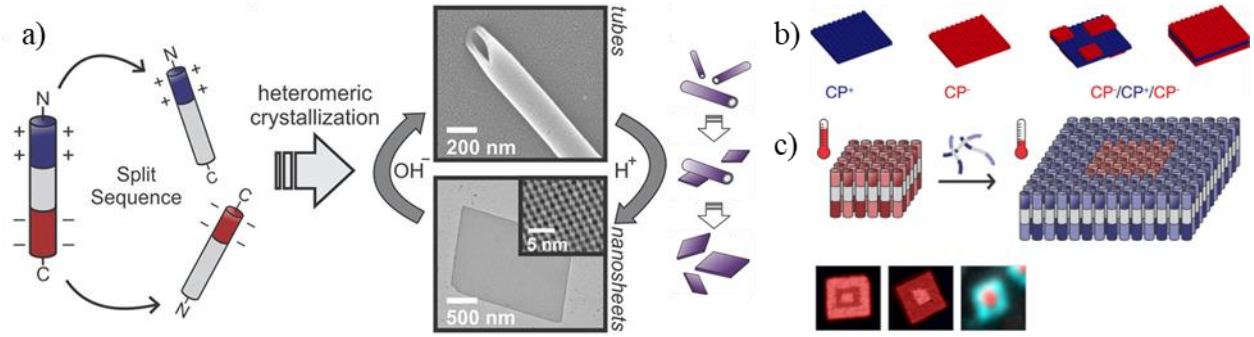

Figure 17. a) pH responsive morphology based on collagen mimetic peptides. Adapted with permission from Ref.215. Copyright © 2020 American Chemical Society; b) schematic representation of a tri-layer. Adapted with permission from Ref.218. Copyright © 2015 American Chemical Society; and c) epitaxial growth of CMPs triggered by temperature. Adapted with permission from Ref.221. Copyright © 2019 American Chemical Society.

Non-natural sequences decorated with functional synthetic motifs have also been used to design new materials with specific properties. In this regard, S. Otto published back in 2010 a self-replicator system based on the incorporation of a 1,3-bencenedithiol moiety into a peptide derivative that formed β-sheet assemblies. The 1,3-bencenedithiol derivative tends to cyclo-oligomerize to form rings ranging from two to seven units through the exchange of disulfide bonds. Interestingly, adjusting for the conditions under which the system evolves (shacking or stirring), hexamers or heptamers were the mostly formed species from the pool (Figure 18a). Both rings self-assemble into long fibers that can be broken under mechanical stress promoting their own selection from the poll of different ring sizes (Figure 18b).[227] In addition, under photoirradiation disulfide exchange induce conversion into polymers, which stabilizes the fibers, promoting a sol to gel transition (Figure 18c).[228] Further experiments also demonstrated the mechanical and chemical control of the length of the supramolecular polymer, which could then act as seeds to promote the formation of a single ring size.[229] Modifications on the peptide scaffold unveiled that the critical parameters to build a self-replicator are its ability to self-assembly and self-replicate.[230] For the first one, the key parameters are the ring size and peptide polarity, while for the second one, it is necessary that its autocatalytic formation outstands the spontaneous formation. The versatility of this system and its on demand tunability has been exploited to mimic behaviors of living systems,

---

[222] T. A. T. Lee, A. Cooper, R. P. Apkarian and V. P. Conticello, *Adv. Mater*., **2000**, *12*, 1105–1110.
[223] S. N. Dublin and V. P. Conticello, *J. Am. Chem. Soc.*, **2008**, *130*, 49–51.
[224] Y. Zimenkov, S. N. Dublin, R. Ni, R. S. Tu, V. Breedveld, R. P. Apkarian and V. P. Conticello, *J. Am. Chem. Soc.*, **2006**, *128*, 6770–6771.
[225] P. Anzini, C. Xu, S. Hughes, E. Magnotti, T. Jiang, L. Hemmingsen, B. Demeler and V. P. Conticello, *J. Am. Chem. Soc.*, **2013**, *135*, 10278–10281.
[226] E. R. Wright, R. A. McMillan, A. Cooper, R. P. Apkarian and V. P. Conticello, *Adv. Funct. Mater*., **2002**, *12*, 149–154.
[227] J. M. A. Carnall, C. A. Waudby, A. M. Belenguer, M. C. A. Stuart, J. J. P. Peyralans and S. Otto, *Science*, **2010**, *327*, 1502–1506.
[228] J. Li, J. M. A. Carnall, M. C. A. Stuart and S. Otto, *Angew. Chem. Int. Ed.*, **2011**, *50*, 8384–8386.
[229] A. Pal, M. Malakoutikhah, G. Leonetti, M. Tezcan, M. Colomb-Delsuc, V. D. Nguyen, J. van der Gucht and S. Otto, *Angew. Chem. Int. Ed.*, **2015**, *54*, 7852–7856.
[230] M. Malakoutikhah, J. J. P. Peyralans, M. Colomb-Delsuc, H. Fanlo-Virgós, M. C. A. Stuart and S. Otto, *J. Am. Chem. Soc*., **2013**, *135*, 18406–18417.

such as adaptability to the environment,[231] formation of new species,[232] dependence on system history (Figure 18d),[233,234] proto-metabolism,[235,236] and parasitic behavior.[237]

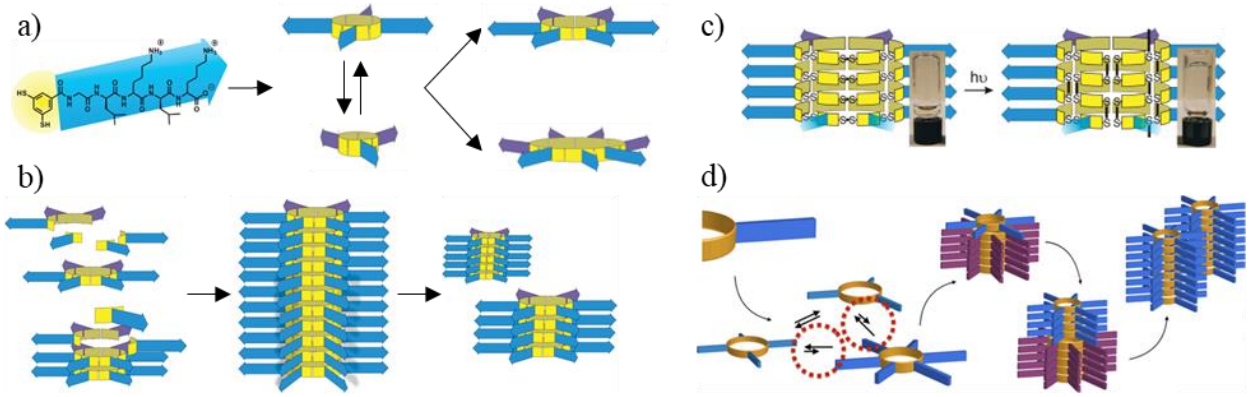

Figure 18. a) Schematic representation of hexamer or heptamer selection under shaking or stirring conditions respectively; b) schematic representation of the hexamer self-assembly into long fibers and their mechanic break. From Jacqui M. A. Carnall *et al.*, Mechanosensitive Self-Replication Driven by Self-Organization. *Science* **327**, 1502-1506 (2010). Reprinted with permission from AAAS.; c) sol to gel transition upon irradiation of the hexamer. Adapted with permission from Ref.228. Copyright © 2011 WILEY-VCH Verlag GmbH & Co. KGaA, Weinheim; and d) selective formation of a hexamer in the presence of an octamer from a different peptide sequence. Reprinted with permission from Ref.233. Copyright © 2017 American Chemical Society.

Another very promising synthetic modification of peptides is the incorporation of an alkyl chain to one end of a short peptide sequence, to form peptide amphiphiles (PA).[238] At this respect, S. Stupp described a PA that self-assemble into fibers triggered by the acidification of the media, forming gels above a critical concentration (Figure 19a).[239] The nanofibers are composed of parallel β-sheets with the peptide pointing towards the water interphase and the alkyl chain in the core of the fiber.[240] These fibers could be further cross-linked by disulfide bonds increasing the structural integrity of the aggregate state. Moreover, the negative charge on the surface of the fibers drives the hydroxyapatite mineralization which aligns along the fibers similar to collagen in bone (Figure 19b).[239] Further studies demonstrated the dynamic behavior of the nanofibers[241] and their tolerance to modifications on the peptide scaffold, which enable the design of fibers containing bioactive sequences.[242] In addition, mixing oppositely charged PAs entails the formation of fibers stable under physiological conditions allowing their use as bio-signals transporters.[243,244] Over the years

[231] G. Leonetti and S. Otto, *J. Am. Chem. Soc*., **2015**, *137*, 2067–2072.
[232] J. W. Sadownik, E. Mattia, P. Nowak and S. Otto, *Nat. Chem*., **2016**, *8*, 264–269.
[233] Y. Altay, M. Tezcan and S. Otto, *J. Am. Chem. Soc.*, **2017**, *139*, 13612–13615.
[234] Y. Altay, M. Altay and S. Otto, *Chem. Eur. J*., **2018**, *24*, 11911–11915.
[235] G. Monreal Santiago, K. Liu, W. R. Browne and S. Otto, *Nat. Chem.*, **2020**, *12*, 603–607.
[236] J. Ottelé, A. S. Hussain, C. Mayer and S. Otto, *Nat. Catal*., **2020**, *3*, 547–553.
[237] M. Altay, Y. Altay and S. Otto, *Angew. Chem. Int. Ed.*, **2018**, *57*, 10564–10568.
[238] H. Cui, M. J. Webber and S. I. Stupp, *Pept. Sci*., **2010**, *94*, 1–18.
[239] J. D. Hartgerink, E. Beniash and S. I. Stupp, *Science*, **2001**, *294*, 1684–1688.
[240] H. Jiang, M. O. Guler and S. I. Stupp, *Soft Matter*, **2007**, *3*, 454–462.
[241] R. M. P. Da Silva, D. Van Der Zwaag, L. Albertazzi, S. S. Lee, E. W. Meijer and S. I. Stupp, *Nat. Commun*., **2016**, *7*.
[242] J. D. Hartgerink, E. Beniash and S. I. Stupp, *Proc. Natl. Acad. Sci. U. S. A*., **2002**, *99*, 5133–5138.
[243] K. L. Niece, J. D. Hartgerink, J. J. J. M. Donners and S. I. Stupp, *J. Am. Chem. Soc*., **2003**, *125*, 7146–7147.
[244] H. A. Behanna, J. J. J. M. Donners, A. C. Gordon and S. I. Stupp, *J. Am. Chem. Soc.*, **2005**, *127*, 1193–1200.

these PAs have found applications in biology and material science such as bone regeneration,[245] spinal cord injury recovery[246,247] and extracellular matrix mimicking (Figure 19c)[248] or dynamic light activated materials (Figure 19d).[249]

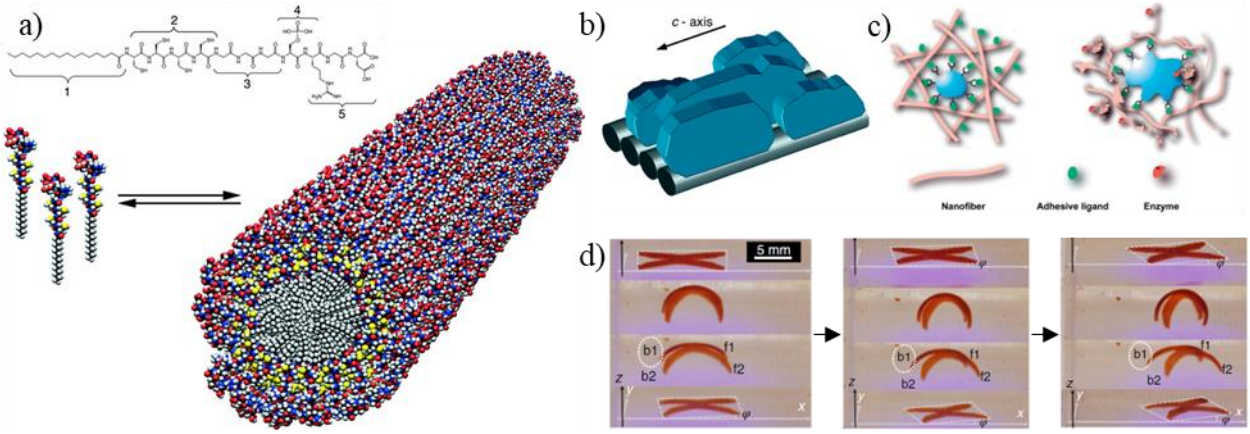

Figure 19. a) PA sequence and schematic fiber formation; b) schematic hydroxyapatite growth align with the peptide fibers. From Jeffrey D. Hartgerink *et al.*, Self-Assembly and Mineralization of Peptide-Amphiphile Nanofibers. *Science* **294**, 1684-1688 (2001). Reprinted with permission from AAAS; c) illustration cell-responsive nanofiber network. Adapted with permission from Ref.248. Copyright © 2005 WILEY-VCH Verlag GmbH & Co. KGaA, Weinheim; and d) light triggered motion of a PA-polymer hybrid. Adapted with permission from Ref.249. Copyright © 2020 Springer Nature Limited.

Another key feature of peptides is their liability to enzymes, which has been exploited by R. V. Ulijn to drive self-assembling process of short peptides (Figure 20a). They demonstrated how hydrogelation of Fmoc-tripeptides could be triggered enzymatically by reversed hydrolysis.[250] This self-assembling strategy amplifies the most stable supramolecular structure providing the system with self-correction and component selection capabilities.[251] Further studies revealed the fundamental role of enzyme concentration,[252] and the residue permissiveness at the second position of the peptide sequence [253] in the self-assembly process of Fmoc-dipeptides. In addition, the reversible nature of the enzymatic reaction pushes the system towards non-equilibrium conditions (Figure 20b).[254] Experiments performed under other assembly inducing stimuli, such as pH, established the important role that agitation plays in supramolecular polymerization,[255] and helped

[245] A. Mata, Y. Geng, K. J. Henrikson, C. Aparicio, S. R. Stock, R. L. Satcher and S. I. Stupp, *Biomaterials*, **2010**, *31*, 6004–6012.
[246] G. A. Silva, C. Czeisler, K. L. Niece, E. Beniash, D. A. Harrington, J. A. Kessler and S. I. Stupp, *Science*, **2004**, *303*, 1352–1355.
[247] Z. Álvarez, A. N. Kolberg-Edelbrock, I. R. Sasselli, J. A. Ortega, R. Qiu, Z. Syrgiannis, P. A. Mirau, F. Chen, S. M. Chin, S. Weigand, E. Kiskinis and S. I. Stupp, *Science*, **2021**, *374*, 848–856.
[248] H. W. Jun, V. Yuwono, S. E. Paramonov and J. D. Hartgerink, *Adv. Mater*., **2005**, *17*, 2612–2617.
[249] C. Li, A. Iscen, H. Sai, K. Sato, N. A. Sather, S. M. Chin, Z. Álvarez, L. C. Palmer, G. C. Schatz and S. I. Stupp, *Nat. Mater*., **2020**, *19*, 900–909.
[250] S. Toledano, R. J. Williams, V. Jayawarna and R. V. Ulijn, *J. Am. Chem. Soc*., **2006**, *128*, 1070–1071.
[251] R. J. Williams, A. M. Smith, R. Collins, N. Hodson, A. K. Das and R. V. Ulijn, *Nat. Nanotechnol.*, **2009**, *4*, 19–24.
[252] A. R. Hirst, S. Roy, M. Arora, A. K. Das, N. Hodson, P. Murray, S. Marshall, N. Javid, J. Sefcik, J. Boekhoven, J. H. Van Esch, S. Santabarbara, N. T. Hunt and R. V. Ulijn, *Nat. Chem*., **2010**, *2*, 1089–1094.
[253] M. Hughes, L. S. Birchall, K. Zuberi, L. A. Aitken, S. Debnath, N. Javid and R. V. Ulijn, *Soft Matter*, **2012**, *8*, 11565–11574.
[254] C. G. Pappas, I. R. Sasselli and R. V. Ulijn, *Angew. Chem. Int. Ed.*, **2015**, *54*, 8119–8123.
[255] W. Helen, P. De Leonardis, R. V. Ulijn, J. Gough and N. Tirelli, *Soft Matter*, **2011**, *7*, 1732–1740.

to reveal the structure of the well-known gelator Fmoc-diphenylalanine (Figure 20c).[256] This fundamental knowledge has paved the way to easily design short peptide nanomaterials[257] with application as water responsive,[258] conductive,[259] cell differentiation,[260] or cosmetic materials.[261]

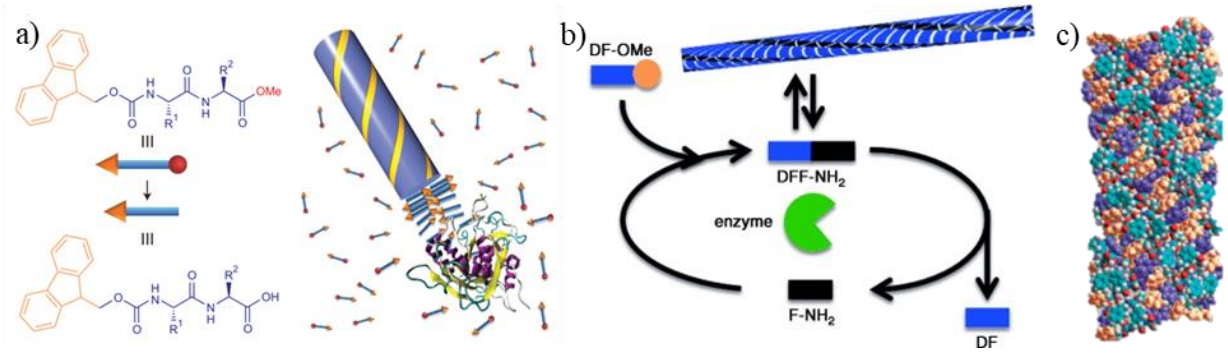

Figure 20. a) Enzyme triggered self-assembly of an Fmoc-dipeptide. Adapted with permission from Ref.252. Copyright © 2010 Springer Nature Limited; b) non-equilibrium enzymatically driven self-assembly of a tripeptide. Adapted with permission from Ref.254. Copyright © 2015 WILEY-VCH Verlag GmbH & Co. KGaA, Weinheim; and c) molecular structure of the Fmoc-FF colored Fmoc (orange) and phenyl (purple). Adapted with permission from Ref. 256. Copyright © 2008 WILEY-VCH Verlag GmbH & Co. KGaA, Weinheim.

4. CYCLIC PEPTIDES

A cyclic peptide (CP) is a peptide chain that forms a closed (cyclic) structure. The closure can be achieved by connecting the N- and C-terminal residues, the N- or C-terminal residue and a complementary side chain group (Glu/Asp or Lys/Orn, respectively), two side chains or other complex arrangements.[262] These peptides are widely found in nature such as ciclosporin or daptomycin with immunosuppressor or antibiotic pharmacological effects, respectively.[263,264] Although natural CPs composed mainly by L-aa have found multiple biological applications,[265] their assembly properties in solution are still very difficult to predict.[266] For this reason, along this thesis when mentioning CP, the term will be referred to the synthetic building block that is able to stack with others through H bonding to form nanotubes. Nowadays many CPs with this capability are known and classified following their composition in α-CPs, β-CPs, α,γ-CPs and so on.

[256] A. M. Smith, R. J. Williams, C. Tang, P. Coppo, R. F. Collins, M. L. Turner, A. Saiani and R. V. Ulijn, *Adv. Mater.*, **2008**, *20*, 37–41.
[257] C. G. Pappas, R. Shafi, I. R. Sasselli, H. Siccardi, T. Wang, V. Narang, R. Abzalimov, N. Wijerathne and R. V. Ulijn, *Nat. Nanotechnol.*, **2016**, *11*, 960–967.
[258] R. Piotrowska, T. Hesketh, H. Wang, A. R. G. Martin, D. Bowering, C. Zhang, C. T. Hu, S. A. McPhee, T. Wang, Y. Park, P. Singla, T. McGlone, A. Florence, T. Tuttle, R. V. Ulijn and X. Chen, *Nat. Mater.*, **2021**, *20*, 403–409.
[259] M. Kumar, N. L. Ing, V. Narang, N. K. Wijerathne, A. I. Hochbaum and R. V. Ulijn, *Nat. Chem.*, **2018**, *10*, 696–703.
[260] E. V. Alakpa, V. Jayawarna, A. Lampel, K. V. Burgess, C. C. West, S. C. J. Bakker, S. Roy, N. Javid, S. Fleming, D. A. Lamprou, J. Yang, A. Miller, A. J. Urquhart, P. W. J. M. Frederix, N. T. Hunt, B. Péault, R. V. Ulijn and M. J. Dalby, *Chem*, **2016**, *1*, 298–319.
[261] A. Lampel, S. A. Mcphee, H.-A. Park, G. G. Scott, S. Humagain, D. R. Hekstra, B. Yoo, P. W. J. M. Frederix, T.-D. Li, R. R. Abzalimov, S. G. Greenbaum, T. Tuttle, C. Hu, C. J. Bettinger and R. V Ulijn, *Science*, **2017**, *356*, 1064–1068.
[262] C. J. White and A. K. Yudin, *Nat. Chem.*, **2011**, *3*, 509–524.
[263] H. Zhang and S. Chen, *RSC Chem. Biol.*, **2022**, *3*, 18–31.
[264] A. A. Vinogradov, Y. Yin and H. Suga, *J. Am. Chem. Soc.*, **2019**, *141*, 4167–4181.
[265] L. Costa, E. Sousa and C. Fernandes, *Pharm.*, **2023**, *16*, 996.
[266] B. Claro, M. Bastos and R. Garcia-Fandino, in *Peptide Applications in Biomedicine, Biotechnology and Bioengineering*, Elsevier, **2017**, *1*, 87–129.

"Independently" of their composition these CPs are designed to adopt a flat conformation with the CO and NH groups of the peptide backbone oriented perpendicular to the plane of the ring, and the aa side chains pointing outward in a pseudo-equatorial position.[267] This planar disposition of the peptide ring allows them to stack forming H-bonds between these groups to provide self-assembling cyclic peptide nanotubes (SCPNs) whose external properties are controlled by the peptide sequence (Figure 21a,b).

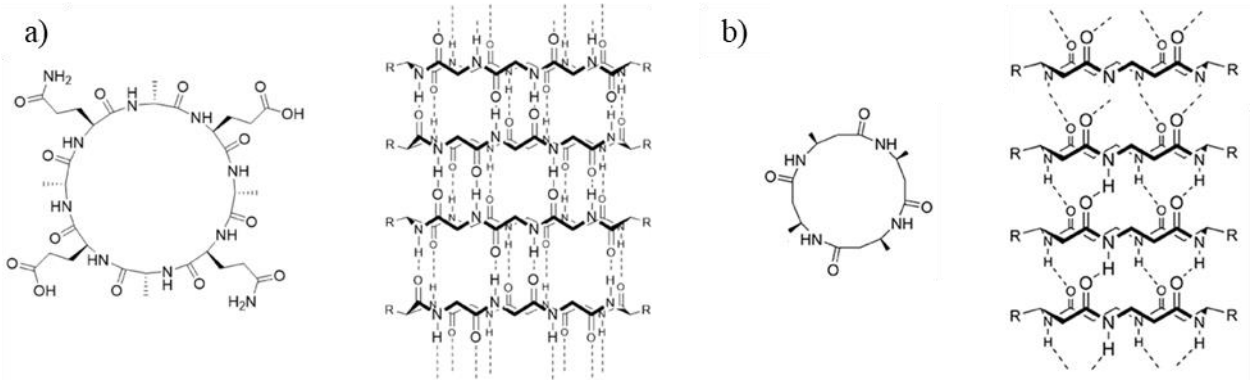

Figure 21. a) Structure of an α-*D,L*-CP (left) and the antiparallel ß-sheet like staking into a NT. Adapted with permission from Ref.269. Copyright © 1993 Springer Nature Limited; and b) structure of an ß-CP (left) and its mandatory parallel ß-sheet like staking. Adapted with permission from Ref.271. Copyright © 1997 Verlag GmbH & Co. KGaA, Weinheim.

These assembling properties of CPs were first stated in 1974 by De Santis *et al.* within the context of theoretical analysis of gramicidin A structure.[268] They concluded that CPs formed by an even number of alternating D- and L-residues could adopt a β-type conformation with CO and NH bonds pointing towards opposite directions perpendicular to the plane. This conformation would allow the stacking of the rings in hollow cylindrical structures through the arrangement of parallel or antiparallel rings that are stabilized by H-bons and van der Waals interactions. This hypothesis was finally demonstrated in 1993, by Ghadiri and collaborators using an α-(*D,L*)-cyclic octapeptide bearing two glutamic acids to trigger the self-assembling process by media acidification. The results clearly confirmed the formation of ordered tubular structures with an internal diameter of 7.5 Å and inter-ring distance of 4.73 Å, in which the CP units formed an antiparallel β-sheet-like structure between peptide backbones of two neighboring units (Figure 21a).[269]

4.1.Control over CP properties

4.1.1. CP-CP stacking interactions

As mentioned before the original alternating α-(*D,L*)-CPs tend to assemble through antiparallel β-sheet interactions. However, parallel stacking is also possible as have been shown by Perrier and collaborators[270] and this can be meticulously controlled by molecular design. For instance, the use

[267] Q. Song, Z. Cheng, M. Kariuki, S. C. L. Hall, S. K. Hill, J. Y. Rho and S. Perrier, *Chem. Rev.*, **2021**, *121*, 13936–13995.
[268] P. De Santis, S. Morosetti and R. Rizzo, *Macromolecules*, **1974**, *7*, 52–58.
[269] M. R. Ghadiri, J. R. Granja, R. A. Milligan, D. E. McRee and N. Khazanovich, *Nature*, **1993**, *366*, 324–327.
[270] M. R. Silk, J. Newman, J. C. Ratcliffe, J. F. White, T. Caradoc-Davies, J. R. Price, S. Perrier, P. E. Thompson and D. K. Chalmers, *Chem. Commun*., **2017**, *53*, 6613–6616.

of β-CPs whose amide groups (CO and NH) are faced on opposite faces of the disc-shaped structure so they can only be stacked forming a parallel β-sheet structure (Figure 21b).[271] Furthermore, the introduction of β-residues into an α-(*D,L*)-CP sequence does not distort the planar conformation and at the same time limits the parallel stacking of the CPs.[272,273] In addition, specific positioning of the side chains of CPs favor antiparallel β-sheet through cross-strand complementary interactions, such as salt bridge Lys/Glu.[274,275]

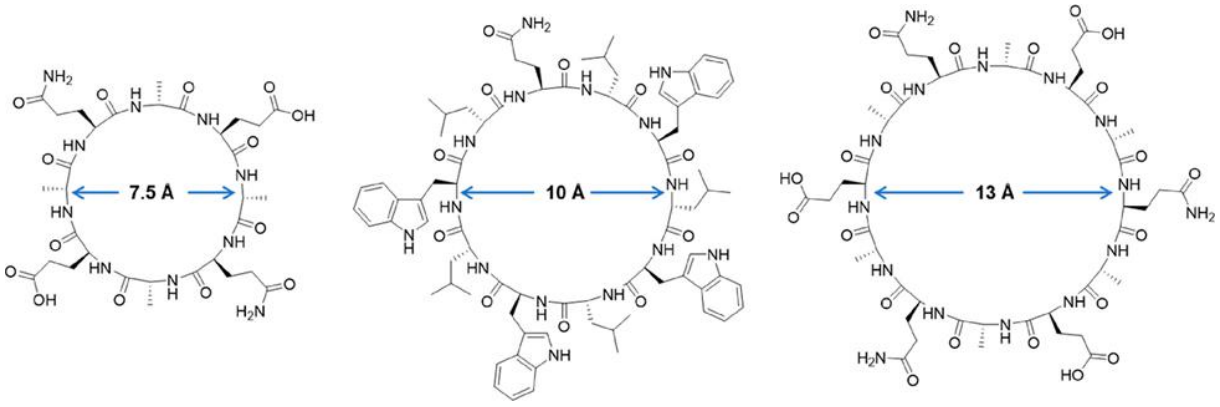

Figure 22. CP structures and their internal diameter for 8, 10 and 12 aa sequences. Reprinted with permission from Ref.267. Copyright © 2021 American Chemical Society.

4.1.2. Internal cavity

The internal properties of these nanotubes and, therefore, their possible applications as 1D hollow materials, are defined by two key parameters, the size and their chemical nature. On the one hand, the diameter size is directly defined by the number and type that make up the cyclic peptide unit. In this sense, the use of 8, 10 or 12 aa in α-(*D,L*)-CP sequences have been used to obtain SCPNs with internal diameters ranging from 7.5 to 13 Å (Figure 22).[276,277] Interestingly, this control on the size of the inner cavity was used to carry selective ion[277] or small molecules transport.[278] Furthermore, the introduction of unnatural residues such as γ- or δ-aa in the peptide sequence provides a tool not only to finely tune the diameter range of the SCPN from 1Å[279] to 30 Å,[274] respectively, but also to modify the internal properties of the self-assembly.

[271] D. Seebach, J. L. Matthews, A. Meden, T. Wessels, C. Baerlocher and L. B. McCusker, *Helv. Chim. Acta.*, **1997**, *80*, 173–182.
[272] F. Novelli, M. Vilela, A. Pazó, M. Amorín and J. R. Granja, *Angew. Chem. Int. Ed.*, **2021**, *60*, 18838–18844.
[273] M. Vilela-Picos, F. Novelli, A. Pazó, A. Méndez-Ardoy, G. Marafon, M. Amorín, A. Moretto and J. R. Granja, *Chem*, **2023**, *9*, 3365–3378.
[274] A. Lamas, A. Guerra, M. Amorín and J. R. Granja, *Chem. Sci.*, **2018**, *9*, 8228–8233.
[275] C. Reiriz, R. J. Brea, R. Arranz, J. L. Carrascosa, A. Garibotti, B. Manning, J. M. Valpuesta, R. Eritja, L. Castedo and J. R. Granja, *J. Am. Chem. Soc.*, **2009**, *131*, 11335–11337.
[276] N. Khazanovich, J. R. Granja, D. E. McRee, R. A. Milligan, M. Reza Ghadiri and A. P. Sloan, *J. Am. Chem. Soc.*, **1994**, *116*, 6011–6012.
[277] M. Reza Ghadiri, J. R. Granja and L. K. Buehler, *Nature*, **1994**, *369*, 301–304.
[278] J. R. Granja and M. Reza Ghadiri, *J. Am. Chem. Soc.*, **1994**, *116*, 10785–10786.
[279] R. J. Brea, L. Castedo and J. R. Granja, *Chem. Comm.*, **2007**, 3267–3269.

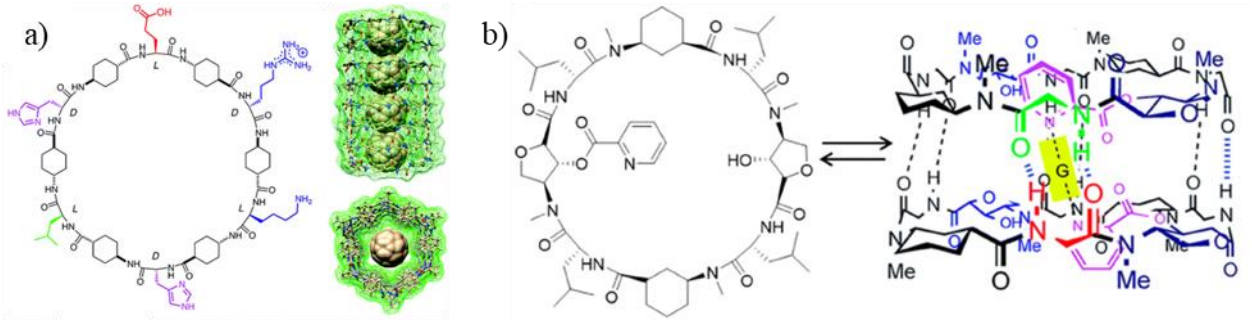

Figure 23. a) α,δ-CP (left) with a hydrophobic cavity to encapsulate fullerene (right). Reproduced from Ref. 274 with permission from the Royal Society of Chemistry; and b) α,γ-CP (left) with a pyridine moiety that allows the encapsulation of silver and oxalic acid (left). Reproduced from Ref. 285 with permission from the Royal Society of Chemistry.

On the other hand, it is well known that α-(*D,L*)-SCPNs possess an internal cavity with hydrophilic properties. However, the introduction of the above-mentioned type of amino acids in the peptide sequence can also modify its inner cavity properties.[280] Synthetic aa such as γ-[281] or δ-residues[282] have been used to form tubular assemblies with hydrophobic cavities. Moreover, hybrid peptide sequences made of these residues with α-(*D,L*)-CPs have been used to modulate the hydrophilic character of these CP assemblies due to projection of methylene moieties into the lumen.[279,283] As a result, big hydrophobic molecules such as fullerenes were encapsulated in the SCPN lumen (Figure 23a).[274] Furthermore, the disposition of the methylene groups and their chemical modification opened the possibility of incorporating functional groups into the internal pore of the nanotube. In this regard, the use of a hydroxylated tetrahydrofuran aa provided an aggregate that had hydroxylic groups pointing into its inner pore.[284] Later, this strategy was used to encapsulate polar molecules or to functionalize the hydroxylic group with a pyridine moiety to expand the encapsulation properties (Figure 23b).[285] Further works also showed that drugs[286] or fluorine atoms[287] could be incorporated into the peptide cavity and use them for cancer therapy or selective anion transport, respectively.

4.1.3. External properties

As previously mentioned, the amino acid side chains are normally pointing outwards on the surface of the SCPNs. This provides control over the external properties of the assembly through the simple design of the peptide sequence used, as long as they do not alter its assembly properties.

---

[280] M. Amorín, L. Castedo and J. R. Granja, *J. Am. Chem. Soc.*, **2003**, *125*, 2844–2845.
[281] L. Li, H. Zhan, P. Duan, J. Liao, J. Quan, Y. Hu, Z. Chen, J. Zhu, M. Liu, Y. D. Wu and J. Deng, *Adv. Funct. Mater.*, **2012**, *22*, 3051–3056.
[282] D. Gauthier, P. Baillargeon, M. Drouin and Y. L. Dory, *Angew. Chem. Int. Ed.*, **2001**, *40*, 4635–4638.
[283] M. Calvelo, A. Lamas, A. Guerra, M. Amorín, R. Garcia-Fandino and J. R. Granja, *Chem. Eur. J.*, **2020**, *26*, 5846–5858.
[284] C. Reiriz, M. Amorín, R. García-Fandiño, L. Castedo and J. R. Granja, *Org. Biomol. Chem.*, **2009**, *7*, 4358–4361.
[285] N. Rodríguez-Vázquez, R. García-Fandiño, M. Amorín and J. R. Granja, *Chem. Sci.*, **2016**, *7*, 183–187.
[286] N. Rodríguez-Vázquez, R. García-Fandiño, M. J. Aldegunde, J. Brea, M. I. Loza, M. Amorín and J. R. Granja, *Org. Lett.*, **2017**, *19*, 2560–2563.
[287] S. S. Burade, T. Saha, N. Bhuma, N. Kumbhar, A. Kotmale, P. R. Rajamohanan, R. G. Gonnade, P. Talukdar and D. D. Dhavale, *Org. Lett.*, **2017**, *19*, 5948–5951.

Furthermore, since some side chains present reactive groups, it is also possible to develop more complex systems through subsequent chemical modifications of these groups.

Over the years many CPs have been functionalized with different aromatic moieties to direct and control their 1D assembly properties while incorporating new electronic and optical properties. The coupling of naphthalenediimide (NDI) through the side chain of the Lys enhances NDI-NDI interactions[288] giving rise to electronically delocalized SCPNs.[289] This Lys functionalization strategy also allowed the alignment of bigger aromatic units, such as fullerenes (Figure 24a).[275] In the same way, using a pyrene moiety as a CP pendant group was exploited to build hybrid nanomaterials directing the noncovalently attachment of the SCPN to single-walled carbon nanotubes[290] (Figure 24b) or molecular silver clusters (Ag_3).[291]

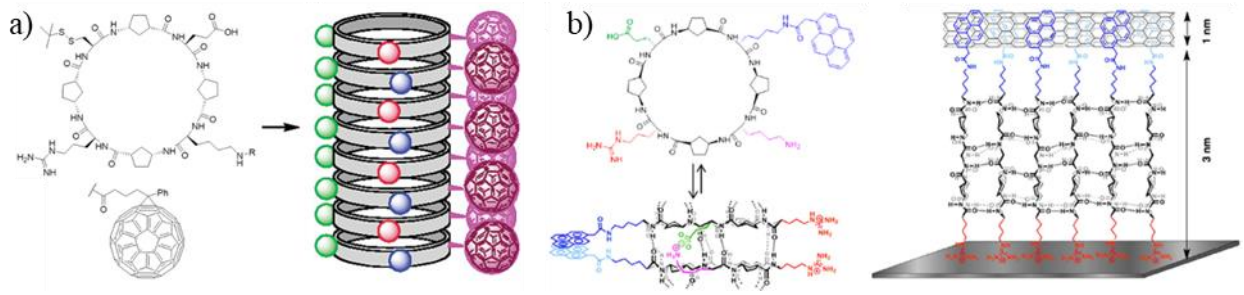

Figure 24. a) α, γ-CP (left) and fullerene alignment (right). Reprinted with permission from Ref.275. Copyright © 2009 American Chemical Society; and b) α,γ-CP-pyrene derivative (left) able to form hybrid materials with SWCN (right). Reprinted with permission from Ref.290. Copyright © 2014 American Chemical Society.

Another functionalization strategy is the attachment of polymer chains to CP. This conjugate forms SCPNs that have the structure of a peptide core coated with a polymer mantle, similar to a molecular brush, which provides greater solubility to the SCPN. This disposition increase its stability in aqueous media due to the steric hindrance caused by the polymer chains and avoiding lateral interactions and therefore aggregation.[267] Interestingly, the control of the polymer length provides a toll to adjust the SCPN length.[292] Over the years three main conjugations around the CP have been done, using the same polymer, [292] different polymers[293] or copolymers[294] giving rise to new structures and applications, some of which will be discussed in the following sections.

Other interesting modifications are the introduction of bulky residues[295] or reactive chemical groups.[296] The first one avoids the supramolecular polymerization of the CP by using *tert*-Leu by means of steric hindrance between homochiral residues. Interestingly, nanotube formation takes

[288] W. S. Horne, N. Ashkenasy and M. R. Ghadiri, *Chem. Eur. J.*, **2005**, *11*, 1137–1144.
[289] N. Ashkenasy, W. S. Horne and M. R. Ghadiri, *Small*, **2006**, *2*, 99–102.
[290] J. Montenegro, C. Vázquez-Vázquez, A. Kalinin, K. E. Geckeler and J. R. Granja, *J. Am. Chem. Soc.*, **2014**, *136*, 2484–2491.
[291] M. Cuerva, R. García-Fandiño, C. Vázquez-Vázquez, M. A. López-Quintela, J. Montenegro and J. R. Granja, *ACS Nano*, **2015**, *9*, 10834–10843.
[292] R. Chapman, K. A. Jolliffe and S. Perrier, *Polym. Chem*., **2011**, *2*, 1956–1963.
[293] M. Danial, C. My-Nhi Tran, P. G. Young, S. Perrier and K. A. Jolliffe, *Nat. Commun*., **2013**, *4*, 2780.
[294] J. Y. Rho, H. Cox, E. D. H. Mansfield, S. H. Ellacott, R. Peltier, J. C. Brendel, M. Hartlieb, T. A. Waigh and S. Perrier, *Nat. Commun*., **2019**, *10*, 4708.
[295] K. Rosenthal-Aizman, G. Svensson and A. Undén, *J. Am. Chem. Soc*., **2004**, *126*, 3372–3373.
[296] Y. Ishihara and S. Kimura, *Pept. Sci*., **2012**, *98*, 155–160.

place by mixing with its enantiomer, forming heterodimeric nanotube in which both CP enantiomers are alternating along the nanotube structure. The second one uses diacetylene residues to covalently link the CPs units once they have self-assembled into SCPN upon UV light induced polymerization.

4.2. Structures based on CPs.

The highly specific control over the properties of the CP and its assembly properties have paved the way for designing different supramolecular structures.

4.2.1. CPs dimers and capsules

Soon after the preparation of the first tubular structures by staking of CPs, the selective N-alkylation of aa with the same chirality to block all amino groups of one face of the CPs was stablish as simple method to restrict the assembling process to dimers.[297] This chemical modification simplifies the study of the CP stacking. Using these simple models was possible to determine the binding constants of the process and determine the energetic differences between the parallel and the antiparallel β-sheet structures that were in agreement with the predominant staking of antiparallel sheets observed in assembled SCPNs.[283,297] Moreover, these N-methylated derivatives have been used to build molecular containers.[285,286] Additionally, the incorporation of a porphyrin cap on the N-alkylated face of an α,γ-CP derivative provided a supramolecular capsule that can selective encapsulate different bipyridine-guests depending on their length (Figure 25a).[298] This promising results could be used for the design of CP-based nanoreactors.

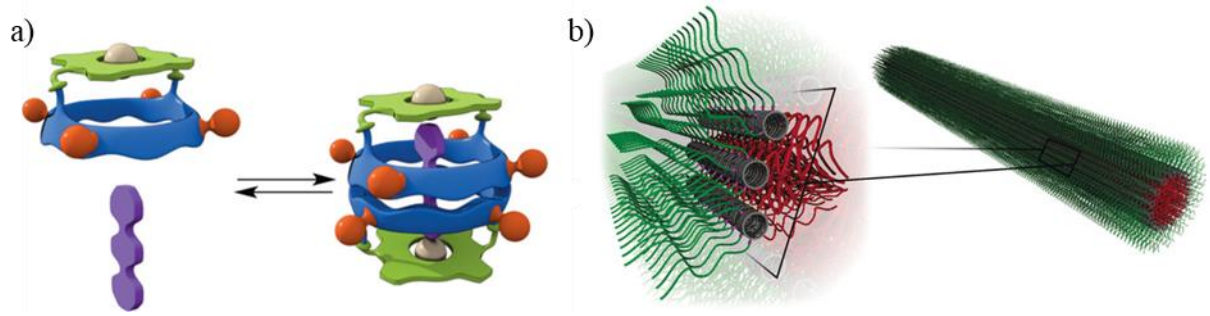

Figure 25. a) α,γ-CP functionalized with a porphyrin cap for pyridine derivatives encapsulation. Adapted with permission from Ref.298. Copyright © 2016 American Chemical Society; and b) CP conjugate to a hydrophilic (green) and hydrophobic (red) polymers for the hierarchically assembly in tubisomes. Adapted with permission from Ref.299. Copyright © 2018 WILEY-VCH Verlag GmbH & Co. KGaA, Weinheim

4.2.2. Tubisomes

As already mentioned, CPs can be asymmetrically decorated with different polymers. A great example was reported by Brendel *et al.* in which a CP was linked to hydrophobic and hydrophilic polymer chains at opposite sides of the CP. This hybrid material forms SCPNs that further interact with others by the hydrophobic chains, thus generating hierarchically assembled tubisomes (Figure

[297] M. Reza Ghadiri, K. Kobayashi, J. R. Granja and D. E. McRee, *Angew. Chem. Int. Ed*., **1995**, *34*, 93–95.
[298] H. L. Ozores, M. Amorín and J. R. Granja, *J. Am. Chem. Soc*., **2017**, *139*, 776–784.

25b).[299] Varying the length and ratio of the polymers, the length of the tubisome can be controlled by molecular design.[300] These structures have shown promising properties as drug delivery vehicles.

4.2.3. Sheets

The possibility to tune the external properties of SCPNs by selecting the aa sequence paved the way to design peptides in which the lateral growth is promoted.[301] Recently, the first example of sheet formation using cyclic peptides that form nanotubes was published. For this purpose, the designed cyclic peptide had a hydrophobic and a hydrophilic domain. As expected, the resulting SCPNs, formed by the formation of H-bonds, generate a hydrophobic surface along the nanotube that further interacts with other tubes to exclude water contact. This lateral growth led to the creation of a nanotubular bilayer formed by nanotubes, burying the hydrophobic faces away from the aqueous environment (Figure 26a). Moreover, systematic structural changes denoted high tolerance to modifications on the hydrophobic core, but no tolerance to substitutions on the Glu-His pair, the residues that are involved in the lateral growth of the sheet.[302] More recently, it has also been demonstrated CP monolayers can be easily design by the incorporation of two hydrophobic faces on opposite side of the peptide sequence to promote the lateral growth.[303]

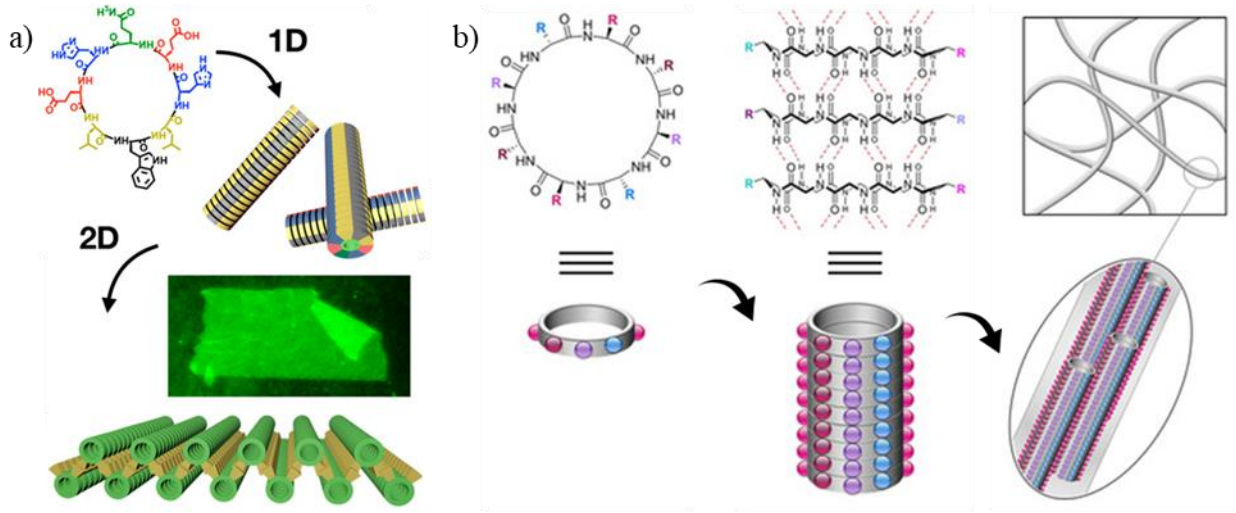

Figure 26. Hierarchical 2 steps self-assembly of CP. First the monomeric CP grows into a 1D-NT and second the NT interact to form a) 2D-sheets or b) NT bundles (fibers). Adapted with permission from Ref.301. Copyright © 2019 American Chemical Society and Ref.305. Copyright © 2018 WILEY-VCH Verlag GmbH & Co. KGaA, Weinheim, respectively.

[299] J. C. Brendel, J. Sanchis, S. Catrouillet, E. Czuba, M. Z. Chen, B. M. Long, C. Nowell, A. Johnston, K. A. Jolliffe and S. Perrier, *Angew. Chem. Int. Ed.*, **2018**, *57*, 16678–16682.
[300] J. C. Brendel, S. Catrouillet, J. Sanchis, K. A. Jolliffe and S. Perrier, *Polym. Chem.*, **2019**, *10*, 2616–2625.
[301] I. Insua and J. Montenegro, *J. Am. Chem. Soc*., **2020**, *142*, 300–307.
[302] S. Díaz, I. Insua, G. Bhak and J. Montenegro, *Chem. Eur. J*., **2020**, *26*, 14765–14770.
[303] I. Insua, A. Cardellini, S. Díaz, J. Bergueiro, R. Capelli, G. M. Pavan and J. Montenegro, *Chem. Sci*., **2023**, *14*, 14074–14081.

4.2.4. Peptide fibers

Recently, Perrier's group and our have demonstrated the ability of certain CPs to form hydrogels.[304,305] This hydrogelation is a hierarchical assembling process in which CPs self-assemble into SCPNs that can further bundle with others to form a 3D fibrillar network that is capable to self-sustain. H. Shaikh et al. studied eleven different CPs that gave rise to organo- or hydrogels depending on the sequence.[305] Additionally, most of the CPs contain pH responsive groups, so strict control of the media conditions is necessary to avoid, in most cases, other side processes such as precipitation (Figure 26b).

In our group, A. Mendez-Ardoy *et al.*[304] designed a CP with two functional domains: i) the hydrophobic part constituted by two Ala and one Lys functionalized with a pyrene moiety, and ii) the hydrophilic block composed by two Ser, two His and one Lys. His residues allowed controlling the assembly process with pH in conditions close to physiological ones. In other words, SCPNs or monomeric subunits are present in alkaline or acidic media, respectively. Moreover, upon increasing the concentration to 2% (w/w) the CP is able to form self-sustainable hydrogels. Interestingly, when the system is encapsulated in microdroplets at acidic pH and these become alkalinized, CP fibrillation take place and induce an alteration on the droplet morphology. In this sense, further understanding and unveiling the structural parameters that determine the viscoelastic behavior of *D,L*-CPs-based hydrogels and their behavior in confined spaces is essential for the design of new CP based systems.

4.3. Application of CP

The wide variety of modifications carried out on the CP and the tunable morphology of the resulting supramolecular structures clearly demonstrates their versatility as functional materials. Herein, some promising results for applicability will be summarized.

4.3.1. Ion and molecular channels

As commented before, the hydrophilic internal cavity of α-(*D,L*)-CPs has been used to transport ions[277] or small polar organic molecules, such as glucose,[278] 5-fluorouracil[306] or glutamic acid,[307] across membranes with high efficiency. Furthermore, systematic studies of the peptide sequence composition showed a tendency to form single or multiple pores when introducing aa neutral or charged side chains, respectively.[308] Interestingly, α,γ-CPs constituted by hydrophobic residues form ion channel structures in lipid bilayers capable of transporting protons or alkaline ions depending on the number of residues (hexa- or octapeptides, respectively).[309] This transport can

[304] A. Méndez-Ardoy, J. R. Granja and J. Montenegro, *Nanoscale Horiz.*, **2018**, *3*, 391–396.
[305] H. Shaikh, J. Y. Rho, L. J. Macdougall, P. Gurnani, A. M. Lunn, J. Yang, S. Huband, E. D. H. Mansfield, R. Peltier and S. Perrier, *Chem. Eur. J*, **2018**, *24*, 19066–19074.
[306] J. Chen, B. Zhang, F. Xia, Y. Xie, S. Jiang, R. Su, Y. Lu and W. Wu, *Nanoscale*, **2016**, *8*, 7127–7136.
[307] J. Sánchez-Quesada, H. S. Kim and M. R. Ghadiri, *Angew. Chem. Int. Ed*., **2001**, *40*, 2503–2506.
[308] M. Danial, S. Perrier and K. A. Jolliffe, *Org. Biomol. Chem*., **2015**, *13*, 2464–2473.
[309] R. García-Fandiño, M. Amorín, L. Castedo and J. R. Granja, *Chem. Sci*., **2012**, *3*, 3280–3285.

also be achieved using functionalized CP dimers as carriers[310] (Figure 27a) and CP-polymer conjugates[311] with selective transport or thermos-responsive behavior respectively.

4.3.2. Antibacterial activity and drug delivery vehicle

The known ability of CPs to interact with lipid membranes was exploited to design a new family of antibiotics.[312] In a first study a small library of CPs was studied against Gram positive and negative bacteria showing the remarkable importance of having an amphipathic character made of a hydrophobic and a charged regions to achieve the antimicrobial activity.[313] A larger systematic study confirmed the activity-structure relationship and the potential of CP antimicrobials since some structures match the antibacterial effect of current treatments.[314] However, they also found that in vitro and in vivo results can vary due to the pharmacokinetics of the CPs. More recently, with the aim of improving the CP antimicrobial activity, peptides incorporating saccharides derived residues[315] or hydrophobic tails[316] were incorporated providing promising results.

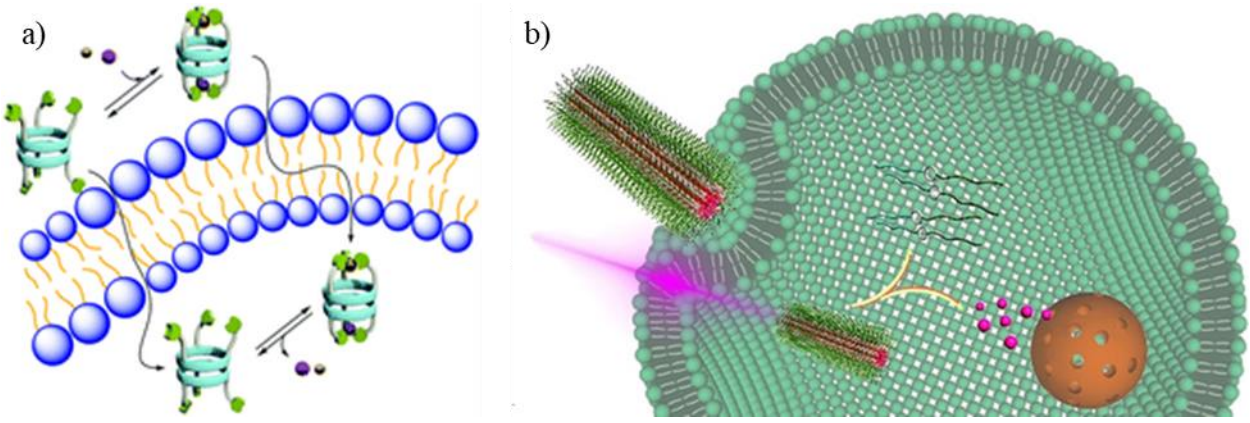

Figure 27. a) Ion transport by a CP dimer functionalized with pyridines. Reproduced from Ref. 310 with permission from the Royal Society of Chemistry; and b) Cell uptake of tubisomes loaded with doxorubicin and drug delivery upon light irradiation. Adapted with permission from Ref.319. Copyright © 2020 WILEY-VCH Verlag GmbH & Co. KGaA, Weinheim.

As commented before, the transport activity of small drugs, such as 5-fluorouracil, of CPs was explored showing a remarkable enhancement of its anti-tumoral activity.[306] In a more complex way, it was also tried to exploit the ability of CP to interact with membranes to deliver big and small bioactive molecules into the cell. The first case was demonstrated by designing a cationic CP that self-assembled into SCPNs that were able to interact with nucleic acids and favors its

[310] A. Fuertes, M. Amorín and J. R. Granja, *Chem. Comm*., **2020**, *56*, 46–49.
[311] M. Danial, C. M. N. Tran, K. A. Jolliffe and S. Perrier, *J. Am. Chem. Soc*., **2014**, *136*, 8018–8026.
[312] N. Rodriguez-Vazquez, H. Ozores, A. Guerra, E. Gonzalez-Freire, A. Fuertes, M. Panciera, J. Priegue, J. Outeiral, J. Montenegro, R. Garcia-Fandino, M. Amorin and J. Granja, *Curr. Top. Med. Chem*., **2014**, *14*, 2647–2661.
[313] S. Fernandez-Lopez, H.-S. Kim, E. C. Choi, M. Delgado, J. R. Granja, A. Khasanov, K. Kraehenbuehl, G. Long, D. A. Weinberger, K. M. Wilcoxen and M. R. Ghadiri, *Nature*, **2001**, *412*, 452–455.
[314] V. Dartois, J. Sanchez-Quesada, E. Cabezas, E. Chi, C. Dubbelde, C. Dunn, J. Granja, C. Gritzen, D. Weinberger, M. R. Ghadiri and T. R. Parr, *Antimicrob. Agents Chemother*., **2005**, *49*, 3302–3310.
[315] L. Motiei, S. Rahimipour, D. A. Thayer, C. H. Wong and M. R. Ghadiri, *Chem. Comm*., **2009**, 3693–3695.
[316] B. Claro, A. Peón, E. González-Freire, E. Goormaghtigh, M. Amorín, J. R. Granja, R. Garcia-Fandiño and M. Bastos, *Colloids Surf. B*, **2021**, *208*, 112086.

internalization and in cell.[317] For the second case, different strategies were followed since the small molecule could be covalently linked to the CP[318] or trapped into the hydrophobic core of the supramolecular aggregate[319] (Figure 27b). In both cases the intracellular release was achieved. All these results confirmed CPs as a promising vehicle for drug delivery.

4.3.3. Other possible applications

As commented above, CPs have the ability to expose different electroactive molecules such as fullerenes[275] or NDIs[289] that can be used in electronic devices. In the same way, CPs have also shown their potential to bring different components in close proximity to favor energy[320] or electron-transfer processes.[321] In addition, CPs are an excellent platform to design 1D-[269], 2D-[301] or 3D-materials[304] at will. Recently, SCPNs have also shown promising results as materials for cell imaging.[322] All the information summarized in this section exhibits the potential of SCPNs in very different areas. However, more information on the structural parameters that direct the assembly and its final morphology, their behavior in confined spaces etc. is needed to fully manipulate CPs on demand, in the construction of functional materials.

[317] M. Li, M. Ehlers, S. Schlesiger, E. Zellermann, S. K. Knauer and C. Schmuck, *Angew. Chem. Int. Ed.*, **2016**, *55*, 598–601.
[318] Y. Wang, S. Yi, L. Sun, Y. Huang, S. C. Lenaghan and M. Zhang, *J. Biomed. Nanotechnol*., **2014**, *10*, 445–454.
[319] J. Yang, J. I. Song, Q. Song, J. Y. Rho, E. D. H. Mansfield, S. C. L. Hall, M. Sambrook, F. Huang and S. Perrier, *Angew. Chem. Int. Ed.*, **2020**, *59*, 8860–8863.
[320] Q. Song, S. Goia, J. Yang, S. C. L. Hall, M. Staniforth, V. G. Stavros and S. Perrier, *J. Am. Chem. Soc*., **2021**, *143*, 382–389.
[321] R. J. Brea, L. Castedo, J. R. Granja, M. A. Herranz, L. Sánchez, N. Martín, W. Seitz and D. M. Guldi, *Proc. Natl. Acad. Sci. U. S. A*., **2007**, *104*, 5291–5294.
[322] J. Yang, X. Yu, J. I. Song, Q. Song, S. C. L. Hall, G. Yu and S. Perrier, *Angew. Chem. Int. Ed.*, **2022**, *61*, e202115208.

OBJECTIVES

As clearly stated in the introduction, supramolecular polymers are very interesting materials with a wide variety of applications. The design of the building blocks is the key element to fit the supramolecular polymer and the desired application. In this sense, polymeric materials based on natural building blocks are specially desired for their inherent biocompatibility and biodegradability. For this reason, the main objective of this thesis is to design, synthesize and study new supramolecular polymers based on α-(*D,L*)-CPs in which the incorporation of aromatic motifs in CP scaffolds can regulate their hierarchical assembly into soft materials and microstructures. Deepening the study that allows unmasking the parameters that govern peptide assemblies is essential for the development of future functional materials.

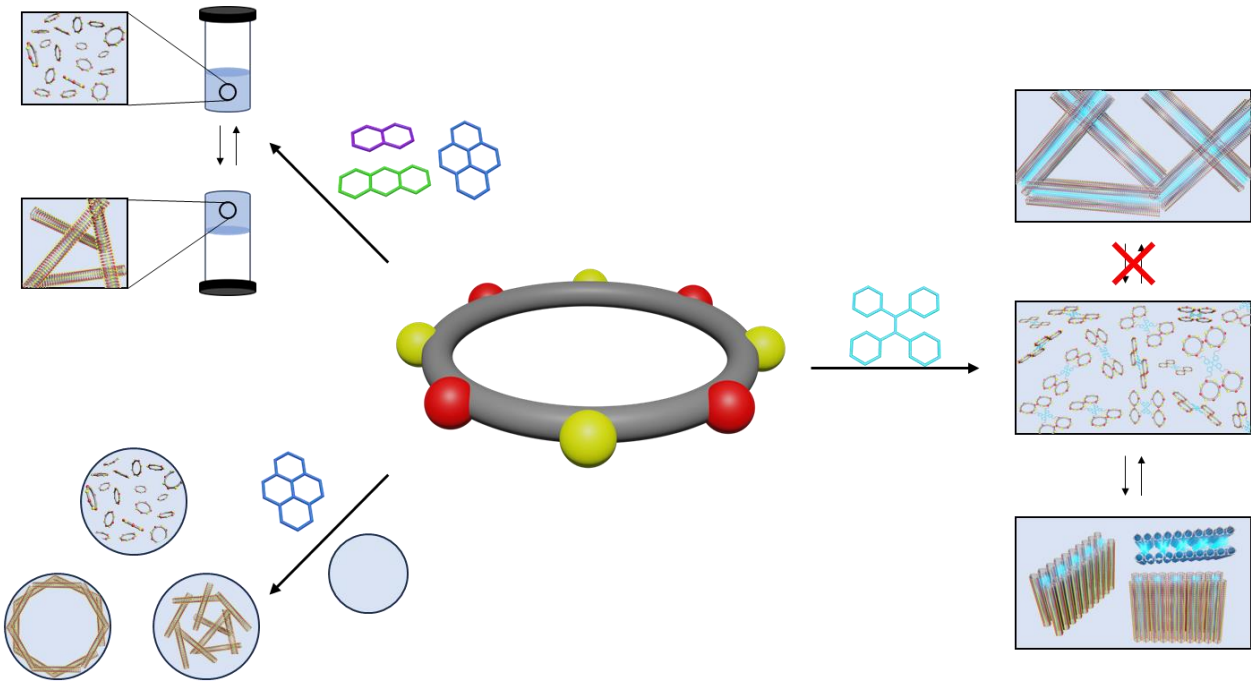

Figure 28. Schematic representation of the objectives of this thesis. On the top left corner, it is shown how the reaction of the CPs with different aromatic units leads to family of pH responsive hydrogelators. On the bottom left corner, the combination of microfluidics with different stimuli (pH and ionic force) leads to the spatial self-assembly. On the right side, the formation of a tetra-CP by the reaction with a TPE unit leads to the formation of 2D materials instead of the expected fibers.

Recently it has been demonstrated that eight residues α-(*D,L*)-CPs specifically modified with a pyrene moiety are able to form a pH responsive hydrogel. Based on these results, the first objective of this work was to develop a family of CPs that would allow controlling their hydrogelation and macroscopic properties through the molecular design of the cyclopeptide units. The key feature of the original design was the incorporation of the aromatic moiety by an oxime condensation between the CP bearing an alkoxyamine and an aromatic aldehyde. This reactive site would allow the condensation with different aldehydes to tune the π,π-stacking interactions. Additionally, a second variable was the use of two peptide scaffolds with one or two alkoxyamine groups. The combination of these two variables would provide the tools to generate the desired library (Figure 28, top left). The characterization of the properties of the resulting hydrogels would

provide the necessary bases to be able to design new CPs hydrogelators on demand according to the desired applications.

The previously mentioned CP-pyrene conjugate also retains its self-assembly capabilities under confined environment behaving as a mimetic of cellular matrix. This capability is fundamental for the design of artificial materials that mimic the behavior of the cell cytoskeleton and help to understand its basic structural functions in which the precise spatiotemporal assembly/disassembly control and orthogonality is required. For this reason, the second objective of this Thesis was to determine whenever the assembly pathway could influence the preferred distribution of CP nanotube bundles within confined spaces. To this end, it was envisaged that the use of finely controlled mixing using microfluidic techniques could be a powerful tool. For this purpose, we chose to use a microfluidic device to evaluate different aspects (concentration of components, mixing flows, addition of different additives, etc.) to achieve high control over the encapsulation process and the ability to respond to external stimuli of the encapsulated CP (Figure 28, bottom left).

The spatial control of the self-assembly of the peptide under different stimulus brought a step closer the objective of mimicking the cytoskeleton. However, the cytoskeleton has an exquisite control over the structure of fiber assemblies, controlling the diameter and the crosslinking points. In the previous studies, we have observed a large size variability of the diameter of the final assemblies. Consequently, we decided to take a step forward to develop homogeneous fibers by covalently attaching a known number of CP units on a central core. Specifically, we thought about using four CP units linked to a tetraphenylethylene core. This central core has also the advantage of reporting their assembly properties thanks to its fluoroscopic properties. However, the preliminary studies showed that the structures resulting from the 4CP-TPE shell-core did not lead to the formation of SCPNs fibers but instead formed 2D sheets (Figure 28, right). This result switched our objective of pursuing homogeneous fibers towards unveiling the structural parameters that drive the 2D growth. To achieve such aim, different CP and TPE derivatives were designed to dilucidated the driving force for the 2D growth.

METHODOLOGY

1. Self-Healing Cyclic Peptides Hydrogels

1.1. Materials

The reagents were acquired from Fluka, Aldrich, Iris Biotech or TCI. ^{1}H NMR was acquired on a Varian 300 MHz spectrometer. Chemical shifts (δ) are reported in ppm relative to TMS (δ = 0). All spectra were normalized with respect to the residual solvent signal. Infrared spectra were recorded on a PerkinElmer Spectrum Two ATR instrument. Analytical HPLC was carried out in an Agilent 1260 Infinity II LC System equipped with an Agilent SB-C18 column and connected to a 6120 Quadrupole LCMS. HR-MS was acquired in a Bruker Microtof instrument. Compounds 1T and **1TP** were prepared as described elsewhere.[304]

1.2. Formation of gels

A solution of the peptide in milliQ water (2.5% w/w) was thoroughly sonicated in milliQ water (30 min to 1 h) until complete solubilization. Then, an aqueous solution of NaOH (0.1 M, 2.3 equiv.) was added, and the concentration was adjusted with milliQ water to give a final CP concentration of 11 mM. The pH of the resulting gel was measured using a pH electrode. The final pH values in these gels ranged from 8.3 to 9.0.

1.3. Measurement of viscoelastic properties of the gel

Viscoelastic properties of gels were measured using an Anton Paar MCR-302 rheometer in a parallel plate (15 mm in diameter) set up with a gap of 0.5 mm. In frequency sweep experiments, storage and loss moduli were recorded at angular frequencies of 0.1–100 rad s^{-1} at a constant shear strain of 5% and 20ºC.

1.4. Fluorescence measurements

Fluorescence measurements were carried out using a Varian Cary Eclipse fluorescence spectrophotometer. Fluorescence spectra were recorded at 20ºC with an averaging time of 0.5 s. The samples were prepared at different pH values and measured using a drop pH meter. The emission measurements were carried out at the excitation indicated in the corresponding figure. For CAC determination, emission spectra of dilutions of CPs in HEPES (10 mM, pH 8) containing 20 μM ThT were obtained at an excitation emission of 440 nm. Fluorescence was normalized by dividing the fluorescence at a given wavelength (I_λ) by the maximum observed fluorescence intensity (at the current acquisition), measured at λ_{max} ($I_{\lambda max}$), that is N.I. = $I_\lambda/I_{\lambda max}$.

1.5. Scanning transmission electron microscopy

Cu grids (300 mesh, coated with carbon grid, Ted Pella) were used to deposit the samples at the concentration of 0.011 mM obtained from gels (pH 8.3–9.0). The samples were stained with 15 μL uranyl acetate (2%) and dried overnight. The STEM images were recorded using a Zeiss Ultra

Plus scanning transmission electron microscope operating at an extra high tension of 20 kV. Nanotube distributions were analyzed manually using ImageJ.[323,324]

1.6. Scanning electron microscopy

Gels were frozen with liquid nitrogen and then broken into small pieces. Fragments belonging to the core of the gel were immediately freeze-dried overnight. The gels were coated with a conductive Ir layer (10 nm) using a Sputter Coater (QUORUM Q150T-S). SEM images were acquired on a Zeiss Ultra Plus scanning transmission electron microscope operating at an extra high tension of 20 kV.

1.7. Fluorescence microscopy

Epifluorescence measurements were carried out at room temperature using an Olympus BX51 microscope with magnifications of 20x and 40x. All images were analyzed using ImageJ.[323,324]

1.8. Atomic force microscopy

Atomic force microscopy measurements were carried out on a Park Systems NX-10 microscope. ACTA tips were used (silicon tips, nominal values: spring constant = 40 N m^{-1}, frequency = 300 kHz, ROC less than 10 nm). Aqueous samples of peptides at pH ca. 8–9 (15–20 μL, 0.11 mM) were deposited in freshly cleaved mica. After 15–20 min equilibration, the micas were thoroughly rinsed with milliQ water and dried with a steam of Ar, and then measured immediately. Image analysis was carried out using Gwyddion.[325] Typically, the profiles were levelled using the mean plane subtraction. Tip strokes were reduced by aligning rows using the means.

1.9. Synthesis of 2T

Cyclic peptides were prepared manually in solid phase as depicted in Scheme **1**. 2-Chlorotrityl chloride resins (2CTC, 500 mg, 1.6 mmol chloride per g resin) were soaked in freshly distilled DCM (4 mL) for 30 min. The solvent was filtered off, and a solution of *N*-α-(9-fluorenylmethyloxycarbonyl)-L-lysine allyl ester hydrochloride (178 mg, 0.4 mmol) and DIEA (350 mL, 2 mmol) in distilled DCM (4 mL) was added to the resin. After 2 h, the solution was filtered off and the resin was washed with DCM (4 mL). A mixture of DCM–MeOH–DIEA (8.5 : 1 : 0.5, 4 mL) was then added and the mixture was shaken for 1 h, filtered and finally successively washed with DCM (3 x 4 mL) and diethyl ether (4 mL). The resulting resin was dried under a high vacuum and the loading was determined by quantification of the Fmoc group.[326] For this, a small portion of the resin (ca. 10 mg) was treated with a solution of piperidine in DMF (1 : 4, 2 mL) for 30 min. An aliquot of this solution (20 mL) is diluted with DMF (1 mL) and the absorbance was

[323] J. Schindelin, I. Arganda-Carreras, E. Frise, V. Kaynig, M. Longair, T. Pietzsch, S. Preibisch, C. Rueden, S. Saalfeld, B. Schmid, J. Y. Tinevez, D. J. White, V. Hartenstein, K. Eliceiri, P. Tomancak and A. Cardona, *Nat. Methods*, **2012**, *9*, 676–682.
[324] C. A. Schneider, W. S. Rasband and K. W. Eliceiri, *Nat. Methods*, **2012**, *9*, 671–675.
[325] D. Nečas and P. Klapetek, *Cent. Eur. J. Phys*., **2012**, *10*, 181–188.
[326] J. Meienhofer, M. Waki, E. P. Heimer, T. J. Lambros, R. C. Makofske and C.-D. Chang, *Int. J. Pept. Protein. Res*., **1979**, *13*, 35–42.

read at 290 and 301 nm. The concentration of the dibenzofulvene–piperidine adduct is obtained using the extinction coefficients tabulated in the literature.

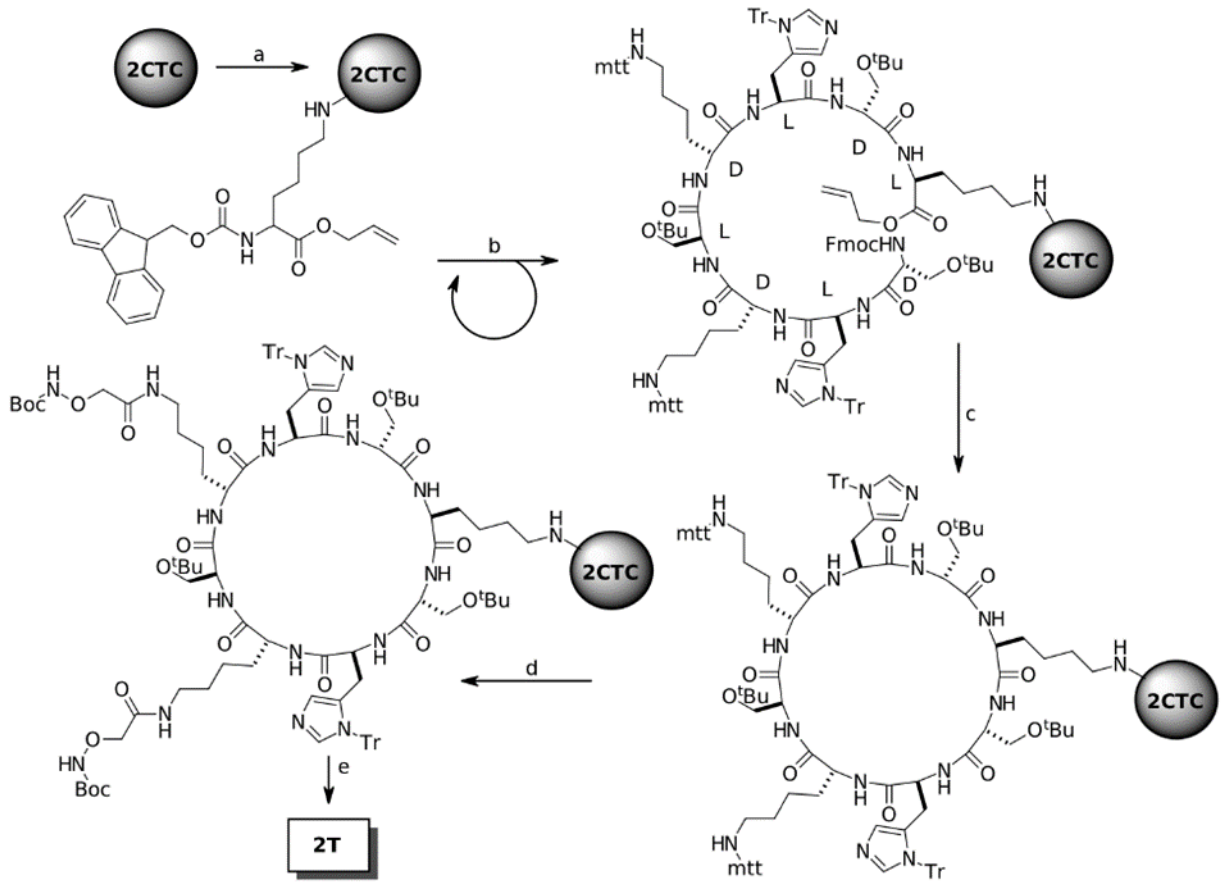

Scheme 1. Preparation of precursor **2T**: a) *N*-α-(9-Fmoc)-L-lysine allyl ester hydrochloride, DIEA, DCM, 2 h; b) i) piperidine/DMF (1:4), 10 min, ii) amino acid, *N*-HBTU, DIEA, DMF, 30 min, repeat 7 cycles with the corresponding aa; c) i) $Pd(OAc)_2$, PPh_3, phenylsilane, 4-methylmorpholine, DCM, overnight, ii) piperidine/DMF (1:4), 10 min, iii) PyAOP, DIEA, DMF, 4 h.; d) i) DCM-TFA-TIS (97.6:1.4:1), 1 h, twice ii) [(*tert*-butoxycarbonyl)aminoxy]acetic acid, *N*-HATU, DIEA, DMF, 45 min; e) TFA-DCM-H_2O-TIS (9:0.5:0.25:0.25).

A portion of resin (0.1 mmol) was used for the synthesis of the peptide. The Fmoc group was removed by treatment with piperidine/DMF (1 : 4, 2–3 mL) for 10 min. The resin was washed with DMF (6 mL) and then treated with a solution of Fmoc-protected amino acid (0.4 mmol), *N*-HBTU[327] (150 mg, 0.4 mmol) and DIEA (100 µL, 0.6 mmol) in DMF (3 mL). The resin was shaken for 30 min and then washed with DMF (3 mL). After the coupling of the last amino acid, the resin was washed with DCM (3 x 3 mL) and a solution of triphenylphosphine (39 mg, 0.15 mmol, 1.5 equiv.), *N*-methylmorpholine (110 µL, 1 mmol, 10 equiv.) and phenylsilane (120 µL, 1 mmol, 10 equiv.) in DCM (2 mL) was added, and the mixture was bubbled with argon for 10 min. Then a solution of $Pd(OAc)_2$ (6.7 mg, 0.03 mmol, 0.3 equiv.) in DCM (0.5 mL) was added dropwise and

[327] A. El-Faham and F. Albericio, *Chem. Rev*., **2011**, *111*, 6557–6602.

the resin was subsequently bubbled with Ar for 2 min. The resulting suspension was stirred for 4 h and then the resin was washed with DCM (4 x 4 mL), DIEA in DMF (2% v/v, 4 x 4 mL), sodium diethyldithiocarbamate (0.5% w/v in DMF, 4 x 4 mL) and DMF (4 x 4 mL). The resin was stirred with piperidine/DMF (1 : 4, 2 mL) for 30 min and finally, it was successively washed with DIEA in DMF (2% v/v, 4 x 2 mL) and DMF (4 x 4 mL).

Cyclization was carried out by adding a solution of PyAOP (208 mg, 0.4 mmol) and DIEA (100 μL, 0.6 mmol) in DMF (3 mL) and the suspension was stirred for at least 3 h. After washing with DMF (3 mL), the reaction was repeated once under the same conditions. For the selective removal of the 4-methyltrityl group, the resin was washed with DCM (3 x 4 mL) and then treated with a mixture of DCM/TFA/TIS (97.6 : 1.4 : 1, 3 mL). After shaking for 20 min, the mixture was filtered off and washed with DCM (3 x 3 mL). This process was repeated under the same conditions and finally the resin was washed with DCM (3 x 3 mL) and DMF (3 x 3 mL). Hereafter, a solution of (*tert*-butoxycarbonylaminoxy)acetic acid (96 mg, 0.5 mmol) and *N*-HATU (188 mg, 0.5 mmol) in DMF (1 mL) was added to the resin followed by the dropwise addition of DIEA (84 μL, 0.5 mmol) in DMF (1 mL). The resulting mixture was mechanically shaken for 45 min and finally, the resin was washed with DMF (3 x 3 mL).

The peptide was released from the resin by treatment with freshly prepared cleavage cocktail (TFA–DCM–H_2O–triisopropylsilane, 90 : 5 : 2.5 : 2.5, 3 mL) for 2 h and then filtered. The resin was washed with TFA (0.5 mL) and the combined acidic solutions were evaporated to 1–2 mL by bubbling argon. The concentrated solution was added dropwise to cold diethyl ether (10 mL diethyl ether per mL TFA). The resulting precipitate was centrifuged for 10 min at 3000 rpm. The supernatant was discarded, then diethyl ether was added, and the suspension was sonicated for 1 min and centrifuged. The sample was dried with a stream of air and dissolved in milliQ water and purified by semipreparative HPLC.

1.10. General procedure of CP conjugation with aromatic aldehydes

A portion of **1T** or **2T** was dissolved in DMSO (100 mL) containing 1.2 and 2.5 equiv. of the corresponding aldehyde, respectively. The solution was stirred at 60ºC until completion of the reaction (monitored by HPLC-MS), typically within 1.5–2 h. The cooled solution was added over diethyl ether (2 mL) and vigorously stirred. The resulting suspension was decanted and the solid was sonicated for 10 min with fresh diethyl ether, centrifuged and decanted. The procedure was repeated twice, and the solid was dried under a high vacuum to give an amorphous powder.

2. SPATIALLY CONTROLLED SUPRAMOLECULAR POLYMERIZATION OF PEPTIDE NANOTUBES

2.1. Materials

Reagents were acquired from Fluka, Aldrich, Iris Biotech or TCI. Pico-Surf™ was purchased from Sphere Fluids. Compound **1TP** was prepared as described elsewhere.[304]

The microfluidic device was produced via soft lithography by using poly(dimethylsiloxane) (PDMS) along with crosslinker (Sylgard 184™ elastomer kit, Dow Corning). Briefly, elastomer and curing agent were mixed in a ratio 10:1, thoroughly mixed and poured into the master. The mixture was degassed until no bubbles were visible, then cured in the oven at 70ºC overnight. The elastomer was cut into pieces with a sharp razor and holes punched with a 1 mm diameter biopsy

punch (kai medical). Glass slides and PDMS chips were treated with oxygen plasma for 10 seconds, then brought to contact and gently pressed. Bonding was completed by heating the chips at 120ºC for 1 h. The chips channels were treated with a solution of trichloro(1*H*,1*H*,2*H*,2*H*-perfluorooctyl)silane 1% in HFE-7500 3M™ Novec™ for a few seconds, then rinsed with fresh HFE-7500, and finally dried with a stream of Ar. Silanization was completed by heating the devices at 65ºC overnight. Solvent pumping was carried out with syringe pumps (New Era NE-4002X double microfluidics syringe pump) through bore polythene tubing (Portex, 0.38 x 0.35 mm).

2.2. Preparation 1TP droplets by microfluidics

Cyclic peptide **1TP** (1 mM) solutions were prepared in milliQ water (pH about 4) and were thoroughly sonicated (30-60 min). The oil phase was prepared by diluting the original Pico-Surf™ solution to a concentration of 0.5% v/v. The formation of droplets was visualized through a high-speed Fastcam Mini camera coupled to a Nikon Eclipse Ti2. The device used is shown in Figure 46 of the manuscript. The size of the channels was 35 x 50 µm. The oil was injected at a flow rate of 500 µL/h. The peptide was injected at a flow rate of 200–150 µL/h, and the triggering solutions at 100 µL/h unless otherwise specified. Droplets were collected over Novec™ containing 0.5% v/v Pico-Surf™.

2.3. Preparation of water-in-oil droplets of 1TP for pico-injection experiments

Droplets of **1TP** in milliQ water intended for pico-injection experiments were prepared in an X-junction chip. The size of the channels was 40 x 40 µm. The flow rates of the oil were 500 µL/h and the aqueous phase at 250 µL/h.

2.4. Pico-injection of NaOH solutions to water-in-oil droplets containing 1TP

Droplets prepared as described above were diluted with an oil stream, and pico-injection was carried out with a solution of NaOH (13 mM). To add the base of NaOH to water-in-oil droplets, the droplets of **1TP** were then reinjected into a pico-injection microfluidic device (Figure 103). Droplets were spaced by two oil inlet channels, and flowed towards a T-shaped junction, where a channel containing an aqueous solution of NaOH was injected continuously. A high voltage square waveform was applied between two electrodes positioned either side of the junction, causing fusion between a microdroplet and aqueous solution of NaOH. The content of each microdroplet is then evenly mixed as it passes through a meandering channel before exiting the device. The subsequent self-assembly process of **1TP** took place in each microdroplet independently.

2.5. STEM measurements

Cu grids (300 mesh, coated with carbon grid, Ted Pella) were used to deposit the samples at concentration as obtained from the microfluidic chip outlet. Samples were stained with 15 µL gadolinium acetate (2%) and dried overnight. STEM images were acquired in a Zeiss Ultra Plus scanning transmission electron microscope operating at an extra high tension of 20 kV.

2.6. Fluorescence microscopy

Epifluorescence measurements were carried out at room temperature using an Olympus BX51 with magnifications of 10x and 40x. All images were analyzed using ImageJ.[323,324] Measurements of percentage of fluorescent area per droplet were carried out by converting fluorescence images

into 8-bit images. Then, a grayscale threshold level was defined in order to shade all the fibers present in the droplets. Circle areas were defined manually in 20 randomly picked individual droplets, and the percentage of fluorescence in each droplet was measured.

2.7. Fluorescence spectroscopy experiments

Fluorescence measurements were carried out in a Varian Cary Eclipse fluorescence spectrophotometer. Fluorescence spectra were acquired at 20ºC with an averaging time of 0.5 s.

2.8. Circular dichroism experiments

Circular dichroism spectra were acquired in a Jasco J-1100 CD spectrometer. Data was obtained at 20ºC in a 2 mm light path quartz cuvette after subtraction of the solvent background signal.

2.9. Laser Scanning Confocal Microscopy

Confocal images were acquired using an Andor DragonFly confocal setup mounted on a Nikon Eclipse Ti-E inverted microscope.

2.10. Preparation of cyclopeptide networks

Typically, 5-10 μL of droplets suspended in HFE-7500 containing Pico-Surf™ (0.5% v/v) were deposited on glass slides, then allowed to dry at room temperature for at least 15 min. Networks were sealed with imaging spacers (Grace Bio-Labs SecureSeal™) and visualized under the fluorescence microscope.

2.11. Charge screening

In order to study the effect of the counterions in the self-assembly of nanotubes, we carried out a comparative study of the addition of NaCl, $CaCl_2$ and Na_2SO_4 at the same calculated ionic strength. Molar ionic strength is given by the following equation:

$$I = \frac{1}{2}\sum_{i=1}^{n} c_i z_i^2$$

where c is the concentration of the ion and z the charge. Taking into account only the more concentrated species (electrolites and MES buffer), the calculated molar ionic strength for NaCl (1.5 M), $CaCl_2$ (0.5 M) and Na_2SO_4 (0.5 M) in MES (50 mM) is about 1.55 M.

2.12. Diffusion of chemical species in the microfluidic device

In order to gain some insights into the diffusion of the chemical species within the microfluidic channels,[328] we estimated the diffusion coefficient for cyclic peptides based on reported hydrodinamic radius (r_H) obtained for peptide dimers in our own group by DOSY experiments. Measured r_H in $CDCl_3$ of 3-aminocyclohexanecarboxylic acids-based octapeptide dimers[329] gave values of $r_H \sim 0.7$ nm. We can estimate the diffusion coefficient in water according the Stokes-

[328] C. Stoffelen, R. Munirathinam, W. Verboom and J. Huskens, *Mater. Horiz.*, **2014**, *1*, 595–601.
[329] A. Fuertes, H. L. Ozores, M. Amorín and J. R. Granja, *Nanoscale*, **2017**, *9*, 748–753.

Einstein equation, that relates the hydrodinamic radius with the diffusion coefficient (D) for particles in liquids at low Reynolds number:

$$D = \frac{kT}{6\pi\eta r_H}$$

where k is the Boltzmann constant, T is the temperature and η is the medium viscosity. Assuming a temperature of 298 K, the diffusion coefficient in water of an octapeptide dimer is about 3.7 x 10^{-10} m^2s^{-1}. Although the expected diffusion coefficient for a monomer will be lower, the calculated value can give us an idea of the extent of diffusion within the microfluidic channel. In this sense, the Einstein-Smoluchowski equation for planar diffusion was used to calculate the time required for the chemical species to reach the other side of the channel:

$$t = \frac{d^2}{2D}$$

where d was estimated as 1/4 of the total microfluidic channel width (35 µm) and D are tabulated[330] and estimated diffusion coefficients in water for the chemical species involved in the assembly within the microfluidic channel. The calculated times are shown in Table 1. Taking into account the dimensions of the channel (35 µm x 50 µm) and that the distance between the two junctions *J*1 and *J*2 is approximately 1100 µm, a flow rate of 350 µL/h will have a residence time of approximately 20 ms.

Table 1. Reported and calculated diffusion coefficients of chemical species injected in the microfluidic device and calculated diffusion time for the chemical species at the interface to reach the other side of the channel.

Chemical species	Diffusion coefficient (m^2s^{-1})	t (ms)
OH^-	52.7 x 10^{-10}	7
Cl^-	20.3 x 10^{-10}	19
Ca^{2+}	7.92 x 10^{-10}	48
CP	3.7 x 10^{-10}	103

We hypothesize that assembly is initiated within the microfluidic device, but final equilibration takes place within the confined aqueous compartment. In this sense, simple theoretical calculation suggests that the diffusion of anions (Cl^-, OH^-) can reach the center of the peptide stream before reaching junction *J*2. On the other hand, fluorescence experiments in bulk solutions indicate that equilibration occurs in more than 10 minutes (Figure 105), which suggests that equilibration cannot take place within the microfluidic channel.

3. 2D Assemblies Based on a Tetraphenylethylene D,L-Cyclic Peptide Scaffold

3.1. Materials

The reagents were acquired from Fluka, Aldrich, Iris Biotech, Carbolution or TCI. All other reagents obtained from commercial suppliers were used without further purification.1H NMR was

[330] D. R. Lide and H. V Kehiaian, *CRC Handbook of Thermophysical and Thermochemical Data*, CRC Press, 1st edn., **1994**.

acquired on a Varian 500 MHz spectrometer. Chemical shifts (δ) are reported in ppm relative to TMS (d = 0). All spectra were normalized with respect to the residual solvent signal. Infrared spectra were recorded on a PerkinElmer Spectrum Two ATR instrument. Analytical HPLC was carried out in an Agilent 1260 Infinity II LC System equipped with an Agilent SB-C18 column and connected to a 6120 Quadrupole LCMS. HR-MS was acquired in a Bruker Microtof instrument.

3.2. UV and Fluorescence measurements

UV and fluorescence measurements were done in a Jasco V-770 and a Varian Cary Eclipse respectively. Both spectra were acquired at room temperature. Samples were prepared at different pH values and measured with a pH meter before measuring. For CAC determination, emission spectra of dilutions of CPs in HEPES (20 mM, pH 8), MES (20 mM, pH 6) or TFA (0.1%, pH 2) containing 10 μM ThT were obtained at an excitation emission of 440 nm.

3.3. Epifluorescence imaging

Epifluorescence measurements were carried out at room temperature using a Nikon Eclipse Ti microscope (1) (DAPI cube: Ex=387/11 nm and Em=447/60 nm; FITC cube: Ex=475/35 nm and Em=530/43 nm; magnifications of 10x, 20x and 60x) or an Olympus BX51 microscope (2) (DAPI cube: Ex=365/5 nm and Em=420 nm; magnifications of 20x and 40x). The general seeding procedure was to equilibrate aqueous samples of peptides (10 μL) for 10 min and right after, rinse them with milliQ water and let them dry. Pipetted and scratched samples were visualized in solution.

3.4. Scanning transmission electron microscopy imaging

Cu grids (300 mesh, coated with carbon grid, Ted Pella) were used to deposit aqueous samples of peptides (10 μL). After 10 min equilibration, the grids were rinsed with milliQ water and dried. The STEM images were recorded using a Zeiss Ultra Plus scanning transmission electron microscope operating at an extra high tension of 20 kV.

3.5. Atomic force microscopy imaging

AFM measurements were carried out on a Park Systems NX-10 microscope. ACTA tips were used (silicon tips, nominal values: spring constant = 40 N m-1, frequency = 300 kHz, ROC less than 10 nm). Aqueous samples of peptides (10 μL) were deposited in freshly cleaved mica. After 10 min equilibration, the micas were rinsed with milliQ water and dried. Image analysis was carried out using Gwyddion. Typically, the profiles were levelled using the mean plane subtraction. Tip strokes were reduced by aligning rows using the means.

3.6. Synthesis of peptides

All CPs were prepared manually in solid phase as shown in Scheme 2.

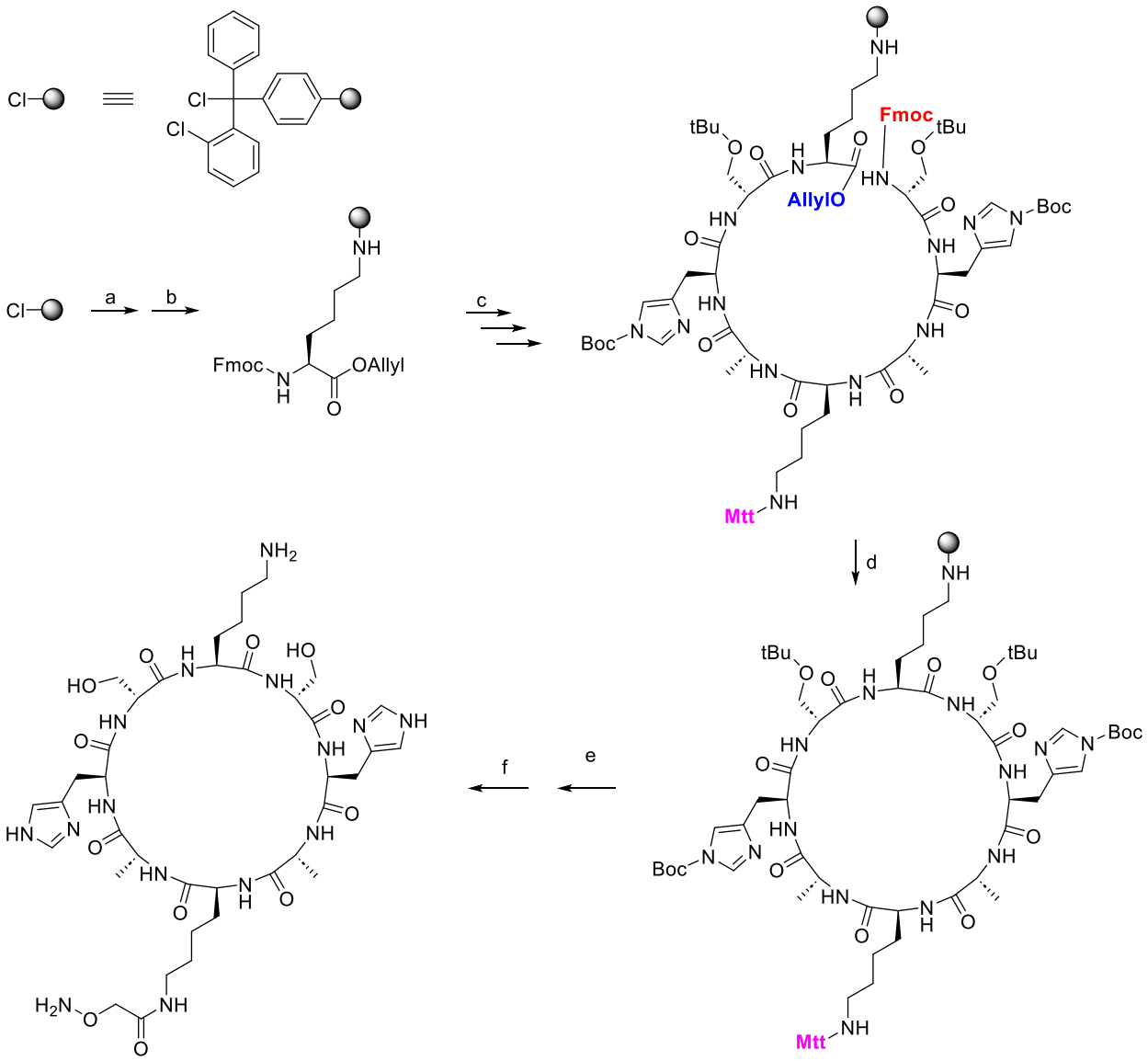

Scheme 2. Solid phase peptide synthesis scheme (e.g., 1T): a)1st aa coupling: Fmoc-L-Lys-OAll*HCl, DIEA, DCM f.d., 2 h; b) Capping: DCM/MeOH/DIEA (8.5:1:0.5), 1h, c) Linear peptide growth: i) piperidine/DMF (1:4), 10 min, ii) aa, N-HBTU, DIEA, DMF, 15 min, repeat 7 cycles with the corresponding aa; d) Cyclization: i) Pd(OAc)2, PPh3, phenylsilane, 4-methylmorpholine, DCM f.d., 4h, ii) piperidine/DMF (1:4), 30 min, iii) PyAOP, DIEA, DMF, 2h, e)Selective modification of Lys residue: i) DCM/TFA/TIS (97.6:1.4:1), 10 min, thrice, ii) (Boc-aminooxy)acetic acid, N-HATU, DIEA, DMF, 45 min, f) TFA/DCM/H2O/TIS (9:0.5:0.25:0.25).

3.6.1. Coupling of the first aa.

a) 2CTC based peptides (CP_{3A}, $CP_{2,8H}$, $CP_{4,6H}$, $CP_{6,8H}$, CP_{7R}, CP_{5Dap}, $CP_{H(Me)}$).

2CTC (500 mg, 1.6mmol/g resin) was swelled in distilled DCM (4 mL) for 10 min. Right after the resin was treated with a solution of Fmoc-L-Lys-OAll*HCl (0.8 mmol) and DIEA (2.4 mmol) in distilled DCM (4 mL) for 2h. Then the resin was washed and a mixture of DCM/MeOH/DIEA (8.5:1:0.5, 4 mL) was added and shaken for 1 h. The resin was washed with DCM (3 x 4 mL) and

diethyl ether (2 x 4 mL). The resulting resin was dried under a high vacuum. The new loading of the resin was determined by quantification of the Fmoc group.[326] For this, a portion of the resin (ca. 10 mg) was treated with piperidine/DMF (1:4, 1mL) for 30 min. An aliquot of this solution (10 μL) is diluted with DMF (990 μL) and the absorbance was read at 290 and 301 nm. The concentration of the dibenzofulvene–piperidine adduct is obtained using the extinction coefficients tabulated in the literature (ε_{290}=5800 and ε_{301}=7800). Only a portion of resin (0.2 mmol) was used for the synthesis of the peptides.

b) Wang-resin based peptides (CP_{1E}).

Wang resin (500 mg, 0.62mmol/g resin) was swelled in distilled DCM (4 mL) for 10 min. Right after the resin was treated with a solution of Fmoc-L-Glu-OAll (1.5 mmol), HOBt (1.24 mmol), DIC (1.24 mmol) and DMAP (0.06 mmol) in distilled DCM/DMF (8:2, 6 mL) for 3h. Then the resin was washed with DMF (3 x 4 mL) and DCM (3 x 4 mL). A mixture of acetic anhydride/2,6-Lutidine (1:1, 4 mL) was added and shaken for 30 min. The resin was washed with DMF (3 x 4 mL), DCM (3 x 4 mL) and diethyl ether (2 x 4 mL). The resulting resin was dried under a high vacuum. The new loading of the resin was determined as in the previous case.

c) Rink Amide-resin based peptides (CP_{1Q}).

The Fmoc-Rink amide resin (0.2 mmol – 315mg, 0.64mmol/g resin) was swelled in DMF (4 mL) for 20 min followed by the Fmoc removal (piperidine/DMF (1:4, 4 mL) for 20 min. After washing the resin with DMF (3 x 4 mL), it is treated with Fmoc-L-Glu-OAll (0.6 mmol), HBTU (0.6 mmol) and DIEA (1.2 mmol) in DMF (4 mL) for 30 min. The resin is washed with DMF (3 x 4 mL).

3.6.2. Linear peptide growth

The resin was swelled in DMF (4 mL) for 10 min followed by the synthesis of the linear peptide. For this, cycles of Fmoc removal (piperidine/DMF (1:4, 4 mL) for 10 min, washes with DMF (3 x 4 mL), aa coupling (Fmoc-protected amino acid (0.6 mmol), HBTU (0.6 mmol) and DIEA (1.2 mmol) in DMF (4 mL) for 15 min) and washes with DMF (3 x 4 mL).

3.6.3. Cyclization

To remove the OAllyl group, the resin was washed with DCM (3 x 3 mL) and a solution of Pd(OAc)2 (0.06 mmol), triphenylphosphine (0.3 mmol), N-methylmorpholine (2 mmol) and phenylsilane (2 mmol) in DCM (4 mL) was added. The mixture was bubbled with argon for 10 min and stirred for 4h. Afterwards, the resin was washed with DCM (3 x 4 mL), DIEA in DMF (2% v/v, 3 x 4 mL), sodium diethyldithiocarbamate (0.5% w/v in DMF, 3 x 4 mL) and DMF (3 x 4 mL). For Fmoc removal the resin was stirred with piperidine/DMF (1:4, 2 mL) for 30 min and washed with DIEA in DMF (2% v/v, 3 x 4 mL) and DMF (4 x 4 mL). Finally, cyclization was carried out by adding a solution of PyAOP (0.6 mmol) and DIEA (1.2 mmol) in DMF (3 mL) for 2 h. After washing with DMF (3 x 4 mL), the reaction was repeated once under the same conditions.

3.6.4. Selective modification of Lys residue

The selective removal of the 4-methyltrityl group was achieved by washing the resin with DCM (3 x 4 mL) and treating it with a mixture of DCM/TFA/TIS (97.6:1.4:1, 4 mL) for 10 min.

This process was repeated under the same conditions twice more. Afterwards, the resin was washed with DCM (3 x 4 mL) and DMF (3 x 4 mL) and treated with a solution of (Boc-aminooxy) acetic acid (0.4 mmol), HATU (0.4 mmol) and DIEA (0.5 mmol) in DMF (4 mL) for 45 min.

3.6.5. Peptide cleavage and purification

The peptide was released from the resin by treatment with cleavage cocktail (TFA/DCM/H2O/TIS, 90:5:2.5:2.5, 4 mL) for 2 h and then filtered. The resin was washed with TFA (0.5 mL) and the solution was evaporated to 1–2 mL under a flow of argon. The concentrated solution was added dropwise to cold diethyl ether (40 mL). The resulting precipitate was centrifuged for 10 min at 4000 rpm. The supernatant was discarded and the solid was washed with diethyl ether twice. The pellet was dried with a stream of air and dissolved in milliQ water. The peptides were all purified by preparative HPLC using a C18 column [equilibration after injection with H2O/0.1% TFA–ACN/0.1% TFA 100:0 for 2 min followed by a gradient of H2O/0.1% TFA–ACN/0.1% TFA 100:0 (2 min) to 80:20 (32 min)]. The corresponding fractions were concentrated in vacuo and lyophilized, giving a white powder in all cases. Retention times, amounts and yields can be observed in Table 2.

Table 2. Retention times, amounts, and yields of the different peptide derivatives.

Peptide	R_t (min)	Amount (mg)	Yield (%)
CP_1	16.8	47.5	19
CP_{1E}	18.9	56.1	24
CP_{1Q}	18.7	57.6	25
CP_{3A}	19.3	28.9	13
CP_{7R}	18.5	55.4	21
CP_{5Dap}	14.9	45.3	16
$CP_{2,8H}$	18.4	55.7	22
$CP_{4,6H}$	17.9	35.4	14
$CP_{6,8H}$	19.1	31.4	12
$CP_{H(Me)}$	16.2	43.8	17

3.7. Synthesis of CP-TPE derivatives

The desired amounts of TPE (e.g., TPE_4, 1mg, 0.0022 mmols) and peptide (e.g., 1T, 19.9mg, 0.0157 mmols, 7 equivalents) were solved in DMSO separately and then mixed. To achieve the condensation of the alkoxyamine with the corresponding aldehydes, the reaction was stirred at 60ºC until the reaction is completed (monitored by HPLC-MS), usually in around 2 h. The reaction was cooled to rt, and the solution was washed with ether (1 mL, x5) to remove DMSO and precipitate the final product. The pellet was dried and dissolved in milliQ water. The peptides were all purified by preparative HPLC using a C18 column [equilibration after injection for 2 min with H2O/0.1% TFA–ACN/0.1% TFA 100:0 followed by a gradient of H2O/0.1% TFA–ACN/0.1% TFA 100:0 (2 min) to 25:75 (32 min)]. The corresponding fractions were lyophilized, giving a light-yellow powder in all cases. Retention times, amounts and yields can be observed in Table 3.

Table 3. Retention times, amounts, and yields of the different CP-TPE derivatives.

Peptide	R_t (min)	Amount (mg)	Yield (%)
4CP$_{1k}$-U-TPE	17.8	8.2	67
4CP$_{1E}$-U-TPE	32.1	5.96	66
4CP$_{1Q}$-U-TPE	30.6	0.6	6
4CP$_{3A}$-U-TPE	29.5	1.97	15
4CP$_{7R}$-U-TPE	18.2	4.6	37
4CP$_{5Dap}$-U-TPE	16.8	7.65	65
4CP$_{2,8H}$-U-TPE	18.2	4.5	46
4CP$_{4,6H}$-U-TPE	17.5	4.0	75
4CP$_{6,8H}$-U-TPE	17.9	1.2	22
4CP$_{H(Me)}$-U-TPE	18.1	7	56
1CP$_{1k}$-U-TPE	26.9	2.5	39
4CP$_{1k}$-U-TPE$_{OH}$	17.2	7.9	52
4CP$_{1k}$-U-TPE$_{PEG}$	18.2	8.6	58

RESULTS

1. SELF-HEALING CYCLIC PEPTIDE HYDROGELS

The results of this chapter have been published in Journal of Material Chemistry B as:

A. Bayón-Fernández,[a] A. Méndez-Ardoy,[a,b] C. Alvarez-Lorenzo,[c] J. R. Granja[a] and J. Montenegro.[a] Self-healing cyclic peptide hydrogels. *J. Mater. Chem. B*. **2023**, *11* (3), 606-617. DOI: 10.1039/d2tb01721k

Affiliations

[a] Centro Singular de Investigación en Química Biolóxica e Materiais Moleculares (CIQUS), Departamento de Química Orgánica, Universidade de Santiago de Compostela, 15782 Santiago de Compostela, Spain.

[b] Institute for Chemical Research, IIQ, CSIC-Universidad de Sevilla, C/Américo Vespucio 49, 41092 Sevilla, Spain.

[c] Departamento de Farmacología, Farmacia y Tecnología Farmacéutica, I+D Farma Group (GI-1645), Facultad de Farmacia, iMATUS and Health Research Institute of Santiago de Compostela (IDIS), Universidade de Santiago de Compostela, 15782 Santiago de Compostela, Spain.

[331] A. Bayón-Fernández, A. Méndez-Ardoy, C. Alvarez-Lorenzo, J. R. Granja and J. Montenegro, *J. Mater. Chem. B*, **2023**, *11*, 606–617.

1.1. Precedents

1.1.1. Gels: definition and classification

Gels can be defined as tridimensional networks formed by a dispersed phase (molecules) that provides rigidity and limits the flow of the dispersant (liquid).[332] Over the years two main classification systems have been developed attending to the nature of their components. On one hand the employed solvent, this is water or an organic solvent, which gives rise to hydro- or organogels, respectively.[333] The dispersant (solvent), since it is the main component of these systems, has a huge impact on the gel applications. In this sense, water is the main solvent in living systems, which is why hydrogels have attracted the attention of scientists due to their numerous biological applications.

Table 4. Summary of some relevant properties for the application of hydrogels in biomedicine. Reprinted with permission from Ref.334. Copyright © 2017 Elsevier Ltd.

	Polymeric		Supramolecular
Properties\Crosslink	Covalent (I)	Non-Covalent (II)	Non-Covalent
Mechanical strength	Very strong	Strong	Weak
Tunability	Poor	Good	Excellent
Bio-stimuli responsiveness	Poor	Good-excellent	Excellent
Biocompatibility	Not good	Good-excellent	Excellent
Mimicry of extracellular matrix	Poor	Excellent	Good-excellent
Reversibility	No	Yes	Yes
Degradation	Poor	Good-excellent	Excellent
Biological functionalities	Poor	Excellent	Excellent

On the other hand, gels can be classified attending to the nature of the material and crosslinking points in polymeric type I (covalent crosslinking), polymeric type II (non-covalent crosslinking) or supramolecular.[334] Both, type of materials and cross-linkings, are extremely related to the properties (Table 4). In this sense, covalent crosslinks provide gels with very high mechanical strength, but at the same time limit their dynamic responsiveness. In addition, the use of toxic components in covalent crosslinking steps limits their possible biological and environmental applications.[335] On the contrary the dynamic nature of the physically crosslinked gels is related with a fast stimuli responsiveness and self-repairing capabilities after damage.[336] These properties paved the way for their use in drug delivery,[337] 3D-cell cultures,[338] or catalysis,[339] among others.[340]

[332] J. D. Ferry, *Viscoelastic properties of polymers*, John Wiley & Sons, New York, 3rd edn., **1980**.
[333] M. A. Kuzina, D. D. Kartsev, A. V. Stratonovich and P. A. Levkin, *Adv. Funct. Mater*., **2023**, *33*, 2301421.
[334] J. Zhou, J. Li, X. Du and B. Xu, *Biomater.*, **2017**, *129*, 1–27.
[335] E. A. Appel, J. del Barrio, X. J. Loh and O. A. Scherman, *Chem. Soc. Rev*., **2012**, *41*, 6195–6214.
[336] Y. S. Zhang and A. Khademhosseini, *Science*, **2017**, *356*, eaaf3627.
[337] J. Li and D. J. Mooney, *Nat. Rev. Mater*., **2016**, *1*, 16071.
[338] G. Fichman and E. Gazit, *Acta Biomater*., **2014**, *10*, 1671–1682.
[339] W. Fang, Y. Zhang, J. Wu, C. Liu, H. Zhu and T. Tu, *Chem. Asian J*., **2018**, *13*, 712–729.
[340] X. Du, J. Zhou, J. Shi and B. Xu, *Chem. Rev*., **2015**, *115*, 13165–13307.

1.1.2. Peptide hydrogels

As mentioned above, control of the physicochemical parameters of gels, such as stiffness or stress relaxation, is essential for the development of adaptive materials to specific applications.[341,342] In this context, supramolecular hydrogels are of particular interest because their assembly and emerging properties can be encoded in small building blocks (hydrogelators).[343] Generally, hydrogelators are amphiphilic molecules soluble in water able to respond to a change in the media conditions, enhancing the interaction between their hydrophobic domains leading to aggregation and gelation.[344] Frequently, the self-assembled structures bury the hydrophobic components in the core of the fiber while exposing the hydrophilic regions to the surrounding medium, determining the properties of the fiber surface.[239]

In general, these supramolecular polymerizations can be triggered by different stimuli, such us temperature, ionic force, pH, redox or catalysis.[345] Although many hydrogelators with different stimuli responsiveness properties have been described over the years, pH changes remain one of the simplest chemical stimuli to trigger the gelation process. Furthermore, these pH variations occur in many natural processes, such us inflammation or cancer diseases, and therefore make them especially suitable for biomedical applications.[346] To achieve this responsiveness, groups susceptible of changing their protonation state under physiological conditions are introduce into the structure of the hydrogelators. It is known that the change in protonation state has a direct impact on the hydrophilic-hydrophobic balance and intermolecular forces,[242] on the strength of H-bonds and the conformation of hydrogelators that promote aggregation and formation of hydrogels.[334,340]

There are many hydrogelators described in the literature, some of which have been mentioned in the general introduction. These are usually classified based on the nature of the structure, such as peptide or DNA hydrogelators, or the presence of a specific chemical group, such as those based on urea or pyridine.[340] Among other designs, peptide hydrogels have attracted the attention for biomedical applications due to their easy synthesis and their inherent biocompatibility and biodegradability.[338] Peptide hydrogelators can self-assemble through non-covalent interactions, such as, H-bonds, electrostatic interactions or π-π stacking, along with hydrophobic effect.[347,348] Moreover, the presence of acid (Glu, Asp) and basic (Arg, Lys, His) amino acids in the peptide scaffold, opens the possibility to design pH responsive hydrogels.[340] Additionally, charge complementarity has also been exploited on pH responsive peptides to enhance the stability of the assemblies over a wider pH range.[243,349] Additionally, the hydrogel mechanical properties can be

---

[341] O. Chaudhuri, L. Gu, D. Klumpers, M. Darnell, S. A. Bencherif, J. C. Weaver, N. Huebsch, H. P. Lee, E. Lippens, G. N. Duda and D. J. Mooney, *Nat. Mater*., **2016**, *15*, 326–334.
[342] O. Chaudhuri, S. T. Koshy, C. Branco Da Cunha, J. W. Shin, C. S. Verbeke, K. H. Allison and D. J. Mooney, *Nat. Mater*., **2014**, *13*, 970–978.
[343] L. A. Estroff and A. D. Hamilton, *Chem. Rev.*, **2004**, *104*, 1201–1217.
[344] T. R. Hoare and D. S. Kohane, *Polymer*, **2008**, *49*, 1993–2007.
[345] N. Chirani, L. Yahia, L. Gritsch, F. L. Motta, S. Chirani and S. Faré, *J. Biomed. Sci*., **2015**, *4*, 1–23.
[346] M. C. Koetting, J. T. Peters, S. D. Steichen and N. A. Peppas, *Mater. Sci. Eng. R Rep*., **2015**, *93*, 1–49.
[347] I. W. Fu, C. B. Markegard and H. D. Nguyen, *Langmuir*, **2015**, *31*, 315–324.
[348] Y. Li, F. Wang and H. Cui, *Bioeng. Transl. Med*., **2016**, *1*, 306–322.
[349] S. Panja, B. Dietrich, O. Shebanova, A. J. Smith and D. J. Adams, *Angew. Chem. Int. Ed*., **2021**, *60*, 9973–9977.

controlled by altering the number[350] or position[351] of aa, modulating the hydrophobicity[350,352] or co-assembling different peptide structures.[353] For all these reasons, peptide scaffolds offer a suitable variety of amino acids to achieve the desired mechanical properties and pH-dependent sol-gel transition.

1.1.3.Examples

Previously (Introduction, section 3.2.2) we briefly introduced some peptide-based materials that can form hydrogels. Here we will further review some of those examples to highlight the mentioned characteristics of peptides and hydrogels. In this sense, there are many different stimuli that can be used to trigger the gel formation. Recently, Pappas *et al*. developed an enzymatically activated peptide gelator.[254] To such aim, they selected the dipeptide methyl ester (H-DF-OMe) able to form transient structures in the presence of α-chymotrypsin. The enzymatic addition of a third amino acid (X = Trp, Tyr, Phe, Leu, Val, Ser, or Thr) should form a family of tripeptides (H-DFX-NH2) with gel capabilities (Figure 29a).[354,355] However, no gel or tripeptide formation was observed for the Trp, Leu, Val, Ser, and Thr derivatives. In contrast, transient peptide formation and gelation was observed when using Phe and Tyr with hydrogel lifetimes of 24 and 4 h, respectively (Figure 29b,c). The higher stability of the hydrogel forming tripeptides, suggest that nanofibers are less prone to enzymatic hydrolysis. Finally, a competitive assay of these derivatives revealed that the kinetic selection of the nanostructures is favored rather than the thermodynamic control.

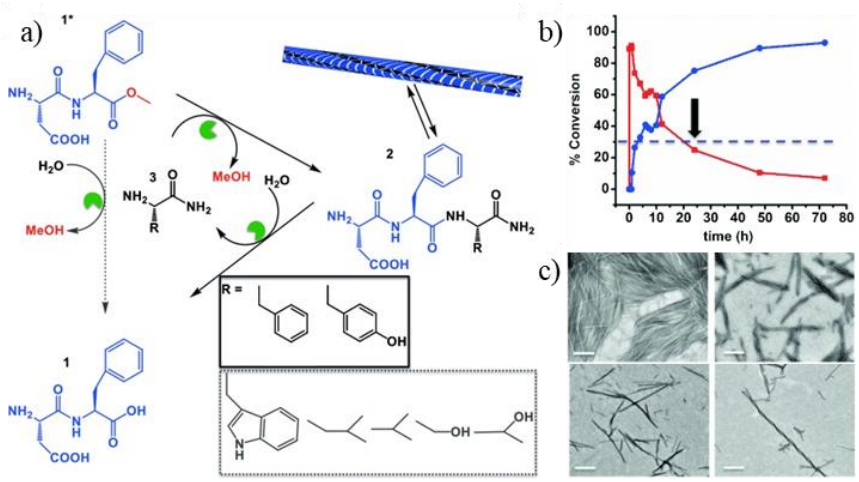

Figure 29. a) Scheme of the transient biocatalytic formation of tripeptide hydrogelator from a dipeptide precursor in the presence of α-chymotrypsin; b) quantitative relation between the DFF tripeptide (red line) and the degradation product DF (blue line); and c) fibers at different times from 0.08 (top left) to 72h (bottom right). Adapted with permission from Ref.254. Copyright © 2015 WILEY-VCH Verlag GmbH & Co. KGaA, Weinheim.

[350] L. M. De Leon Rodriguez, Y. Hemar, J. Cornish and M. A. Brimble, *Chem. Soc. Rev*., **2016**, *45*, 4797–4824.
[351] D. E. Clarke, C. D. J. Parmenter and O. A. Scherman, *Angew. Chem. Int. Ed*., **2018**, *57*, 7709–7713.
[352] E. T. Pashuck, H. Cui and S. I. Stupp, *J. Am. Chem. Soc*., **2010**, *132*, 6041–6046.
[353] J. M. Anderson, A. Andukuri, D. J. Lim and H. W. Jun, *ACS Nano*, **2009**, *3*, 3447–3454.
[354] J. Fastrez and A. R. Fersht, *Biochem*., **1973**, *12*, 2025–2034.
[355] P. W. J. M. Frederix, G. G. Scott, Y. M. Abul-Haija, D. Kalafatovic, C. G. Pappas, N. Javid, N. T. Hunt, R. V. Ulijn and T. Tuttle, *Nat. Chem*., **2015**, *7*, 30–37.

Another interesting stimulus mediated gelation is based on a peptide conformational change. In order to achieve this goal, Li *et al.* have chosen the decapeptide sequence that forms a β-sheet at the interface of the irisin dimer[356] and split it into two complementary pentapeptides (Figure 30a,b).[357] However, the conformation of the protein domain in nature is related with the conformational restriction imposed by the protein itself.[358] To overcome this limitation they coupled a pyrene moiety at the C termini (Figure 30a,b).[357] Individual solutions of the pentapeptides exhibited an α-helix-like conformation. Interestingly, the mixture of both peptides causes a conformational change to a β-sheet-like structure that triggers hydrogelation. The concept explained here opens the possibility to use aromatic interactions to mimic the restriction imposed by natural proteins and trigger the gelation by conformational changes.

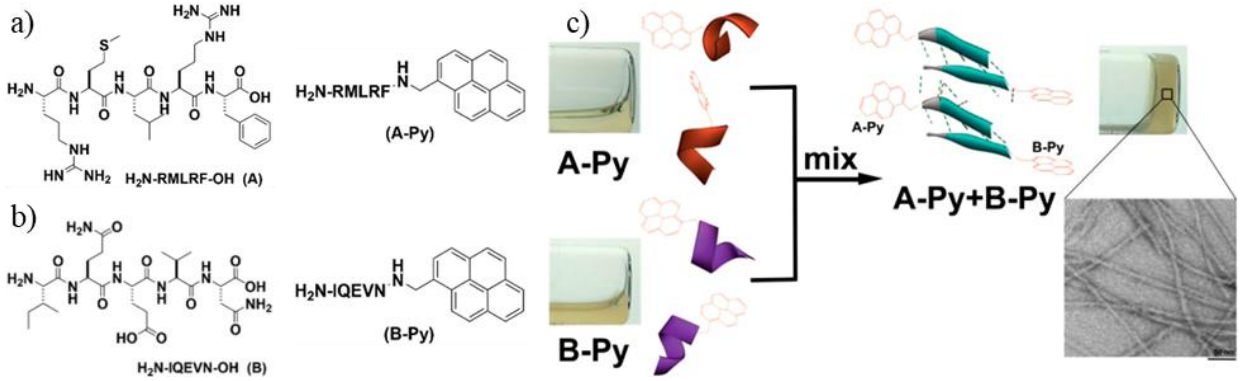

Figure 30. a) and b) Pentapeptide structures (left) and pyrene derivative (right) for A and B; and c) schematic representation of the conformational transition and subsequent gelation upon mixing both segments. Adapted with permission from Ref.357. Copyright © 2016 American Chemical Society.

Although, as seen in these examples, hydrogelation can be triggered by different stimuli, the change in pH is one of the most interesting chemical signals to drive gel formation. Over the years, many aromatic peptides have been used to design pH responsive hydrogelators with controlled mechanical properties,[359,360] leaving the field of non-aromatic peptide scaffolds less explored. Recently, Clarke *et al*. reported three different pentapeptides composed of Ile and Asp residues that can self-assemble into pH-responsive hydrogels with tunable viscoelastic properties.[351] They investigated the structure-assemblies relationship by systematically altering the position of the charged Asp residues (Figure 31a,b). The acidification of the peptide solutions triggered the gel formation, which stiffness could be modulated across two orders of magnitude (2–200 kPa) depending on the concentration and charge distribution (Figure 31c). All three peptides formed β-sheet structures, more twisted when the polar groups are at the ends and the Ile residues are together. The supramolecular nature of the hydrogels conferred self-healing and shear-thinning capabilities making them very suitable for biological or 3D printing applications.

---

[356] M. A. Schumacher, N. Chinnam, T. Ohashi, R. S. Shah and H. P. Erickson, *J. Biol. Chem*., **2013**, *288*, 33738–33744.
[357] J. Li, X. Du, S. Hashim, A. Shy and B. Xu, *J. Am. Chem. Soc*., **2017**, *139*, 71–74.
[358] J.-M. Lehn, *Supramolecular Chemistry: Concepts and Perspectives*, Wiley-VCH, New York, **1995**.
[359] J. K. Gupta, D. J. Adams and N. G. Berry, *Chem. Sci*., **2016**, *7*, 4713–4719.
[360] M. Ma, Y. Kuang, Y. Gao, Y. Zhang, P. Gao and B. Xu, *J. Am. Chem. Soc*., **2010**, *132*, 2719–2728.

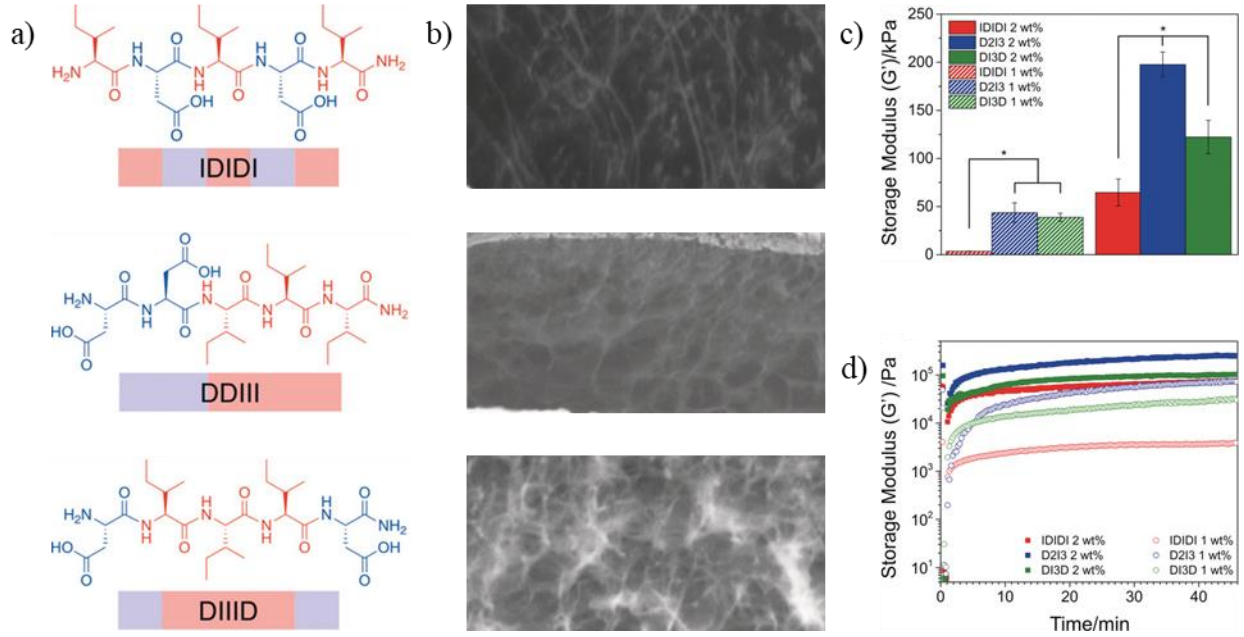

Figure 31. a) and b) Chemical structures and hydrogel Cryo-TEM micrographs of the three pentapeptide sequences; c) storage moduli taken from frequency sweeps at 0.1 % strain; and d) sequential step strain sweeps: 0.1 % strain (30 s), 200 % strain (30 s) and 0.1 % strain (45 min). Adapted with permission from Ref.351. Copyright © 2018 WILEY-VCH Verlag GmbH & Co. KGaA, Weinheim.

Another remarkable example of non-aromatic peptide hydrogels are the peptide amphiphiles with adjustable assembling properties developed by S. Stupp and collaborators.[352,361] In the first design, Hartgerink *et al.* attempted to mimic bone extracellular matrix using a pH-responsive PA.[239] To this aim, four regions were introduce in the PA sequence: i) four Cys able to ensure fibers robustness through disulfide bonds; ii) a phosphoserine residue to display a highly phosphorylated surface to promote the HA mineralization;[362] iii) the sequence Arg-Gly-Asp (RGD) known to promote integrin-mediated cell adhesion;[363] and iv) a sixteen-carbon tail to provide amphiphilicity to the peptide derivative (Figure 19a). As expected, the peptide showed pH and redox responsiveness properties promoting fiber formation and alkaline stabilization, respectively. Furthermore, the nanofibers exposed the peptide segments on the outer surface, which allowed control over HA mineralization (Figure 19b). This proof of concept paved the way for in vivo applications.[245] Initially, subtle changes on the peptide sequence were carried out to adjust the hydrogel properties. Also, the RGD and phosphoserine groups were located in different peptides to test their individual and collective effect on bone regeneration (Figure 32a). Quantification of bone regeneration for the peptide co-assembled with the phosphoserine derivative demonstrated good bone regeneration properties when compared to a clinically used matrix (Figure 32b).

[361] M. P. Hendricks, K. Sato, L. C. Palmer and S. I. Stupp, *Acc. Chem. Res.*, **2017**, *50*, 2440–2448.
[362] S. Mann, J. M. Webb and R. J. P. Williams, *Biomineralization : chemical and biochemical perspectives*, VCH, New York, **1989**.
[363] M. D. Pierschbacher and E. Ruoslahti, *Nature*, **1984**, *309*, 30–33

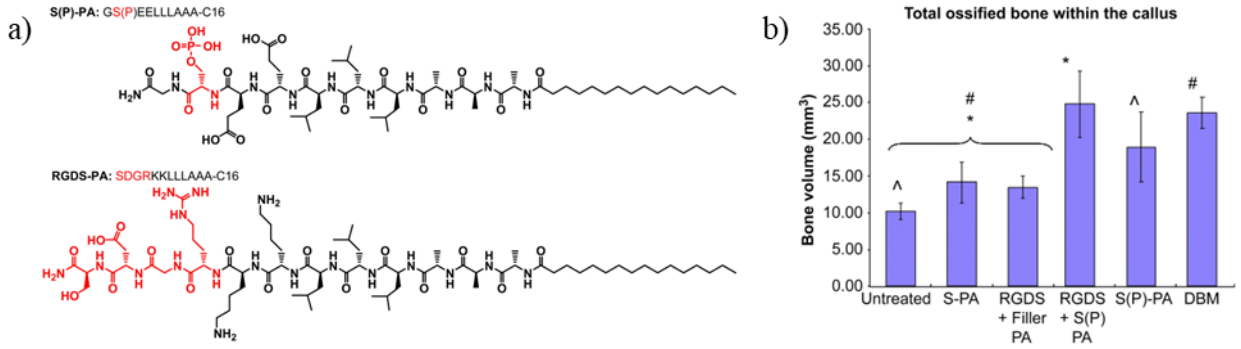

Figure 32. a) Chemical structures of the functionalize peptides (functionalization marked in red); and b) quantification of the in vivo bone regeneration. Note that S-PA and Filler-PA (controls) structures are not shown in the image and DBM corresponds to allogenic matrix used as positive control. Reprinted with permission from Ref. 245. Copyright © 2010 Elsevier Ltd.

Up to this point we have seen some examples of peptide hydrogels with different properties and applications shoes formation was triggered by different stimuli. However, why is so important the control over the rheological properties? As mentioned above, the control of mechanical properties is key to developing some applications. For example, stem cells are known to differentiate in response to the chemical and mechanical properties of the culture.[364,365] This dependency on matrix elasticity[364] was exploited by Alakpa *et al*. to promote cell differentiation with peptide hydrogels (Figure 33a).[260] To this end, they employed the cytocompatible co-assemblies of Fmoc-Phe-Phe and Fmoc-Ser with gelation and crosslinking capabilities, respectively.[366] Visual examination and rheological measures of different peptide concentrations (5-40 mM) exhibited a great control over the elastic moduli (0.1-32 kPa) (Figure 33b).[260] Subsequent studies revealed the attachment of cells to the fibers probably mediated by serum proteins (Figure 33c). Finally stem cells were cultured on soft, stiff, and rigid gels (1, 13 and 32 kPa, respectively) giving rise to neuronal, chondrogenic, and osteogenic differentiation, respectively (Figure 33d). Moreover, they performed a metabolomics analysis during the cell differentiation process, identifying bioactive lipids that can also be used in the differentiation of stem cells and demonstrating that the use of peptide hydrogels can be a great platform for cell differentiation and the search for new drug candidates.

Cyclic peptides can also be used as source of hydrogels, although they still have moderate mechanical properties.[304,305] However, systematic studies have not yet been carried out to control its viscoelastic behavior. As we have seen in the previous example, the control over the mechanical properties of the hydrogels is key for their application. Therefore, understanding how monomer structure can be translated to macroscopic properties through the precise control of molecular self-assembly is crucial to control the functionality of these materials.[367] Additional information about the rheological measurements can be found on the appendix (1).

---

[364] A. J. Engler, S. Sen, H. L. Sweeney and D. E. Discher, *Cell*, **2006**, *126*, 677–689.
[365] P. M. Tsimbouri, R. J. McMurray, K. V. Burgess, E. V. Alakpa, P. M. Reynolds, K. Murawski, E. Kingham, R. O. C. Oreffo, N. Gadegaard and M. J. Dalby, *ACS Nano*, **2012**, *6*, 10239–10249.
[366] V. Jayawarna, S. M. Richardson, A. R. Hirst, N. W. Hodson, A. Saiani, J. E. Gough and R. V. Ulijn, *Acta Biomater.*, **2009**, *5*, 934–943.
[367] J. H. Van Esch, *Langmuir*, **2009**, *25*, 8392–8394.

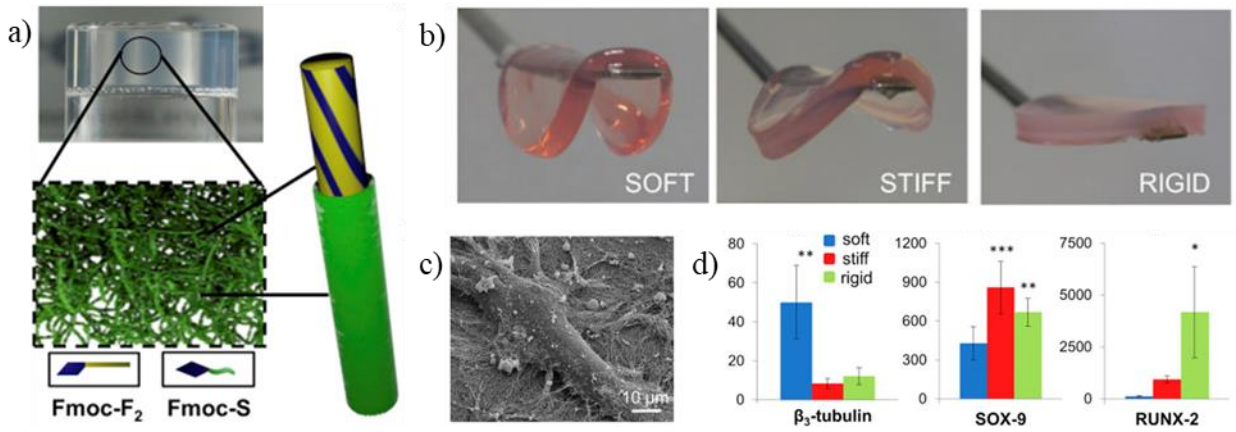

Figure 33. a) Schematic presentation of proposed core-shell assemblies; b) macroscopic images for 10, 30, 40 mM gels in culture media; c) SEM image of a MSC attached to Fmoc-F2/S gel fibers (scale bar 10 µm); and d) differentiation check upon expression of ß3-tubulin (neural cells), SOX-9 (chondrocytes), and RUNX2 (osteoblasts). Adapted with permission from Ref.260. Copyright © 2016 Elsevier Ltd.

1.2. Objectives

Previously in our group it has been demonstrated that an α-(*D,L*)-CP modified with a pyrene pendant is able to form hydrogels triggered by media alkalinization, in which the pyrene moiety contribute to nanotube fibrillation in the hierarchical supramolecular pathway.[304] Based on this, we hypothesize that the incorporation of a set of aromatic pendant units could provide a tool to modulate the self-assembly capabilities driven by π-π stacking interactions and hydrophobic effects. This, in turn, will influence the phase segregation responsible for the formation of hydrogels, and therefore expanding the properties of the new CPs family of hydrogelators. With this aim, the main objective of this chapter is to present the principles of the design and synthesis of this new class of hydrogelators based on α-(*D,L*)-CP that allow to adjust their hydrogel properties in a simple and efficient manner. To achieve such a goal, we propose the following steps:

- Design, synthetize and characterize two α-(*D,L*)-CP scaffolds bearing one or two alkoxyamines groups to anchor different arenes to generate a new family of CP derivative precursors.
- Condensation of these precursors with different arenecarboxyaldehydes to provide amphipathic hydrogelators.
- Study the self-assembling properties of the CP conjugates and establish a correlation with the structural properties.
- Study the hydrogelation capabilities and their mechanical properties and, again, establish a correlation with the number and nature of the arenes in the different derivatives.

1.3. Discussion

1.3.1. Design

The alkoxyamine equipped CP scaffolds were named **1T** and **2T** depending on the number of reacting moieties, in which this number stands for one or two tails (alkoxyamine) per cyclic peptide (Figure 34a). These amphiphilic peptide precursors were designed to segregate hydrophobic and hydrophilic domains for a controlled one-dimensional hierarchical self-assembly growth. The cyclic peptide monomers were designed incorporating the following structural elements: (i) basic aa (e.g., His, Lys) to control the self-assembling process by protonation/deprotonation of their side chain groups; (ii) serine residues in the hydrophilic domain to enhance water solubility; (iii) alkoxyamine groups at the opposite side of the hydrophilic core to allow the incorporation of arene moieties to modulate the hydrophobic character. For cyclic peptide **2T**, both alkoxyamine moieties will be placed at residues (Lys) of the same chirality and placing a Ser between both reactive tails to improve the solubility. The use of the same chirality on this CP would facilitate the formation of antiparallel-like stacking similarly to **1T**. To retain most of the structural features in both peptides, the mentioned Lys would have *D*-chirality and would substitute the Ala residues of **1T**. Fmoc solid-phase peptide synthesis, employing orthogonal protecting groups, was employed to prepare both CPs (Scheme **1**, Section 1.9). After HPLC purification, oxime formation with a variety of aldehydes was accomplished by mixing either peptides **1T** or **2T** with the corresponding aldehydes (2-naphthaldehyde (**N**), 9-anthracenecarboxaldehyde (**A**) and 1-pyrenecarboxaldehyde(**P**)) in DMSO at 60ºC for 30 min. The final peptides were purified by precipitating and washing in diethyl ether to give peptides **1TN**, **1TA**, **1TP**, **2TN**, **2TA** and **2TP** (Figure 34b). The purity of the products was analyzed by HPLC-MS, ^{1}H NMR and infrared spectroscopy (Figure 69-Figure 92). The molecular hydrophobicity character of the resulting CPs was estimated by the 1-octanol/water partition coefficient (log*P*) (Table 5). These values were used to rank CP derivatives according to their hydrophobicity. As expected, log*P* values expressed the polarity differences according to the nature and number of aromatic moieties.

1.3.2. Hydrogelation capabilities

O-alkyloxime functionalized CPs (TFA salts from HPLC) were solubilized in milliQ water at the concentrations required for hydrogelation (~2% w/w) giving in all cases acidic solutions. Addition of small amounts of aqueous solution of NaOH (0.1 M) induced the sol–gel transitions at room temperature after reaching a pH around 8.0, which was reversible upon acidification (Figure 93). Only CPs with higher log*P* values (Table 5) were able to form stable hydrogels (log*P* > -3.5), which indicates positive correlation between hydrogelation capabilities and hydrophobic character. The self-assembly occurred by the antiparallel β-sheet stacking of the CP units (Figure 34c and d), followed by further assembly induced by the interdigitation of the aromatic pendants that are exposed to the aqueous medium that produces networks of intertwined nanotubes. Figure 34e shows the results of inversion vial test, which indicated that most of the derivatives were able to form self-sustained hydrogels. No phase segregation was not observed for any of the examples, except for the two-tailed naphthalene hydrogel (**2TN**) after storage longer than one month.

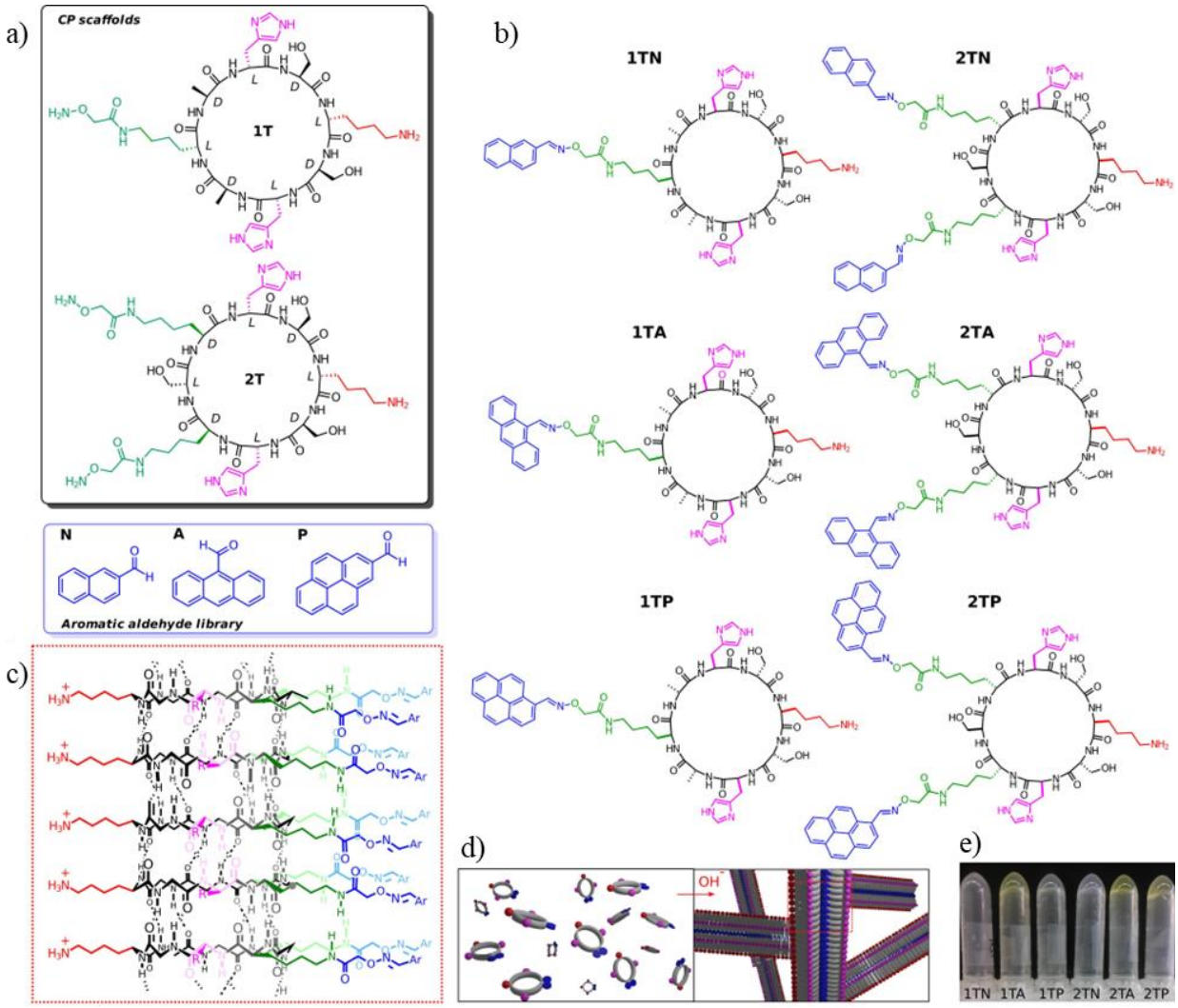

Figure 34. a) Building blocks based on cyclic peptides **1T** and **2T** and aromatic aldehydes 2-naphthaldehyde (**N**), 9-anthracenecarboxaldehyde (**A**) and 1-pyrenecarboxaldehyde (**P**); b) library of hydrogelators prepared by condensation between aldehydes and alkoxyamines described above; c) representation of the antiparallel ß-sheet assembly of cyclic peptides **2T** proposed with stacked aromatic units as the basic model for nanotube formation. The final structures assemble based on a balance between hydrogen bonding interactions, π-π stacking of the aromatic moieties, and electrostatic repulsions; d) schematic representation of the formation of gels triggered by pH changes; e) inverted vial test of 11 mM CPs solutions in basic aqueous solutions (pH 8.3-9.0).

1.3.3. Spectroscopic characterization

Spectroscopic characterization of the hydrogel was then carried out to gain further insights on the self-assembly mechanism. ATR-FTIR spectra obtained from freeze-dried alkaline solutions revealed Amide I stretching bands at ca. 1673 cm^{-1} and 1625 cm^{-1}, which are characteristics of antiparallel β-sheet aggregates (Table 5 and Figure 94).[368] Additionally, all peptide derivatives

[368] R. Sarroukh, E. 1.4Goormaghtigh, J. M. Ruysschaert and V. Raussens, *Biochim. Biophys. Acta*, **2013**, *1828*, 2328–2338.

exhibit the same wavelength for the Amide A band at ca. 3274 cm^{-1} which confirms the similar interaction between the CPs units (Figure 94).

Table 5. Summary of the properties of the CPs described in this work.

CP	logP[a]	Amid. I (cm^{-1})[b]	Gel[c]	CAC (μm)[d]	Crit. Strain[e] (%)	G'/G"[f]	G' (Pa)[f]	G" (Pa)[f]	Recovery[g] (%)
1T	-6.8	n.d.	No	n.d.	n.d.	n.d.	n.d.	n.d.	n.d.
2T	-8.7	n.d.	No	n.d.	n.d.	n.d.	n.d.	n.d.	n.d.
1TN	-3.5	1624, 1683	No	17	n.d.	n.d.	n.d.	n.d.	n.d.
1TA	-2.4	1624, 1678	Yes	7	0.8	4.9	239	49	59
1TP	-1.8	1622, 1674	Yes	6	1.2	6.1	859	141	92
2TN	-2.1	1622, 1673	Yes	6	13.0	2.7	148	55	78
2TA	0.2	1621, 1673	Yes	3	1.1	6.5	13013	1993	66
2TP	1.4	1622, 1673	Yes	2	2.0	8.5	6436	760	82

n.d. stands for not determined. [a]Calculated log*P* for amphiphilic derivatives using the A log*P*98 algorithm.[369] [b]Wavelength of maximum intensity corresponding to the Amide I stretching bands obtained from ATR-FTIR spectra in Figure 94. [c]Formation of hydrogels (11 mM) after alkalinization to pH 8.3-9.0. [d]CAC was determined by thioflavin T fluorescence emission (Figure 95). [e]Critical strain determined visually from strain sweep experiments as the threshold where G'/G" starts to decrease. [f]Determined at a strain of 1% from strain sweep experiments. [g]Determined from the self-healing experiments. Values denote the percentage of G' recovered after the last recovery cycle.

The peptides **1TN**, **1TA**, **1TP**, **2TN**, **2TA** and **2TP** were then studied at different pH under diluted aqueous conditions. As previously reported,[304] the alkalinization of the **1TP** (Figure 35a and b and Figure 96c) caused variations in the absorbance and the fluorescence emission spectra, such as an emission red-shift from 430 nm to 500 nm, which is attributed to the excimer emission due to the stack of the pyrene moieties.[370] This suggests that at acidic pH, the aromatic moieties are distant from each other, while alkalinization brings pyrene units in close proximity guided, most likely, by the CP assembly (Figure 34c and d). However, in contrast to our observations with **1TP**, the two pyrene tails' derivative (**2TP**) shows a certain level of excimer emission even at acidic pH (Figure 35c and Figure 96d, pH 3.6), which indicates a certain level of self-assembly even under the starting acidic conditions and/or a proximity between intramolecular pyrene units. The decrease of the excimer band with initial alkalinization from pH 3.6 to 4.4 (Figure 35c and Figure 96d) suggests a structural reorganization of the pyrene moieties upon initial deprotonation. However, the alkalinization assembly could also be confirmed, as the ratio between the monomer and the excimer emission with increasing pH showed a sharp transition around 6 for the **1TP** (Figure 35b) and between pH 4.5 and 5.5 for the **2TP** (Figure 35d and Figure 96d), which indicates that small fractions of deprotonated imidazolium moieties rapidly trigger the supramolecular process. This is consistent with a critical aggregation concentration (CAC) at the low μM range for both derivatives (Table 5 and Figure 95). We also observed spectral changes in the fluorescence spectra of derivatives **1TA**, **2TA**, **1TN** and **2TN**. Fluorescence spectra after alkalinization of the anthracene

[369] A. K. Ghose, V. N. Viswanadhan and J. J. Wendoloski, *J. Phys. Chem. A*, **1998**, *102*, 3762–3772.
[304] A. Méndez-Ardoy, J. R. Granja and J. Montenegro, *Nanoscale Horiz.*, **2018**, *3*, 391–396.
[370] F. M. Winnik, *Chem. Rev.*, **1993**, *93*, 587–614.

peptide derivatives, also resulted in the formation of excimers[371] as shown by the intensity variations and bathochromic shifts (Figure 35e,g and Figure 96b,e). A similar trend was found for the **1TN** and **2TN**, where the intensity of an emission shoulder at 450 nm increased after alkalinization and the formation of the corresponding excimer (Figure 35i,k, Figure 96a,d).[372] In agreement with the pyrene derivatives, these changes took place at pH values close to 5–6 (Figure 35f,h,j, and l), which might indicate a higher critical aggregation concentration of naphthalene and anthracene CPs in comparison to pyrene counterparts (Table 5). In all CP derivatives the excimer emission is higher in the two-tail peptide than the one-tail derivative, suggesting higher assembling properties for the **2T** peptides.

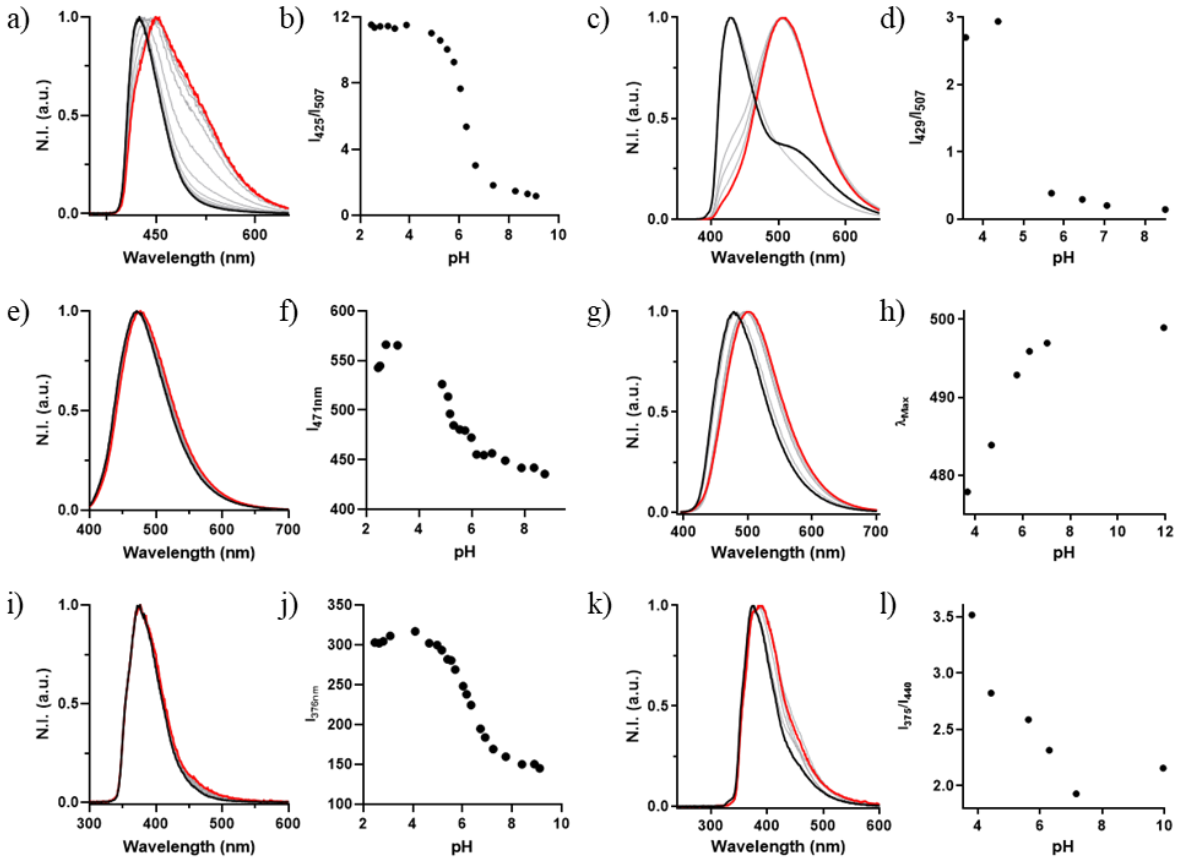

Figure 35. Spectroscopic studies at different pH values of aqueous solutions of CPs (400μM) bearing pyrene, anthracene and naphthalene moieties, at λ_{exc} = 340nm, 385nm and 230nm, respectively; a) normalized fluorescence spectra of **1TP** from pH 2.5 (black) to 9.1 (red); b) fluorescence intensity ratio as a function of pH for **1TP**; c) normalized fluorescence spectra of **2TP** from pH 3.5 (black) to 8.5 (red); d) fluorescence intensity ratio as a function of pH for **2TP**; e) normalized fluorescence spectra of **1TA** from pH 2.5 (black) to 8.8 (red); f) intensity maxima (471 nm) as a function of pH for **1TA**; g) normalized fluorescence spectra of **2TA** from pH 3.6 (black) to 11.8 (red); h) wavelength of maximum emission intensity as a function of pH for **2TA**;); i) normalized fluorescence spectra of **1TN** from pH 2.5 (black) to 9.1 (red); j) intensity maxima (376 nm) as a function of pH for **1TN**; k) normalized fluorescence spectra of **2TN** from pH 3.8 (black) to 9.9 (red); l) fluorescence intensity ratio as a function of pH for **2TN.**

[371] P. K. Lekha and E. Prasad, *Chem. Eur. J.*, **2010**, *16*, 3699–3706.
[372] T. H. Ghaddar, J. K. Whitesell and M. A. Fox, *J. Phys. Chem. B*, **2001**, *105*, 8729–8731.

The self-assembly of all CPs (**1TN**, **1TA**, **2TN**, **2TA** and **2TP**) was also studied via UV-visible spectroscopy (Figure 36). As expected, basified aqueous solutions exhibited a lower absorbance compared to the acidic solutions in the range of the wavelengths studied, which is consistent with the aggregation of the dyes.

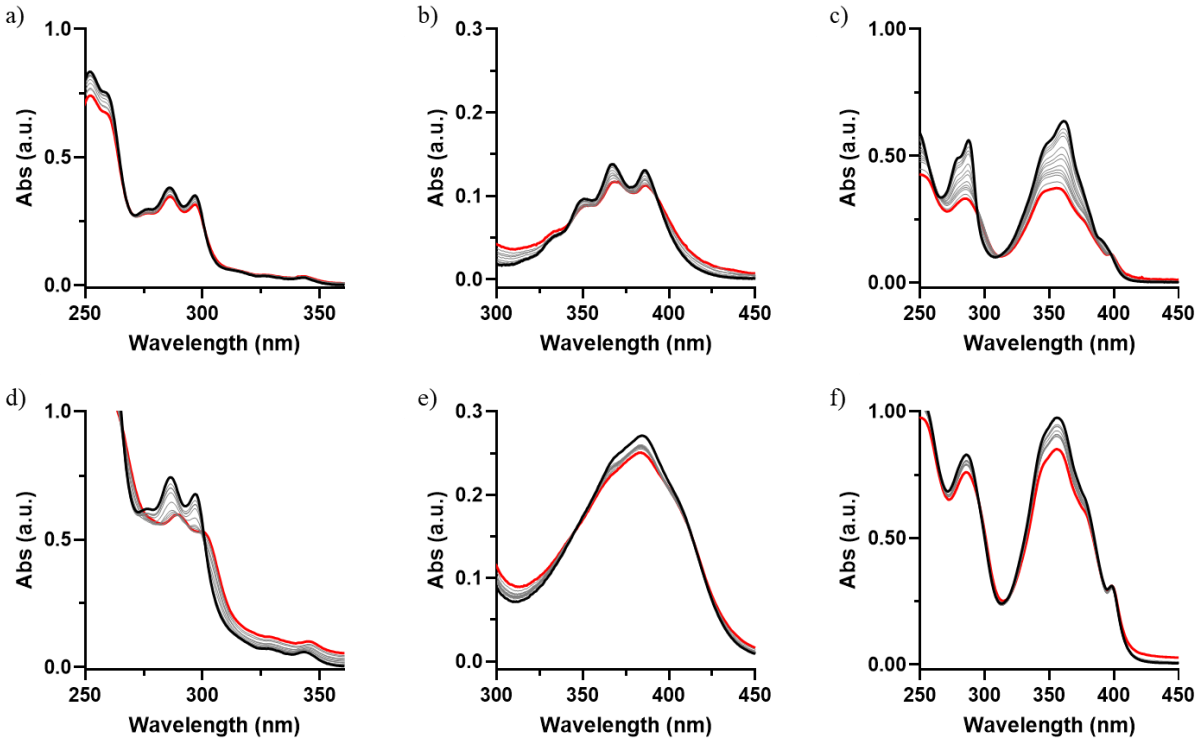

Figure 36. UV spectra of CPs (50 μM, water) at different pH values, from 1.9-2.0 (black line) to 8.6-8.9 (red line); a) **1TN**; b) **1TA**; c) **1TP**; d) **2TN**; e) **2TA**; f) **2TP.**

1.3.4. Microscopy characterization

The self-assembly of the different CPs was then studied via scanning transmission electron microscopy (STEM, Figure 37). In order to visualize individual nanotubes, dilutions of hydrogels (final concentration 11 μM) were prepared, and the resulting equilibrated solutions were deposited in carbon-coated grids. After staining with uranyl acetate, the substrates were visualized by STEM and the resulting micrographs showed the presence of fibrillar assemblies for all the CPs (**1TA**, **1TP**, **2TN**, **2TA** and **2TP**), while worm micelles-like structures were observed for **1TN** (Figure 37a). Nanotube diameters measured from STEM micrographs from different samples of **1TA**, **1TP**, **2TN**, **2TA** and **2TP** ranged from 4 to 8 nm, which is in agreement with bundles made of at least two single nanotubes, considering that single nanotubes derived from cyclic octapeptides with pyrene tails should have diameter in the range of 2.0–2.5 nm.[304] The nanotube diameter was further assessed by atomic force microscopy (AFM) after depositing a solution of 2TP (0.11 mM) on a mica surface (Figure 37b). The images showed the presence of nanotubes with a diameter of 2.5 to 4 nm that could be assigned to single or double nanotubes in a parallel packed architecture. It was observed that certain cyclic peptide samples (e.g. **1TA**, **2TN**) showed nanotubular structures with

shorter and lower persistence lengths (Figure 37a). Despite challenging, length distribution control of supramolecular polymers provides insights into the assembly/disassembly mechanisms and eventually the macroscopic properties of the resulting materials.[495,373] For qualitative assessment, the length of a significant number of nanotubes was determined in the low-magnification STEM images and then plotted as histogram charts (Figure 37c and Figure 97-Figure 101). The nanotube length distribution charts revealed substantial differences depending on aromatic aldehyde moieties (Figure 37c). In general, samples from CPs conjugated to the pyrene aldehyde gave distributions shifted to longer nanotube sizes.

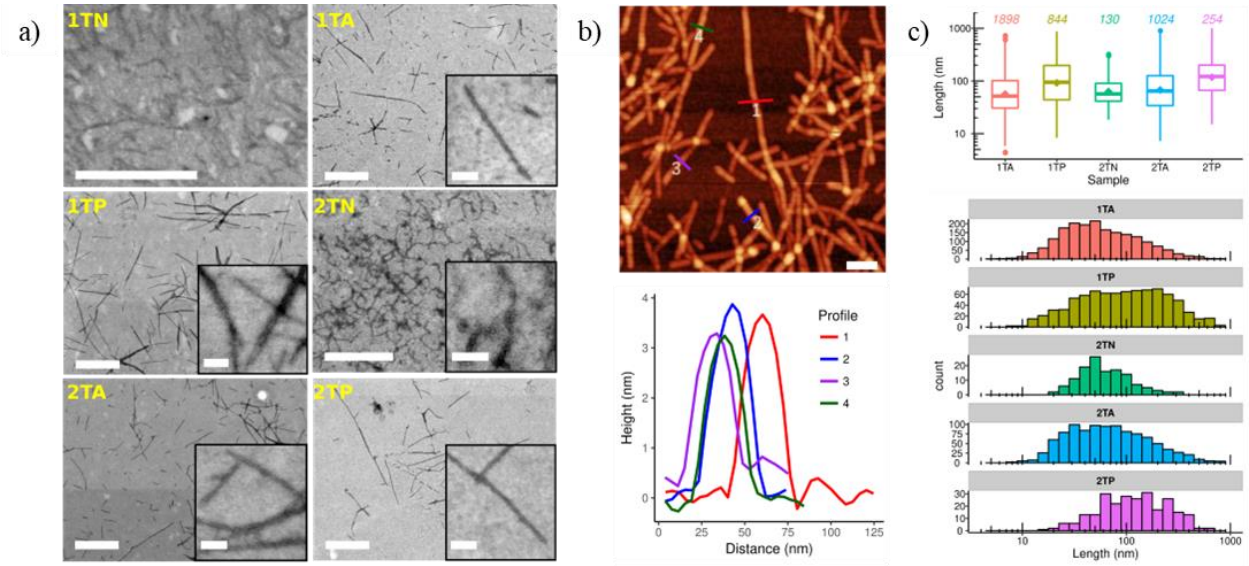

Figure 37. Scanning transmission electron microscopy (STEM) of compounds **1TN**, **1TA**, **1TP**, **2TN**, **2TA** and **2TP** deposited on carbon-coated grids after diluting the corresponding gels (pH 8.3-9.0) in water to a final concentration of 11 μM. a) STEM micrographs of the nanotubes (high magnification in the inset). Scale bars are 400 nm for low magnification pictures and 50 nm for insets; b) non-contact AFM images after the dilution of the 2TP hydrogel (top) and deposition on freshly cleaved mica sheets and the corresponding height profiles (bottom) at a CP concentration of 0.11 mM. Scale bar denotes 100 nm; c) nanotubes' length distribution obtained from STEM micrographs plotted as boxplots (top) and histograms (bottom). Length distributions were obtained from an average of 4 STEM micrographs per compound and several individual nanotubes between 130 and 1898. The median lengths were 52, 95, 58, 65 and 122 nm for **1TA**, **1TP**, **2TN**, **2TA** and **2TP**, respectively. Numbers on top of boxplots denote the individual nanotubes measured for each compound, and diamonds represent the length mean.

To investigate the morphology of the gels at a higher scale, the freeze-dried gel (xerogel) was prepared and observed by scanning electron microscopy (SEM, Figure 38). A homogeneous network of stiff nanotubes was visualized in the hydrogels of **1TA**, **1TP**, **2TA** and **2TP**. The diameters of the thinner bundles observed were of 28 ± 6, 27 ± 4, 27 ± 4 and 28 ± 5 nm, respectively (averaged from at least 11 diameter measurements). This higher diameter should result from the bundling of the individual nanotubes into thicker fibers. These data again suggested that increasing the size or the number of aromatic rings has a minor influence on the diameter distribution of the nanotube bundles. On the other hand, no clear fibers were observed for the two-tail naphthalene

[373] F. Tantakitti, J. Boekhoven, X. Wang, R. V. Kazantsev, T. Yu, J. Li, E. Zhuang, R. Zandi, J. H. Ortony, C. J. Newcomb, L. C. Palmer, G. S. Shekhawat, M. O. De La Cruz, G. C. Schatz and S. I. Stupp, *Nat. Mater.*, **2016**, *15*, 469–476.

peptide (**2TN**), which showed globular-like aggregates through all the xerogel surface. Although we confirmed by STEM that this derivative (**2TN**) self-assembles into nanotubes (see above), the presence of these aggregates might suggest that they bundle poorly into high persistence length micron sized fibers. We also observed the presence of regions where thicker fibers were formed. For example, in Figure 38b, the SEM images of the 1TP xerogel showed the presence of clearly differentiated fibers with diameters that range from 20 to 140 nm and lengths at the micrometer scale. Careful inspection reveals that these thicker fibers, as expected, are composed of bundles of thinner fibers (Figure 38b and Figure 102).

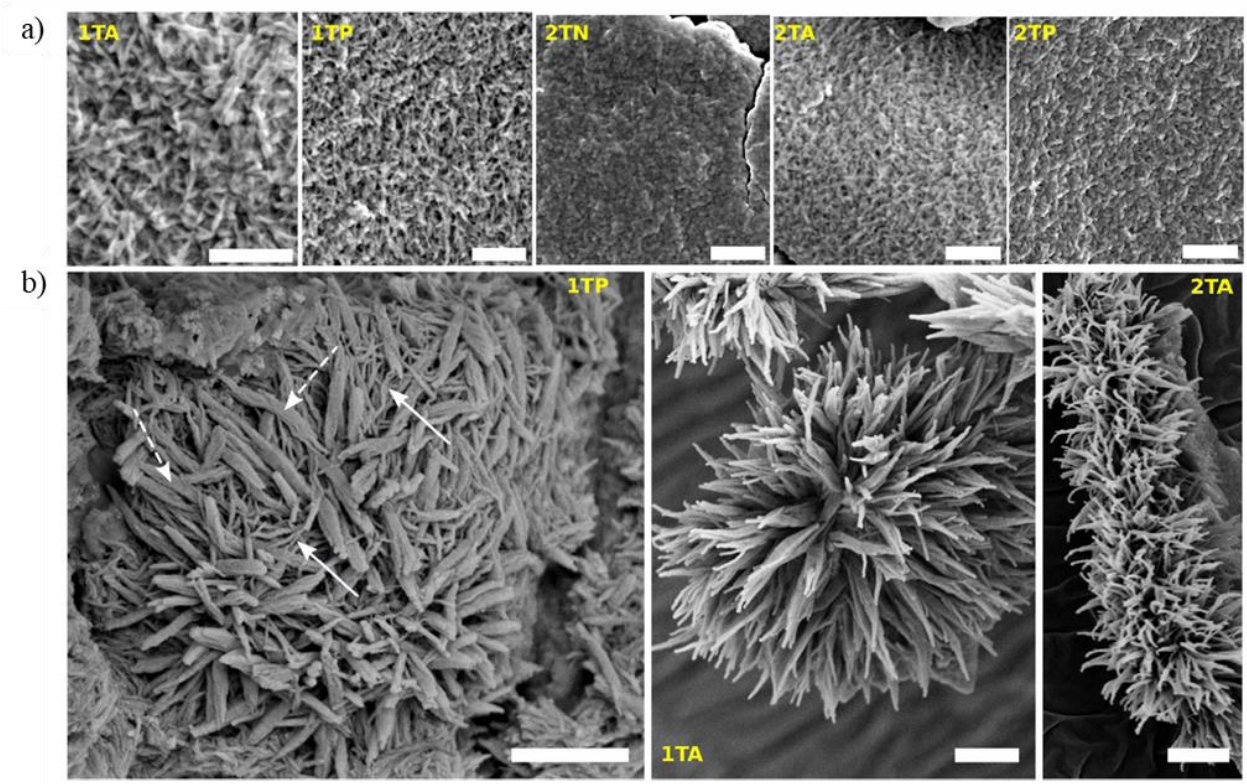

Figure 38. (a) SEM images of freeze-dried gels of compounds **1TA**, **1TP**, **2TN**, **2TA** and **2TP**. Scale bars are 400 nm; (b) details of nanotube bundles observed in the specific region of the gels. The dashed arrows denote wider bundles of nanotubes, while plain arrows indicate the presence of thinner bundles. Scale bars are 800 nm.

The intrinsic fluorescence of the attached aryl moieties was next employed to visualize the gels in the wet state by fluorescence microscopy (Figure 39). Clear fibrillar structures were also observed in the gels obtained from single and double pyrene tails (**1TP** and **2TP**). The micrographs confirmed the propensity of the self-assembled structures derived for these peptides to bundle and form microscopic size fibers. This is in agreement with our previous observations with compound **1TP**, where fibers of a few micrometers long were observed by laser confocal microscopy.[304] Overall, data collected by spectroscopic and imaging techniques indicate that (i) the hydrogels are constituted by nanotube bundles, where the aromatic moieties are in close proximity; (ii) the bundling can be manifested in the formation of micrometer sized fibers; (iii) the stiffness of the fibers/bundles depends on the structural design (e.g. **2TN** vs. **2TP**) and (iv) the dilution of the gels revealed different nanotube length distributions.

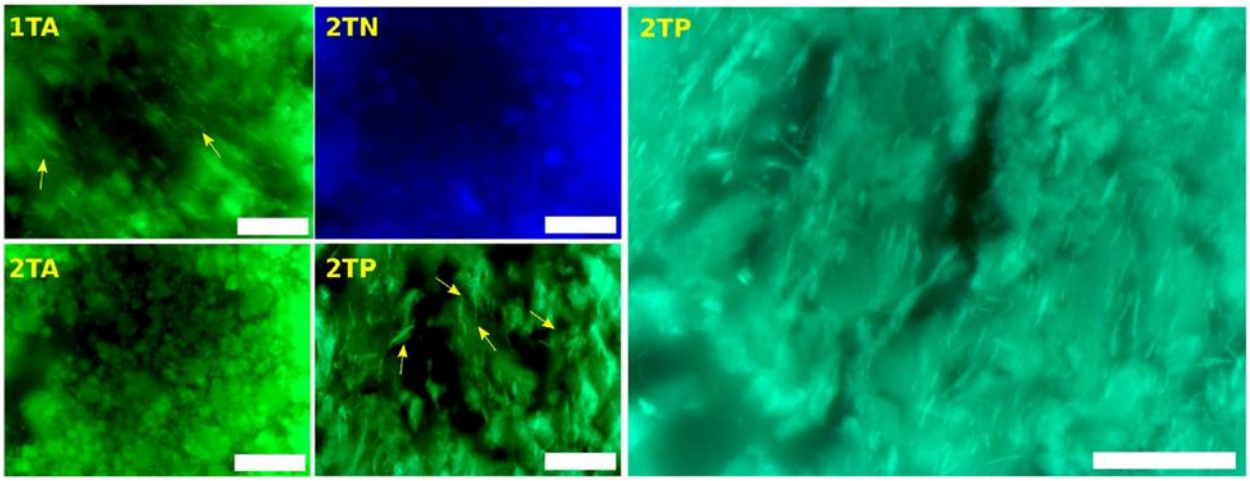

Figure 39. Epifluorescence images obtained from hydrogels formed by a 11 mM aqueous basic (8.5–9.0) solution of **1TA**, **2TN**, **2TA** and **2TP**. Scale bars are 50 μm. Yellow arrows indicate the presence of fibers or elongated gel structures.

1.3.5. Rheological characterization

Rheological measurements were carried out to probe the viscoelastic response of cyclic peptide-based gels towards increasing strains. The response of the storage (elastic, G') and loss (viscous, G'') moduli to an increased shear strain is shown in Figure 40a. At low strains (below 1%), the storage modulus is higher than the loss one, indicating the presence of hydrogel-like networks with tie-junctions that can store mechanical energy.[495] Increasing the strain eventually leads to structural deconstruction and the drop of the storage modulus values. We observed that the critical strain required for deconstructing the hydrogel network is dependent on the hydrogelator structure (Table 5) and remains close to 1% strain, except for the two-tail naphthalene-based gels (**2TN**), where the critical strain approaches 10%. The G'/G'' ratio was then compared to test the prevalence of the gel solid-like properties (Figure 40b).[495] At low strains, the hydrogelators with higher hydrophobic character (**2TA** and **2TP**) exhibited the highest elastic response, while **2TN** exhibited the greatest contribution of the viscous component. The storage modulus increased with the number of tails (e.g., **1T** < **2T**) and also with the number of fused aromatic rings (**N** < **A** < **P**). Therefore, this strategy allowed the tuning of the storage modulus of a common molecular structure at a constant hydrogelator concentration, in a range that expands two orders of magnitude (100–10000 Pa, Table 5) and that was 50 times stiffer than the stiffest cyclopeptide hydrogelators reported up to date (G' ~ 200 Pa at 5% strain).[305]

The gel relaxation timescale was then analyzed by frequency-dependent experiments at 5% constant strains. Despite certain strain values were in the non-linear viscoelastic regime, the storage and loss moduli remained independent of the radial frequency for the range of frequencies studied (Figure 40c). Considering that the main interactions holding the hydrogel tubular nanostructure are intrinsically supramolecular, any mechanical damage to the network will lead to a non-equilibrium

condition that should evolve back to restore the supramolecular interactions.[374,375] Therefore, supramolecular network recovery after strain-induced deconstruction was characterized by different methods. First, we manually sliced pieces of the two pyrene tails cyclic peptide tubular network (**2TP**) and then we manually join them together (Figure 40d). A single solid hydrogel piece without any observable internal crack was readily recovered, which already suggested self-healing capabilities of the corresponding hydrogel.

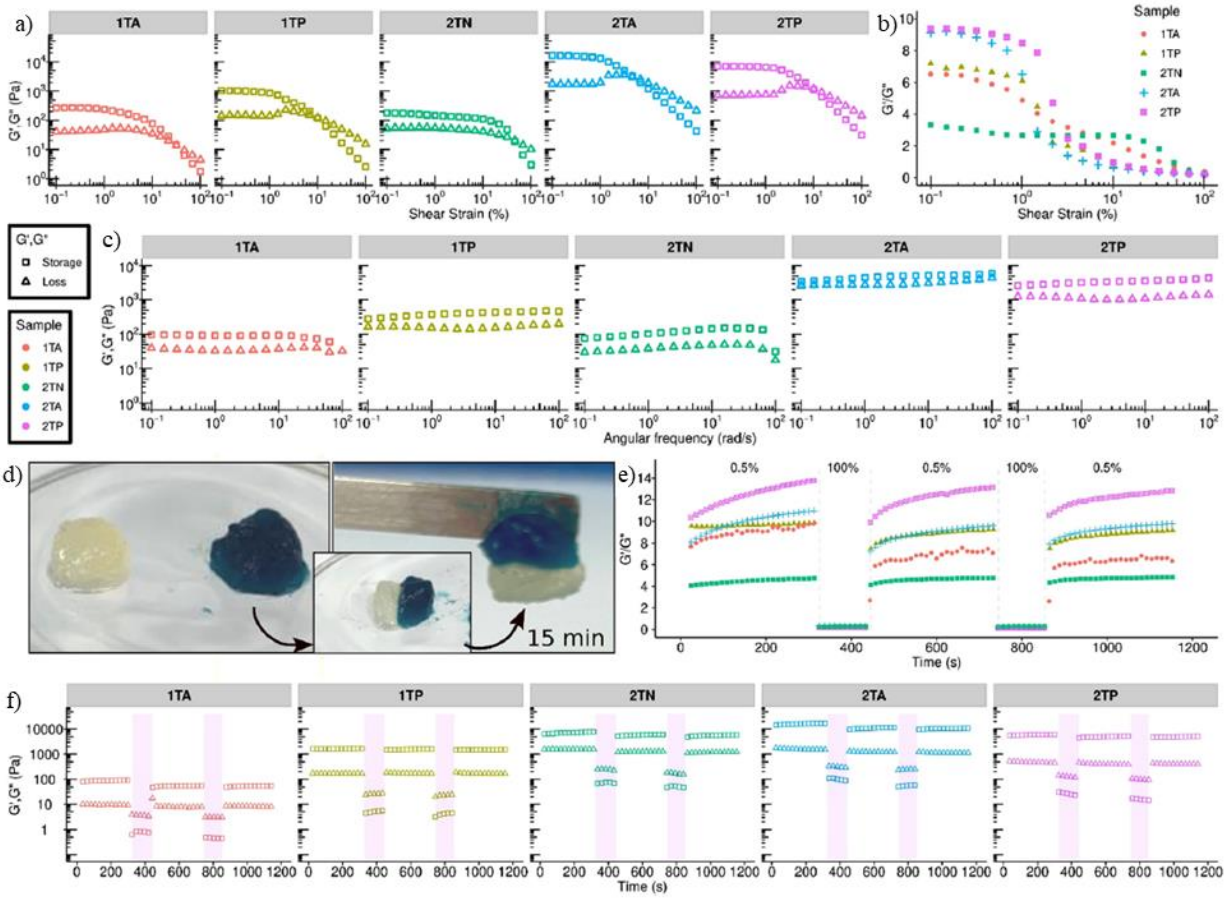

Figure 40. a) Strain sweeps of hydrogels prepared from compounds **1TA**, **1TP**, **2TN**, **2TA** and **2TP** at 11 mM concentration (1.1–1.7% w/w, pH 8.3–9.0, 20ºC); b) strain sweeps expressed as the function of tan δ (G'/G''); c) dynamic frequency spectra at a constant strain of 5%; d) macroscopic self-healing of the 2TP hydrogel (5% w/w) after cutting a gel piece using a sharp razor and join the pieces. One half was stained with 1–2 mg methylene blue before joining; e) comparative continuous step strain experiments carried out on **1TA**, **1TP**, **2TN**, **2TA** and **2TP** gels at a CP concentration of 11 mM in basic solutions. The strain steps varied from 0.5% to 100% for defined time intervals; f) individual strain step experiments. The shaded regions denote an applied strain of 100%.

Step strain experiments, by application of a sustained small strain of 0.5% for 300 s, were carried out to quantify the kinetics of the healing process (Figure 40e).[374] The G'/G'' ratio increased slowly during this step, which indicated a structural rearrangement of the aqueous tubular network.

[374] E. Borré, J. Stumbé, S. Bellemin-Laponnaz and M. Mauro, *Angew. Chem. Int. Ed.*, **2016**, *55*, 1215–1264.
[375] A. Campanella, D. Döhler and W. H. Binder, *Macromol. Rapid. Commun.*, **2018**, *39*, 1700739.

Application of a strain step of 100% for 100 s triggered a sharp drop of the G'/G'' ratio because of a dramatic drop of the storage modulus, which becomes smaller than the loss modulus (Figure 40f). This observation clearly indicated a structural damage of the network, with loss of tie-junctions or entanglements among the self-assembled structures. However, restoring the strain to the initial 0.5% resulted in a recovery of part of the original viscoelastic properties of the hydrogels in less than 12 seconds, which indicated a rapid self-healing of the initial network interactions (~50% for **1TA** and **2TA**, and ~75% for **1TP**, **2TN** and **2TP**). Upon extended healing times, recovery ranged from 59 to 92% (Table 5). Repeating number of damaging strain step cycles could be applied to the supramolecular hydrogel material without losing hydrogel viscoelastic properties (Table 5).

This rheological characterization confirmed that the viscoelastic properties of the described cyclic peptide hydrogels, prepared from **1TA**, **1TP**, **2TN**, **2TA** and **2TP**, were strongly modulated by the hydrophobic moiety installed on the CP ring. This experimental evidence is consistent with the differences in nanotube lengths' distributions and/or stiffness, which in turn are derived from the different molecular structures of the cyclic peptide monomers. To illustrate this correlation, the distribution of nanotube lengths obtained from diluted gel samples was plotted against the loss tangent δ (G'/G'') (Figure 41). This plot showed that the cyclic peptides forming the longer nanotubes have a higher propensity to generate dense networks. However, we hypothesize that many other elements play a significant role in the network structure and dynamics and determine the elastic capabilities; for example, nanotube persistence length, bundling (which additionally increases persistence length) and the network crosslinking are fundamental parameters that govern these material properties.[376]

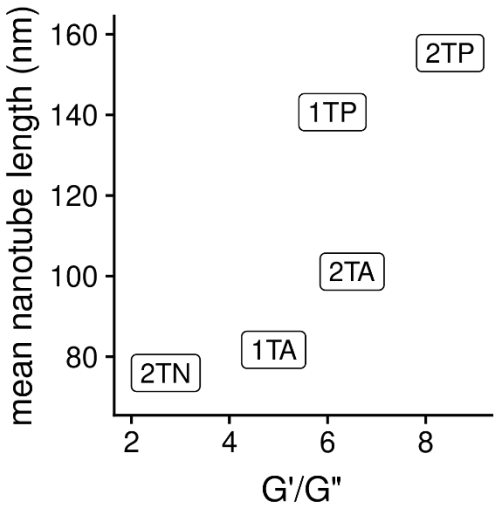

Figure 41. Correlation between loss tangent (G'/G'') observed (hydrogels at 11 mM concentration, 20ºC) and mean nanotube length obtained in diluted solutions (11 μM, 20ºC).

[376] J. W. McAllister, J. R. Lott, P. W. Schmidt, R. L. Sammler, F. S. Bates and T. P. Lodge, *ACS Macro. Lett*., **2015**, *4*, 538–542.

1.4. Conclusions

In this chapter we have introduced the molecular design principles of a new family of self-healing hydrogelator-based self-assembling cyclic peptide nanotubes. These cyclic peptide monomers are easily accessible building blocks and constitute optimal scaffolds for the precise orientation of hydrophobic or charged components, providing a simple route to fine-tune intermolecular interactions.

Other important aspects of this chapter are:

- Exploitation of the highly efficient alkoxyamine-aldehyde condensation to access a discrete library of amphiphilic CPs, which showed an excellent capacity of maintaining the one-dimensional hierarchical self-assembly from the nano to the micron scale.
- The rheological characterization indicated that the viscoelastic properties of these gels could be perfectly modulated by tuning the number and nature of the aromatic tails attached to the cyclopeptide monomer.
- SEM and STEM of gels revealed the presence of entangled networks of hierarchically associated nanotube fibers at the micron size scale.
- The observed degree of correlation between the length distributions and the viscoelastic character of the gels can be attributed to the formation of a different degree of entanglement of the nanotubes.
- The supramolecular nature of this strategy allowed the preparation of self-healing viscoelastic materials that can be easily tuned by molecular design.
- This work gives access to a new type of a la carte self-healing hydrogels made of simple and versatile cyclic peptide monomers with a high chemical functionalization potential and structural control.

2. Spatially Controlled Supramolecular Polymerization of Peptide Nanotubes

The results of this chapter have been published in Angewandte Chemie International Edition as:

A. Méndez-Ardoy,[a] A. Bayón-Fernández,[a] Z. Yu,[b] C. Abell,[b] J. R. Granja[a] and J. Montenegro.[a] Spatially Controlled Supramolecular Polymerization of Peptide Nanotubes by Microfluidics. *Angew. Chem. Int. Ed.* **2020**, *59* (17), 6902-6908. DOI: 10.1002/anie.202000103

Affiliations

[a]Centro Singular de Investigación en Química Biolóxica e Materiais Moleculares (CIQUS), Departamento de Química Orgánica, Universidade de Santiago de Compostela, 15782 Santiago de Compostela, Spain.

[b]Department of Chemistry, University of Cambridge, Cambridge, CB2 1EW, United Kingdom.

[377] A. Méndez-Ardoy, A. Bayón-Fernández, Z. Yu, C. Abell, J. R. Granja and J. Montenegro, *Angew. Chem. Int. Ed*., **2020**, *59*, 6902–6908.

2.1. Precedents

In the previous chapter we have demonstrated the possibility to use cyclic peptide as a powerful scaffold to build hydrogels with tunable mechanical behavior. In nature, the cellular environment is sustained by hydrogel-like phases generated by association of protein-based building blocks.[378-380] The understanding on the underlying principles of how fibrillar systems interact with the confinement is an important scientific challenge, which requires the use of simplified, tunable models.[380]

2.1.1. A brief introduction of the cytoskeleton

The cytoskeleton has been regarded as an active polar gel[381,382] formed by a network of crosslinked supramolecular polymers and regulatory proteins.[383] As previously mentioned in the general introduction, the major components of the cytoskeleton are actin filaments, microtubules, and intermediate filaments (Figure 42a).[382-384] All three assemblies are formed under out of equilibrium conditions making this system highly dynamic.[382] The exquisite control of the dynamic behavior of the gel by cytoskeletal binding proteins or other regulatory mechanisms, such as phosphorylation, are essential to adjust the mechanical properties of the cell in response to certain stimuli (Figure 42b).[384] This is important since the cytoskeleton viscoelastic behavior directly affect the cell shape, movement, cargo transport and division.[382,383]

The most studied components of the cytoskeleton are the actin filaments and the microtubules. The first one is form by the assembly of actin monomers into filaments with a diameter of 8 nm,[384] and with a shorter persistent length and greater flexibility than the microtubules.[383] However, these filaments in the presence of crosslinkers can be further arranged into crosslinked gels, rigid bundles, or regular arrays.[384] In animal cells, they are mainly localized close to the membrane and form the cell cortex that controls the mechanical properties of the cell and participates in cell locomotion.[381,384]

On the other hand, microtubules are formed by the assembly of α- and β-tubulins into protofilaments that interact laterally to form rigid microtubules[62,63] whose external and internal diameters are 25 and 10 nm, respectively.[384] Normally, microtubules grow individually from the centrosomes in the center of the cell toward the actin cortex.[381,384] However, when the cell enters the division cycle they evolve gradually to form the mitotic spindle that separates the genetic material of the born cells.[383]

Both filaments and microtubules are polar, meaning that all the subunits within any filament are oriented in the same direction.[382,384] This property in conjunction with the associated motor proteins allows the directional transport and organization of cargos and organelles across the cell.[384] Additionally, this disposition of the individual units promotes that the addition (growth) or removal

---

[378] M. C. Catoira, L. Fusaro, D. Di Francesco, M. Ramella and F. Boccafoschi, *J. Mater. Sci. Mater. Med.*, **2019**, *30*, 115.
[379] U. Blache and M. Ehrbar, *Adv. Wound Care*, **2018**, *7*, 232–246.
[380] Y. Bashirzadeh and A. P. Liu, *Soft Matter*, **2019**, *15*, 8425–8436.
[381] R. A. Meyers, *Encyclopedia of Complexity and Systems Science*, Springer, New York, NY, 1st edn., **2009**.
[382] J. Prost, F. Jülicher and J. F. Joanny, *Nat. Phys*., **2015**, *11*, 111–117.
[383] D. A. Fletcher and R. D. Mullins, *Nature*, **2010**, *463*, 485–492.
[384] S. K. Maciver, in *Encyclopedia of Life Sciences*, John Wiley & Sons, **2001**.

(disassembly) of subunits occur in opposite ends. This process is known as treadmilling and plays a crucial role on cell movement (Figure 42c).[381] During this process, the total length of the filament remains constant, while their center of mass moves.

Unlike the components mentioned above, intermediate filaments are assembled from a large family of proteins that form a coiled-coil antiparallel dimer prior to the polymerization.[384] The resulting filaments have an intermediate diameter of 10 nm and lack of polarity.[381,384] They can interact with themselves or with the other cytoskeleton fibrillar structures.[383] However, their main contribution is related with the structural and elastic properties of the cell,[381] such as maintaining the integrity of the nucleus.[383]

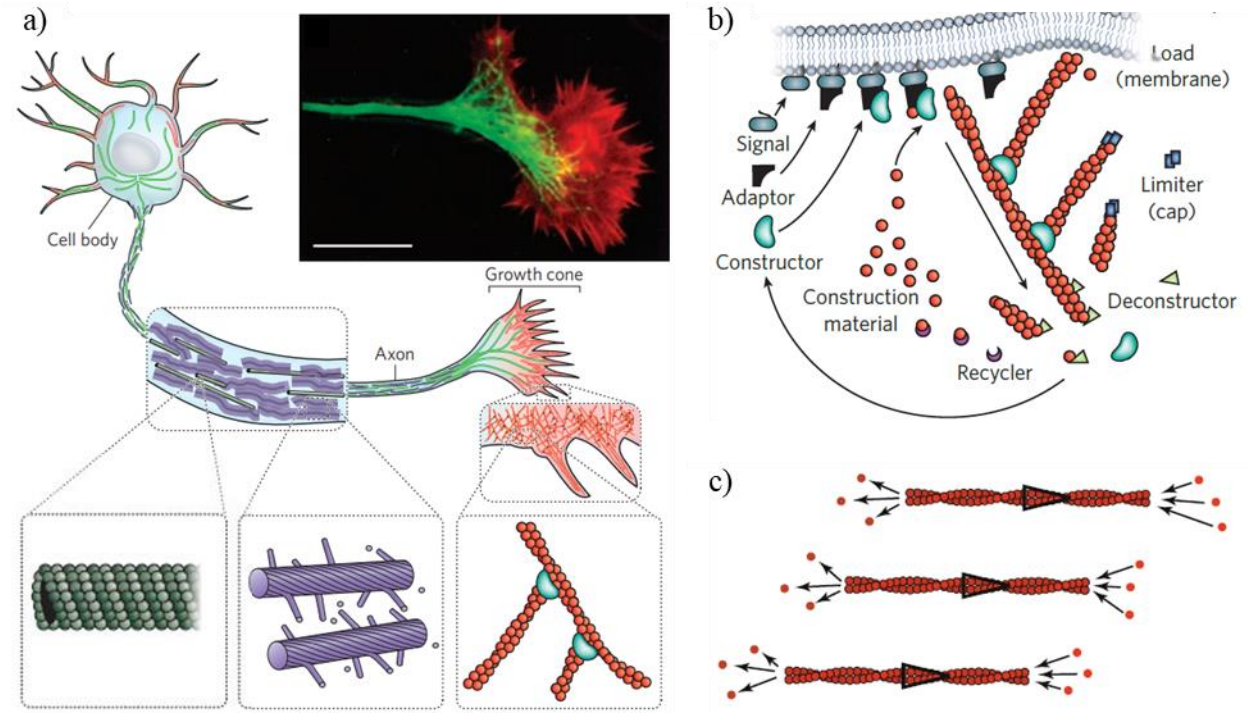

Figure 42. a) Schematic representation and confocal micrograph of a neuron cytoskeleton; b) formation of protrusive and branched actin filaments. Adapted with permission from Ref.383. Copyright © 2010 Springer Nature Limited; and c) a treadmilling actin filament (arrows indicate the polarity). Reprinted with permission from Ref.381. Copyright © 2009 Springer-Verlag New York.

2.1.2. Bottom-up approach to cytoskeleton mimicking systems

Over the years, the growing knowledge about this cell machinery has pointed the scientific focus towards the development of a fully synthetic cytoskeleton that could provide fundamental understanding of the natural counterpart. However, the lack of knowledge about the behavior of confined artificial systems and the functional complexity of the cytoskeleton makes, at the moment, not possible to include all the characteristics at once. Here we will focus our attention on two basic features, the confinement, and the spatiotemporal control over the assembly.

On the one hand, cells are physically separated from the extracellular media by a membrane.[385] This spatial confinement strongly affects the spatial organization of microtubules and actin filaments, influencing mitotic spindle positioning, cellular contractility, and polarity.[386,387] Moreover, studies in bulk and confined spaces have shown differences in the actin bundling threshold, diminishing up to 5 times when is confined.[388] This points out the importance of studying in limited spaces the systems that try to mimic the cytoskeleton.

On the other hand, cells need precise control over the dynamics of the cytoskeleton to be able to carry out processes as complex as division.[389] As commented before, during the interphase the microtubules are found in a radial disposition,[381,384] that have to evolve towards a much dynamic and organized structure during mitosis, the spindle.[390] In this sense, it is necessary to have a right moment for the separation of the centromeres and their final location since the mitotic spindle, responsible for separating the genetic material of the cell, will grow from them. Additionally, while this process is taking place, an actin contractile ring is assembled at the equatorial cell position, to promote the final cell separation.[391] As thought, any misplace of these processes would lead to division failure. This is just one example that emphasize the spatiotemporal control as one of the minimum requirements for designing any synthetic system that mimics the natural cytoskeleton.[392] However, in nature there are many other processes that also require this meticuolous control over the polymerization, such as tip growth,[393] or cell motion.[381]

However, the development of an organic structure with controlled spatiotemporal polymerization in a confined space is just a small step towards the development of an artificial cytoskeletal model. Other characteristics that should be introduce later in these models are their chemical stability to reach out of equilibrium systems,[60] the responsiveness to intra- or extra-cellular changes,[380,383] or the heterogeneous polymeric nature to interact with each other and form a unit.[383]

2.1.3. Microfluidics as confinement methodology

As mentioned above, compartmentalization is one of the minimal requirements to build a synthetic cytoskeleton or any cell mimicking system. Over the years multiple designs have been used to simulate the membrane physical barrier such as polymersomes,[394] proteinosomes,[395] giant

---

[385] M. J. Langton, *Nat. Rev. Chem*., **2021**, *5*, 46–61.
[386] F. C. Tsai and G. H. Koenderink, *Soft Matter*, **2015**, *11*, 8834–8847.
[387] F. Fanalista, A. Birnie, R. Maan, F. Burla, K. Charles, G. Pawlik, S. Deshpande, G. H. Koenderink, M. Dogterom and C. Dekker, *ACS Nano*, **2019**, *13*, 5439–5450.
[388] M. Soares E Silva, J. Alvarado, J. Nguyen, N. Georgoulia, B. M. Mulder and G. H. Koenderink, *Soft Matter*, **2011**, *7*, 10631–10641.
[389] A. F. Straight and C. M. Field, *Curr. Biol*., **2000**, *10*, 760–770.
[390] H. M. Syred, J. Welburn, J. Rappsilber and H. Ohkura, *Mol. Cell. Proteom*., **2013**, *12*, 3135–3147.
[391] M. Miyazaki, M. Chiba, H. Eguchi, T. Ohki and S. Ishiwata, *Nat. Cell. Biol*., **2015**, *17*, 480–489.
[392] F. C. Keber, E. Loiseau, T. Sanchez, S. J. Decamp, L. Giomi, M. J. Bowick, M. C. Marchetti, Z. Dogic and A. R. Bausch, *Science*, **2014**, *345*, 1135–1139.
[393] C. S. Bascom, P. K. Hepler and M. Bezanilla, *Plant Physiol*., **2018**, *176*, 28–40.
[394] R. J. R. W. Peters, M. Marguet, S. Marais, M. W. Fraaije, J. C. M. van Hest and S. Lecommandoux, *Angew. Chem. Int. Ed*., **2014**, *53*, 146–150.
[395] F. Liu, Y. Cai, H. Wang, X. Yang and H. Zhao, *J. Mater. Chem. B*, **2021**, *9*, 1406–1413.

vesicles,[396] coacervates,[397] water-in-oil droplets and so on.[304] More recently, the development of microfluidics technology[398,399] allow the obtention of the above mention structures[400-406] with a higher level of control over critical parameters such as shape, size, volume, composition, and internal concentration.[404,407] Furthermore, the tuning of the mixing regimes using microfluidics also favors precise selection of the self-assembly conditions and pathways in supramolecular assemblies.[408] This features have promoted their use to build artificial cells.[400,407,409]

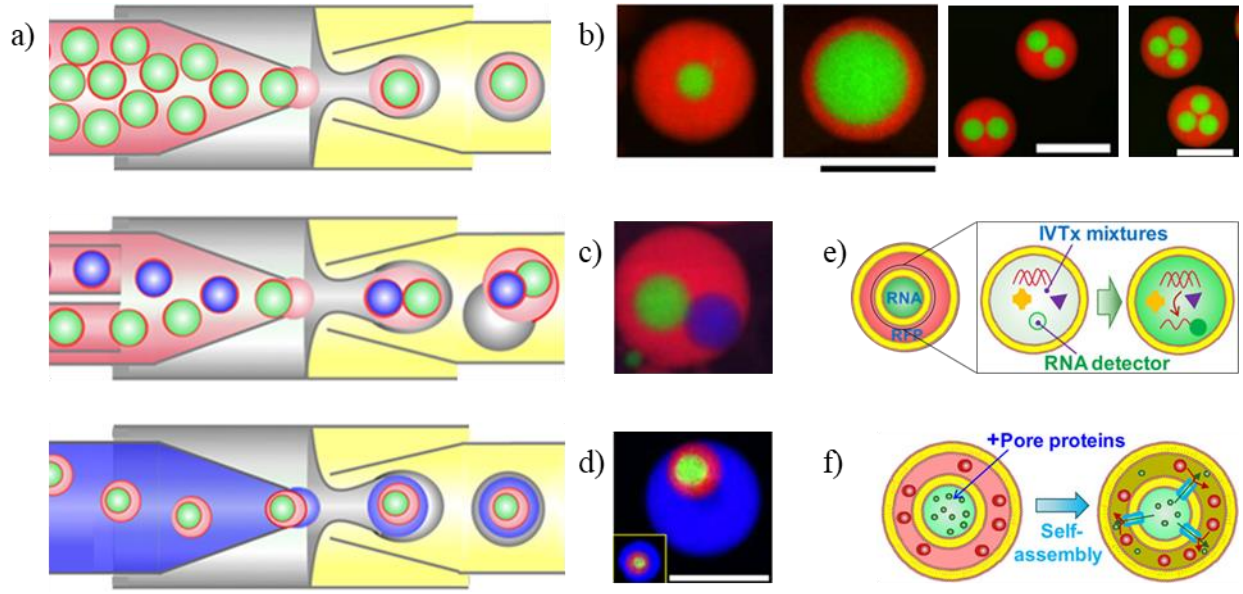

Figure 43. a) Schematic representations of the different microfluidics systems; b), c) and d) confocal images of the different vesosomes; e) and f) schematic representation of the cell mimicking processes of RNA transcription and pore transport. Reprinted with permission from Ref.401. Copyright © 2017 American Chemical Society.

Recently Deng et al. have exploited the versatility of microfluidics to build vesosomes.[401] Vesosomes are multicompartmental liposomal structures with potential applications as drug delivery vehicles, bioreactors, and artificial cells. However, conventional methods do not allow the control of the size, complexity or encapsulation. In this sense, Deng et al. designed multistep microfluidic strategies that produce monodispersed vesosomes with low variability in their

[396] R. Krishna Kumar, X. Yu, A. J. Patil, M. Li and S. Mann, *Angew. Chem. Int. Ed*., **2011**, *50*, 9343–9347.
[397] N. A. Yewdall, A. A. M. André, T. Lu and E. Spruijt, *Curr. Opin. Colloid. Interface. Sci*., **2021**, *52*, 101416.
[398] J. K. Nunes and H. A. Stone, *Chem. Rev*., **2022**, *122*, 6919–6920.
[399] N. Convery and N. Gadegaard, *Micro Nano Eng*., **2019**, *2*, 76–91.
[400] Y. Ai, R. Xie, J. Xiong and Q. Liang, *Small*, **2020**, *16*, 1903940.
[401] N. N. Deng, M. Yelleswarapu, L. Zheng and W. T. S. Huck, *J. Am. Chem. Soc*., **2017**, *139*, 587–590.
[402] N. N. Deng, M. A. Vibhute, L. Zheng, H. Zhao, M. Yelleswarapu and W. T. S. Huck, *J. Am. Chem. Soc.*, **2018**, *140*, 7399–7402.
[403] D. van Swaay, T.-Y. D. Tang, S. Mann and A. de Mello, *Angew. Chem. Int. Ed*., **2015**, *54*, 8398–8401.
[404] R. K. Shah, H. C. Shum, A. C. Rowat, D. Lee, J. J. Agresti, A. S. Utada, L.-Y. Chu, J.-W. Kim, A. Fernandez-Nieves, C. J. Martinez and D. A. Weitz, *Mater. Today*, **2008**, *11*, 18–27.
[405] M. Ugrinic, A. Zambrano, S. Berger, S. Mann, T. Y. D. Tang and A. Demello, *Chem. Comm*., **2018**, *54*, 287–290.
[406] A. Martin, P. Lalanne, A. Weber-Vax, A. Mutschler and S. Lecommandoux, *Int. J. Pharm*., **2023**, *642*, 123157.
[407] A. Salehi-Reyhani, O. Ces and Y. Elani, *Exp. Biol. Med*., **2017**, *242*, 1309–1317.
[408] A. Sorrenti, R. Rodriguez-Trujillo, D. B. Amabilino and J. Puigmartí-Luis, *J. Am. Chem. Soc*., **2016**, *138*, 6920–6923.
[409] C. Martino and A. J. deMello, *Interface Focus*, **2016**, *6*, 20160011.

diameters (< 5%) (Figure 43a). With this strategy they were able to control the content, vesicles size, and the number and nature of the interior liposomes (Figure 43b-f). To explore their behavior as artificial cells, they form vesosomes able to carry out the synthesis of RNA in the nucleus (inner liposome) and proteins in the cytoplasm (outer liposome) (Figure 43e). Furthermore, they explore the inclusion of size-selective pores in the membrane by inserting the membrane protein melittin into the core liposomes. The encapsulation of low and high molecular weight molecules in the different compartments demonstrated the selectivity of the transport size of the channels (Figure 43f). This study highlights the meticulous control that microfluidics allows over the encapsulation process and its potential to build artificial cell models.[410-412]

2.1.4. Natural proteins encapsulation

Since it was found that the cytoskeleton plays a fundamental role in many cellular processes, scientists have devoted a great deal of effort trying to fully understand it. However, replicating this behavior in the laboratory is an extremely difficult task. With this aim in mind, two different strategies have been used up to date to try to simulate the performance of the cytoskeleton.

The first approach consists of the encapsulation of individual components of the cytoskeleton. This methodology provides a way to mimic some of the properties of the cytoskeleton, but also to gather better knowledge about the behavior of the individual constituents, providing new insights about their role in the cellular behavior.[380] For example, Miyazaki et al. reported the spontaneous formation of an actin contractile ring at the equatorial position of water droplets (Figure 44a).[391] For this to happen it was necessary to have bundling factors, a small, round droplet, and for polymerization to begin after encapsulation. Furthermore, the presence of myosin caused the contraction of the ring, the magnitude of which was directly proportional to the concentration of myosin (Figure 44b). These results help explain how cells coordinate the shape and activities of actomyosin to direct cytokinesis. Other complex natural processes such as shape control have also been achieved by encapsulating actin filaments[386] or microtubules.[413]

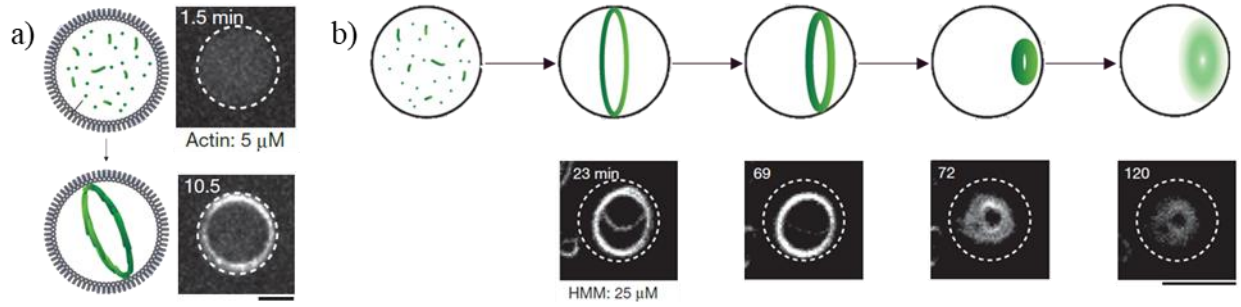

Figure 44. Schematic representations and microscopy micrographs of a) the spontaneous ring formation and b) the myosin triggered ring contraction. Adapted with permission from Ref.391. Copyright © 2015 Springer Nature Limited.

[410] S. Majumder, N. Wubshet and A. P. Liu, *J. Micromech. Microeng.*, **2019**, *29*, 083001.
[411] P. Schwille, J. Spatz, K. Landfester, E. Bodenschatz, S. Herminghaus, V. Sourjik, T. J. Erb, P. Bastiaens, R. Lipowsky, A. Hyman, P. Dabrock, J. Baret, T. Vidakovic-Koch, P. Bieling, R. Dimova, H. Mutschler, T. Robinson, T. -Y. D. Tang, S. Wegner and K. Sundmacher, *Angew. Chem. Int. Ed.*, **2018**, *57*, 13382–13392.
[412] K. Kamiya and S. Takeuchi, *J. Mater. Chem. B*, **2017**, *5*, 5911–5923.
[413] Y. Sato, Y. Hiratsuka, I. Kawamata, S. Murata and S.-I. M. Nomura, *Sci. Robot.*, **2017**, *2*, eaal3735.

2.1.5. Synthetic systems encapsulation

Despite much having advanced with natural proteins, the confined self-assembly of artificial minimal systems that can be engineered by rational design has been much less explored. After many years of designing supramolecular polymers, some of them were able to resemble cytoskeleton properties but in bulk state.[414-417] However, it was not until recently when scientist started to study the behavior of different DNA,[418] polymer,[419] peptide[420] or amino acid[396,396] based materials in confined spaces. For example, R. Booth et al. recently reported a family of linear peptide amphiphiles able to self-assemble into fibers.[421] The redesign of a promising amphiphile precursor that was split in two parts, the peptide precursor and the hydrophobic tail, allowed the in situ generation of the self-assembling peptide amphiphile (Figure 45a).[422] Additionally, the confinement of the peptide precursor in water in oil droplets and the later addition of the octanal caused an homogeneous fibrillation of the PA with a trend to accumulate at the cortex with time. These fibrillar networks placed at the cortex were involved in droplet fusion, cargo uptake and cargo exchange capacities (Figure 45b,c). These results suggest that supramolecular polymers have an important role on the behavior of the droplet and the interactions with its surroundings.

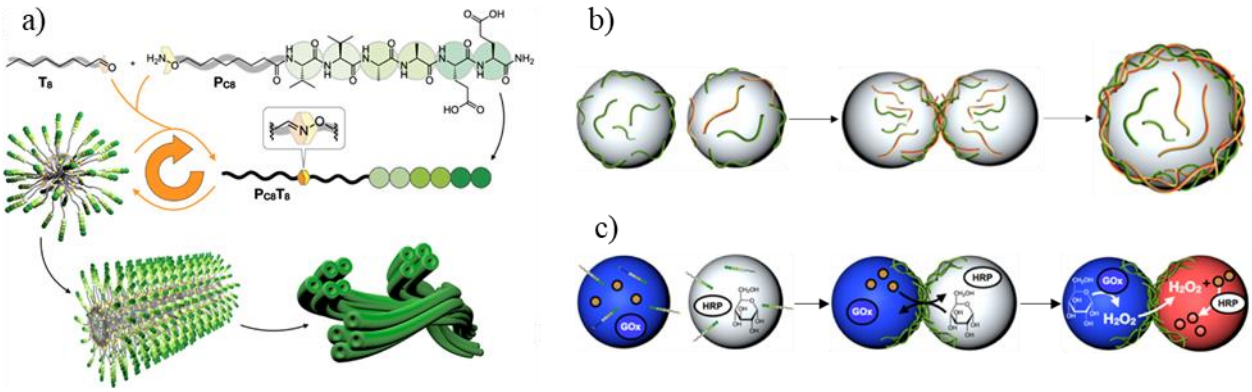

Figure 45. Schematic representations of the a) autocatalytic formation and hierarchical assembly; b) coalescence and c) droplet communication. Adapted with permission from Ref.422. Copyright © 2021 Springer Nature Limited.

As previously commented in the general introduction, our group has designed cyclic peptides that were encapsulated in water droplets that exhibit self-assembling capabilities upon alkalinization, similar to the ones observed in bulk solution. Moreover, this fibrillation caused the deformation of the droplets.[304] However, despite the progresses made with pure synthetic systems

[414] J. Leira-Iglesias, A. Tassoni, T. Adachi, M. Stich and T. M. Hermans, *Nat. Nanotechnol*., **2018**, *13*, 1021–1027.
[415] D. Bochicchio, S. Kwangmettatam, T. Kudernac and G. M. Pavan, *ACS Nano*, **2019**, *13*, 4322–4334.
[416] J. W. Fredy, A. Méndez-Ardoy, S. Kwangmettatam, D. Bochicchio, B. Matt, M. C. A. Stuart, J. Huskens, N. Katsonis, G. M. Pavan and T. Kudernac, *Proc. Natl. Acad. Sci. U. S. A*., **2017**, *114*, 11850–11855.
[417] R. Otter and P. Besenius, *Org. Biomol. Chem*., **2019**, *17*, 6719–6734.
[418] S. Zhou, X. Cai, Y. Zhang, Q. Chen, X. Yang, K. Wang, L. Jian and J. Liu, *J. Mater. Chem. B*, **2022**, *10*, 8322–8329.
[419] Q. Xu, S. Li, M. Qi, J. Gao, C. Chen, P. Huang, Y. Wang, C. Yu, W. Huang and Y. Zhou, *Angew. Chem. Int. Ed*., **2022**, *61*, e202204440.
[420] R. Martí-Centelles, J. Rubio-Magnieto and B. Escuder, *Chem. Comm*., **2020**, *56*, 14487–14490.
[421] R. Booth, I. Insua, G. Bhak and J. Montenegro, *Org. Biomol. Chem*., **2019**, *17*, 1984–1991.
[422] R. Booth, I. Insua, S. Ahmed, A. Rioboo and J. Montenegro, *Nat. Commun*., **2021**, *12*, 6421.

and the importance of the precise location of intracellular supramolecular networks, the control over the spatiotemporal control of synthetic fibrillar networks has not been experimentally achieved.

2.2. Objectives

As just mentioned, cyclic peptides maintain their hierarchical assembling capabilities intact when confined in water in oil droplets.[304] The higher control over the encapsulation process offered by microfluidics inspired us to further study the CPs as artificial building blocks to design synthetic cytoskeleton mimics. In this sense, the main objective of this chapter is to spatially control the supramolecular polymerization of cyclic peptide nanotubes in aqueous droplets. Along the way to achieve the final goal, it was necessary to:

- Find two different polymerization inputs that provided the final assemblies with different characteristics, in our case the changes in pH and ionic strength were selected as chemical stimuli.
- Study the self-assembling behavior of the CP under ionic strength in bulk and compare it with the previously known behavior under alkaline conditions.
- Compare the polymerization response of the CP when subjected to the different stimuli in confined spaces.

2.3. Discussion

2.3.1. Design

Cyclic peptide monomers were employed as building blocks, as they can be precisely designed to trigger their one-dimensional hierarchical polymerization from the nanoscale[269] to the mesoscale.[304] The CP depicted in Figure 46a (**1TP**) is positively charged at acidic pH (pH ~ 4) due to protonation of the lysine and the histidines residues, which prevents **1TP** assembly due to electrostatic repulsions. Attenuation of the repulsive forces by either deprotonation (alkalinization) or by counterion shielding (ionic strength) would favor inter-monomer interactions, triggering the formation of the corresponding self-assembled cyclic peptide nanotubes. In the resulting tubular architecture, the hydrogen-bonded antiparallel β-sheets are stabilized by the π-π stacking interactions and hydrophobic effects of the pyrene units (Figure 46a). However, owing to the distance mismatch between β-sheets (~4.7 Å) and π– π stacks (~3.5 Å), the pyrene moieties should intercalate each other to spread the one-dimensional hierarchical arrangement of the corresponding micrometer-sized tubular bundles (Figure 46a, bottom).[304] As previously reported, the pH control of solutions of **1TP** allowed peptide self-assembly assisted by pyrene stacking as has been shown by the quenching and bathochromic shift of the fluorescence emission due to excimer formation.[290, 291, 304]

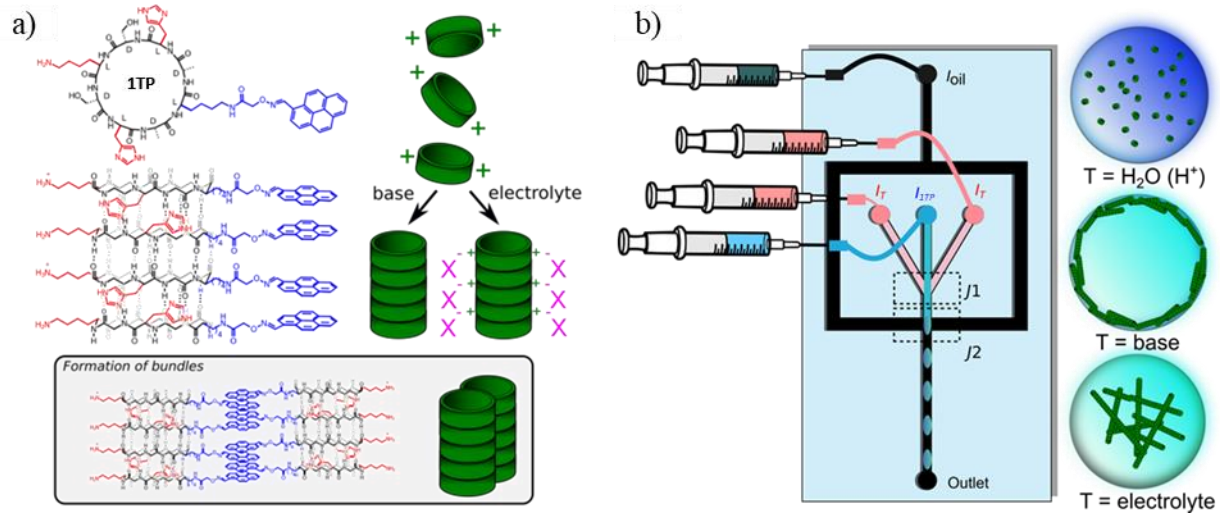

Figure 46. Spatially controlled supramolecular fibrillation. a) Structure and model of pH-triggered self-assembly of cyclic peptide **1TP**. Basic amino acids are in red, pyrene moiety in blue. b) Microfluidic device for the in situ fibrillation. Channels dimensions: 35x50 µm. **1TP** in aqueous conditions (1 mM, milliQ water, pH 3-4) was injected in inlet I_{1TP} (blue) at flow rates of 200-150 µLh^{-1} and assembled upon mixing with inlets I_T containing water, base (NaOH 3.5 mM) or an electrolyte (such as CaCl2 1M) in junction *J*1 (pink) at flow rates of 100 mLh^{-1}. The aqueous stream converges with the oil phase (HFE 7500 3M Novec with 0.5% v/v Pico-Surf as surfactant, black) by I_{oil} inlet in *J*2 for droplet generation at flow rates of 500 mLh^{-1}. Droplets are collected in the outlet.

2.3.2. Ionic strength responsiveness

We hypothesized that ionic strength could also be employed to trigger the self-assembly of **1TP** by shielding electrostatic repulsions by counterion scavenging. Typically, electrostatic repulsions decrease by decreasing Debyes double layer thickness, which is inversely proportional

to the ionic strength.[423] Therefore, addition of electrolytes should allow the self-assembly of protonated peptide nanotubes.[424,425] These two different trigger signals (pH and ionic strength) would thus lead to different tubular networks with potential different interactions with the environments of the water droplet, that is, interface or aqueous inner volume. To test this hypothesis, we initially studied the self-assembly of protonated **1TP** in bulk aqueous buffer by adding a variety of different electrolytes such as $CaCl_2$, NaCl, or Na_2SO_4 (Figure 47). The increase of the Cotton effect, assigned to the π-π^* transition of the pyrene moiety, confirmed that self-assembly of **1TP** is triggered by the ionic strength modulation (Figure 47a). As expected, this process was more efficient for multivalent anions (SO_4^{2-} vs. Cl^-) than multivalent cations (Ca^{2+} vs. Na^+). A quenching in the fluorescence emission of the pyrene was also observed, as would be expected due to the ionic shielding of the cationic charge of the peptide monomers (Figure 47b). Fluorescence microscopy confirmed that ionic strength triggered the fibrillar assembly of **1TP**, which was dependent on the concentration and the chemical nature of the added counterions (Figure 48) revealing a higher tendency towards aggregation in the presence of multivalent anions (SO_4^{2-}, Figure 48 bottom). The corresponding one-dimensional hierarchical bundles of cyclic peptide nanotubes were also confirmed by STEM electron microscopy (Figure 104).

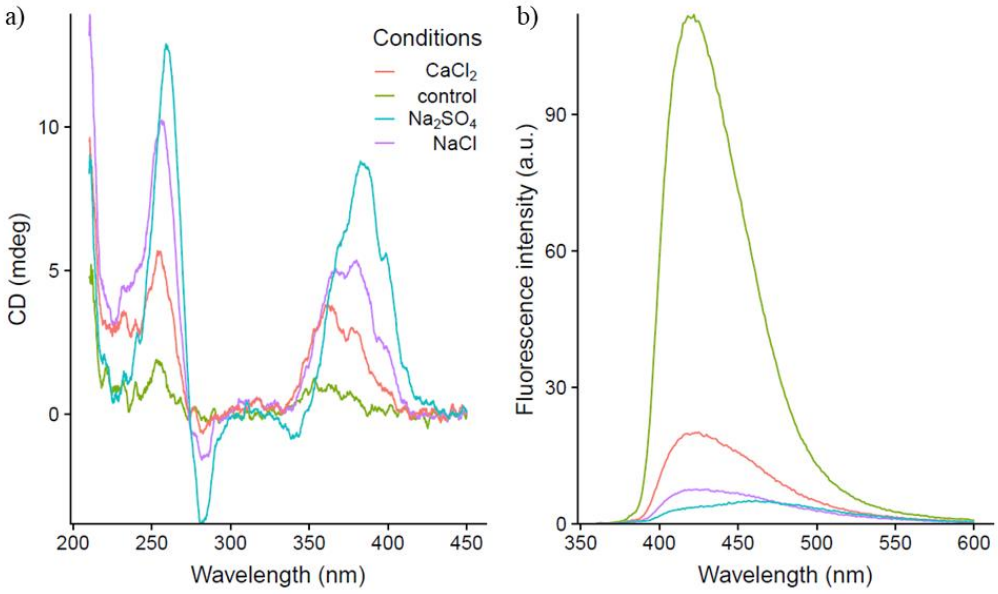

Figure 47. Assembly of **1TP** (50 μM) in MES (50 mM) at pH 5.6 at a molar ionic strength of approximately 1.5 M. Control experiments indicate the absence of salt (green line). The electrolytes were $CaCl_2$ (0.5 M, red line), NaCl (1.5 M, purple line) and Na_2SO_4 (0.5 M, blue line): a) circular dichroism experiments and b) fluorescence experiments, λ_{exc} = 340 nm.

[423] G. M. Kontogeorgis and S. Kiil, *Introduction to applied colloid and surface chemistry*, John Wiley & Sons, Chichester, 1st edn., **2016**.
[424] D. A. Walker, B. Kowalczyk, M. O. De La Cruz and B. A. Grzybowski, *Nanoscale*, **2011**, *3*, 1316–1344.
[425] J. C. Stendahl, M. S. Rao, M. O. Guler and S. I. Stupp, *Adv. Funct. Mater.*, **2006**, *16*, 499–508.

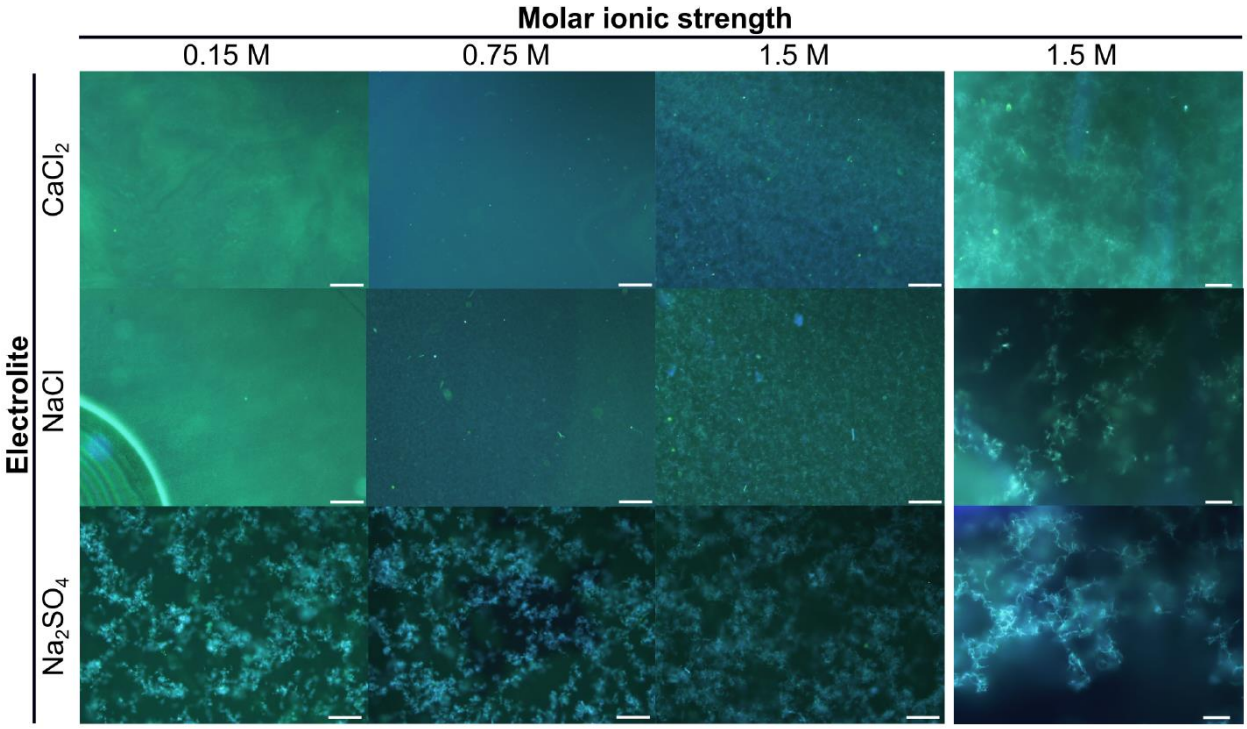

Figure 48. Effect of electrolyte concentration in the self-assembly of **1TP** visualized by fluorescence microscopy. Scale bars are 100 μm for low magnification (left block) and 20 μm for high magnification (right block).

2.3.3. Microfluidic encapsulation

After confirming the efficient hierarchical self-assembly of cyclic peptides by modulation of the ionic strength, we hypothesized that the microfluidic-controlled tandem encapsulation and self-assembly of cyclic peptides using different trigger signals (that is, pH or ionic strength) could be applicable to adjust the packing degree, the chemical nature and the spatial positioning of the resulting supramolecular peptide fibers. The microfluidic device shown in Figure 46b was employed to control the tandem assembly and droplet confinement of **1TP** in the presence or absence of different stimuli. We initiated peptide nanotube assembly in junction J_1 by merging the streams of I_{1TP}, containing a diluted aqueous **1TP** solution (1 mm) and I_T, containing the assembly-triggering solution (that is, base or highly concentrated saline solutions). Assembly kinetics and theoretical calculations suggest that although self-assembly might be initiated before droplets formation, equilibration takes place within the droplet (Experimental section 2.12). Droplet encapsulation was immediately achieved in junction J_2 by flow focusing the aqueous stream with an oil stream composed of HFE 7500 3M Novec and 0.5% v/v Pico-Surf as surfactant (I_{oil}).[426] This set up was employed to adjust the flow rates at (I_T) and the different stimuli for the spatially controlled distribution of the nanotubes within the aqueous droplets.

[426] C. Holtze, A. C. Rowat, J. J. Agresti, J. B. Hutchison, F. E. Angilè, C. H. J. Schmitz, S. Köster, H. Duan, K. J. Humphry, R. A. Scanga, J. S. Johnson, D. Pisignano and D. A. Weitz, *Lab Chip*, **2008**, *8*, 1632–1639.

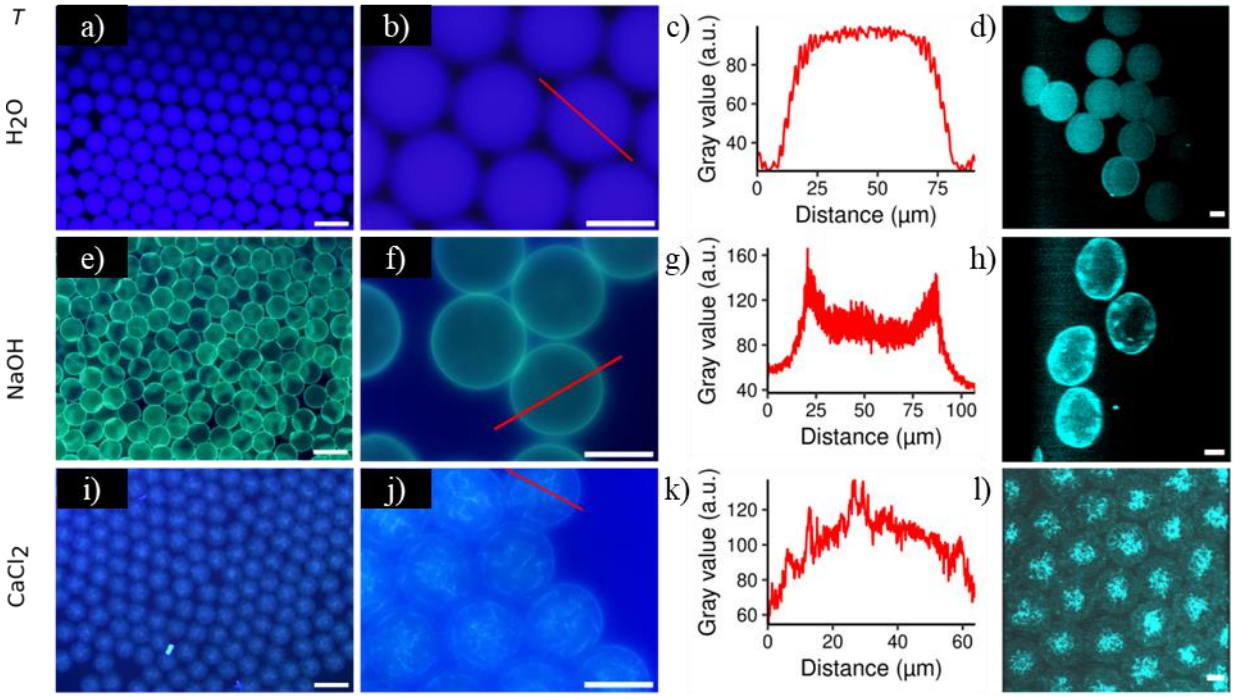

Figure 49. Self-assembly of **1TP** in microfluidic generated droplets (water-in-oil) as function of composition of inlet I_T. Top, middle, and bottom rows show the results when I_T is water, NaOH (3.5 mM) and $CaCl_2$ (1M) respectively. a), e), i) Low-magnification images (scale bars: 100 μm). b), f), j) High-magnification images (scale bars: 50 μm). c), g), k) Profiles extracted from high magnification images (red lines in b, f, j). d), h), l) Confocal 3D projections of the droplets (scale bars: 25 μm). Flow rates: I_{oil} = 500 μLh^{-1}; I_{1TP} = 200-150 μLh^{-1}; I_T = 100 μLh^{-1}.

Initial experiments were performed by flowing pure water in the assembly inlets (I_T), which merged in J_1 with acidic (pH ~ 4) aqueous solution of **1TP** (I_{1TP}) and the resulting solution was encapsulated in droplets (J_2). Fluorescence microscopy analysis of these droplets showed the typical blue fluorescence emission that belongs to dispersed CPs and monomeric pyrene (Figure 49a,b). As expected, fluorescence profile of the droplets and the corresponding confocal planes showed that the pyrene emission was equally distributed along the droplet interior (Figure 49c,d). However, when an alkaline solution (NaOH 3.5 mM) was injected in I_T, a redshifted green fluorescent halo was observed in the periphery of the dropelt (Figure 49e,h). The corresponding micrographs indicated a preferential adsorption of the supramolecular peptide nanotubes and microfibers at the perimeter of the water-droplet interface (Figure 49g,h) in capsule-like structures.[427,428] Similar results were observed in fibrillation experiments using HEPES buffer (50 mm, pH 8) as to precisely control the pH increase (Figure 106). Microfluidic fibrillation experiments by direct base pico-injection ($NaOH_{aq}$), in preformed droplets loaded with homogeneously dispersed **1TP** (pH ~ 4), again showed the assembly of a fluorescent droplet cortex,

[427] J. Zhang, R. J. Coulston, S. T. Jones, J. Geng, O. A. Scherman and C. Abell, *Science*, **2012**, *335*, 690–694.
[428] J. Zhang, J. Liu, Z. Yu, S. Chen, O. A. Scherman and C. Abell, *Adv. Funct. Mater.*, **2018**, *28*, 1800550.

which was reminiscent of reconstituted actin[429] or DNA[430] cortical shells (Figure 107). These pico-injection experiments unambiguously confirmed that the spatial control of the supramolecular polymerization was caused by the modulation of the chemical signal. In contrast to the pH stimulus, the use of a solution of high ionic strength ($CaCl_2$, 1M), resulted in the fibrillar networks concentrating in the core of the droplet from where they spanned throughout the internal volume of the droplets (Figure 49i-l). As shown in the corresponding fluorescent profile, a much lower absorption at the droplet surface and a maximal fiber concentration at the droplet core could be traced (Figure 49k,l). Confocal planes further supported these observations (Figure 108 and Figure 109).

2.3.4. Spectroscopic characterization in droplets conditions

To rationalize these results, the fluorescence emission, the UV/Vis absorbance, and the circular dichroism (CD) were measured and compared under exactly the same conditions to those used in the fibrillation experiments in the microscope (Figure 50). The CD spectra indicated that the chirality of resulting the assemblies was similar regardless of the chemical stimulus used (Figure 50a). However, comparison of the fluorescence emission of the CP solutions under acidic, alkaline and high ionic strength conditions showed a stronger fluorescence quenching for the fibrillar assemblies at alkaline pH (Figure 50b). Additionally, the normalized fluorescence emission spectra again indicated a stronger excimer signal also for the higher pH solution suggesting stronger packing of the pyrene units,[290] as expected for the assembled deprotonated monomers (Figure 50b inset).

To further study the assembly process, we employed Thioflavin T (ThT), a fluorescent probe that enhances its fluorescence emission in its planar state when trapped within β-sheets.[431,432] In these experiments, the self-assembly of **1TP** would bring into close contact with the thioflavin probe and the pyrene of the peptide, which should give rise to fluorescence resonance energy transfer (FRET) between the pyrene donor and the ThT exogenous acceptor.[304] The ThT emission (FRET effect) was higher for peptide assembled upon alkalinization, which indicated a more efficient and compact nanotube packing of the cyclic peptides assembled under basic conditions (Figure 50c). UV-Vis spectra also showed a greater decrease in the extinction coefficient of pyrene under basic conditions, which was again a clear indication of a stronger association of pyrene in the resulting nanotubes (Figure 50c). These results were consistent with a more compact supramolecular packing of the more hydrophobic deprotonated fibers obtained by alkalinization, which would have a higher affinity for the droplet oil–water interface. In contrast, fibers assembled under high ionic strength were found to be charged and less packed to allow higher electrostatic interactions between nanotubes. These more hydrophilic tubular bundles have a lower affinity for the droplet interface and, therefore, they concentrate at the droplet core. These series of experiments

[429] L. Limozin, M. Bärmann and E. Sackmann, *Eur. Phys. J. E*, **2003**, *10*, 319–330.
[430] C. Kurokawa, K. Fujiwara, M. Morita, I. Kawamata, Y. Kawagishi, A. Sakai, Y. Murayama, S. I. M. Nomura, S. Murata, M. Takinoue and M. Yanagisawa, *Proc. Natl. Acad. Sci. U. S. A.*, **2017**, *114*, 7228–7233.
[431] L. S. Wolfe, M. F. Calabrese, A. Nath, D. V Blaho, A. D. Miranker and Y. Xiong, *Proc. Natl. Acad. Sci. U. S. A.*, **2010**, *107*, 16863–16868.
[432] P. K. Singh, A. K. Mora and S. Nath, *Chem. Commun.*, **2015**, *51*, 14042–14045.

confirmed that the assembly pathway can lead to different supramolecular polymers with particular affinities for different environments in a single water droplet.

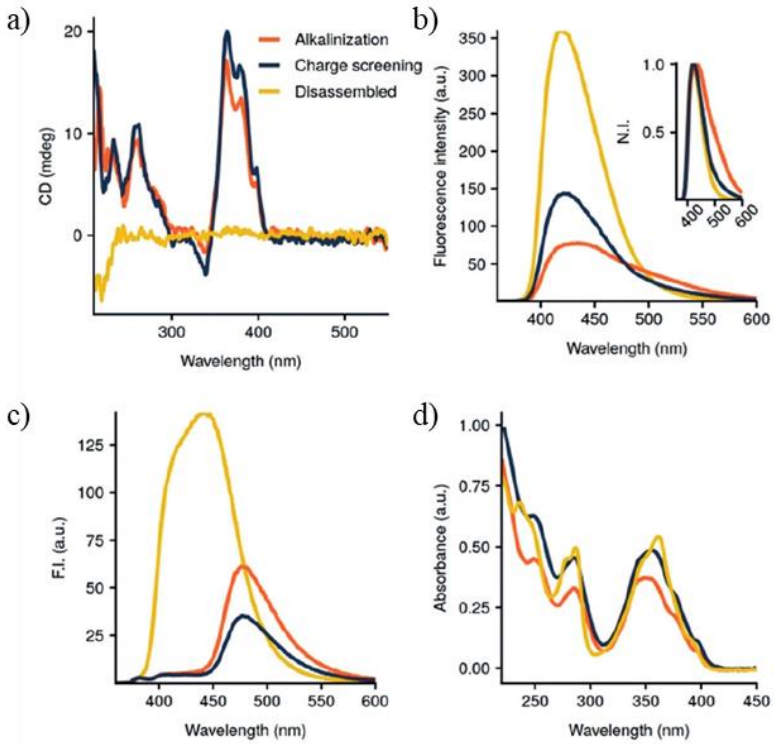

Figure 50. Spectroscopic characterization of **1TP** self-assembly. In all cases,the different conditions are highlighted by different colors: acidic (HCl pH ~ 4) in yellow, HEPES (50 mM, pH 8) in orange, and $CaCl_2$ (500 mM) in dark blue. a) Circular dichroism of **1TP** (200 μM); b) Pyrene fluorescence emission. (λ_{exc} = 340 nm). Conditions: pH (80% quenching) and ionic strength (60% quenching); c) FRET between pyrene and ThT fluorophores[304] ([ThT]=20 μM; λ_{exc} = 340 nm). d) UV absorbance spectra to monitor self-assembly of **1TP** (200 μM) at different conditions.

2.3.5. Control over the spatial behavior

The experimental confirmation of the different assembly pathway and chemical nature of microfluidic-triggered fibrillar networks, prompted us to explore the potential spatial positioning of supramolecular polymers by tuning the flow rate of the corresponding trigger. In this case, modulation of the flow of electrolyte (I_T) would control the molar ratio between the anions and the cationic peptide monomers and thus allow a different degree of ionic shielding of the resulting supramolecular fibers. Therefore, cyclic peptide self-assembly was triggered by controlling the flow of multivalent anions (such as $SO4^{2-}$) to adjust ionic strength and electrostatic crosslinking and thus adapt the density of the peptide fibrillar network and its spatial position inside the droplet container. Gratifyingly, the corresponding micrographs confirmed the gradual and precise adjustment of the fibers along the droplet by regulating the flow rates of the electrolyte injection (Figure 51a). An electrolyte shock employing high flow rates of Na_2SO_4 of 150 μLh^{-1} led to a strong ionic shielding of the peptide monomers and a crosslinking degree of the protonated microtubular networks. As a consequence, these hydrophilic fibrillar networks concentrated at the core of the droplets (Figure 51a, top). However, the decrease the electrolyte ($SO4^{2-}$) flow rate (for

example, 20 μLh^{-1}) provided the gradual distribution of the supramolecular fibers throughout the water droplet internal volume (Figure 51a, bottom).[433] Quantification of the fluorescent area in droplet populations confirmed that the higher the electrolyte flow rate, the less the fibrillated fluorescent area per individual droplet (Figure 51b). Comparatively, changes in flow rates using NaOH or $CaCl_2$ did not show such finely tuned trends (Figure 110).

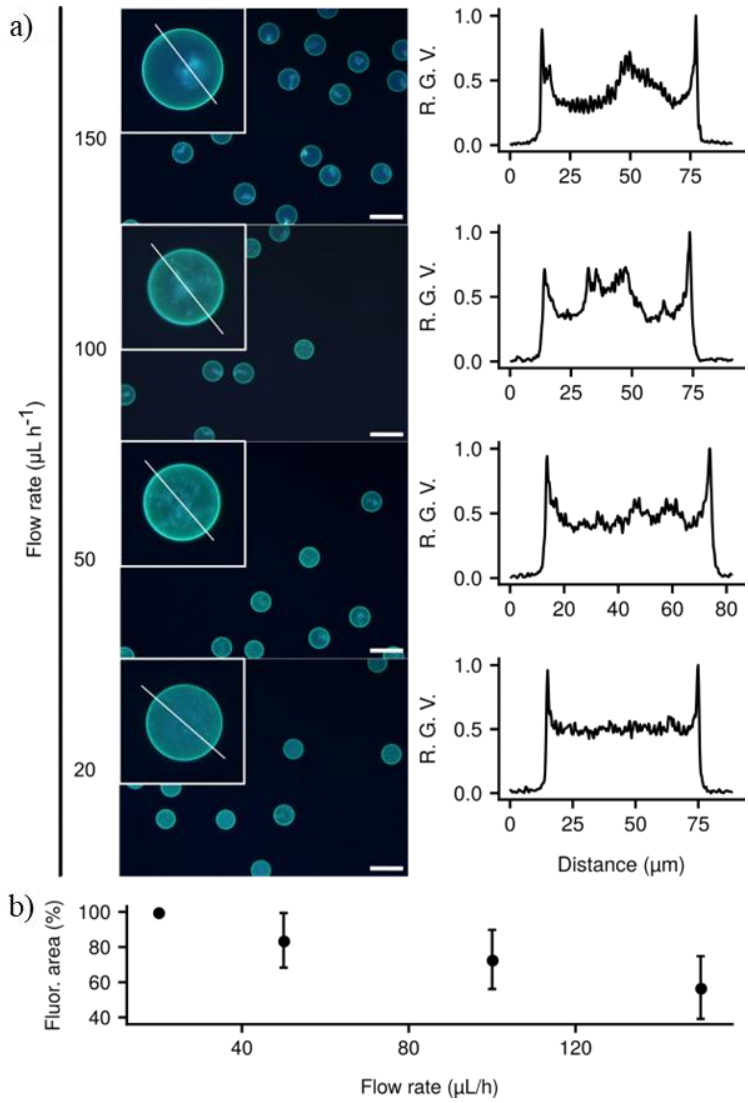

Figure 51. a) Fluorescence micrographs showing network density in the self-assembly of **1TP** in W/O droplets. The peptide (1 mM) was assembled by co-flowing it with Na_2SO_4 5 mM at different flow rates. Flow rates of I_{oil} and I_{1TP} were constant (500 μLh^{-1} and 200 μLh^{-1} respectively). Flow rates of I_T Na_2SO_4 5 mM were varied from 150 to 20 μLh^{-1}. Insets: the traced profile for a representative droplet. Scale bars: 100 µm. b) Percentage of fluorescence area per droplet by image analysis. Average area with standard deviation for the analysis of 20 random droplets. R.G.V.=relative gray value.

[433] S. Mellouli, B. Monterroso, H. R. Vutukuri, E. Te Brinke, V. Chokkalingam, G. Rivas and W. T. S. Huck, *Soft Matter*, **2013**, *9*, 10493–10500.

Spatial control of supramolecular polymerization regulates different communication processes in living systems such as active uptake, multicellular assembly or cell to cell communication.[434] Populations of artificial droplets have also shown adaptive interactions or even tissue-like self-organization.[435-437] Additionally, micro-printing technology has recently allowed the patterning of tissue-like synthetic materials with single droplet resolution.[438] Inspired by functional natural fibrillar networks and the growing importance of droplet micro-patterning, we decided to test if the positional control of the supramolecular polymer could be used to tune assembly of droplet populations.[439]

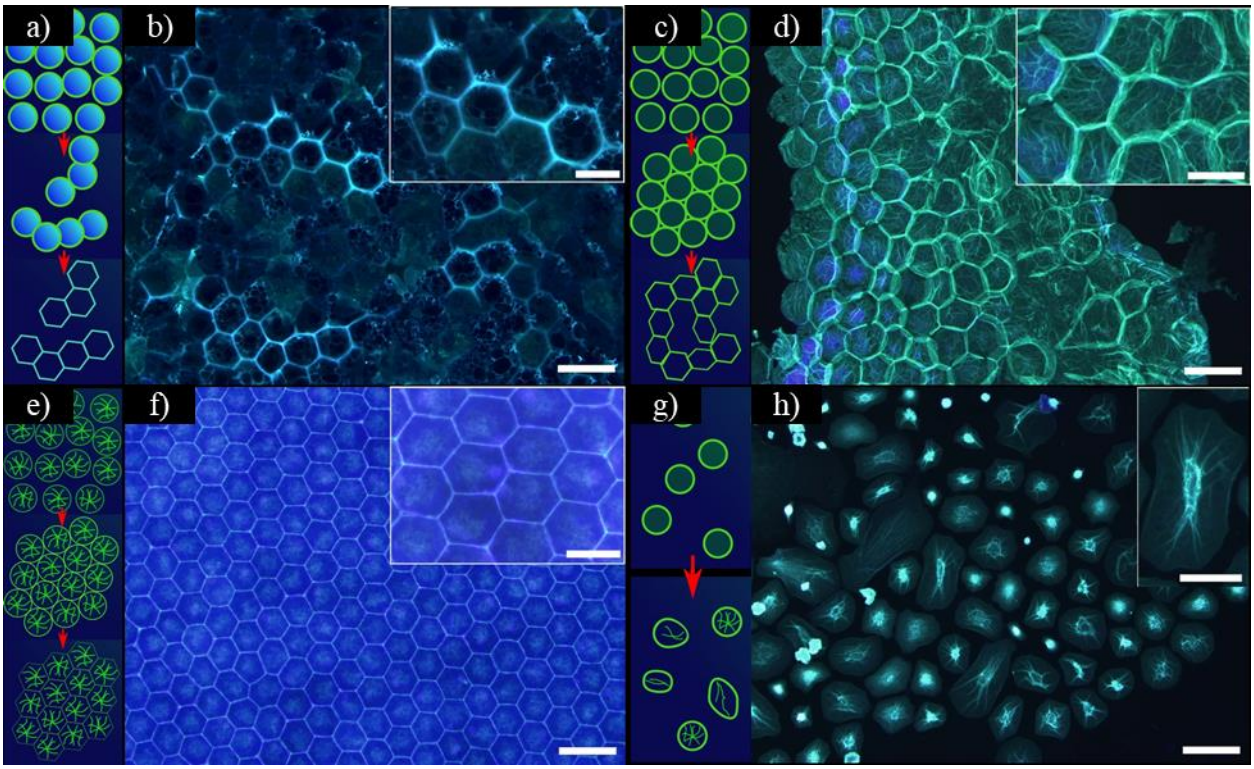

Figure 52. Depictions of the process of Novec oil evaporation and fluorescence microscopy images showing 2D droplet networks after oil evaporation. Red lines in cartoons denote the effect of time lapse. a), b) Induced droplet assembly in homogenously dispersed **1TP** droplets. c) and d) Induced droplet assembly in cortex-fibrillated droplets (NaOH 3.5 mM); e), f) Induced droplet assembly in core-fibrillated droplets ($CaCl_2$, 1M). g), h) Induced assembly in diluted droplet suspensions over a higher boiling point oil Fluorinert-FC70 (HEPES 50 mM pH 8). a), c), e), g) Representation of the process, b), d), f), h) epifluorescence images. Scale bars: 100 μm (low magnification) and 50 μm (high magnification).

Therefore, the fluorinated oil was carefully evaporated to promote the assembly of water droplets where the polymerization of supramolecular peptide fibers was induced at different

[434] M. Baker, *Nature*, **2017**, *549*, 322–324.
[435] H. Niederholtmeyer, C. Chaggan and N. K. Devaraj, *Nat. Commun.*, **2018**, *9*, 5027.
[436] P. Gruner, B. Riechers, B. Semin, J. Lim, A. Johnston, K. Short and J. C. Baret, *Nat. Commun.*, **2016**, *7*, 10392.
[437] K. M. Chang, M. R. R. de Planque and K. P. Zauner, *Sci. Rep.*, **2018**, *8*, 12656.
[438] G. Villar, A. D. Graham and H. Bayley, *Science*, **2013**, *340*, 48–52.
[439] P. Zhu, T. Kong, C. Zhou, L. Lei and L. Wang, *Small Methods*, **2018**, *2*, 1800017.

positions (Figure 52). Amorphous networks were observed for the assembly of droplets loaded with dispersed cyclic peptides (pH ~ 4), which suggested an uncontrolled aggregation of the droplet suspensions mainly due to disordered surfactant interactions (Figure 52a,b). In contrast, cortex fibrillated droplets (Figure 52c,d) showed the formation of a roughly assembled network with a green-shifted thick peptide wall with irregular hexagonal and pentagonal patterns. The high curvature topologies and the bathochromic shift of the pyrene emission suggested a strong droplet aggregation triggered by the bundling of the peptide fibers located at the perimeter (Figure 52c,d). However, highly regular hexagonal honeycomb patterns (Figure 52e,f) were formed when the assembly was carried out from droplets suspensions where the fibers were located at the internal core of the droplets (Figure 49i-l). These highly regular networks indicated a more controlled assembly process when the fibers from the droplet core gradually coalesced at the network interface (Figure 52e,f). Finally, anisotropic supramolecular structures, reminiscent of natural fibrillar networks, could also be detected when a droplet emulsion was allowed to dry over a higher boiling point oil (Fluorinert-FC70; Figure 52g,h). In this case, the synthetic tubular networks were projected from the droplet core to its periphery and randomly distributed for the smaller spherical droplets. In contrast, anisotropic growth of the supramolecular polymers was confirmed in the direction of the aqueous distribution pattern in elongated droplets (Figure 52h).

2.4. Conclusions

In this chapter, we have demonstrated the control over the supramolecular polymerization of synthetic fibers in artificial minimal models and suggests the important role of the different chemical environments for the distribution of natural fibrillar networks in simple primitive protocells.

Other important conclusions that can be taken from this chapter are:

- The assembly of the cyclic peptide pyrene derivative is strongly influenced by the ionic strength, both in bulk and in confined spaces.
- Both spectroscopic and microscopy studies suggest a higher degree of packing under alkaline conditions compared to the increase of ionic strength.
- It is possible to spatially control the polymerization of supramolecular fibers in water droplets by the adjustment using microfluidic techniques of the chemical signals that trigger the self-assembling process.
- The microfluidic tuning of the chemical nature or flow rates of the polymerization stimuli made it possible to modulate the structure of the tubular network and its precisely adjusted spatial position under the different physicochemical environments of a water droplet container (interface vs. aqueous core).
- This technology can be further applied in the generation of well-ordered two-dimensional droplet networks by exploiting the spatially adjusted self-assembly of CP nanotubular bundles.

3. 2D ASSEMBLIES BASED ON A TETRAPHENYLETHYLENE D,L-CYCLIC PEPTIDE SCAFFOLD

3.1. Precedents

In chapter I and chapter II, we have exploited the ability of cyclic peptides modified with aromatic units that self-assemble into 1D structures stabilized by H-bonds and π-π stacking, which continue to interact hierarchically to form bundles of SCPNs thanks to further π-π interactions and hydrophobic effect. In addition, recently it has been also demonstrated that specifically designed CPs can promote the lateral interaction of SCPNs giving rise to 2D materials.[301,302]

3.1.1. 2D Nanomaterials

The scientific focus on the development of 2D materials started back in 2004 when K.S. Novoselov et al. discovered graphene and its outstanding electrical properties.[440] From that time, the use of different materials to control the properties of the 2D systems paved the way to their use in optoelectronics, catalysis, or sensing, among others.[441,442] However, many of these materials need harsh conditions and tedious exfoliation procedures for their synthesis pointing out the urgency for the development of suitable methodologies that allowed the bottom up synthesis of well-defined materials with tuned properties.[442]

In the recent years, molecular self-assembly has gained nanotechnological importance since it allows controlling the organization of nanostructures by encoding information at the molecular level.[443,444] In this sense, supramolecular structures with known propensity to form 1D aggregates, such as peptides,[445-447] peptoids,[168,448] proteins,[216,449] nucleic acids,[196,450,451] polymers[155,452,453] and others,[454-456] have been designed to grow in a second dimension. The exquisite control over the monomer properties have paved the way for their use in a wide variety of applications like nanotechnology,[450,452] catalysis[447] or biology.[168,448,449] From the variety of scaffolds, peptides and proteins are of particular interest since they combine the physical and chemical properties of 2D

---

[440] K. S. Novoselov, A. K. Geim, S. V Morozov, D. Jiang, Y. Zhang, S. V Dubonos, I. V Grigorieva and A. A. Firsov, *Science*, **2004**, *306*, 666–669.
[441] X. Zhuang, Y. Mai, D. Wu, F. Zhang and X. Feng, *Adv. Mater*., **2015**, *27*, 403–427.
[442] C. E. Boott, A. Nazemi and I. Manners, *Angew. Chem. Int. Ed*., **2015**, *54*, 13876–13894.
[443] T. Govindaraju and M. B. Avinash, *Nanoscale*, **2012**, *4*, 6102–6117.
[444] I. Insua, J. Bergueiro, A. Méndez-Ardoy, I. Lostalé-Seijo and J. Montenegro, *Chem. Sci*., **2022**, *13*, 3057–3068.
[445] Y. Lin, M. Penna, M. R. Thomas, J. P. Wojciechowski, V. Leonardo, Y. Wang, E. T. Pashuck, I. Yarovsky and M. M. Stevens, *ACS Nano*, **2019**, *13*, 1900–1909.
[446] Y. Lin, M. R. Thomas, A. Gelmi, V. Leonardo, E. T. Pashuck, S. A. Maynard, Y. Wang and M. M. Stevens, *J. Am. Chem. Soc.*, **2017**, *139*, 13592–13595.
[447] T. Kim, J. Hong, J. Kim, J. Cho and Y. Kim, *J. Am. Chem. Soc.*, **2023**, *145*, 1793–1802.
[448] A. Battigelli, J. H. Kim, D. C. Dehigaspitiya, C. Proulx, E. J. Robertson, D. J. Murray, B. Rad, K. Kirshenbaum and R. N. Zuckermann, *ACS Nano*, **2018**, *12*, 2455–2465.
[449] S. Zhang, J. Zhang, W. Fang, Y. Zhang, Q. Wang and J. Jin, *Nano Lett*., **2018**, *18*, 6563–6569.
[450] X. Wang, H. Jun and M. Bathe, *J. Am. Chem. Soc.*, **2022**, *144*, 4403–4409.
[451] P. Wang, S. Gaitanaros, S. Lee, M. Bathe, W. M. Shih and Y. Ke, *J. Am. Chem. Soc.*, **2016**, *138*, 7733–7740.
[452] L. Han, M. Wang, X. Jia, W. Chen, H. Qian and F. He, *Nat. Commun*., **2018**, *9*, 865.
[453] A. Rajak and A. Das, *Angew. Chem. Int. Ed*., **2022**, *61*, e202116572.
[454] M. Kawaura, T. Aizawa, S. Takahashi, H. Miyasaka, H. Sotome and S. Yagai, *Chem. Sci*., **2022**, *13*, 1281–1287.
[455] J. Dong, L. Liu, C. Tan, Q. Xu, J. Zhang, Z. Qiao, D. Chu, Y. Liu, Q. Zhang, J. Jiang, Y. Han, A. P. Davis and Y. Cui, *Nature*, **2022**, *602*, 606–611.
[456] Q. Zhang, R. J. Xing, W. Z. Wang, Y. X. Deng, D. H. Qu and H. Tian, *iScience*, **2019**, *19*, 14–24.

structures, attributed to their large surface area and flexibility,[457,458] with intrinsic biopolymer properties such as biocompatibility, bioactivity and tunable assembling properties.[459,460]

Lin et al. have recently designed a peptide amphiphile bearing six phenylalanine, one hydrophobic tail, and glutamic acids able to assemble into Janus 2D structures with single-layer thickness (Figure 53a,b).[446] The phenylalanine segment promotes the growth in one direction though the formation of β-sheets structures and in a second via aromatic interactions, both strengthen by the hydrophobic effect of the alkyl chain. Further experiments demonstrated that co-assembly with the functionalized peptide was possible without any morphological change being observed in the nanosheets. In this way, the surface could display biotin allowing the decoration of the lamina with avidin-enzymes complexes to enhance their catalytic activity (Figure 53c). Moreover, the self-sorting between peptide β-strands and hydrocarbon chains[461] enables the heterofunctionalization of the asymmetric layers. However, subtle modifications on the peptide scaffold such as removing one phenylalanine gave rise to twisted fibers highlighting the importance of the molecular design to build new 2D supramolecular systems.

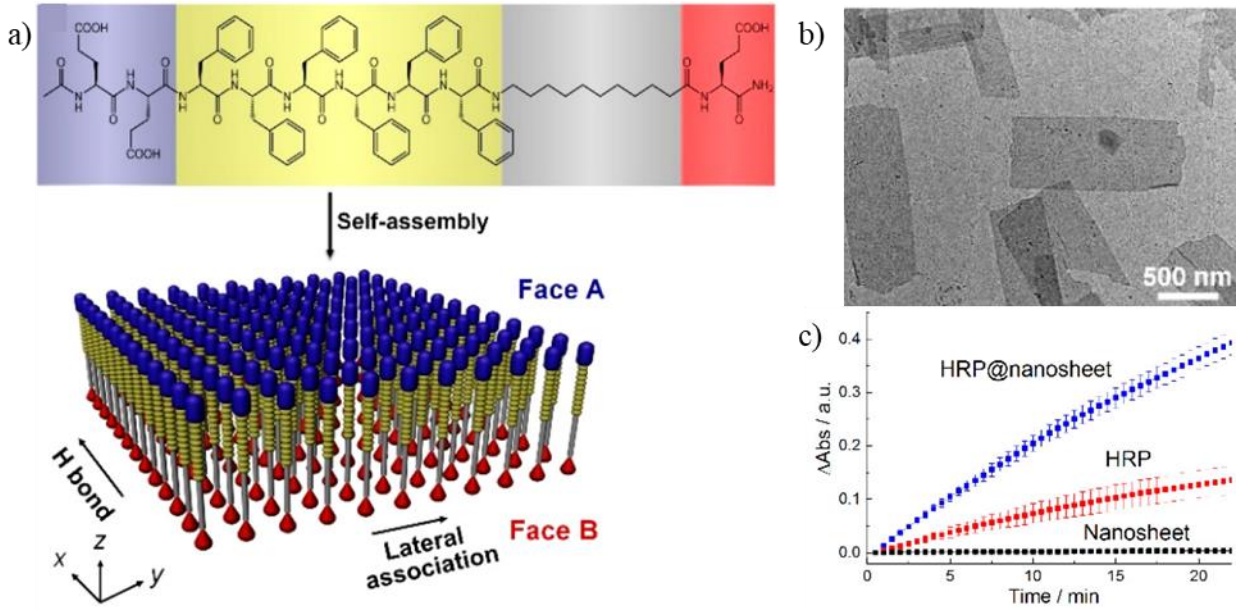

Figure 53. a) Chemical structure and self-assembling scheme into Janus nanosheets; b) TEM micrograph of the nanosheets; and c) enhancement of the catalytic activity of the enzyme when displayed on the surface of the 2D system. Adapted with permission from Ref.446. Copyright © 2017 American Chemical Society.

Kim et al. report the use of a bioactive peptide (DGEA)[461] synthetically modified with pyrene that was able to transition from supramolecular vesicles to 2D nanostructures[447] through the formation of arene–perfluoroarene stackings in presence of octafluoronaphthalene (OFN) (Figure

[457] B. Shen, Y. Kim and M. Lee, *Adv. Mater.*, **2020**, *32*, 1905669.
[458] T. Kim, J. Y. Park, J. Hwang, G. Seo and Y. Kim, *Adv. Mater.*, **2020**, *32*, 2002405.
[459] A. Lampel, R. V. Ulijn and T. Tuttle, *Chem. Soc. Rev.*, **2018**, *47*, 3737–3758.
[460] C. C. Huang, M. Kang, S. Shirazi, Y. Lu, L. F. Cooper, P. Gajendrareddy and S. Ravindran, *Acta Biomater.*, **2021**, *126*, 199–210.
[461] Z. Yu, F. Tantakitti, L. C. Palmer and S. I. Stupp, *Nano Lett.*, **2016**, *16*, 6967–6974.

54a,b).[462] The OFN addition results in the formation of a pyrene-OFN monolayer with both sizes covered with peptides residues. Moreover, the enzymatic stability and the low cellular uptake of the 2D system compared to the vesicles counterpart and the abiotic nature of the OFN, encourage them to study the effect of DGEA upon binding integrin α2β1 involved in cell adhesion, proliferation, and differentiation.[463] To demonstrate that 2D materials could be used to enhance cell proliferation and differentiation they compare the activity of DGEA coated sheets and vesicles on C2C12 cells, showing the 2D system a significantly higher performance (Figure 54c). These results reveal how peptide-based 2D materials can be used to improve biological activity of peptides.

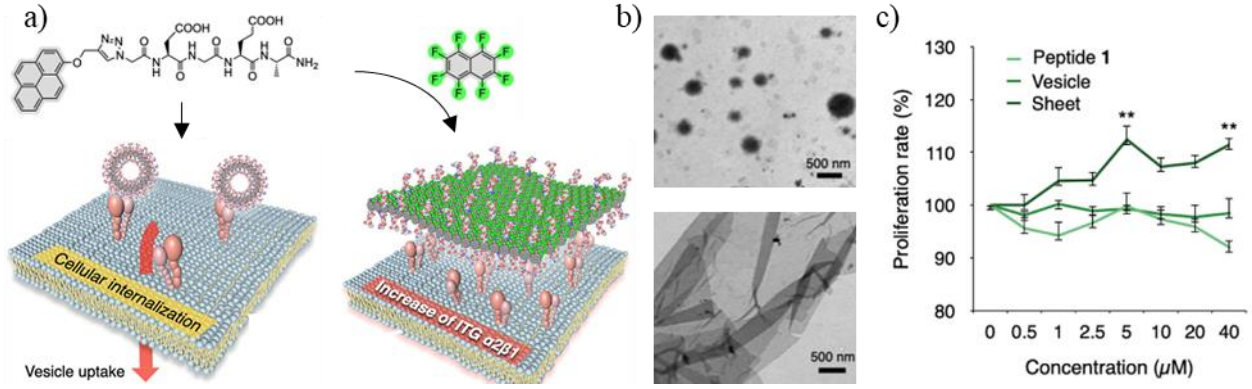

Figure 54. a) Chemical structure of pyrene modified peptide and OFN (top), and the assembly into vesicles or nanosheets (bottom); b) TEM images of the different aggregated morphologies; and c) Proliferation assay in C2C12 cells with different peptide concentrations. Adapted with permission from Ref.447. Copyright © 2023 American Chemical Society.

In addition, some examples based on natural (3.2), artificial (3.1) and cyclic peptide (4.2.3) scaffolds have already been described. The recent discovery of the cyclic peptides ability to grow in a second dimension generating 2D systems has open the door for new designs and applications.

3.1.2. Aggregation-Induced Emission

Around the same dates that graphene was reported, Luo *et al*. introduced the concept of aggregation-induced emission (AIE) using 1-methyl-1,2,3,4,5-pentaphenylsilole.[464] Contrary to what happens with the commonly used dyes, which are susceptible to suffer aggregation-caused quenching (ACQ), the AIE chromogens exhibit weak luminescence in bulk solution but their emission properties increase as they form aggregates.[465,466] Their fundamental properties[467] have

[462] G. Y. Lee, E. Hu, A. L. Rheingold, K. N. Houk and E. M. Sletten, *J. Org. Chem*., **2021**, *86*, 8425–8436.
[463] K. Sivaraman and C. Shanthi, *Life Sci*., **2018**, *214*, 22–33.
[464] J. Luo, Z. Xie, Z. Xie, J. W. Y. Lam, L. Cheng, H. Chen, C. Qiu, H. S. Kwok, X. Zhan, Y. Liu, D. Zhu and B. Z. Tang, *Chem. Comm*., **2001**, *18*, 1740–1741.
[465] Y. Tu, Z. Zhao, J. W. Y. Lam and B. Zhong Tang, *Natl. Sci. Rev*., **2021**, *8*, nwaa260.
[466] J. Mei, Y. Hong, J. W. Y. Lam, A. Qin, Y. Tang and B. Z. Tang, *Adv. Mater*., **2014**, *26*, 5429–5479.
[467] Z. Zhao, H. Zhang, J. W. Y. Lam and B. Z. Tang, *Angew. Chem. Int. Ed*., **2020**, *59*, 9888–9907.

made them suitable for implementation in various applications like optoelectronics, sensors, smart material or biomedicine among others.[466-470]

Even though many AIE luminogens of different nature have been synthesize over the years, tetraphenylethene (TPE) based dyes are one of the most important AIE families.[470] The TPE core presents a central ethene surrounded by four phenyl rings with high rotational freedom, that serves as a non-radioactive channel when the molecules are found isolated in dilute solutions. However, upon aggregation this rotation is physically constrained enhancing the fluorescence decay pathway providing TPE and derivatives with AIE properties.[465,466] Moreover, TPE is really easy to synthesize with the desired chemical modifications making it suitable to achieve more complex systems.[471] Recently, TPE has been decorated with different pendants such as peptides,[472-474] polymers,[322,475,476] and other organic molecules,[477-479] combining the properties of the individual components. The resulting supramolecular aggregates have shown promising activity in sensing,[475,477] optoelectronics,[478] and imaging.[322,472,479]

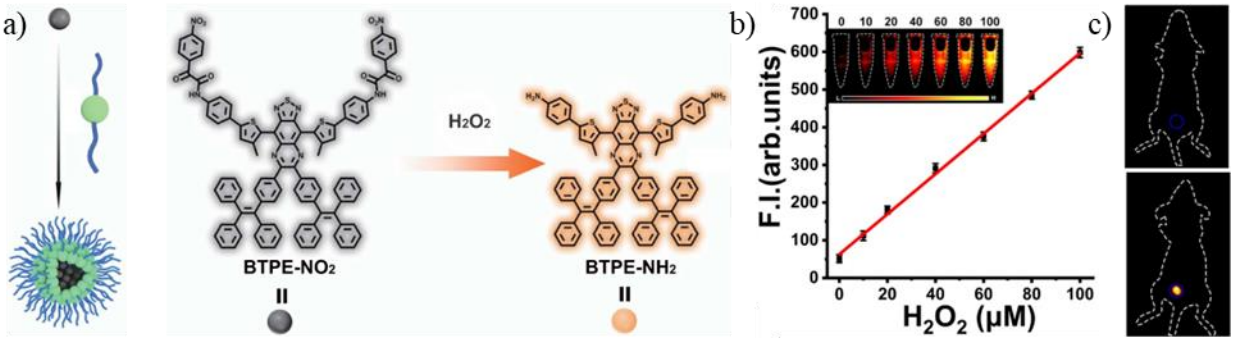

Figure 55. a) Schematic representation of the encapsulation (left) and chemical transformation of the dye upon exposure to H_2O_2; b) fluorescence intensity growth depending on the H_2O_2 levels; and c) NIR-II fluorescence images ninety minutes after injection of the control (top) and the treated mouse (bottom). Adapted with permission from Ref.476. Copyright © 2021 Springer Nature Limited.

For example, NIR-II fluorophores are very interesting dyes since they enable real-time imaging at high depths with great resolution and better disease diagnosis and monitoring. In this sense, benzothiadiazole-core fluorophores are really promising dyes since their fluorescence is

[468] Y. Zuo, H. Shen, F. Sun, P. Li, J. Sun, R. T. K. Kwok, J. W. Y. Lam and B. Z. Tang, *ACS Bio. and Med. Chem. Au.*, **2022**, *2*, 236–257.
[469] M. Kang, Z. Zhang, N. Song, M. Li, P. Sun, X. Chen, D. Wang and B. Z. Tang, *Aggregate*, **2020**, *1*, 80–106.
[470] J. Mei, N. L. C. Leung, R. T. K. Kwok, J. W. Y. Lam and B. Z. Tang, *Chem. Rev.*, **2015**, *115*, 11718–11940.
[471] Z. Zhao, J. W. Y. Lam and B. Z. Tang, *Curr. Org. Chem.*, **2010**, *14*, 2109–2132.
[472] S. K. Talloj, M. Mohammed and H. C. Lin, *J. Mater. Chem. B*, **2020**, *8*, 7483–7493.
[473] E. Suárez-Picado, M. Coste, J. Y. Runser, M. Fossépré, A. Carvalho, M. Surin, L. Jierry and S. Ulrich, *Biomacromolecules*, **2022**, *23*, 431–442.
[474] Y. Wang, T. Pan, X. Wei, F. Su, A. Li, Y. Tai, T. Wei, Q. Zhang, D. Kong and C. Zhang, *Commun. Chem.*, **2022**, *5*, 81.
[475] Z. Wang, X. He, T. Yong, Y. Miao, C. Zhang and B. Zhong Tang, *J. Am. Chem. Soc.*, **2020**, *142*, 512–519.
[476] J. Chen, L. Chen, Y. Wu, Y. Fang, F. Zeng, S. Wu and Y. Zhao, *Nat. Commun.*, **2021**, *12*, 6870.
[477] Y. Wang and M. Lee, *Chempluschem*, **2020**, *85*, 711–714.
[478] J. De, A. H. Abdul, R. A. K. Yadav, S. P. Gupta, I. Bala, P. Chawla, K. K. Kesavan, J. H. Jou and S. K. Pal, *Chem. Comm.*, **2020**, *56*, 14279–14282.
[479] H. Shen, F. Sun, X. Zhu, J. Zhang, X. Ou, J. Zhang, C. Xu, H. H. Y. Sung, I. D. Williams, S. Chen, R. T. K. Kwok, J. W. Y. Lam, J. Sun, F. Zhang and B. Z. Tang, *J. Am. Chem. Soc.*, **2022**, *144*, 15391–15402.

easily extended to NIR-II range, and they have excellent photostability and large stoke shifts.[480] However, they lack stimuli responsiveness to pathological biomarkers and their poor water solubility and fluorescence quenching limit their use in biological applications. To overcome these limitations J. Chen *et al*. designed a new benzothiadiazole-core bearing two TPE groups, providing the system with AIE properties, and two nitrophenyloxoacetamide units, that provide H_2O_2 responsiveness to detect inflammatory diseases (Figure 55a).[476] The further encapsulation of the probe in Pluronic F127 showed great biocompatibility, water-dispersibility and stability. The response of the system towards increasing concentrations of H_2O_2 exhibited the expected AIE behavior (Figure 55b) and the selectivity towards this stimulus, even in the presence of possible interfering substances. Additionally, the in vivo detection of inflammatory diseases such as interstitial cystitis or liver injuries (Figure 55c) demonstrated how AIE dyes can be exploited to overcome problems like ACQ.

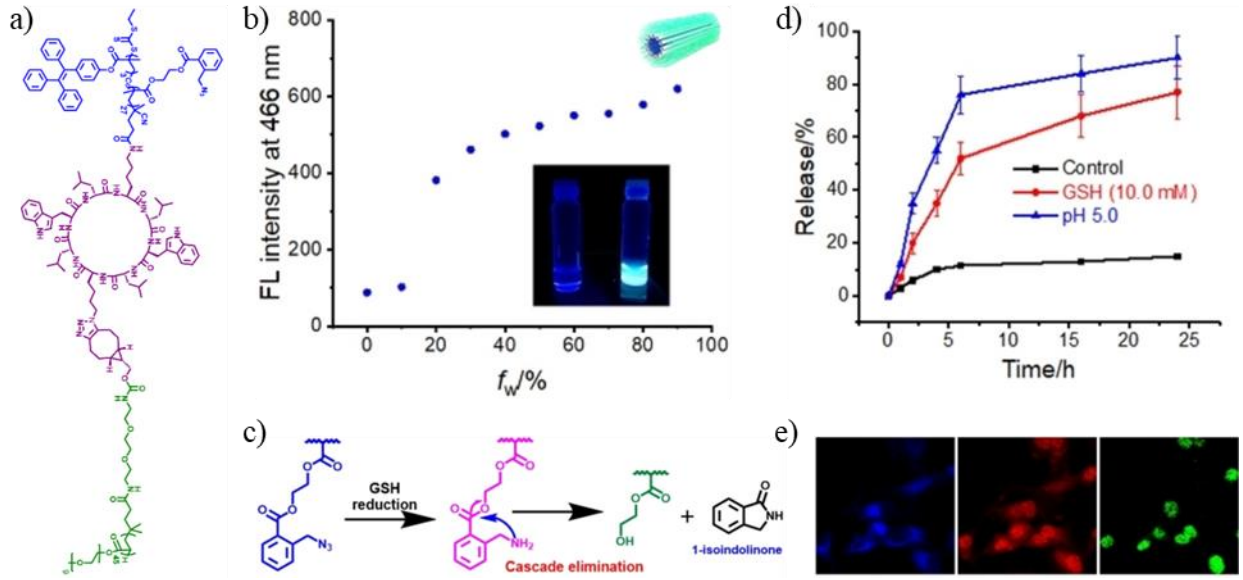

Figure 56. a) Chemical structure of the CP-polymer conjugate; b) TPE fluorescence maxima depending on the water content; c) elimination of the 2-azido-methylbenzoate in the presence of glutathione; d) time dependent drug release; and e) TPE, doxorubicin and Hoechst channels of MDA-MB-231 cells after 8h of incubation with tubisomes showing the colocalization of doxorubicin with the cell nucleus while tubisomes remain in the cytoplasm. Adapted with permission from Ref.322. Copyright © 2021 WILEY-VCH Verlag GmbH & Co. KGaA, Weinheim.

As previously mentioned in section 0 of the introduction, cyclic peptides decorated with hydrophilic and hydrophobic segments can form Janus amphiphilic nanotubes, which present a hydrophobic internal channel and a hydrophilic shell. In this context J. Yang et al. have recently designed a TPE modified polymer to follow the self-assembly and drug delivery process of these CPs-polymer conjugates.[322] Additionally, to target the reductive intracellular environment characteristic of cancer cells,[481] a glutathione sensitive motif (2-azido-methylbenzoate) was included in the hydrophobic segment (Figure 56a,c). First, they demonstrated that the tubisome

[480] Q. Zhu, F. Sun, T. Li, M. Zhou, J. Ye, A. Ji, H. Wang, C. Ding, H. Chen, Z. Xu and H. Yu, *Small*, **2021**, *17*, 2007882.
[481] L. Kennedy, J. K. Sandhu, M. E. Harper and M. Cuperlovic-culf, *Biomolecules*, **2020**, *10*, 1429.

growth could be followed by the TPE emission (Figure 56b), corroborated by SANS and TEM. Moreover, the ACQ of doxorubicin and its FRET with TPE could be exploited to follow the drug encapsulation by emission quenching. Although the loaded tubisomes showed no morphology alteration and high stability under physiological conditions, in the presence of glutation the azido group was reduced, releasing 1-isoindolinone and transforming the hydrophobic segment into a hydrophilic one with the corresponding drug release (Figure 56c,d). Finally, in vitro experiments demonstrate that tubisomes maintain their great capacity to release the cargo inside cancer cells, where doxorubicin end up localizing within the cell nucleus while the vehicle remains in the cytosol (Figure 56d). This example clearly confirms the potential use of AIE derivatives for imaging-guided drug delivery vehicles.

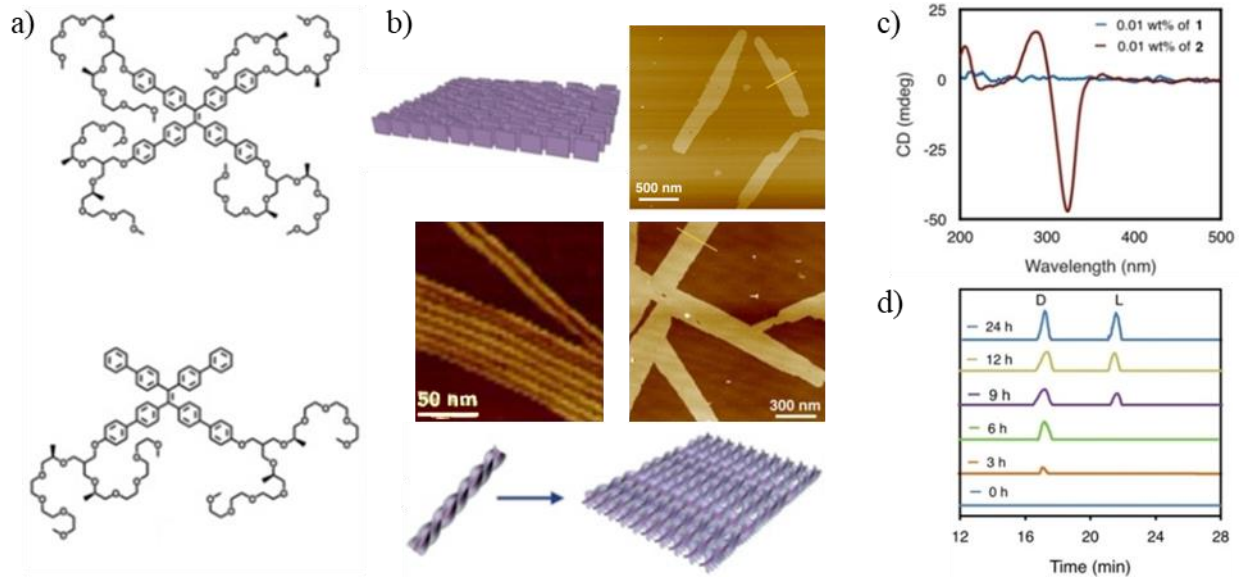

Figure 57. a) Chemical structure of the tera- (top) and di-substituted (bottom) TPE derivatives; b) schematic representation and AFM images of the modified TPE assemblies; c) circular dichroism of both compounds; and d) HPLC showing selective adsorption of D-phenylalanine to the chiral sheets after 6 h. Adapted with permission from Ref.477. Copyright © 2020 WILEY-VCH Verlag GmbH & Co. KGaA, Weinheim.

As we have seen, AIE properties can be incorporated into different molecules by chemical modification allowing previously ACQ system to be fluorescent upon aggregation or to follow specific process such as drug delivery. However, their assembling properties can also be used to rationally design supramolecular polymers. In this sense, Y. Wang et al. have reported TPE decorated with chiral polyethylene glycol able to hierarchically self-assemble into a chiral 2D structure.[477] To do this, they designed two TPE derivatives bearing two or four oligoether groups (Figure 57a). Both monomeric species solved in methanol exhibit a huge increase in fluorescence upon the addition of different fractions of aqueous salts (50 mM KF). Even though TEM and AFM showed sheets, only the disubstituted TPE derivative have chiral behavior in circular dichroism (Figure 57c). Additional studies at lower concentrations revealed that tetrasubstituted TPE forms a monolayer with the hydrophilic segments at the surface that grows with increasing concentrations, while the disubstituted TPE forms helical fibers at low concentrations that can subsequently assemble laterally to form structures with sheet forms at higher concentrations (Figure 57b).

Finally, HPLC analysis in the presence of a racemic mixture of phenylalanine reveal that chiral sheets have a preferential biding for the D enantiomer (Figure 57d), which causes an increase in fluorescence suggesting their possible application as separation materials or sensors.

Summarizing this section, it is clear the need to gain further insights on the design of new supramolecular 2D materials that can incorporate the desired functionalities towards specific applications. In this sense, AIE probes appear as interesting moieties to include in the main structure of responsive systems since they can simplify the characterization and visualization of the assembled structures as well enhancing stability and packing of the new materials.

3.2. Objectives

In chapters I and II, we have employed cyclic peptides bearing one or two aromatic units to form hydrogels. These moieties are attached to the side chain of the cyclic peptide to enhance the 1D growth of the nanotube structure and also to promote further hierarchical assembly into SCPN bundles though π-π stacking and hydrophobic effects. However, this bundling process, made of a hydrophobic internal wire appears to be very difficult to control, giving rise to fibers of different lengths and diameters. In this sense we hypothesize that by adjusting the number of cyclic peptides and, consequently, nanotube units surrounding the internal hydrophobic "wire", the diameter of the fibers could be determined with great precision. For this reason, we anticipated that the use of a poly-substituted hydrophobic entity with a given number of CPs should generate fibers with a homogeneous diameter. In this sense, the use of an easily synthesized tetraphenylethylene core with the desired structural modifications (carboxyaldehydes) seemed to be an excellent basic scaffold on which to build this new approach.[482] However, the first experimental observations showed the tendency of this scaffold to grow in two dimensions switching our initial idea. For this reason, the main objective of this chapter is to evaluate tetrakis-(CP)TPE scaffold for the design of new 2D materials. To achieve such a goal, it was necessary to:

- Design and synthetize all CP-TPE derivatives.
- Characterize the self-assembling properties of the different derivatives using spectroscopic and imaging techniques.
- Study the relationship between the structure and the assembled state.
- Search for an application in which we can take advantage of the 2D-assemblies.

[482] All TPEs derivatives functionalized with four carboxyaldehydes (**TPE-(CHO)$_4$, TPE-(PEG)$_4$, TPE-(OH)$_4$**) were kindly provided by our collaborator Sebastien Ulrich from Université de Montpellier.

3.3. Discussion

3.3.1. Design

As already mentioned in previous chapters, studies carried out with **CP_{1k}** (Figure 58, **1T** in the first chapter) functionalized with different aromatic residues has shown the ability to self-assemble into hydrogels under neutral or basic conditions. In this hierarchical process, the monomeric peptides first stack with each other forming SCPNs with all the aromatic units aligned along the tubular structure. These SCPNs interact with each other though the aromatic units forming bundles (fibers) that crosslinks, swell and retain water molecules within their structure to give rise to self-sustainable hydrogels with different viscoelastic properties.[304] The resulting fibers are constituted by a central hydrophobic core, aromatic wire, constituted by arene moieties subrounded by the assembled CPs in which the polycyclic arene dominates the nanotube packing.[483] Moreover, as demonstrated in chapter two, the polymerization of **1TP** (**CP_{1k}-pyrene**) derivative in confined spaces can be spatially controlled by media conditions. This exquisite control over where these supramolecular structures are formed brings us one step closer to building a minimal artificial model of the cell cytoskeleton. Unfortunately, the size of the fibers cannot be precisely controlled depending on the relative spatial orientation of the pyrene moieties that bring together the SCPNs. In this sense, with the aim of making a simpler system with a homogeneous fiber diameter, we designed this novel peptide component in which four cyclic peptides were attached to a tetraphenylethene moiety (**$4CP_{1k}$-U-TPE**). The TPE moiety should resemble the pyrene central core with the additional advantage of their AIE properties that should provide the characteristic emission upon assembly.

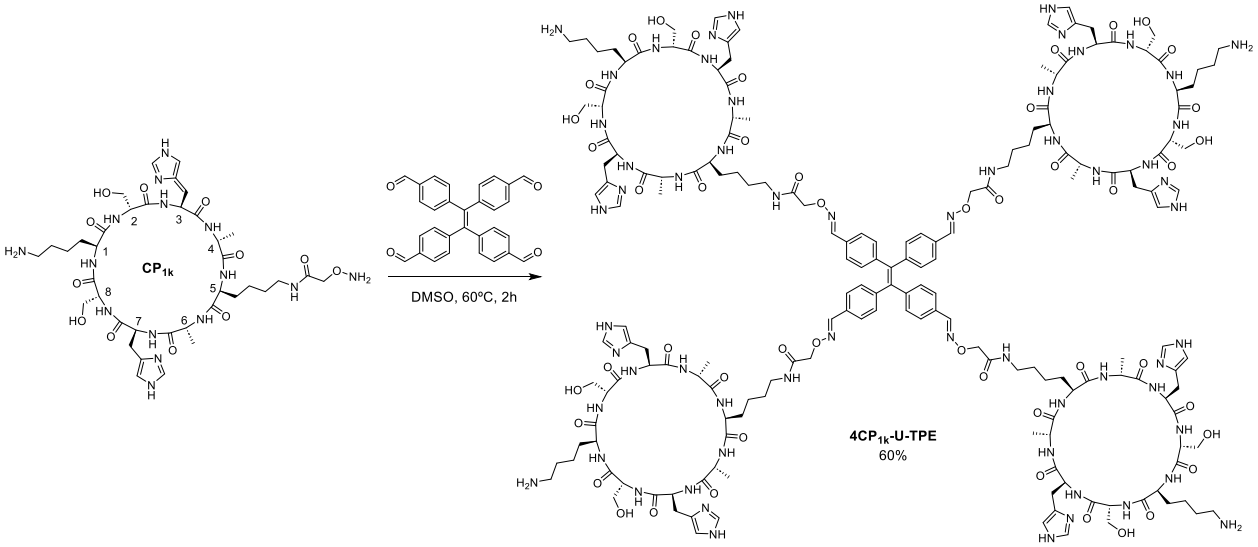

Figure 58. Synthetic scheme used in the preparation of **$4CP_{1k}$-U-TPE**.

[483] J. Guo, S. T. Rich-New, C. Liu, Y. Huang, W. Tan, H. He, M. Yi, X. Zhang, E. H. Egelman, F. Wang and B. Xu, *Chem*, **2023**, *9*, 2530–2546.

Cyclic peptide **CP_{1k}** was prepared by Fmoc solid phase peptide synthesis as previously reported,[304] and then condensed with the TPE derivative containing four para substituted aldehydes (**TPE-$(CHO)_4$**)[482] to provide **$4CP_{1k}$-U-TPE** in a 60% yield, after heating at 60ºC in DMSO for 2h (Figure 58).HRMS probed the existence of our product mass found: 4050.9398 (calculated for $C_{182}H_{256}N_{60}O_{48}^{+}$: 4050.9469). HPLC-MS, ^{1}H NMR and IR spectroscopy confirmed the identity of the product (Figure 122, Figure 123).

3.3.2. Spectroscopic characterization

Once confirmed the preparation of **$4CP_{1k}$-U-TPE** in order to understand it self-assembling properties, pH titrations were carried out and the spectral changes monitored by fluorescence and UV-vis spectroscopy (Figure 59). Alkalinization of an aqueous solution of **$4CP_{1k}$-U-TPE** (50 μM, pH 3) revealed an increase in fluorescence emission at a wavelength of 495 nm with a blueshift of the maximum, which can be attributed to the stacking of the aromatic rings and the consequent inhibition of the molecular rotation of the phenyl groups of the dye (Figure 59a, Figure 135a).[465,471] UV absorption profile showed a redshift of the absorbance maximum and a slight decrease in extinction coefficient, compatible with the packing of the TPE moiety (Figure 59b, Figure 135b).[477] To verify that emission of the AIE dye was concomitant with β-sheet structures, pH titrations were carried out in the presence of Thioflavin T.[301,431,432] ThT is the gold-standard in the detection of amyloid fibrils, due to its ability to stain "cross-β" structures. Insertion of the dye increases its fluorescence emission and induces a red shift of the absorbance maximum from 412 up to 440nm. As expected, alkalinization of **$4CP_{1k}$-U-TPE** solutions to pH 8.5 in the presence of the dye results in an increase of 50 times the fluorescence intensity and a shift from 412 to 440nm in the absorbance spectra (Figure 59c, Figure 135c). Plotting fluorescence emission at 495 nm (I_{max}) and the maximum absorption (Abs_{max}) versus pH, it is observed a clear transition around pH 6 (Figure 59d). This supports that histidine deprotonation (pKa~6) drives the supramolecular polymerization. At the final titration point (pH 8.5), the lysine side chains are partially protonated and strongly solvated, thus preventing the system from aggregation.[484]

The reversibility of the system with pH and temperature was then evaluated. Initially, we demonstrated that the process is fully reversible with pH changes. Afterward, we checked the influence of temperature at fixed pH. At pH2, the tetrameric compound is unstable causing partial cleavage of the oxime bond upon increasing the temperature, giving rise to the deletion of one or two CPs after heating at 90ºC for a few minutes. At pH 6 the molecule is stable, allowing to study the full cycle. Under this conditions, the system is completely reversible, with the emission of the TPE and ThT completely switching off when 90 ºC are reached (Figure 59e,f, Figure 136a). However, at pH 8 the system remains assembled even when heated to 90 ºC for 1h (Figure 59g,h, Figure 136b, Figure 144), confirming its greater stability under these pH conditions. Finally, the Critical Assembling Concentration at different pH confirms the monomeric state of **$4CP_{1k}$-U-TPE** at pH 2, but no remarkable differences were observed at more basic conditions, such as pH 6 and 8 (Figure 137).

[484] G. Gasparini, E. K. Bang, J. Montenegro and S. Matile, *Chem. Comm.*, **2015**, *51*, 10389–10402.

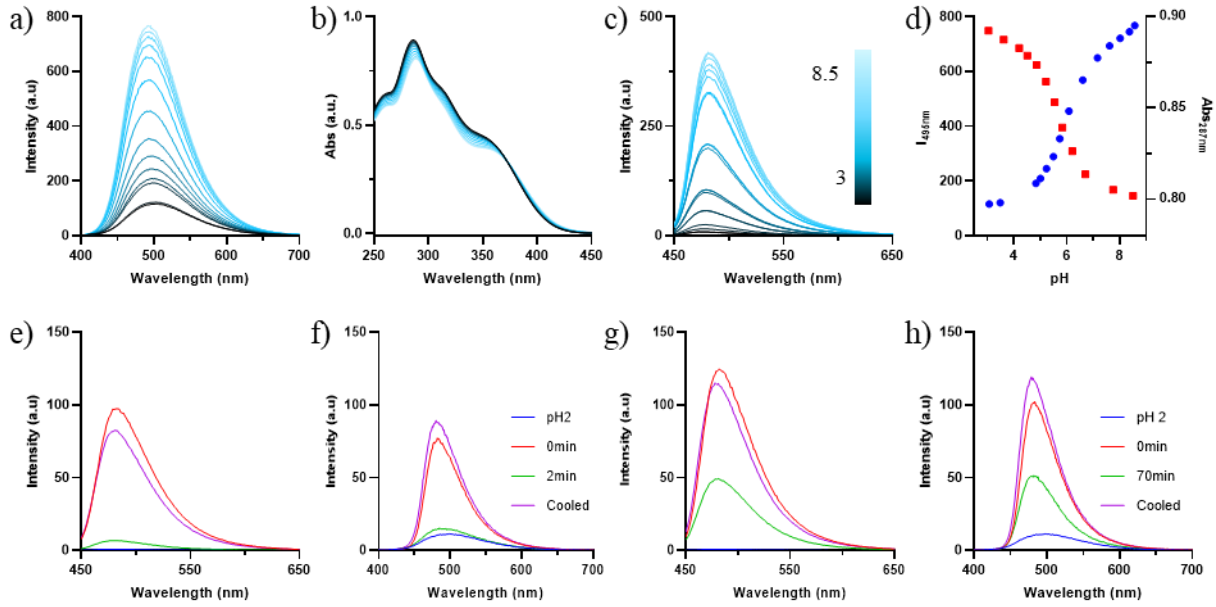

Figure 59. Spectroscopic characterization of **4CP$_{1k}$-U-TPE** (50μM) in aqueous media at different pHs. a) Fluorescence spectra (λ_{exc} = 365 nm); b) UV-VIS spectra; c) Fluorescence spectra of ThT (10 μM) in presence of the peptide (λ_{exc} = 440 nm); d) changes on maximum emission (I_{max} = 495 nm, blue dots) and absorbance wavelength (Abs_{max} = 287 nm, red squares) with pH; e) and f) fluorescence spectra of ThT 10 μM and TPE heated to 90 ºC at pH 6 (20 mM MES); and g) and h) fluorescence spectra of ThT 10 μM and TPE heated to 90 ºC at pH 8 (20 mM HEPES). Notice for e-f: pH 2 fluorescence is shown as the control for disassembled state, also a lower concentration of ThT and lower slits are used to avoid saturation of the equipment.

3.3.3. Microscopy characterization

In sharp contrast with our expectations, alkalinization of a solution of **4CP$_{1k}$-U-TPE** (20 μM) did not result in the formation of well-defined fibers consisting of four parallel nanotubes that could lead to sol-gel transitions. Instead, 2D supramolecular microscopic assemblies were observed using different microscopy techniques (Figure 60).

As already confirmed by spectroscopy techniques, **4CP$_{1k}$-U-TPE** preserves the AIE properties of the TPE moiety. Epifluorescence microscopy was employed to visualize the assemblies at alkaline pH (20mM HEPES, pH 8). The fluorescence micrographs revealed a continuous fluorescence layer that expands through large areas. In some areas, different cracks and fractures appear in the sheets, most likely as a consequence of the deposition process (Figure 60a, Figure 138, smaller sheets in Figure 140). To confirm that this fluorescence layer found in solution corresponds to large sheets, they were mechanically broken by scratching them with a spatula or shaking them vigorously, giving rise to the subsequent appearance of smaller sheets (Figure 139). The addition of ThT to this solution resulted in the expected overlap of emissions (Figure 60b, Figure 141), confirming that these layers are formed by assembled nanotubes that grow laterally to form the 2D structures.

Scanning transmission electron microscopy (STEM) micrographs further confirmed the presence of the sheets (Figure 60c, Figure 143 and Figure 144), in which sharp boundaries and folded edges could be observed. To accurately measure the sheet height, aliquots of the aqueous solution of **4CP$_{1k}$-U-TPE** (20 μM) were deposited on mica surfaces. Non-contact AFM

micrographs of the resulting samples revealed the presence of long sheet-like structures with an average height of 3.7±0.2 nm, which correspond quite well with the diameter of two nanotubes (Figure 60d, Figure 142). Unmodified octa-CP previously reported in the literature showed heights of 1.6nm for a single SCPN and 3.2 nm for a bilayer,[301] while pyrene modified SCNTs can go up to 2.5nm.[304] Taking these values as reference, we can calculate that our molecule would have a height of approximately 4nm. In any case, considering that the aromatic moiety could be oriented tilted with respect to the plane defined by the CPs to compensate the smaller distance between the stacked arenes and that of the β-sheets,[483] the observed height coincides quite well with that estimated from the existing data (Figure 61a,b). Similarly, 2D materials were also obtained at lower pH (pH 6, 20mM MES, Figure 145).

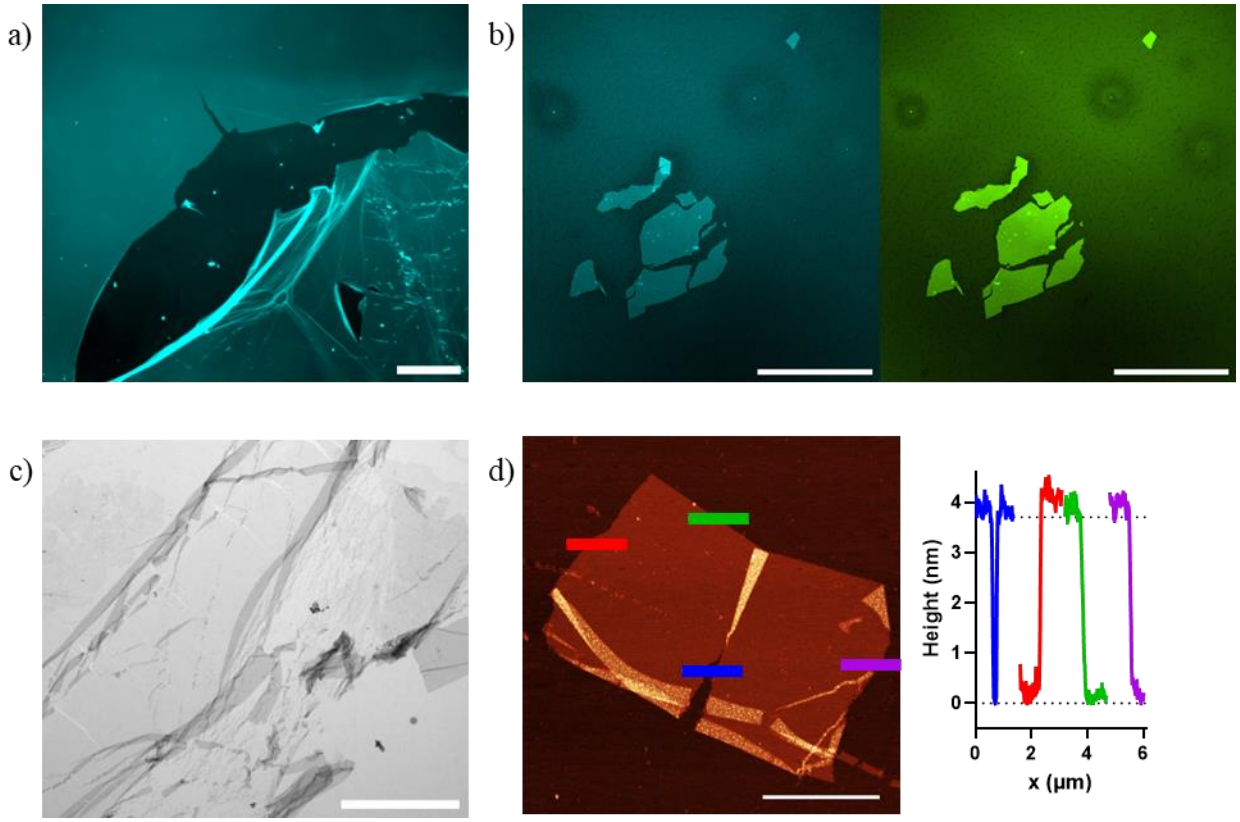

Figure 60. Imaging characterization of **4CP$_{1k}$-U-TPE** (20 μM) in an aqueous solution of HEPES (20 mM, pH8) demonstrating the presence of sheet-like structures. a) Epifluorescence imagen (scale bar 200 μm); b) epifluorescence picture of this solution in the presence of ThT (10 μM) (scale bar 200 μm); c) STEM (scale bar 4 μm); d) AFM micrograph on the left (scale bar 3 μm) and height profile on the right.

3.3.4. Scaffold versatility

Considering the observed pH dependence on the formation of 2D-plates, we initially proposed a hierarchical mechanism model based on the formation of four nanotubes fibers, in which hydrogen-bonding interaction and TPE stacking direct this assembly (Figure 61a,b). As a consequence of the pairing between His, the four resulting nanotubes are arranged into two pairs leaving the stacked TPE moieties located in between the two pairs. On both sides of these pairs there are still imidazole rings along the SCPNs with the capability to continue interacting with two

other pairs of nanotubes to grow in the same direction of the plane, forming the corresponding laminas completely solvated by a lysine shield.

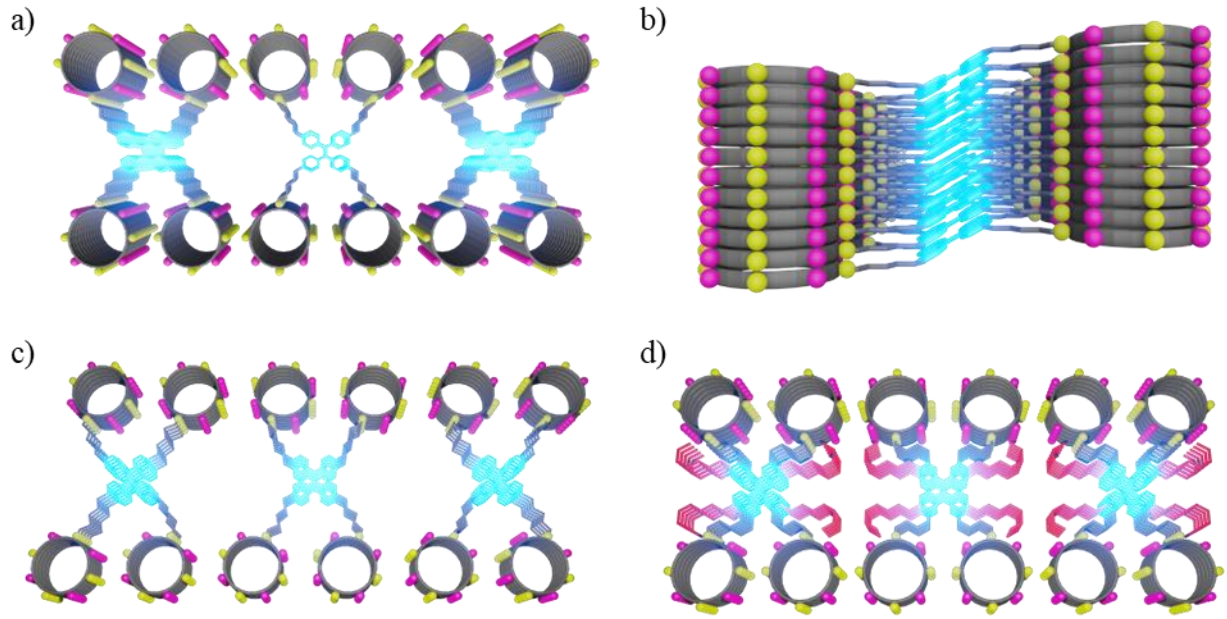

Figure 61. Schematic representations of different assembling possibilities with D-aa (pink) and L-aa (yellow). His-His matching proposed for the assembly of **4CP$_1$-U-TPE** from a zenithal a) or side b) point of view; c) His-His mismatch due to the linking chain flexibility; and d) plausible empty space filling for the **4CP$_1$-U-TPE$_{PEG}$**.

With the aim of unveiling the mechanism of lateral growth that promotes the enlargement and stability of these assemblies in two dimensions, we decided to make different modifications in key amino acids of the peptide sequence (Table 6, entry 1-10) as well as on the TPE central core (Table 6, entry 11-13) based on our initial mechanistic proposal of lateral assembly of SCPNs (Figure 61a,b). To check the importance of the positive charge of the canonical lysine, we substituted the former for a glutamine (uncharged) or a glutamic acid (acid). The relevance of the connector length between CP and TPE moiety was also checked by reducing the four carbon of Lys side chain to one. In addition, the role played by the position of His in the CP sequence and its protonation stage was also evaluated, alternating or changing these residues for other.

Once the peptides were prepared (for details on the CPs structures and synthesis, see 3.6), and attached to the TPE moieties the formation of 2D-structures was evaluated by spectroscopic and microscopy techniques (Figure 62, Figure 63, Figure 64, Figure 146-Figure 157). In general, most of the new derivatives provided again 2D- structures, although some aspect should be mentioned. The substitution of the lysine by a glutamine (**4CP$_{1Q}$-U-TPE**, entry 2), gives rise to similar morphologies (Figure 62a, Figure 146b) although less stable at higher pH, conditions at which the appearance of a precipitate is observed (Figure 146a). This confirms the importance of the protonated lysine in maintaining the stability of the aggregated state in solution and in preventing it from aggregating with other sheets. On the other hand, the substitution by glutamic acid (**4CP$_{1E}$-U-TPE**, entry 3) promotes the disassembly of the formed sheets above pH 6.5 (Figure 62b, Figure 147c), therefore, reducing the pH range at which these sheets are stable. This might be caused by

the increasing repulsion between negatively charged carboxylates of neighboring stacked CPs once both histidines are deprotonated (Figure 63b). To reduce the distance and flexibility of the TPE connectors with CPs, the lysine at position 5 was substituted by Dap (**4CP$_{5Dap}$-U-TPE**, entry 4), thus reducing its length by three carbons. This change did not provide any significant change on the assembling properties, giving rise to aggregates similar to those observed for **4CP$_{1k}$-U-TPE** (Figure 62c, Figure 148c).

Table 6. Structural modifications **4CP$_{1k}$-U-TPE**. Aa substitutions and TPE modifications are shown in red and alterations on aa positioning are shown in green. Aa positioning can be seen in **Figure 58**.

Entry	*Name*	*1*	*2*	*3*	*4*	*5*	*6*	*7*	*8*
1	**4CP$_{1}$-U-TPE**	K	S	H	A	K-Oxime-4-TPE	A	H	S
2	**4CP$_{1Q}$-U-TPE**	Q	S	H	A	K-Oxime-4-TPE	A	H	S
3	**4CP$_{1E}$-U-TPE**	E	S	H	A	K-Oxime-4-TPE	A	H	S
4	**4CP$_{5Dap}$-U-TPE**	K	S	H	A	Dap-Oxime-4-TPE	A	H	S
5	**4CP$_{2,8H}$-U-TPE**	K	H	S	A	K-Oxime-4-TPE	A	S	H
6	**4CP$_{4,6H}$-U-TPE**	K	S	A	H	K-Oxime-4-TPE	H	A	S
7	**4CP$_{6,8H}$-U-TPE**	K	S	A	A	K-Oxime-4-TPE	H	S	H
8	**4CP$_{3A}$-U-TPE**	K	S	A	A	K-Oxime-4-TPE	A	H	S
9	**4CP$_{H(Me)}$-U-TPE**	K	S	H(Me)	A	K-Oxime-4-TPE	A	H(Me)	S
10	**4CP$_{7R}$-U-TPE**	K	S	H	A	K-Oxime-4-TPE	A	R	S
11	**1CP$_{1}$-U-TPE**	K	S	H	A	K-Oxime-1-TPE	A	H	S
12	**4CP$_{1}$-U-TPE$_{PEG}$**	K	S	H	A	K-Oxime-4-TPE(PEG)	A	H	S
13	**4CP$_{1}$-U-TPE$_{OH}$**	K	S	H	A	K-Oxime-4-TPE(OH)	A	H	S

Moreover, two sets of modifications were carried out on His at positions 3 and 7. As mentioned above, we hypothesized that these residues, once partially deprotonated, could promote the lateral growth of **4CP$_{1k}$-U-TPE** nanotubes though H-bonding, perhaps mediated by water molecules, with others.[485-487] The first set of modifications consisted of altering the positions occupied by the His. These residues were exchanged with Ser (**4CP$_{2,8H}$-U-TPE**, entry 5), with Ala (**4CP$_{4,6H}$-U-TPE**, entry 6) or moved to the same side of the cycle, breaking the symmetric distribution of residues at both sides of the aromatic component, (**4CP$_{6,8H}$-U-TPE**, entry 7). None of those changes led to the formation of structures other than 2D-plates (Figure 62d-f, Figure 149-Figure 151c). The second set of modifications consisted of the replacement of one or both His with other aa. To avoid the mentioned lateral H-bond formation, His3 or His7 were substituted, respectively, by an alanine (**4CP$_{3A}$-U-TPE**, entry 8) a non-polar residue, or an arginine **(4CP$_{7R}$-U-TPE**, entry 10) a positively charged residue that, in principle, should increase inter-tube lateral repulsion. Additionally, both His were replaced by His with the imidazole ring N-methylated (**4CP$_{H(Me)}$-U-TPE**, entry 9) with the aim of blocking the possible H-bonding between His. To our surprise, all these peptide

[485] A. H. Iyer, R. N. V. Krishna Deepak and R. Sankararamakrishnan, *J. Phys. Chem. B*, **2018**, *122*, 1205–1212.
[486] J. Heyda, P. E. Mason and P. Jungwirth, *J. Phys. Chem. B*, **2010**, *114*, 8744–8749.
[487] M. Hennig and B. H. Geierstanger, *J. Am. Chem. Soc.*, **1999**, *121*, 5123–5126.

derivatives behaved similarly to the initial structure (Figure 62g-i, Figure 152c, Figure 153c, Figure 154c), forming again the corresponding 2D structures. Interestingly, **4CP$_{7R}$-U-TPE** derivative provided greater stability into the pH range. We attributed this to the presence of the positive charge of Arg, which could also be involved in the lateral growth though cation-π interactions.

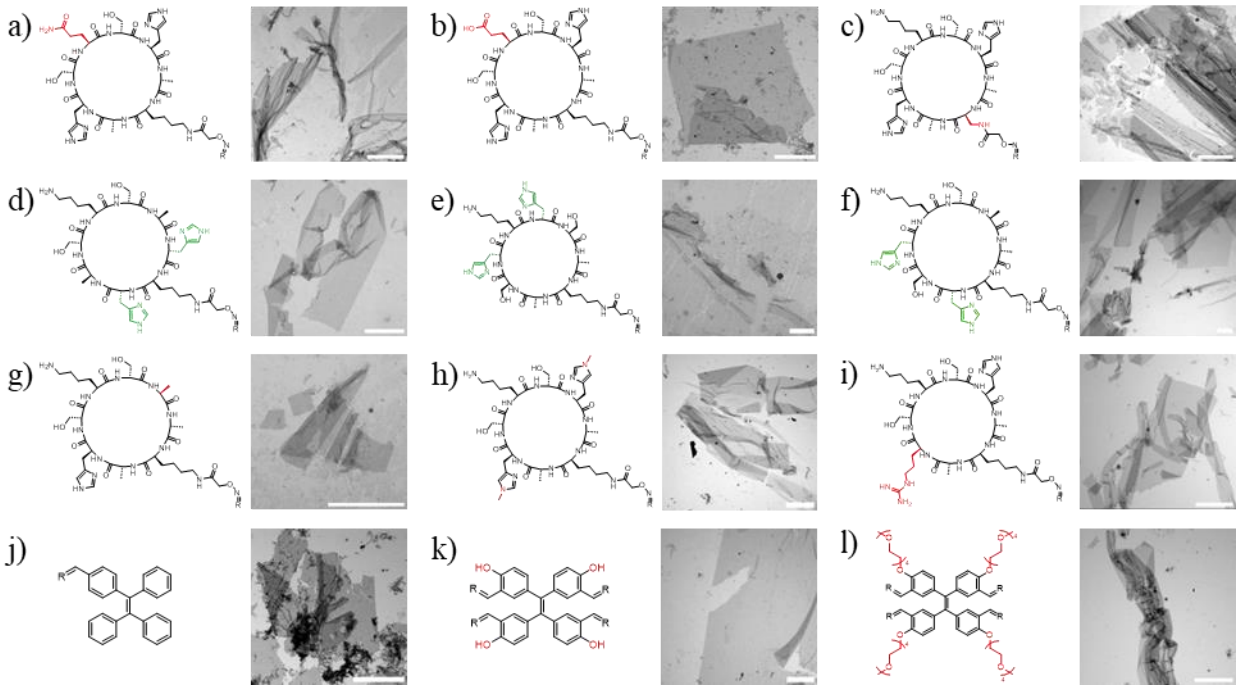

Figure 62. Partial chemical structure showing structural changes with respect to the initial structure (**4CP$_1$-U-TPE**) and STEM showing sheet like structures at 50 μM for a) **4CP$_{1Q}$-U-TPE** (pH 5.9), b) **4CP$_{1E}$-U-TPE** (pH 6.3), c) **4CP$_{5Dap}$-U-TPE** (pH 6.9), d) **4CP$_{4,6H}$-U-TPE** (pH 8.1), e) **4CP$_{2,8H}$-U-TPE** (pH 8.1), f) **4CP$_{6,8H}$-U-TPE** (pH 8.3), g) **4CP$_{3A}$-U-TPE** (pH 8.1), h) **4CP$_{H(Me)}$-U-TPE** (pH 7.3), i) **4CP$_{7R}$-U-TPE** (pH 7.9), j) **1CP$_1$-U-TPE** (pH 9.0), k) **4CP$_1$-U-TPE$_{PEG}$** (pH 6.0) and l) **4CP$_1$-U-TPE$_{OH}$** (pH 7.23). Scale bars are 3μm.

Additionally, three different TPE derivatives were also studied. The monosubstituted TPE derivative was synthesized (**TPE-(CHO)$_1$**) and condensed with **CP$_{1k}$** (**1CP$_{1k}$-U-TPE,** entry 11). This derivative was designed with the aim of leaving TPE moiety exposed to the solvent as in the previous pyrene precursor[304] (**1TP**, Chapters I and II) and also break the apparent C4 symmetry of the tetra substituted derivative. The morphology of the assembled state analyzed by STEM experiments showed a mixture between sheets and linear (1D) aggregates that could correspond to SCPNs (Figure 62j, Figure 155c). The second approach was based on the hydroxylated derivative (**4CP$_{1k}$-U-TPE$_{OH}$**, entry 12) which has the CP pendant on the meta position creating different isomers depending on the relative orientation with respect to each other. Such design was intended to favor intertubular interactions in the four SCPN subunits, which reduces the 2D polymerization. However, final morphology was not affected by this change (Figure 62k). The spectroscopic behavior is very similar to the **4CP$_{1E}$-U-TPE** starting to disassembly at pHs higher than 6 (Figure 63k, Figure 64k). This could be related with the deprotonation of the phenols on the TPE ring that might cause charge repulsion. Third, the pegylated derivative (**4CP$_{1k}$-U-TPE$_{PEG}$**, entry 11) provided similar morphologies to the original design (Figure 62j), confirming that the effect on the hydroxylated derivatives comes from the OH and not the substitution on the meta position. In

summary, all designed scaffolds have shown a tendency to assemble into laminas similar to the original design, with some stability differences for Gln, Glu and **TPE$_{OH}$** derivatives. Interestingly, the only case where SCPNs can be visualized is in the monosubstituted TPE, whose structure resembles the nanotube forming CPs from Chapters I and II.

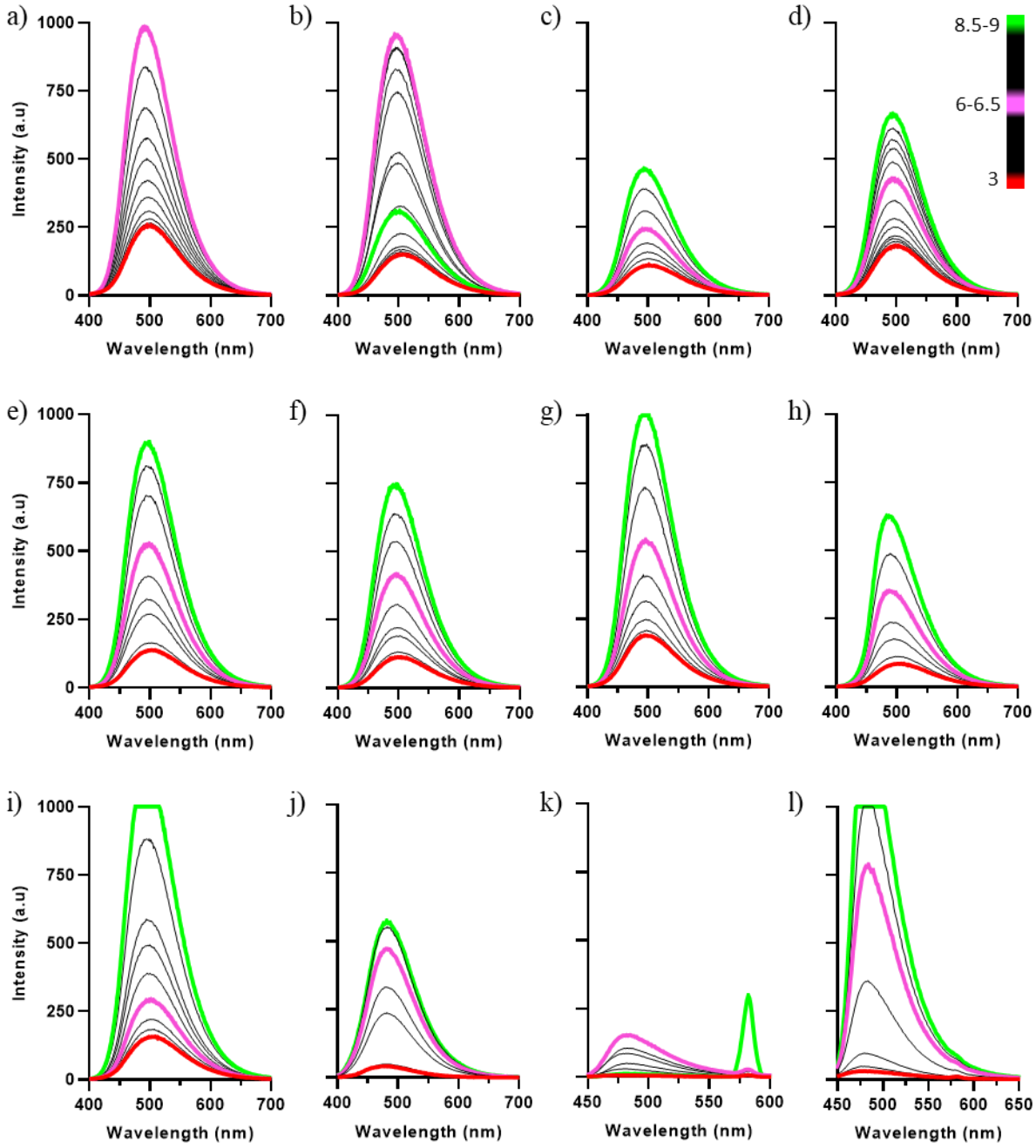

Figure 63. TPE fluorescence characterization of the designed derivatives (50μM) in aqueous media at different pHs (λ_{exc} = 365 nm). a) **4CP$_{1Q}$-U-TPE**, b) **4CP$_{1E}$-U-TPE**, c) **4CP$_{5Dap}$-U-TPE**, d) **4CP$_{3A}$-U-TPE**, e) **4CP$_{2,8H}$-U-TPE**, f) **4CP$_{6,8H}$-U-TPE**, g) **4CP$_{4,6H}$-U-TPE**, h) **4CP$_{H(Me)}$-U-TPE**, i) **4CP$_{7R}$-U-TPE**, j) **1CP$_1$-U-TPE**, k) **4CP$_1$-U-TPE$_{OH}$** and l) **4CP$_1$-U-TPE$_{PEG}$**.

Notice: last pH (green line) for **4CP$_{7R}$-U-TPE** and **4CP$_1$-U-TPE$_{OH}$** are 10.8 and 10.5, respectively.

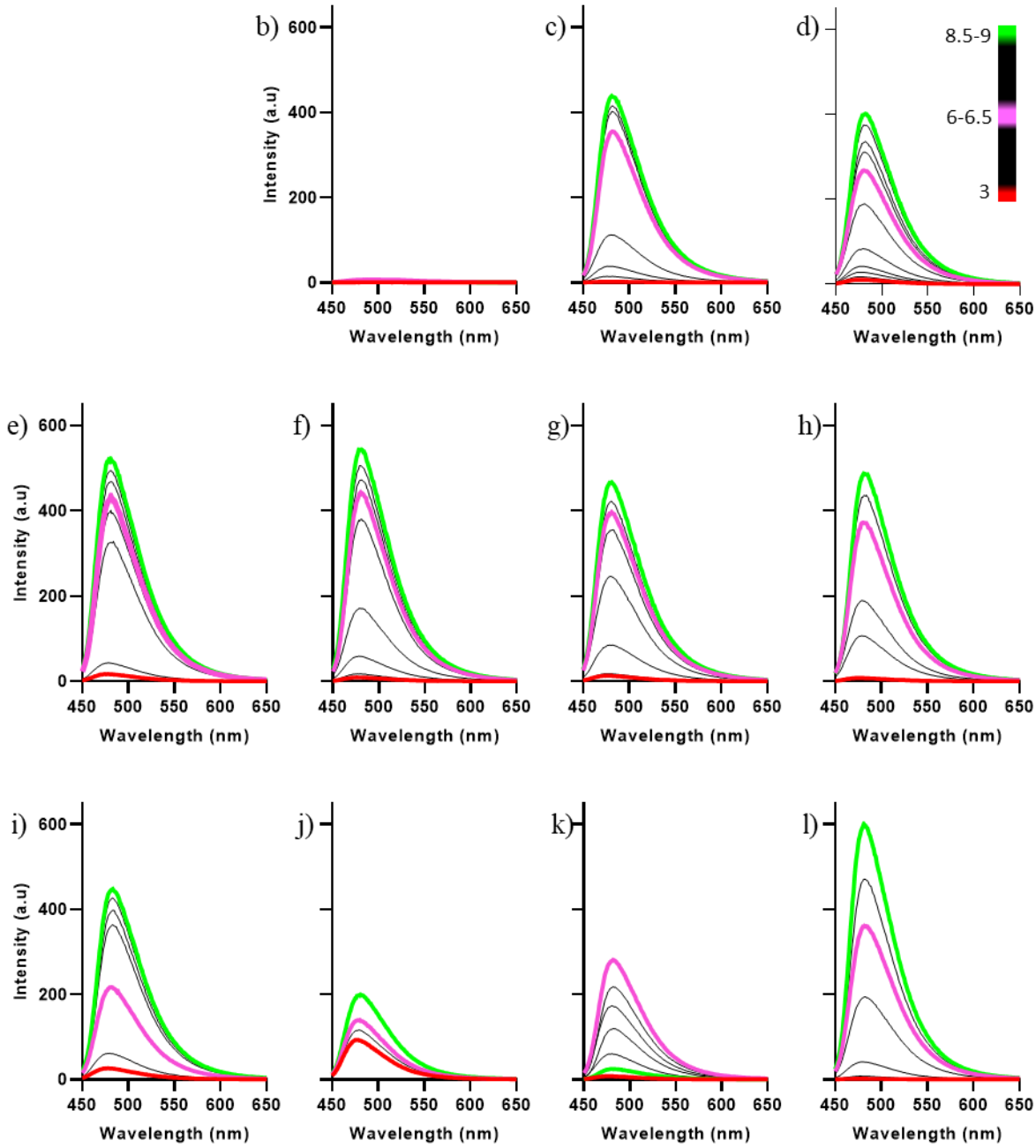

Figure 64. ThT fluorescence characterization of the designed derivatives (50 μM) in aqueous media with ThT (20 μM) at different pHs (λ_{exc} = 440 nm). b) **4CP$_{1E}$-U-TPE**, c) **4CP$_{5Dap}$-U-TPE**, d) **4CP$_{3A}$-U-TPE**, e) **4CP$_{2,8H}$-U-TPE**, f) **4CP$_{6,8H}$-U-TPE**, g) **4CP$_{4,6H}$-U-TPE**, h) **4CP$_{H(Me)}$-U-TPE**, i) **4CP$_{7R}$-U-TPE**, j) **1CP$_1$-U-TPE**, k) **4CP$_1$-U-TPE$_{OH}$** and l) **4CP$_1$-U-TPE$_{PEG}$**.

Notice: last pH (green line) for **4CP$_{1E}$-U-TPE**, **4CP$_{7R}$-U-TPE** and **4CP$_1$-U-TPE$_{OH}$** are 10.1, 11.2 and 10.5, respectively. Also, intermediate pH (pink line) for **1CP$_{1K}$-U-TPE** is 5.5.

Generally speaking, all systems present similar spectroscopic properties to **4CP$_{1K}$-U-TPE** (Figure 63, Figure 64 and Figure 146-Figure 157a,b). The most general observation that calls our

attention is the difference in fluorescence intensity depending on the CP derivative used. However, this effect can be easily explained by differences in the packing state and the final peptide/ThT concentration. As can be seen in the absorbance spectra, there could be differences in concentration up to 20% between the peptide derivatives. On the other hand, the TPE derivatives present different absorption spectra, making direct comparison difficult (Figure 146-Figure 157a). In addition, derivative **1CP$_{1K}$-U-TPE** has four times less CP on solution resulting in a less intense ThT spectra (Figure 64i). Unexpectedly, the ThT spectra of **4CP$_{1E}$-U-TPE** (Figure 64b) does not show an emission enhancement with pH. We suggest this might be associated with the presence of negative charges on the surface of the sheet that might sequester the ThT, avoiding its insertion in the β-sheet structure.[488] Its self-assembling behavior is similar to **4CP$_1$-U-TPE$_{OH}$** since both compounds start to disassemble at high pH values (Figure 63 and Figure 64b,k). The insertion of ThT in this case where the negative charges are found in the core, supports this hypothesis. Although more data is needed to confirm this hypothesis, the imaging and spectroscopic data suggest that the TPE linked to His bearing CPs could be a great scaffold for building pH responsive 2D systems.

3.3.5. Catalytic evaluation

To evaluate the surface accessibility of imidazole rings of His residues, their potential catalytic activity was evaluated. We envisaged that imidazole aligned along the nanotube could participate in catalytic transformation as acid/base pairs or through coordination to attach a metal center capable of catalyze new reactions. For this purpose, we study the hydrolysis of p-Nitrophenol acetate, commonly used to check hydrolase activity,[489] on the surface of the laminas (Figure 65). This process can be followed by monitoring the absorbance of the p-nitrophenol (hydrolytic product) at 400 nm. Moreover, Zn^{+2} ions can potentially coordinate imidazole rings increasing the catalytic activity upon coordination with His.[490,491] As clearly visualized in the graphic of Figure 65a, the p-Nitrophenol acetate is hydrolyzed faster in the presence of a metal ion . In this sense, **4CP$_{1K}$-U-TPE** showed a higher activity than the controls, that could also be enhanced by the presence of Zn^{+2}. However, analysis of the resulting cyclic peptide with time showed partial acetylation of the Lys side chain, suggesting that the observed activity might be accelerated for the nucleophilic character of the amino group. Further studies with other cyclic peptides in which amino group is removed, for example substituting the Lys by an Arg, should be carried out to confirm this catalytic activity.

[488] V. Babenko and W. Dzwolak, *Chem. Comm.*, **2011**, *47*, 10686–10688.
[489] C. Zhang, R. Shafi, A. Lampel, D. MacPherson, C. G. Pappas, V. Narang, T. Wang, C. Maldarelli and R. V. Ulijn, *Angew. Chem. Int. Ed*., **2017**, *56*, 14511–14515.
[490] L. Zhou, S. Li, Y. Su, X. Yi, A. Zheng and F. Deng, *J. Phys. Chem. B*, **2013**, *117*, 8954–8965.
[491] D. Nakatake, Y. Yokote, Y. Matsushima, R. Yazaki and T. Ohshima, *Green Chem*., **2016**, *18*, 1524–1530.

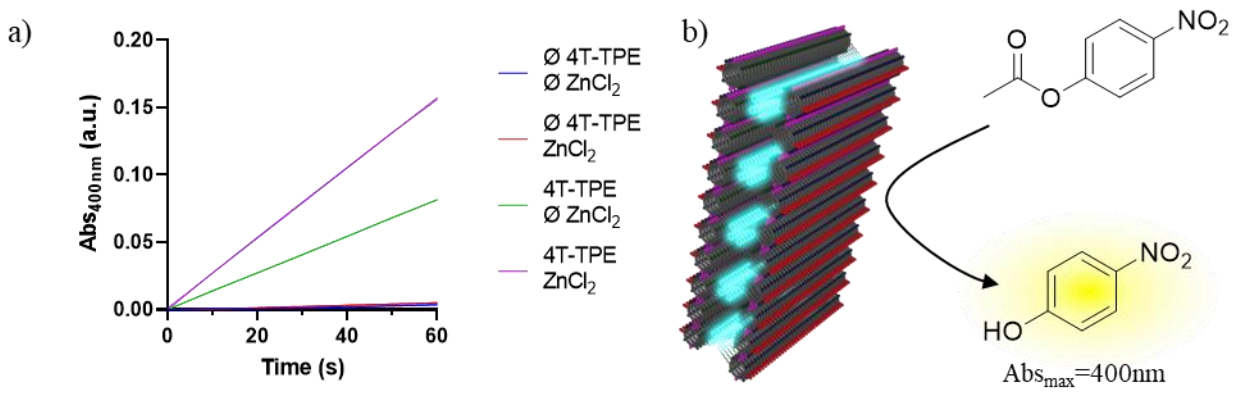

Figure 65. a) Catalytic activity of **4CP$_{1K}$-U-TPE** (50 μM) at pH8 in the presence of 200 μM of p-NPA. b) Catalytic scheme showing the hydrolytic activity of the peptide sheets.

3.4. Conclusions

In this chapter, we have shown a new cyclic peptide scaffold with propensity to hierarchically assemble into fluorogenic 2D structures through β-sheet type hydrogen bonding interactions, π-π stacking and hydrophobic effects. The scaffold is based on a TPE moiety surrounded by four cyclic peptides bearing His as assembling modulators.

Other important aspects of this chapter are:

- The use of the highly efficient alkoxyamine/aldehyde condensation easily gives access to a library of CPs-TPE derivatives.
- Microscopic imaging and spectroscopic characterization revealed the tendency to this scaffold to form 2D structures, which exhibit good thermal- and pH responsiveness.
- AFM measurements confirmed the presence of a monolayer of this tetrameric nanotube in which the positively charged lysines prevent the system from collapsing.
- The TPE and ThT spectroscopic characterization revealed that the properties of the individual components remain intact in the final assembly, showing the characteristic behavior of AIE probes and β-sheets of CPs.
- The modifications on the CP sequence and the TPE structure confirmed the high versatility of the system to build new 2D materials with desired functionalization.
- Preliminary studies suggest great potential for the use of these supramolecular nanosheets as catalysts.

CONCLUSIONS

Throughout this thesis we have demonstrated how side chains functionalization on α-D,L-cyclic peptides can be exploited to control the morphology of the aggregate state opening the possibility to employ such scaffolds in multiple applications such as soft materials, catalysis or biology.

First, we have successfully synthesized a library of CP hydrogelators bearing one or two aromatic moieties. The spectroscopic and imaging characterization reveal a hierarchical gelling process (Figure 66), in which CP monomers assembled into nanotubes upon alkalinization that could further interact with each other forming bundles (fibers). Moreover, the viscoelastic properties of the obtained self-healable hydrogels could be related with the number and nature of the pendants groups providing structural principles to obtain new materials with properties adapted to the desired applications.

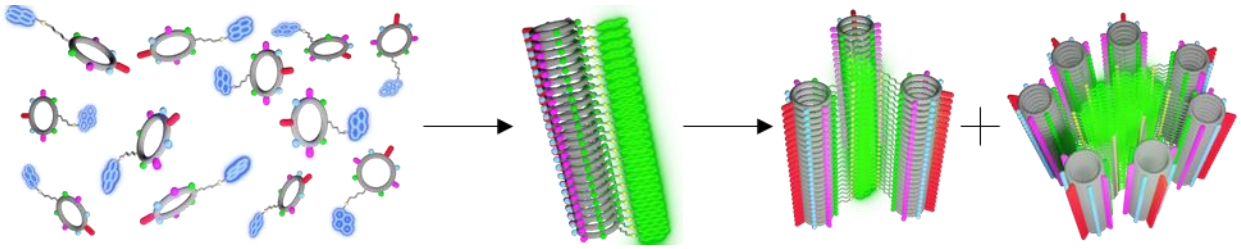

Figure 66. Schematic representation of the hierarchical assembling process of **1TP**.

Second, we demonstrated how by controlling the assembly pathway of CP monomers within confined spaces determines the spatial distribution in droplet systems. Taking advantage of the exquisite control that offers microfluidics, we triggered the peptide derivative assemblies with different stimuli controlling the positioning of the assemblies in the final droplet (Figure 67). The obtained structures resembled some basic behavior of cells cytoskeleton.

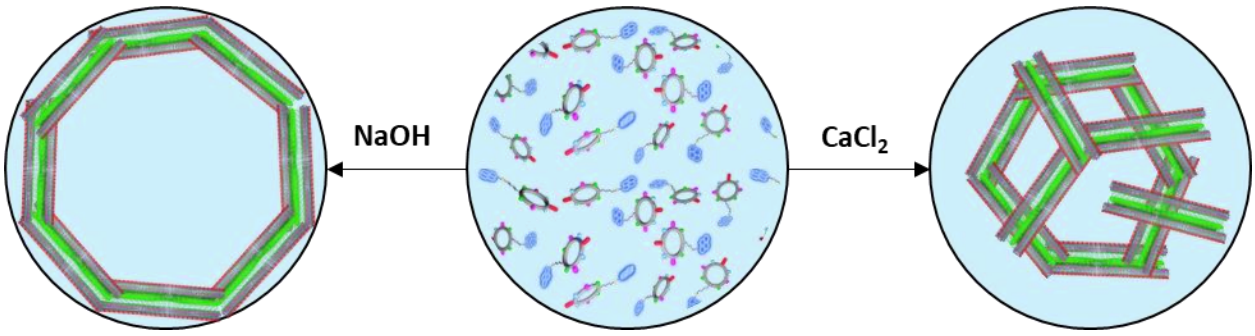

Figure 67. Representation of the peripheric (left) or core (left) positioning of the fibrillar aggregates upon triggering the assembling process by alkalinization or ionic shock, respectively.

Finally, in our search for homogeneous cyclopeptide fibers that would allow a better control over the diameter and length of the fibers, we found a tetrakis(CP)-TPE scaffold capable of hierarchically self-assembly into SCPNs whose lateral interactions are enhanced, forming 2D nanostructures (Figure 68). These new materials exhibit potential catalytic activity. Moreover, the different modifications on the peptide scaffold did not affect the two-dimensional growth of the

system, suggesting that specifically functionalized sheets can be obtained by molecular design using a TPE central core as common component.

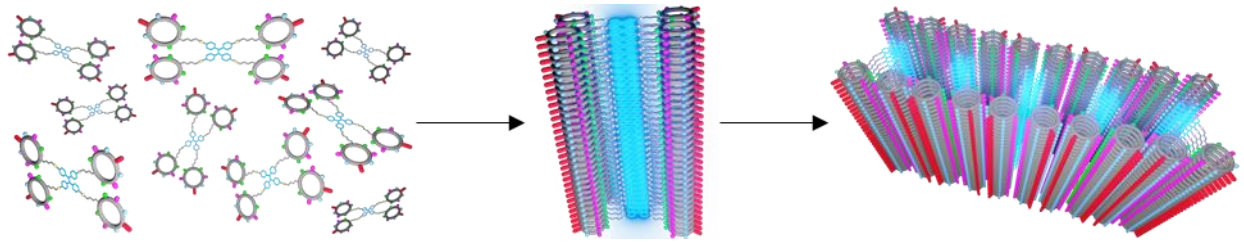

Figure 68. Schematic representation of the hierarchical assembling process of tetrakis(CP)-TPE derivatives.

BIBLIOGRAPHY

All references have been inserted as footnotes the first time they were cited to facilitate the reading of the Thesis.

EXPERIMENTAL SECTION

1. Self-Healing Cyclic Peptide Hydrogels

1.1. Characterization

1.1.1. 2T

Semipreparative HPLC purification of 2T using a C18 column [gradient of H_2O–0.1% TFA–acetonitrile–0.1% TFA 95 : 5 (0 min) to 70 : 30 (20 min)] gave 20.5 mg of **2T** (19%); Rt = 7.35 min, RP-uHPLC (C18, H_2O–acetonitrile (dopped with 0.1% TFA) 100 : 0 (0 min) - 25 : 75 (20 min)); ^{1}H NMR (300 MHz, D_2O) δ: 8.62 (s, 2 H), 7.25 (s, 2 H), 4.70–4.65 (m, water overlapped), 4.45 (s, 4 H), 4.40–4.30 (m, 5 H), 4.22 (m, 1 H), 3.82 (d, J = 6 Hz, 4 H), 3.74 (d, J = 6 Hz, 2 H), 3.31 (m, 2 H), 3.22–3.03 (m, 6 H), 2.95 (t, J = 6 Hz, 2 H), 1.90–1.10 (m, 18 H); FTIR (neat): 3273, 1667, 1621, 1535, 1435, 1190, 1133, 838, 903, 799, 723, 632 cm^{-1}; HRMS calculated for $C_{43}H_{72}N_{17}O_{15}^+$: 1066.5388, found: 1066.5395.

1.1.2. 1TN

1T (4.8 mg, 5.2 mmol) was reacted with 2-naphthaldehyde (1.2 mg, 7.7 mmol) to provide 4.1 mg of **1TN** as a white powder (74%). Rt = 7.98 min, RP-uHPLC (C18, H_2O–acetonitrile (dopped with 0.1% TFA) 95 : 5 (0 min) - 5 : 95 (15 min)); ^{1}H NMR (300 MHz, DMSO-d_6) δ: 8.75 (s, 2 H), 8.48 (s, 1 H), 8.30 (m, 3 H), 8.10–7.91 (m, 7 H), 7.77 (d, *J* = 9 Hz, 1 H), 7.68–7.56 (m, 3 H), 7.26, 7.22 (2 s, 2 H), 5.10 (bs, 2 H), 4.55 (m, 3 H), 4.32 (m, 5 H) 3.54–2.87 (m, overlapped water), 2.73 (bs, 2 H), 1.70–1.18 (m, 14 H); FTIR (neat): 3270, 1669, 1625, 1537, 1201, 1181, 1132, 1074, 833, 798, 721, 697 and 628 cm^{-1}; HRMS calculated for $C_{49}H_{68}N_{15}O_{12}^+$: 1058.5166, found: 1058.5159.

1.1.3. 1TA

1T (16.6mg, 18 mmol) was reacted with 9-anthracenecarboxaldehyde (5.6 mg, 27 mmol) to provide 16.4 mg of **1TA** as a yellow solid (82%). Rt = 8.41min, RP-uHPLC (C18,H_2O–acetonitrile (dopped with 0.1% TFA) 95 : 5 (0min)-5 : 95 (15min)); ^{1}H NMR (300 MHz, DMSO-d_6) δ: 9.41 (s, 1 H), 8.75 (m, 3 H), 8.47–7.97 (m, 9 H), 7.59 (m, 4 H), 7.28, 7.24 (2 s, 2 H), 5.10 (bs, 2 H), 4.55 (m, 3 H), 4.32 (m, 5 H), 3.54–2.87 (m, overlapped water), 2.73 (bs, 2 H), 1.70–1.06 (m, 14 H); FTIR (neat): 3270, 1669, 1622, 1534, 1453, 1202, 1179, 1132, 1048, 1029, 1006, 723, 704 and 627 cm^{-1}; HRMS calculated for $C_{53}H_{70}N_{15}O_{12}^+$: 1108.5323, found: 1108.5316.

1.1.4. 2TN

2T (8.2 mg, 7.7 mmol) were reacted with 2-naphthaldehyde (3.6 mg, 23 mmol) to provide 7.6 mg of **2TN** as a white powder (74%) Rt = 7.99 min, RP-uHPLC (C18, H_2O–acetonitrile (dopped with 0.1% TFA) 95 : 5 (0 min) - 5 : 95 (12 min)); ^{1}H NMR (300 MHz, DMSO-d_6) δ: 8.75 (b, 3 H), 8.48 (s, 2 H), 8.39–8.17 (m, 3 H), 8.09–7.85 (9 H), 7.77–7.50 (m, 7 H), 7.23 (m, 2 H), 5.04 (bs, 2 H), 4.57 (s, 4 H), 4.38–4.15 (m, 5 H), 3.60–2.83 (m, overlapped water), 2.73 (broad, 2 H), 1.70–1.00 (m, 12 H); FTIR (neat): 3272, 2923, 2857, 1624, 1533, 1199, 1179, 1129, 1077, 896, 821, 721, 629 and 477 cm^{-1}; HRMS calculated for $C_{65}H_{84}N_{17}O_{15}^+$: 1342.6327, found: 1342.6326.

1.1.5. 2TA

2T (15.8 mg, 14.8 mmol) was reacted with 9-anthracenecarboxaldehyde (9.1 mg, 44 mmol) to provide 16.2 mg of **2TA** as a yellow powder (76%). Rt = 8.64 min, RP-uHPLC (C18, H_2O–acetonitrile (dopped with 0.1% TFA) 95 : 5 (0 min) - 5 : 95 (12 min)); ^{1}H NMR (300 MHz, DMSO-d_6) δ: 9.40 (s, 2 H), 8.90 (b, 2 H), 8.73 (s, 2 H), 8.48–7.94 (m, 16 H), 7.66–7.56 (m, 8 H), 7.31, 7.28 (2 s, 2 H), 5.03 (bs, 2 H), 4.67 (m, 5 H), 4.43–4.20 (m, 5 H), 3.64–2.80 (m, overlapped water), 2.73 (b, 2 H), 1.71–1.05 (m, 12 H); FTIR (neat): 3268, 1668, 1622, 1535, 1199, 1179, 1136, 1048, 1020, 835, 800, 787, 719 and 629 cm^{-1}; HRMS calculated for $C_{73}H_{88}N_{17}O_{15}^+$: 1442.6640, found: 1442.6644.

1.1.6. 2TP

2T (19.3 mg, 18.1 mmol) was reacted with 1-pyrenecarboxaldehyde (13 mg, 57 mmol) to provide 20.8 mg of **2TP** as a yellow powder (77%). Rt = 9.21 min, RP-uHPLC (C18, H_2O–acetonitrile (dopped with 0.1%TFA) 95 : 5 (0 min)-5 : 95 (12min)); ^{1}H NMR (300 MHz, DMSO-d_6) δ: 9.33 (s, 2 H), 8.87 (b, 2 H), 8.75 (d, J = 9 Hz, 2 H), 8.58 (s, 2 H), 8.40–7.94 (m, 18 H), 7.82 (b, 2 H), 7.64 (b, 2 H), 7.25 (b, 2 H), 5.00 (bs, 2 H), 4.68 (m, 5 H), 4.32 (m, 5 H), 3.64–3.00 (m, overlapped water), 2.73 (b, 2 H), 1.73–1.07 (m, 12 H); FTIR (neat): 3263, 1662, 1624, 1533, 1199, 1179, 1131, 1077, 1046, 1024, 1003, 856, 717 and 627 cm^{-1}; HRMS calculated for $C_{77}H_{88}N_{17}O_{15}^+$: 1490.6640, found: 1490.6637.

1.2. Figures

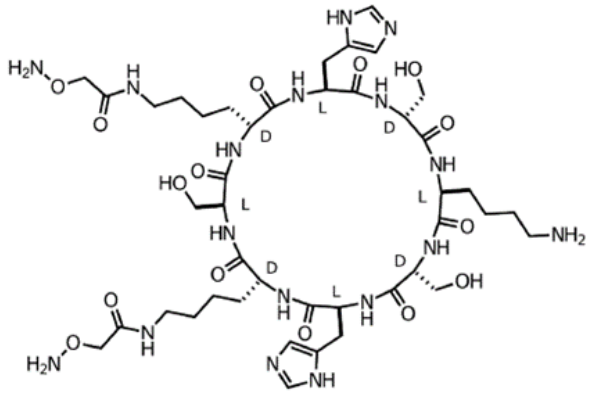

Figure 69. Chemical structure of CP **2T**.

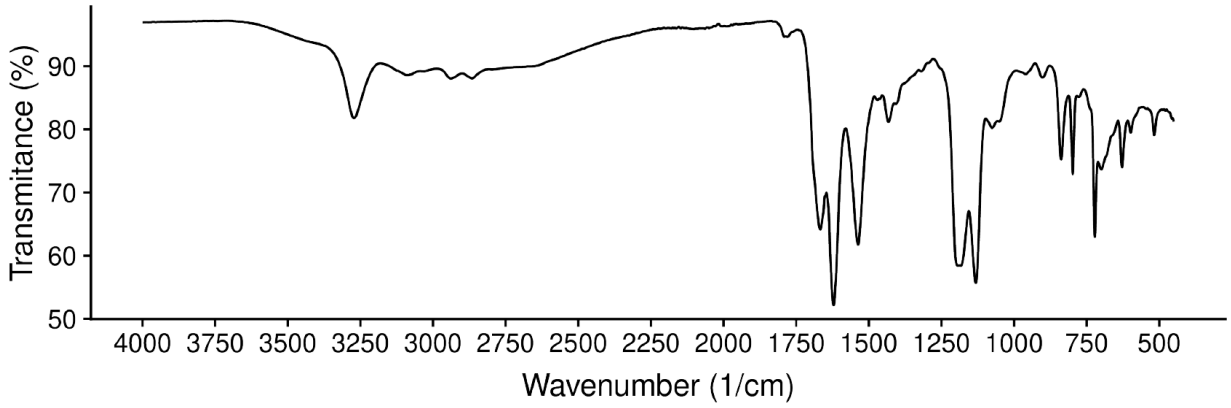

Figure 70. FTIR-ATR of **2T**.

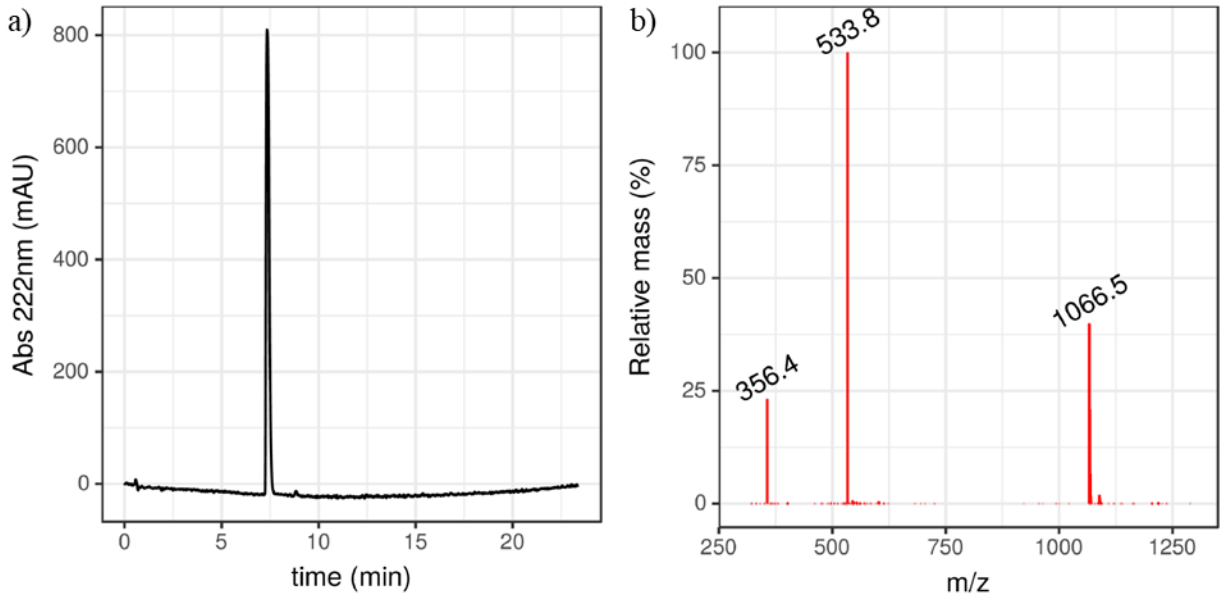

Figure 71. a) HPLC chromatogram of peptide **2T**. Gradient of 0% to 75% ACN (0.1% TFA) in 20 min; b) MS spectra of the main peak.

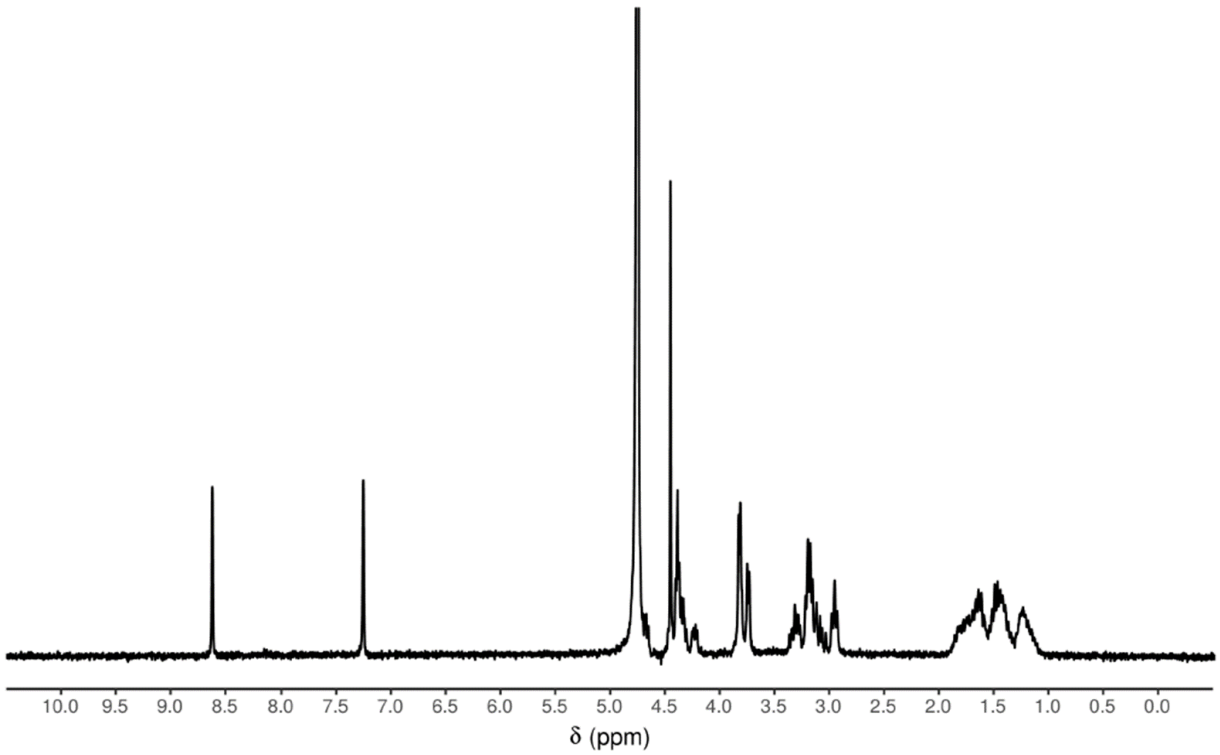

Figure 72. ^{1}H NMR spectra (300 MHz, D_2O, room temperature) of cyclic peptide **2T**.

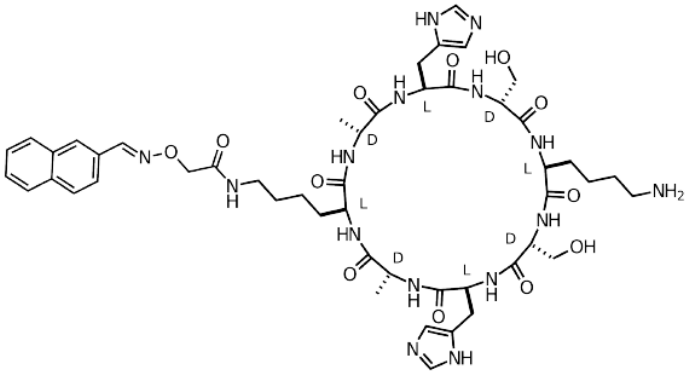

Figure 73. Chemical structure of CP **1TN**.

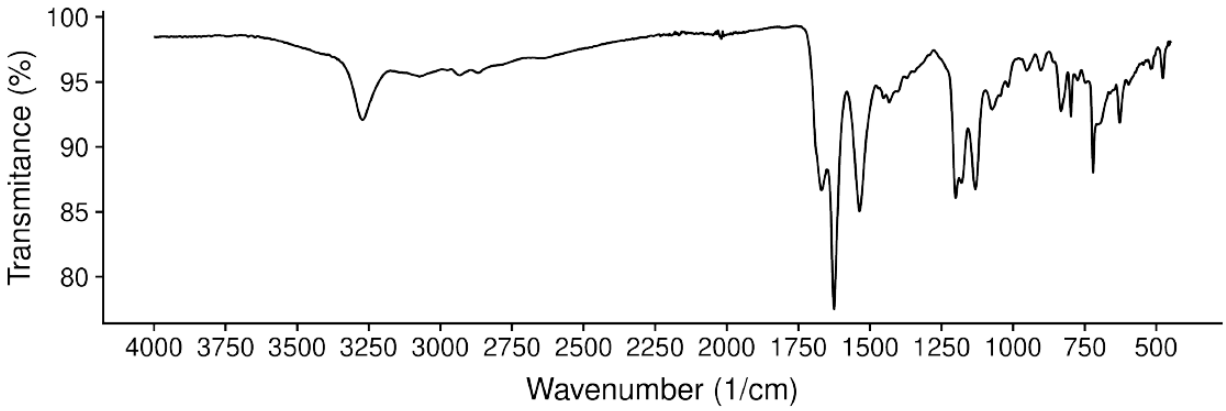

Figure 74. FTIR-ATR of **1TN**.

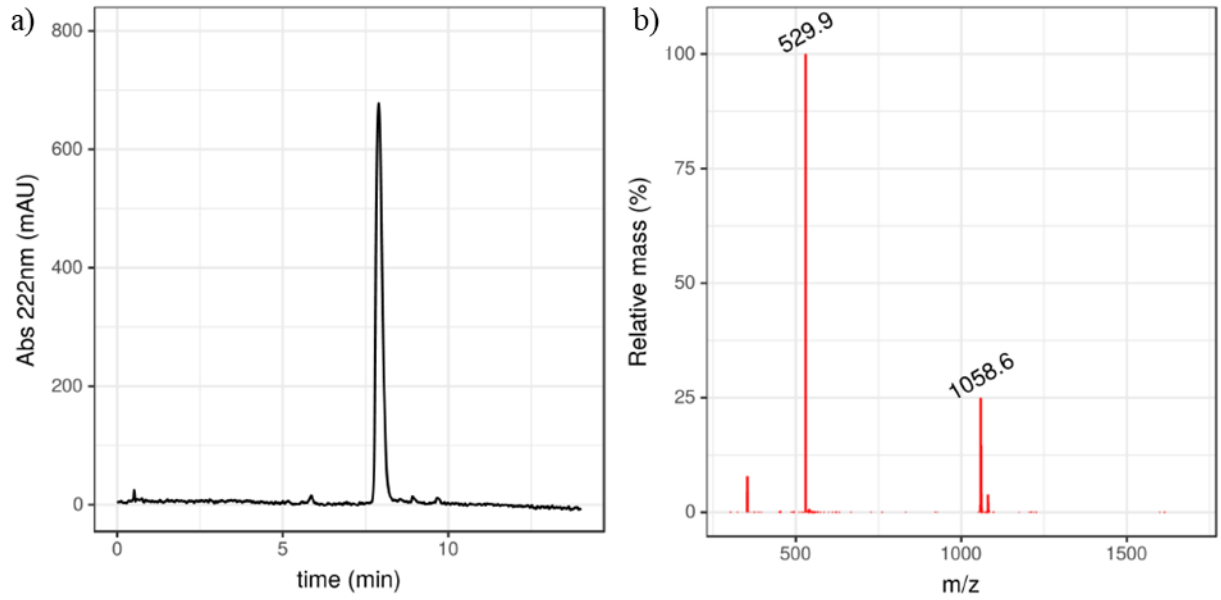

Figure 75. a) HPLC chromatogram of peptide **1TN**. Gradient of 5% to 95% ACN (0.1% TFA) in 15 min; b) MS spectra of the main peak.

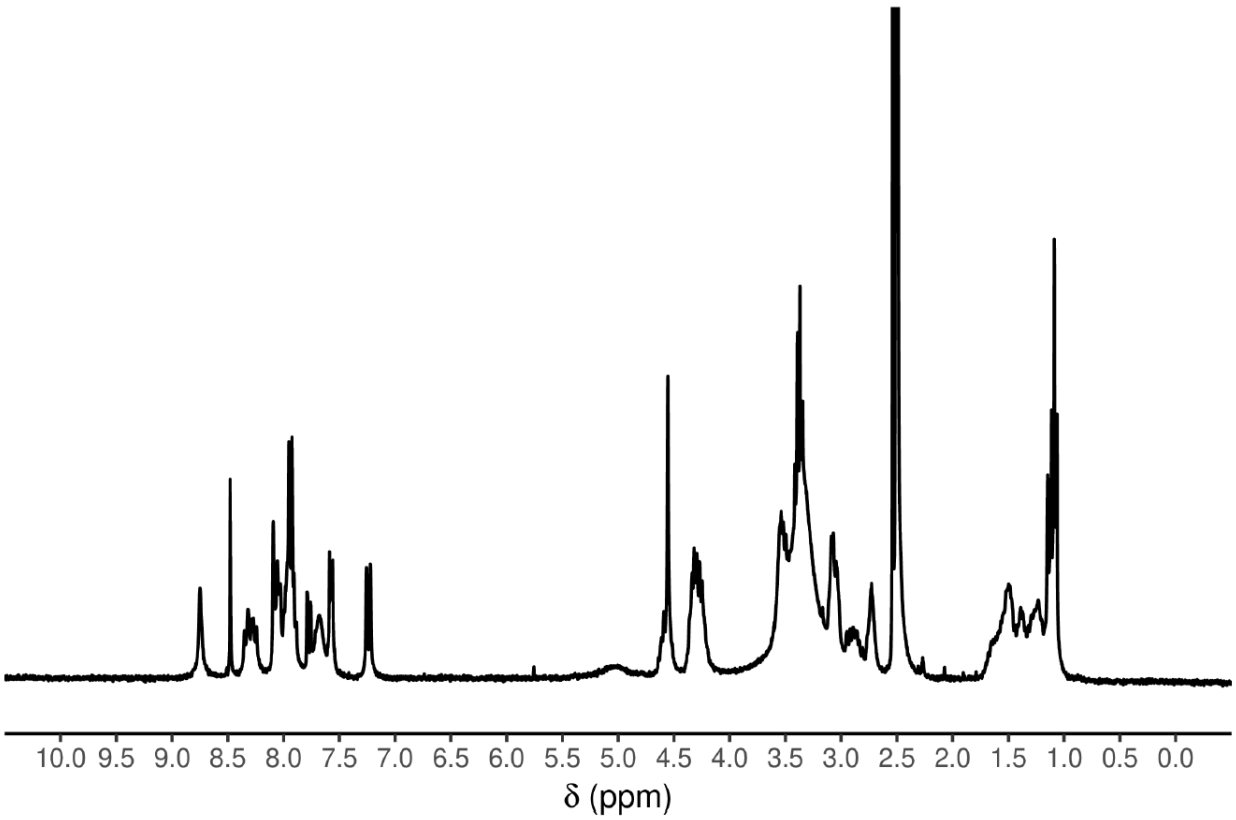

Figure 76. ^{1}H NMR spectra (300 MHz, DMSO-d_6, room temperature) of cyclic peptide **1TN**.

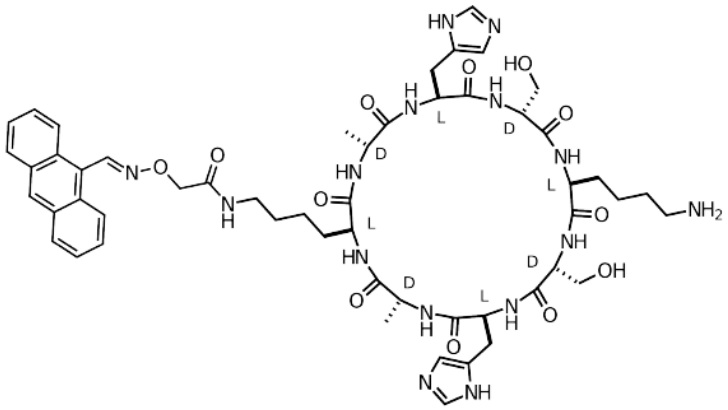

Figure 77. Chemical structure of CP **1TA**.

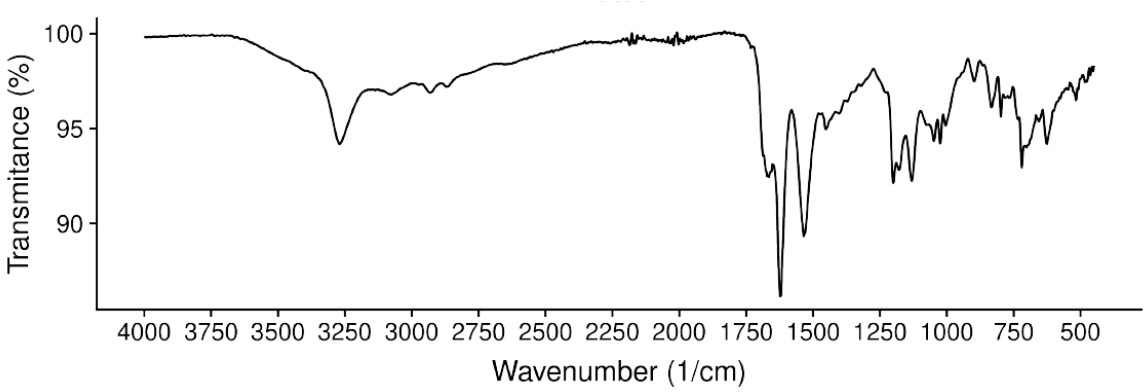

Figure 78. FTIR-ATR of **1TA**.

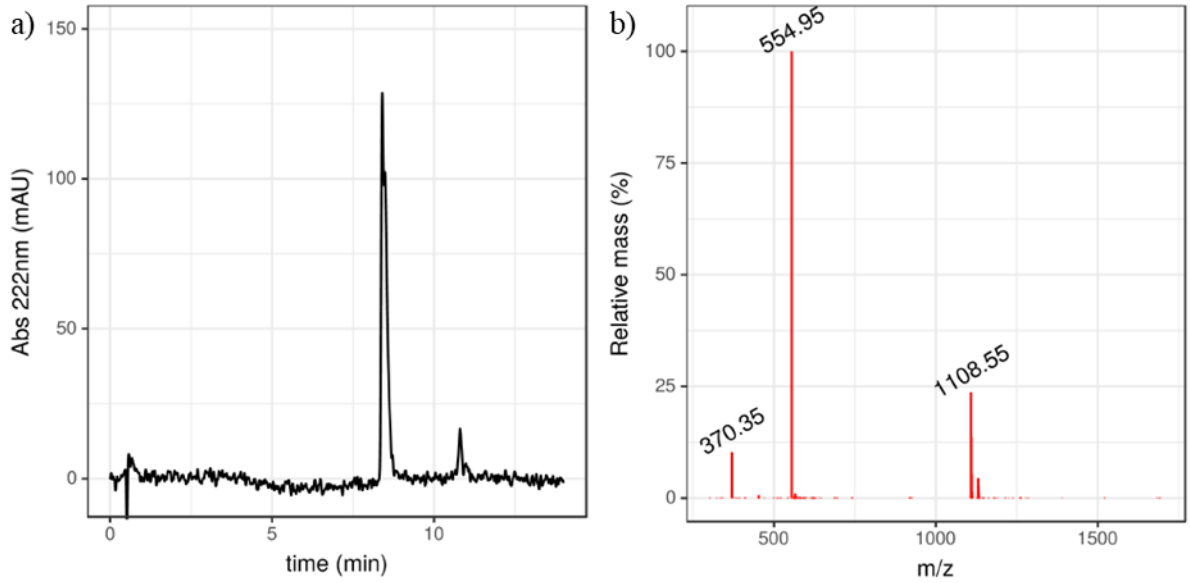

Figure 79. a) HPLC chromatogram of peptide **1TA**. Gradient of 5% to 95% ACN (0.1% TFA) in 15 min; b) MS spectra of the main peak.

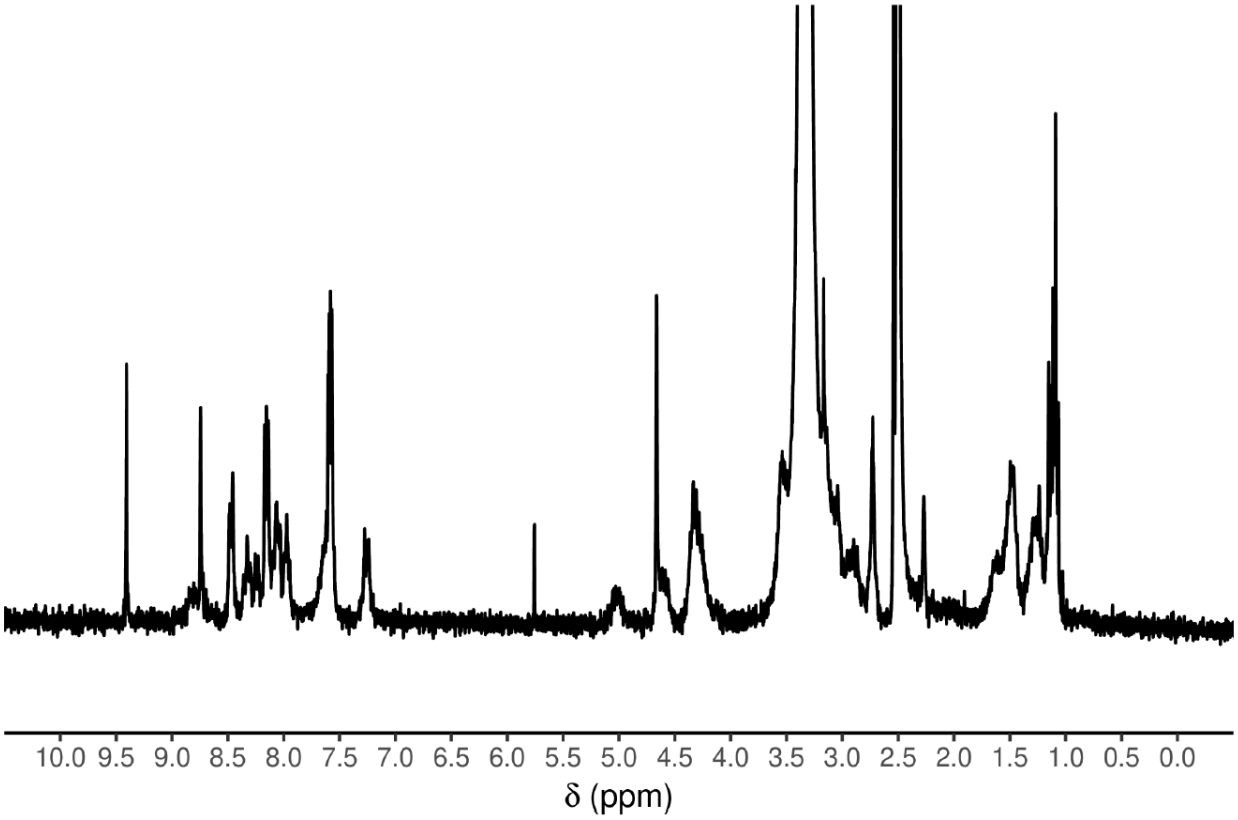

Figure 80. ^{1}H NMR spectra (300 MHz, DMSO-d_6, room temperature) of cyclic peptide **1TA**.

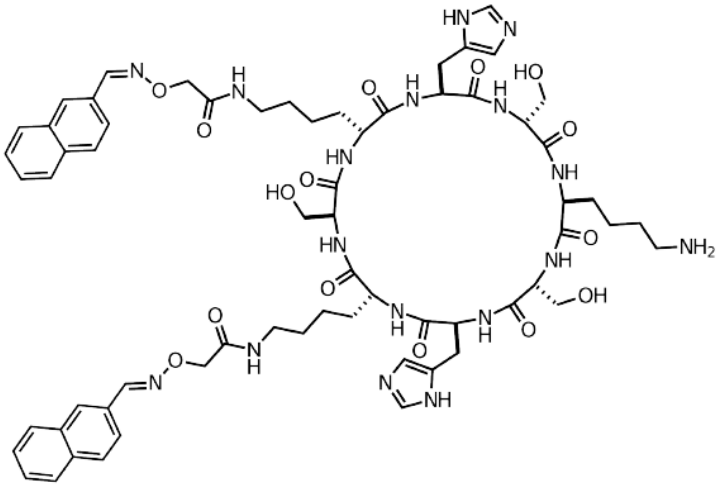

Figure 81. Chemical structure of CP **2TN**.

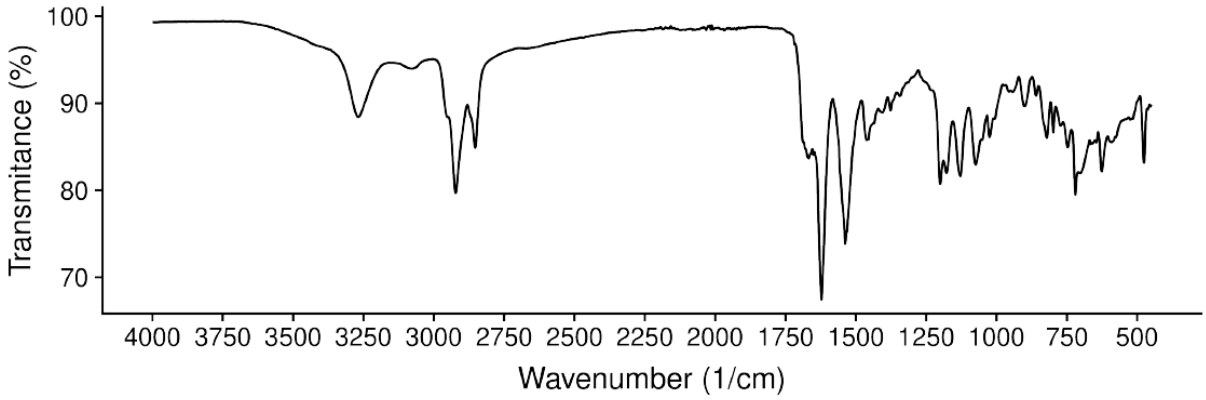

Figure 82. FTIR-ATR of **2TN**.

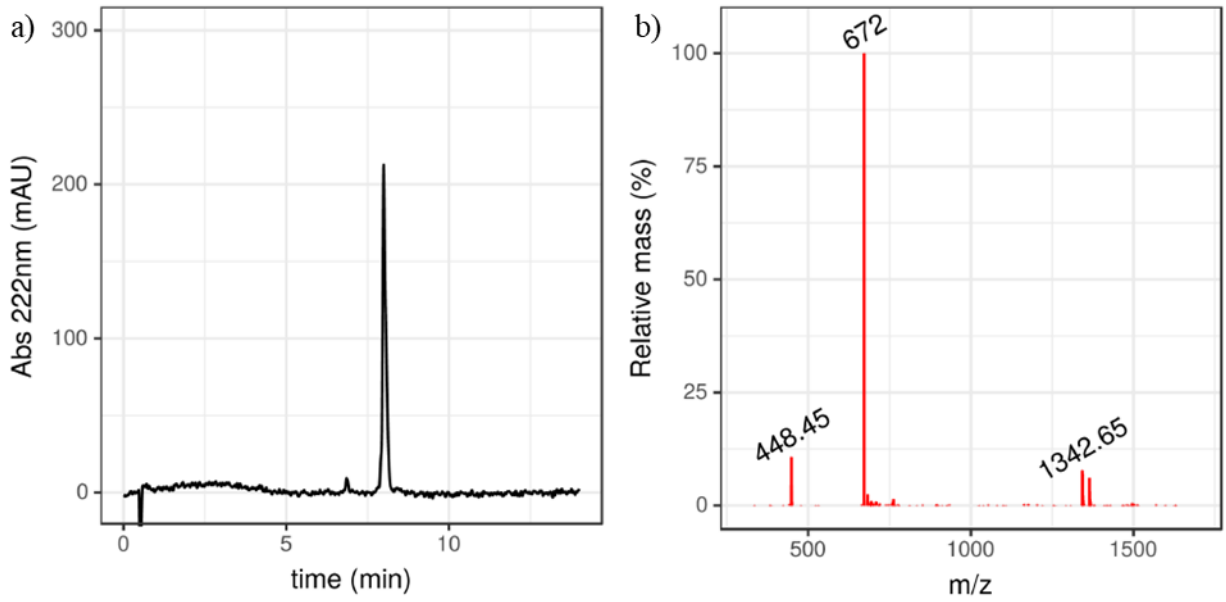

Figure 83. a) HPLC chromatogram of peptide **2TN**. Gradient of 5% to 95% ACN (0.1% TFA) in 12 min; b) MS spectra of the main peak.

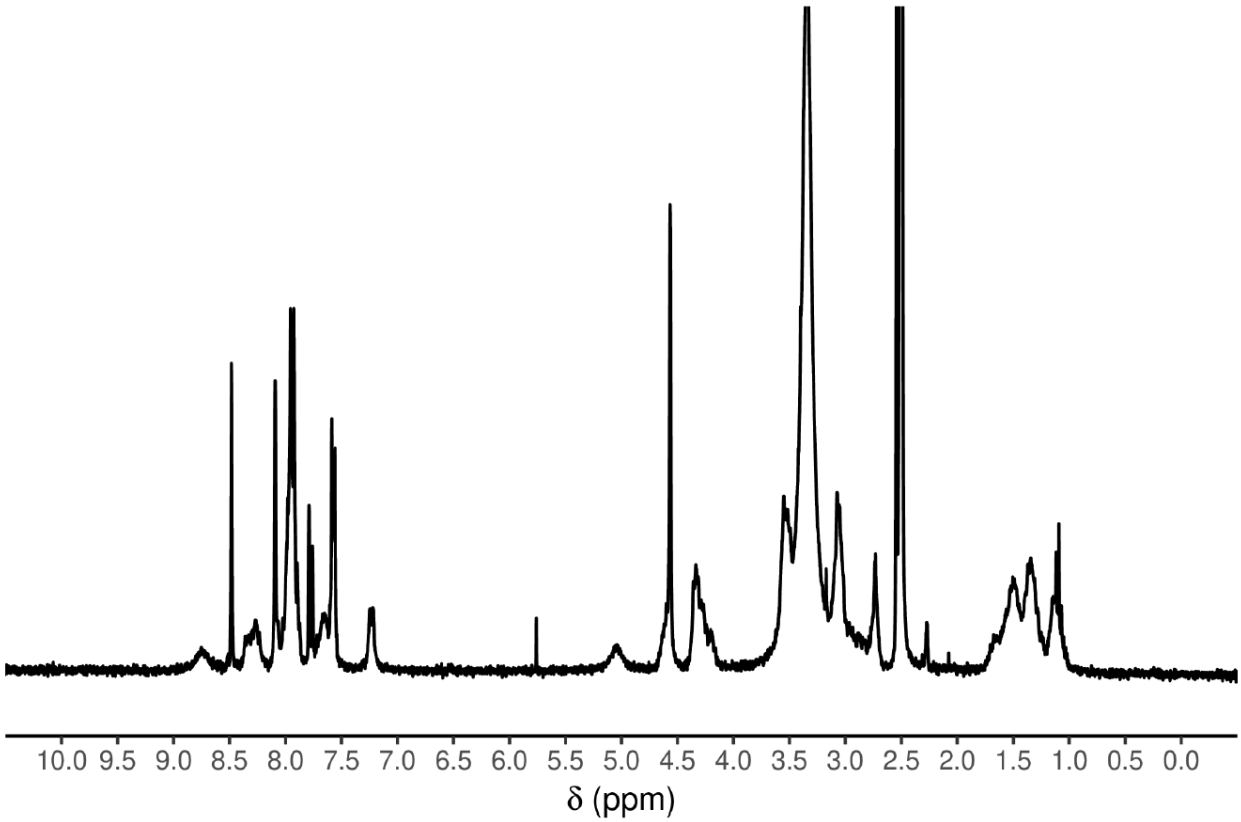

Figure 84. ^{1}H NMR spectra (300 MHz, DMSO-d_6, room temperature) of cyclic peptide **2TN**.

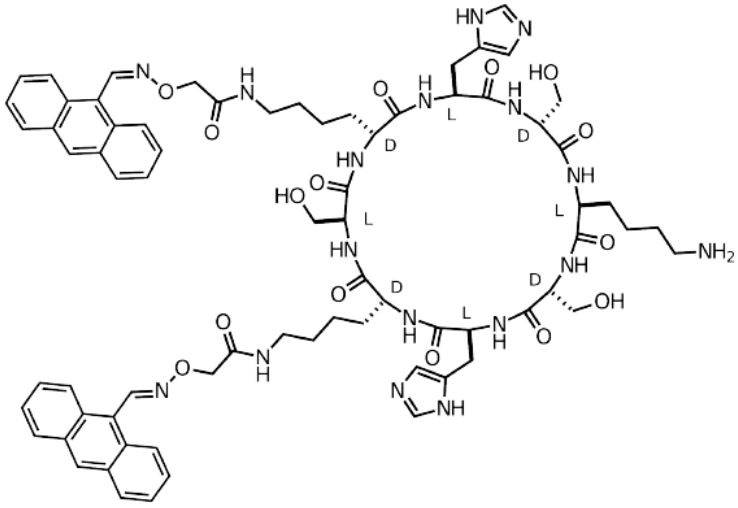

Figure 85. Chemical structure of CP **2TA**.

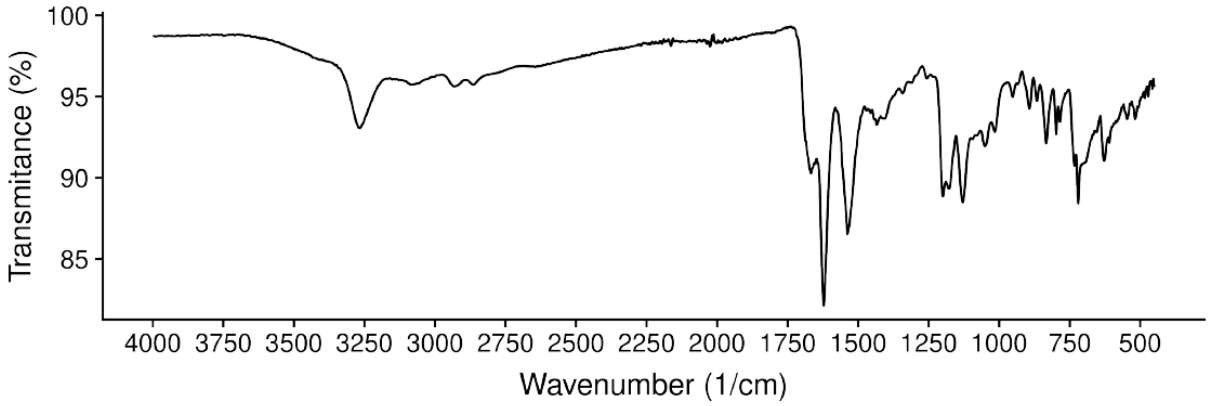

Figure 86. FTIR-ATR of **2TA**.

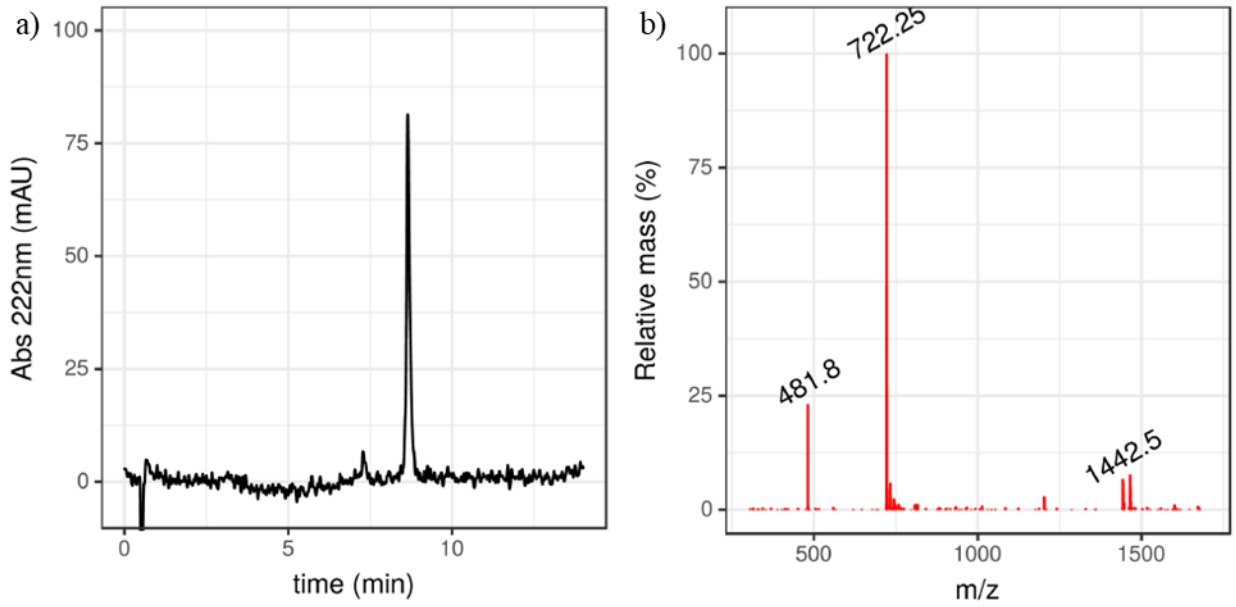

Figure 87. a) HPLC chromatogram of peptide **2TA**. Gradient of 5% to 95% ACN (0.1% TFA) in 12 min; b) MS spectra of the main peak.

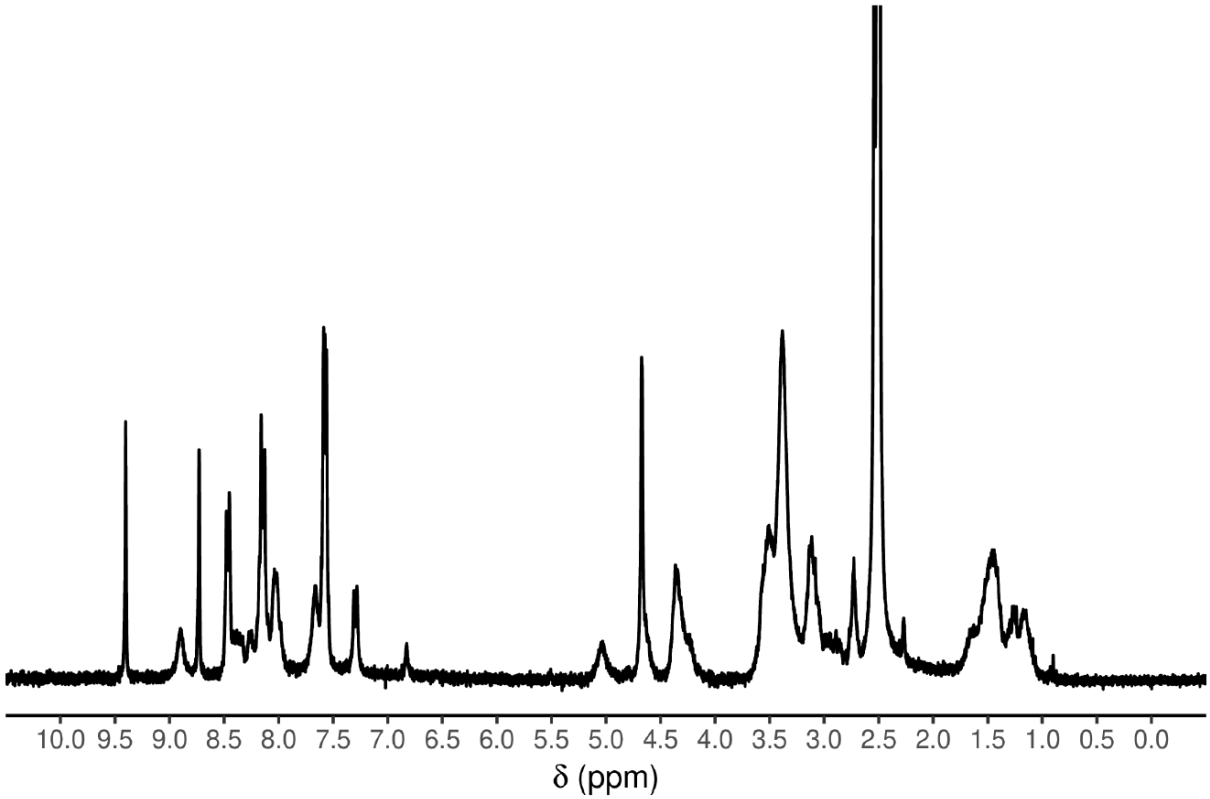

Figure 88. ^{1}H NMR spectra (300 MHz, DMSO-d_6, room temperature) of cyclic peptide **2TA**.

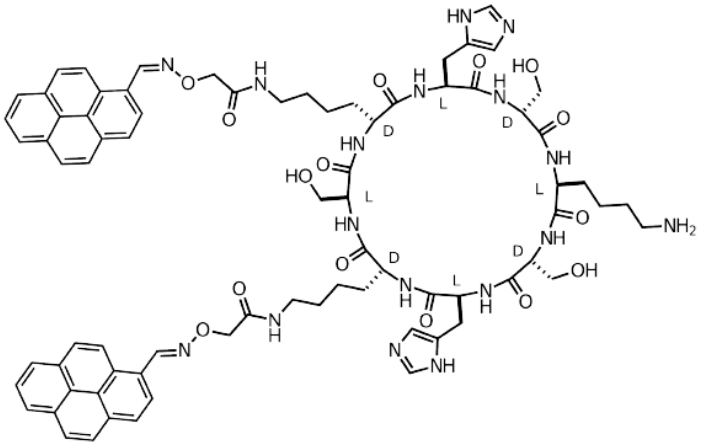

Figure 89. Chemical structure of CP **2TP**.

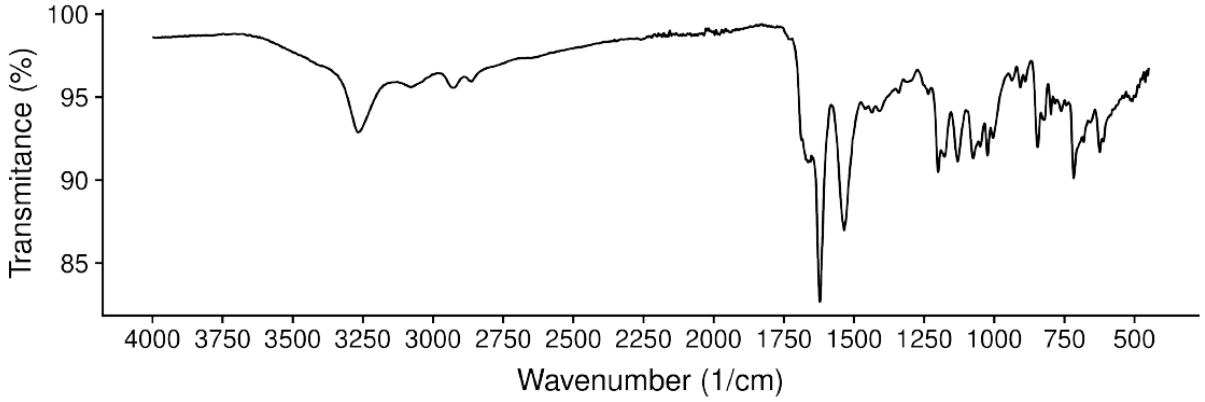

Figure 90. FTIR-ATR of **2TP**.

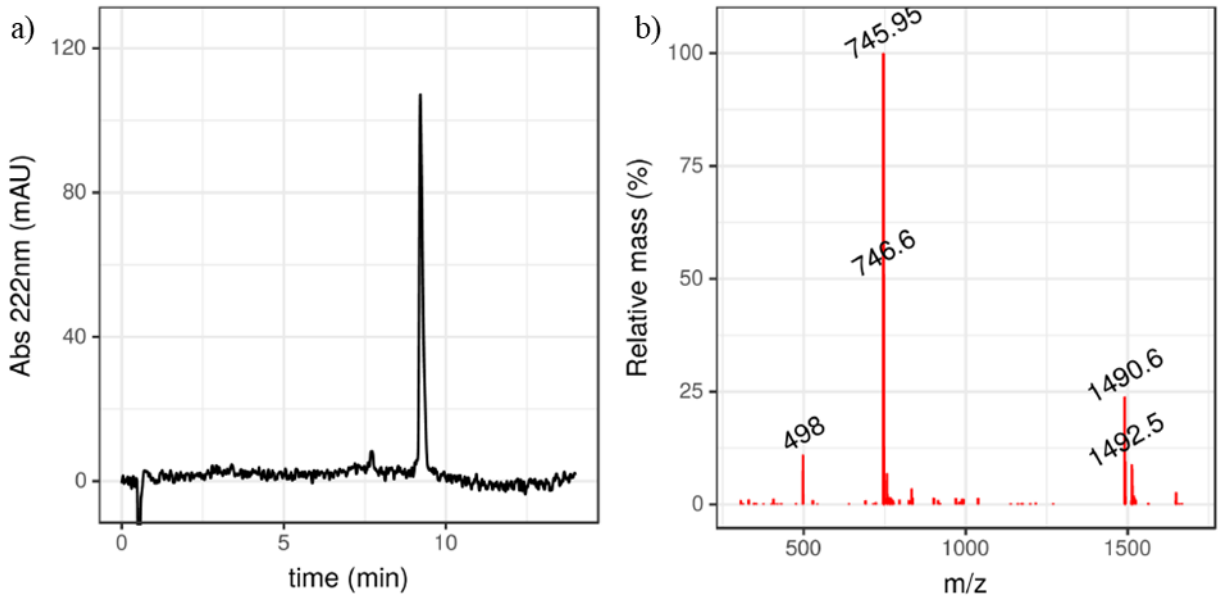

Figure 91. a) HPLC chromatogram of peptide **2TP**. Gradient of 5% to 95% ACN (0.1% TFA) in 12 min; b) MS spectra of the main peak.

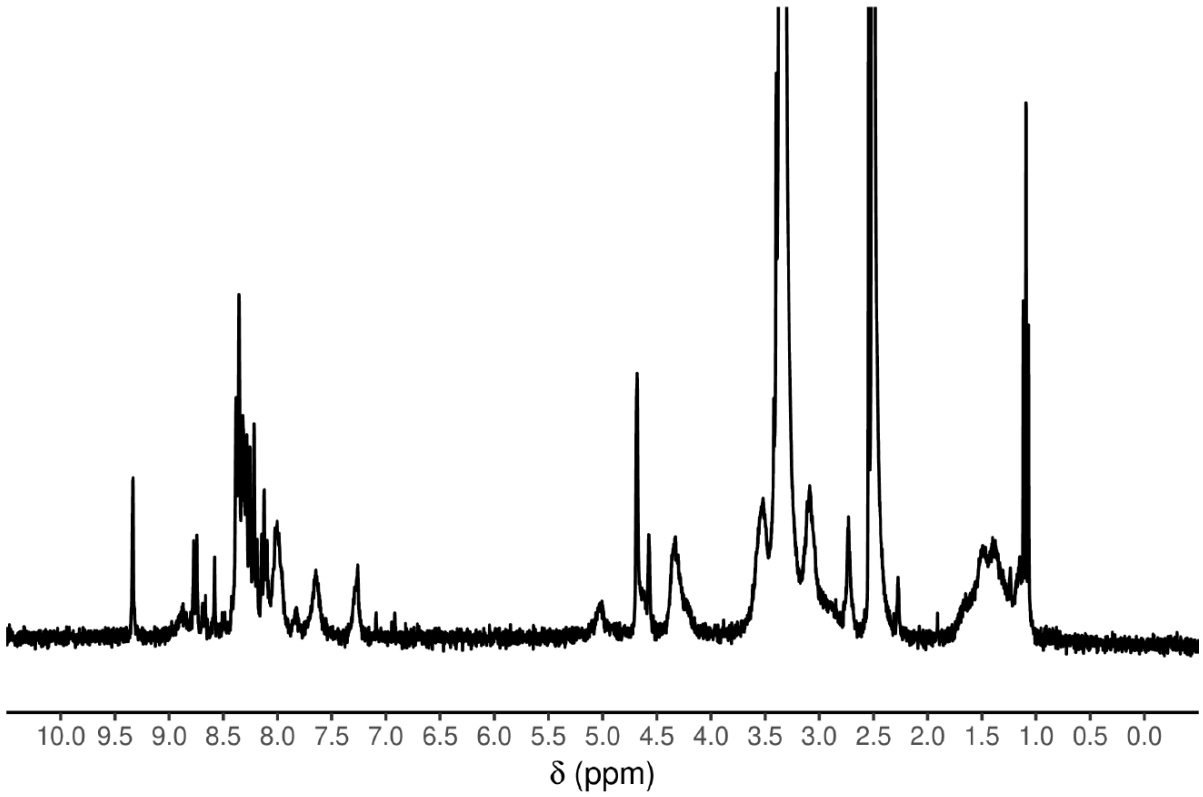

Figure 92. ^{1}H NMR spectra (300 MHz, DMSO-d_6, room temperature) of cyclic peptide **2TP**.

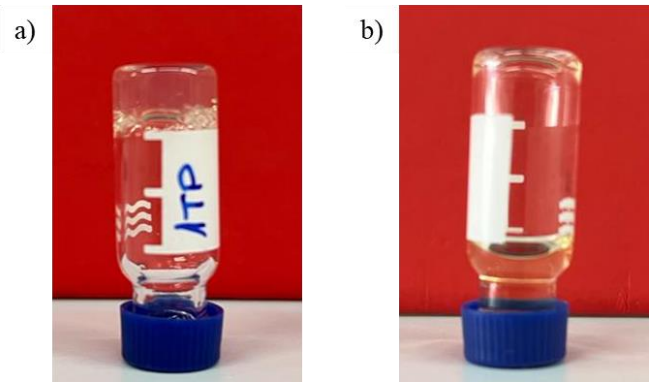

Figure 93. Reversible gel-sol transition upon acidification of **1TP** hydrogels a) Preformed hydrogel (2% w/w, pH 8-9); b) Transition to a solution state after addition of concentrated acid.

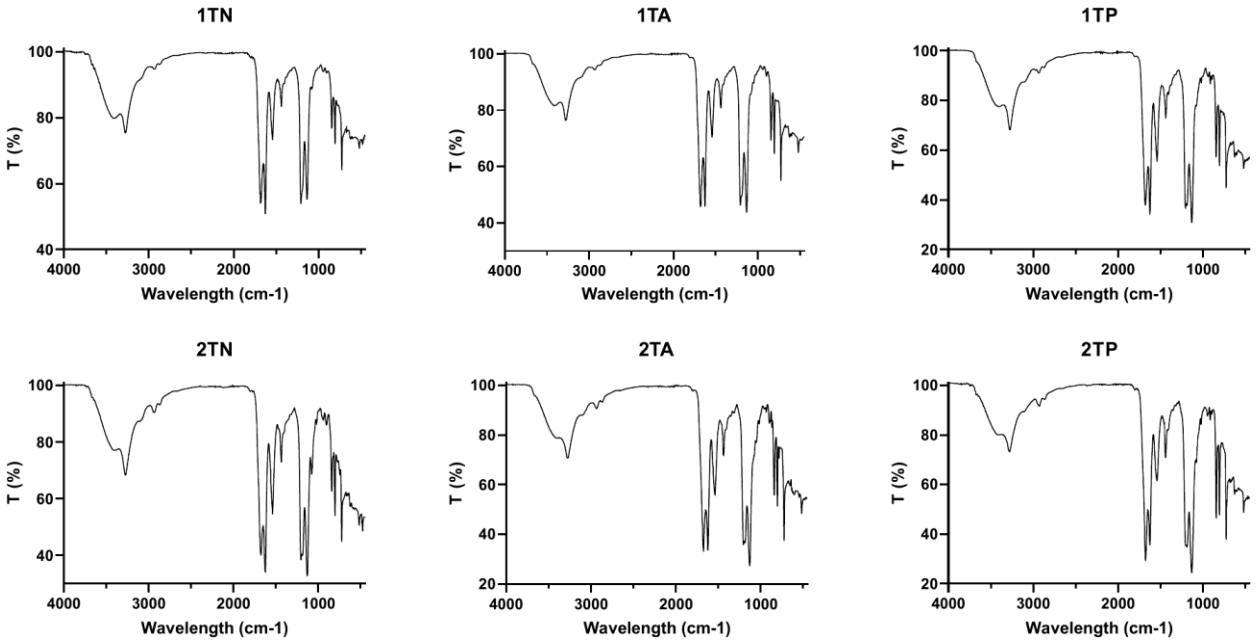

Figure 94. ATR-FTIR spectra for freeze-dried alkaline samples of **1TN**, **1TA**, **1TP**, **2TN**, **2TA** and **2TP**.

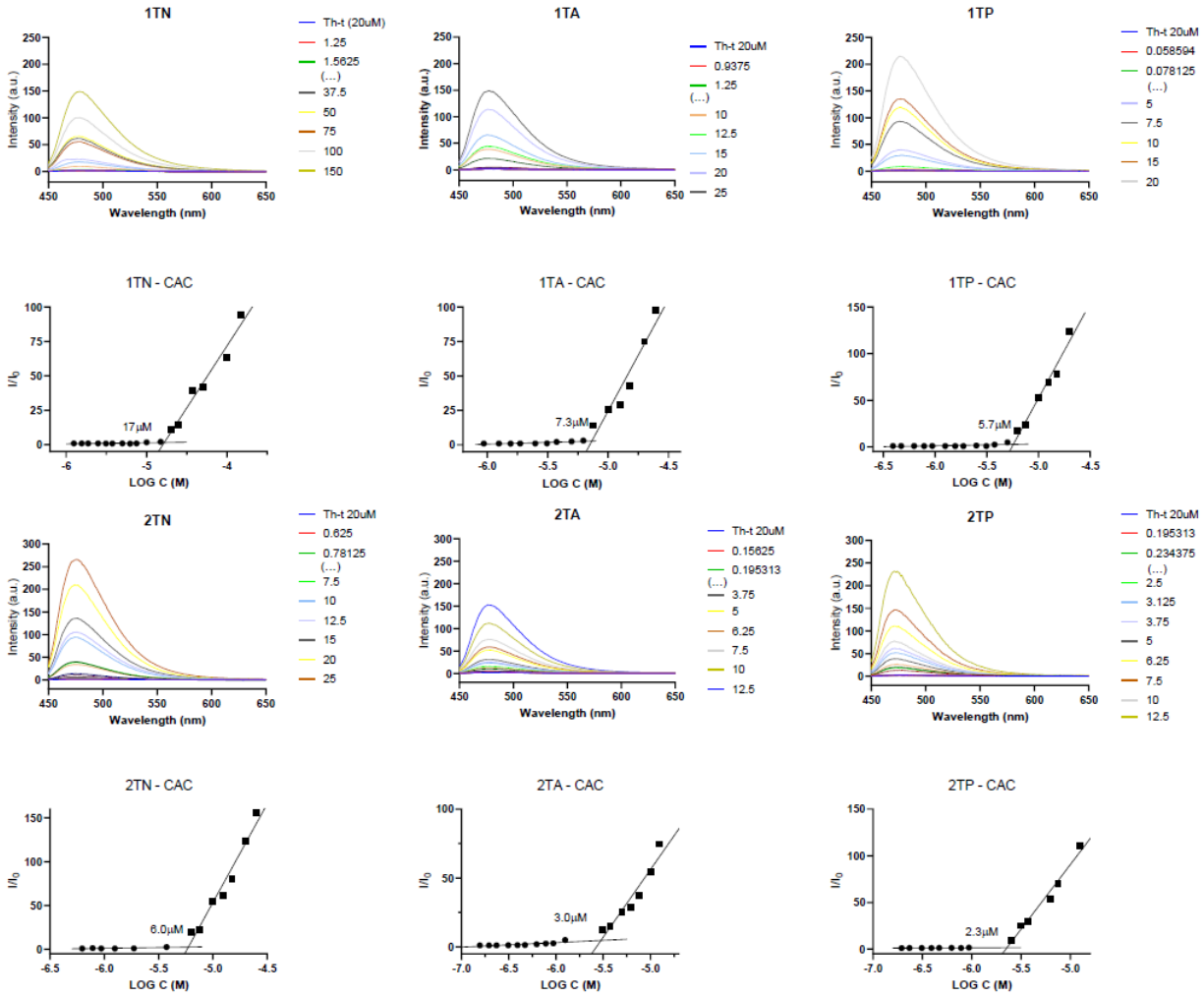

Figure 95. Determination of critical aggregation concentration (CAC) by fluorescence experiments in the presence of ThT (20 μM).

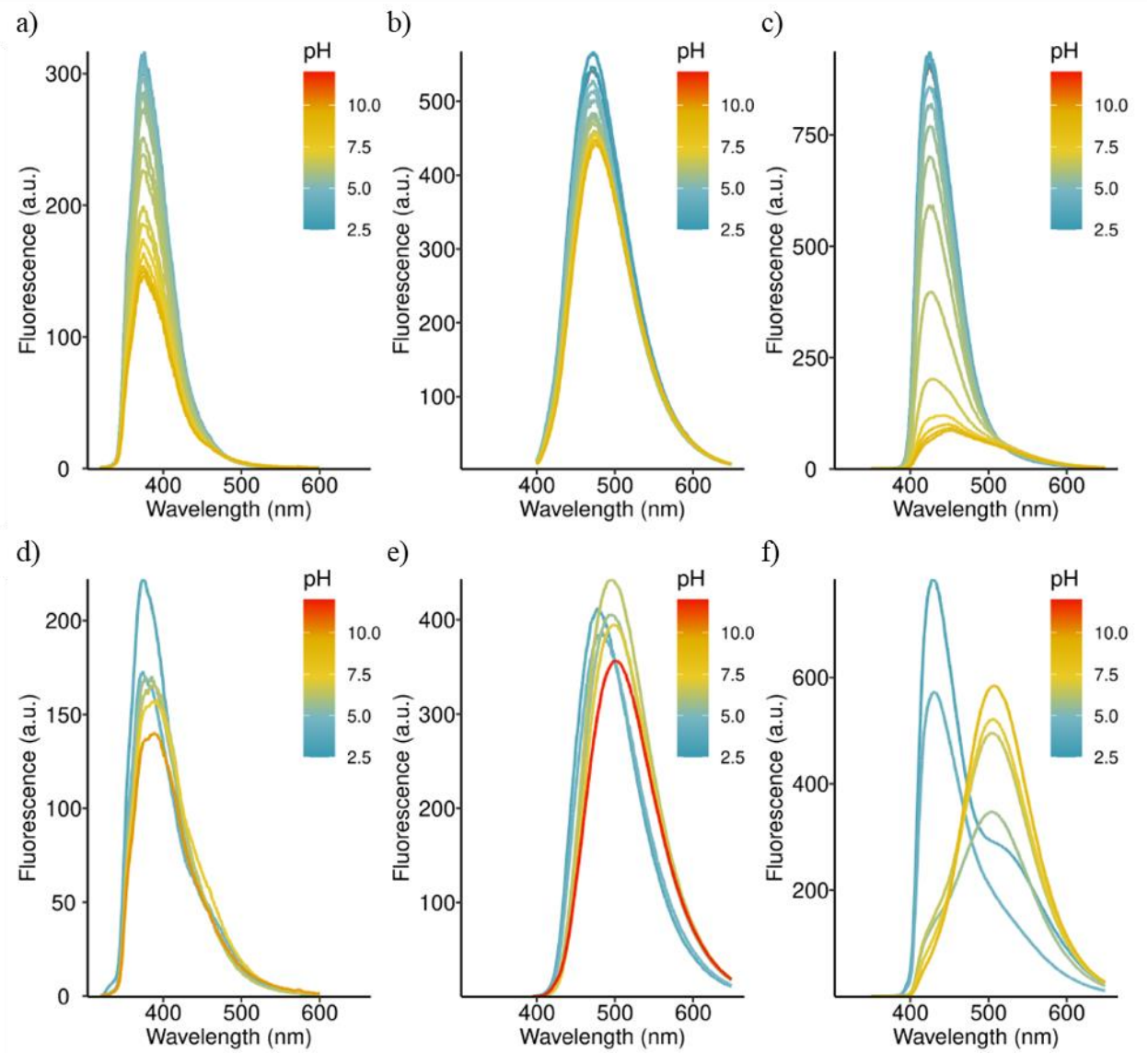

Figure 96. Fluorescence emission spectra of CPs (400 μM, water) at different pH values. The parameters are: a) **1TN**: λ_{exc} = 230 nm; b) **1TA**: λ_{exc} = 385 nm; c) **1TP**: λ_{exc} = 340 nm: d) **2TN**: λ_{exc} = 230 nm; e) **2TA**: λ_{exc} = 385 nm; f) **2TP**: λ_{exc} = 340 nm.

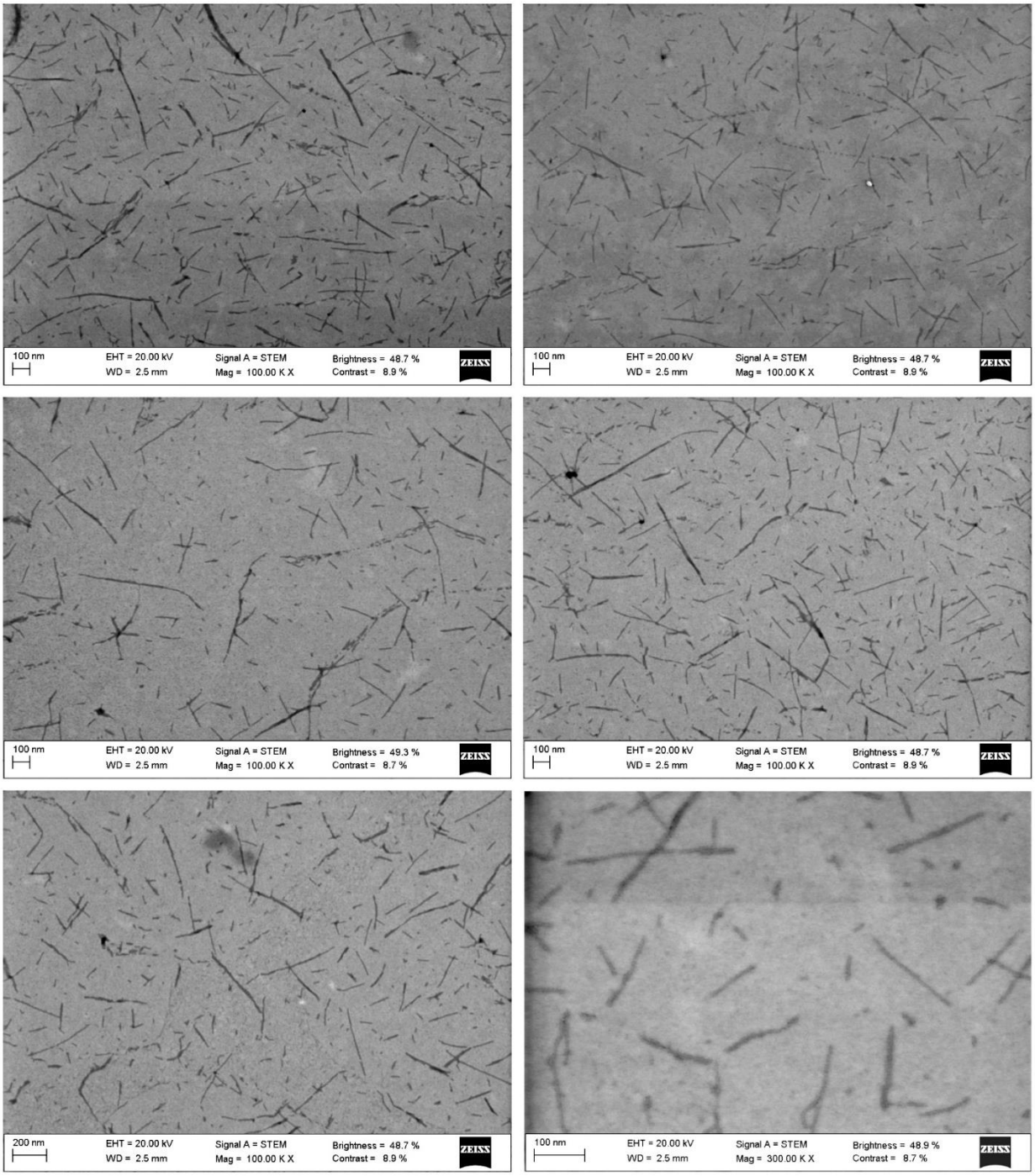

Figure 97. STEM micrographs of dilutions of **1TA** gels (final concentration 11 μM) after staining with uranyl acetate.

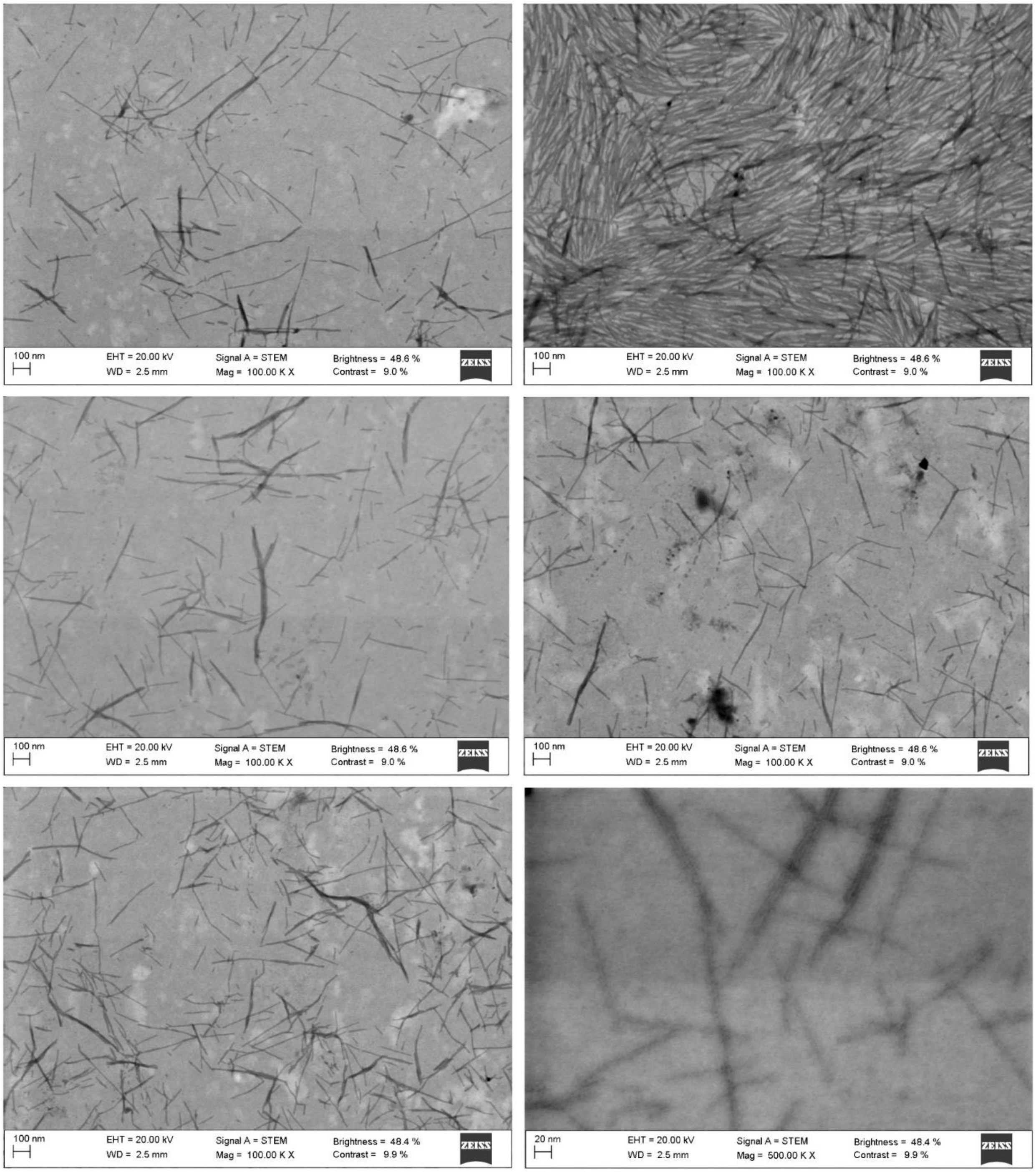

Figure 98. STEM micrographs of dilutions of **1TP** gels (final concentration 11 μM) after staining with uranyl acetate.

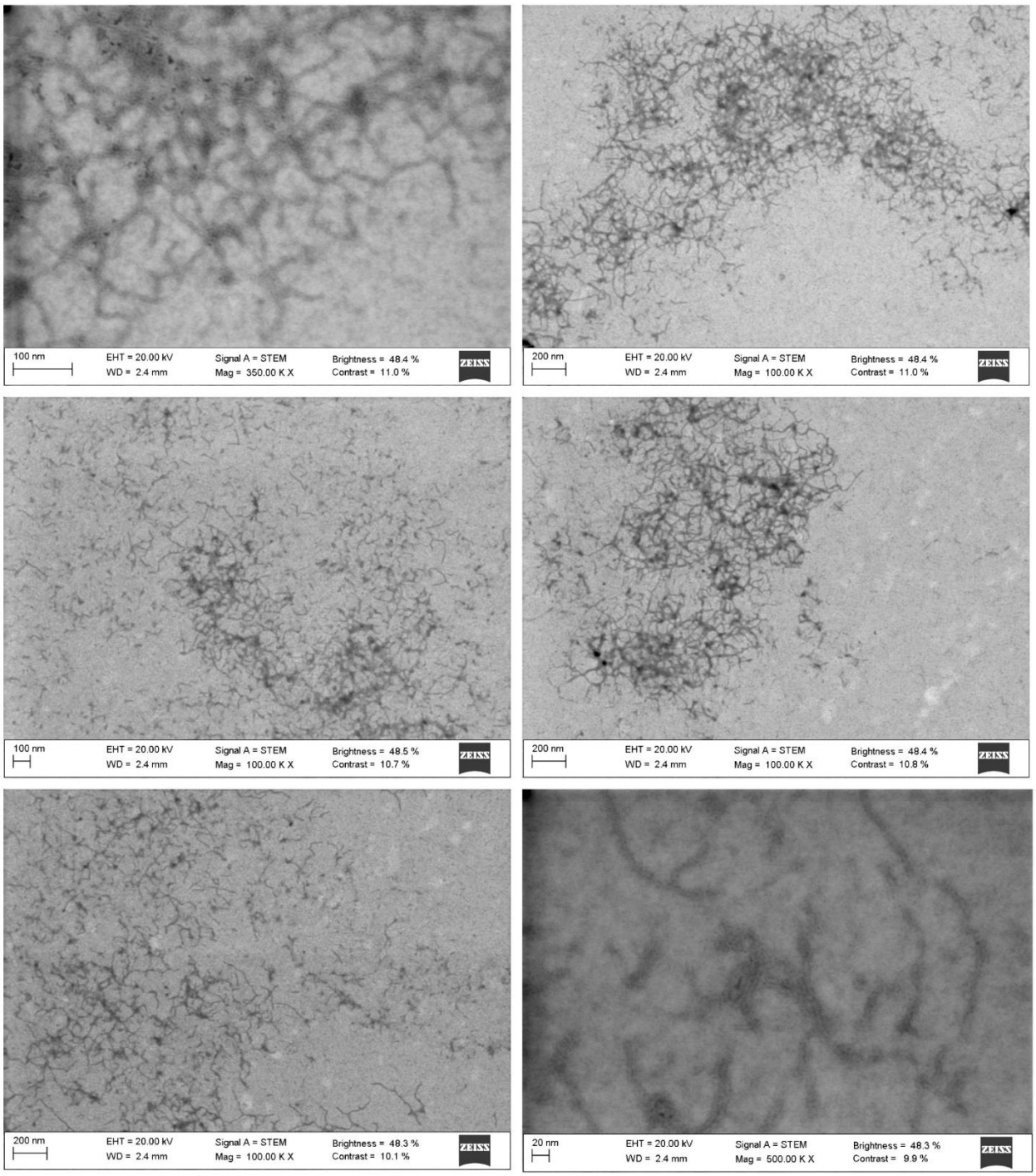

Figure 99. STEM micrographs of dilutions of **2TN** gels (final concentration 11 μM) after staining with uranyl acetate.

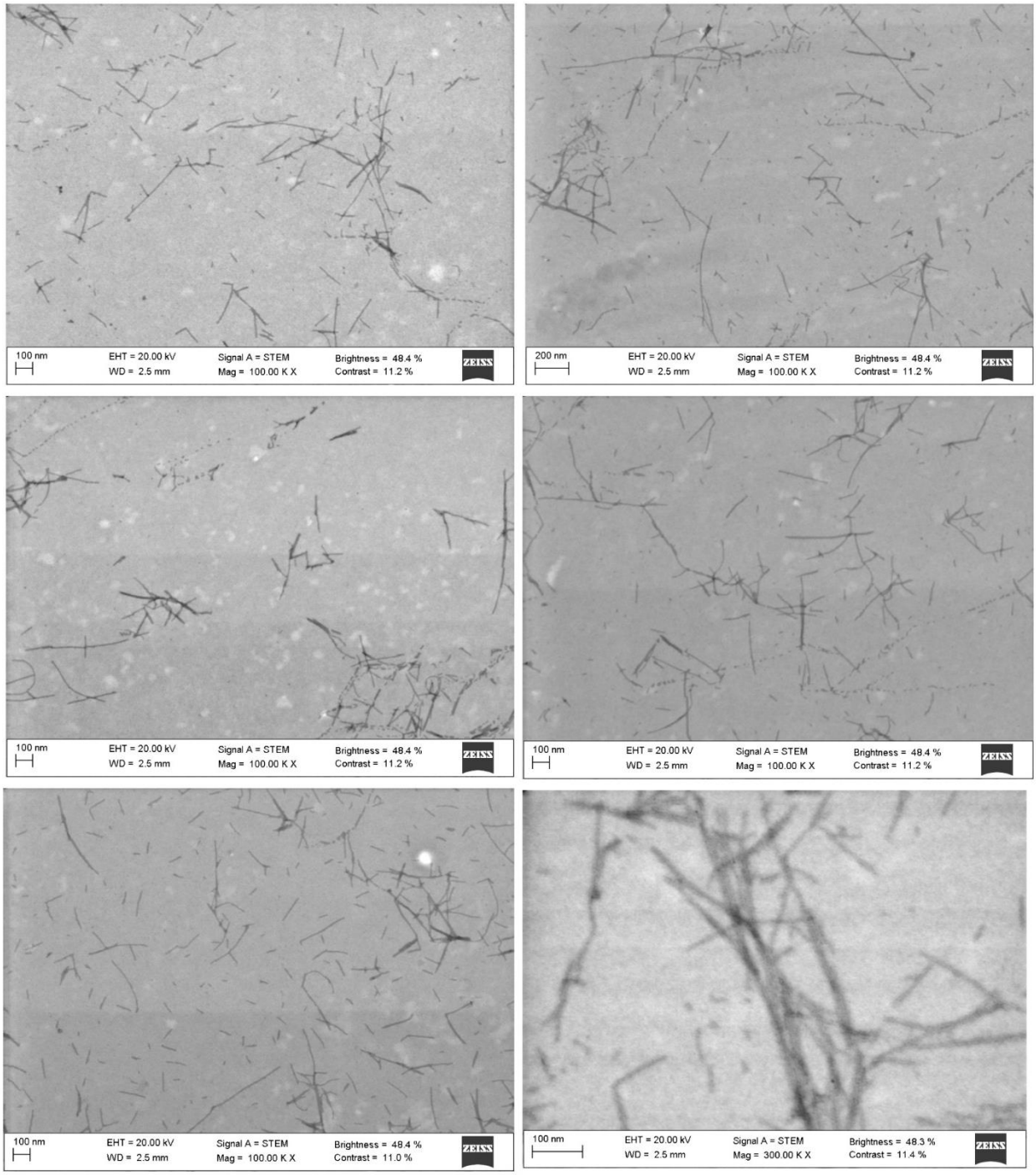

Figure 100. STEM micrographs of dilutions of **2TA** gels (final concentration 11 μM) after staining with uranyl acetate.

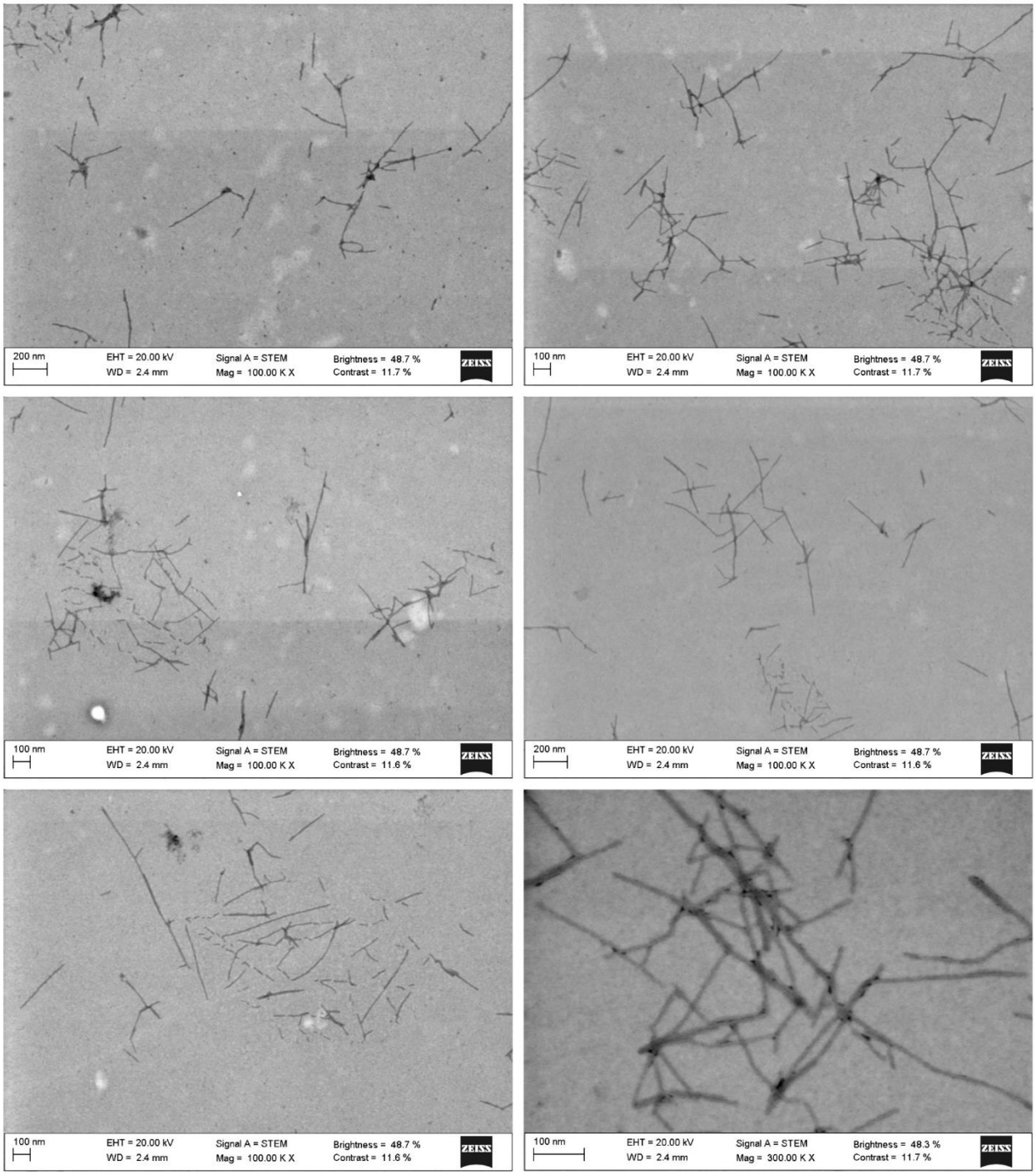

Figure 101. STEM micrographs of dilutions of **2TP** gels (final concentration 11 μM) after staining with uranyl acetate.

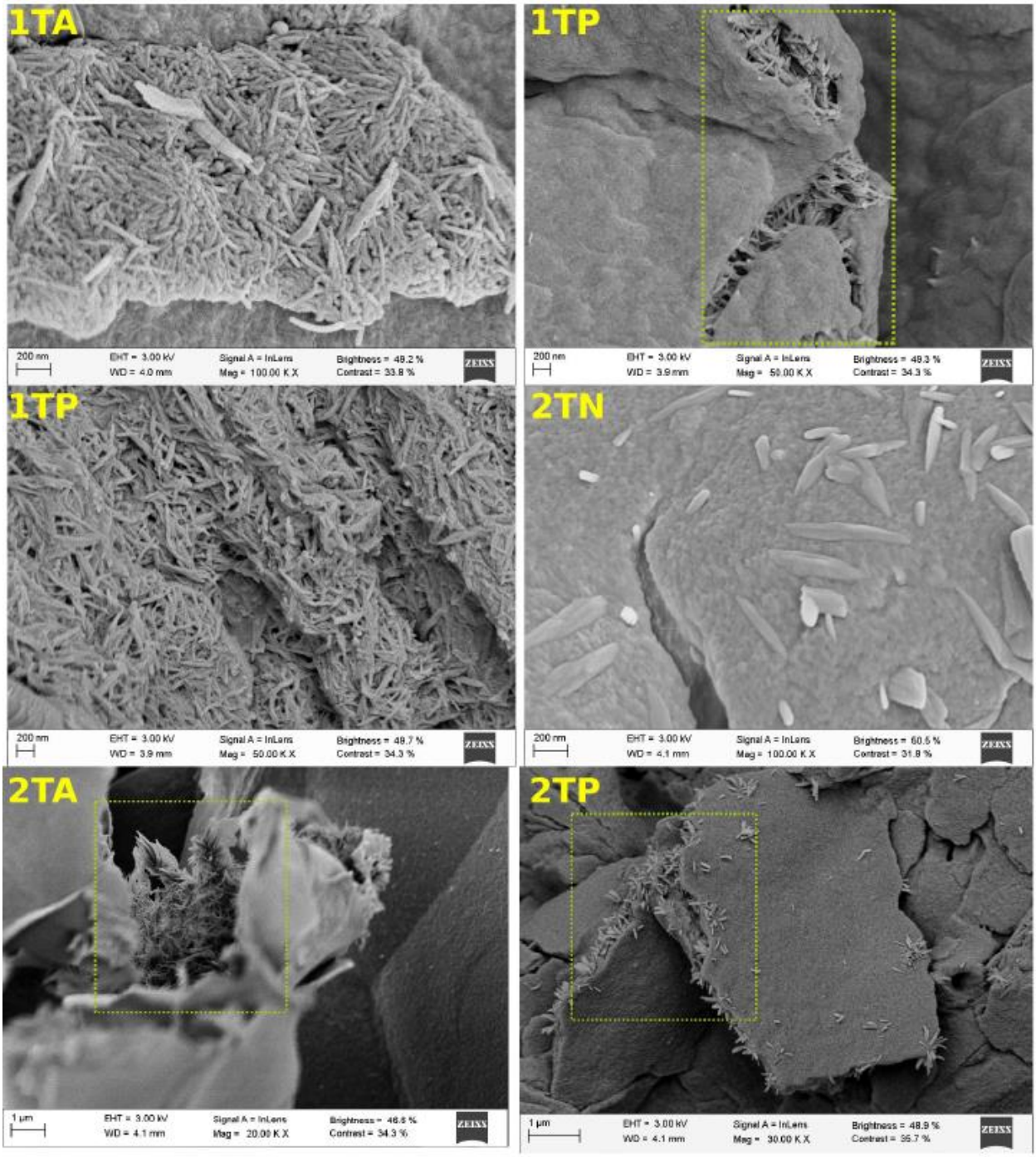

Figure 102. SEM images of **1TA**, **1TP**, **2TN**, **2TA** and **2TP** freeze-dried gels showing local regions where nanotubes are clearly visualized. The dashed boxes highlight the presence of nanotubes under the surface.

2. Spatially Controlled Supramolecular Polymerization of Peptide Nanotubes

2.1.Figures

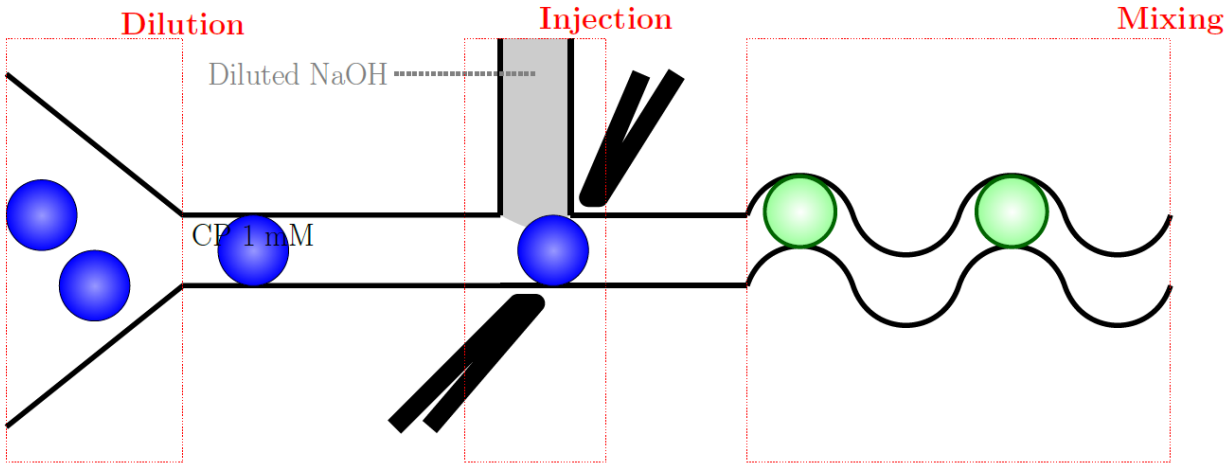

Figure 103. Schematic representation of the pico-injection device.

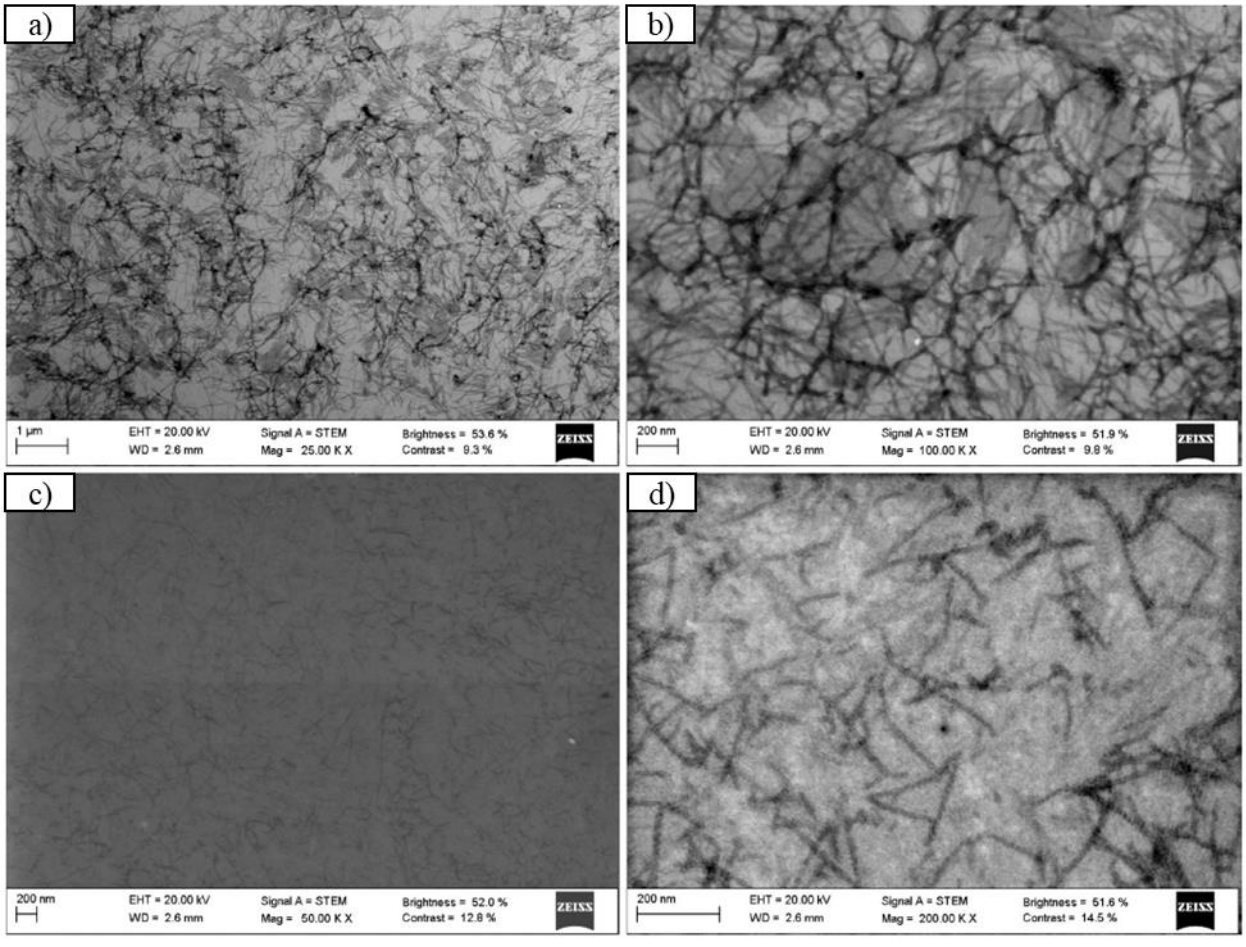

Figure 104. Formation of 1TP nanotubes when assembled by charge screening (final $CaCl_2$ concentration approximately 500 mM) visualized by STEM microscopy at a) low and b) high magnification; or c) and d) assembled by using NaOH 3.5 mM.

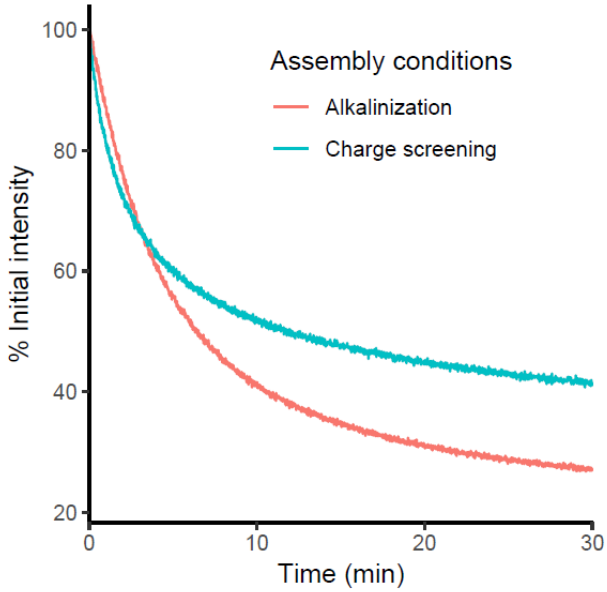

Figure 105. Kinetics for the quenching of pyrene monomer (λ_{exc} = 340 nm, λ_{em} = 420 nm) for **1TP** (50 μM) in the presence of $CaCl_2$ (0.5 M, red line) or HEPES pH 8 (50 mM, red line).

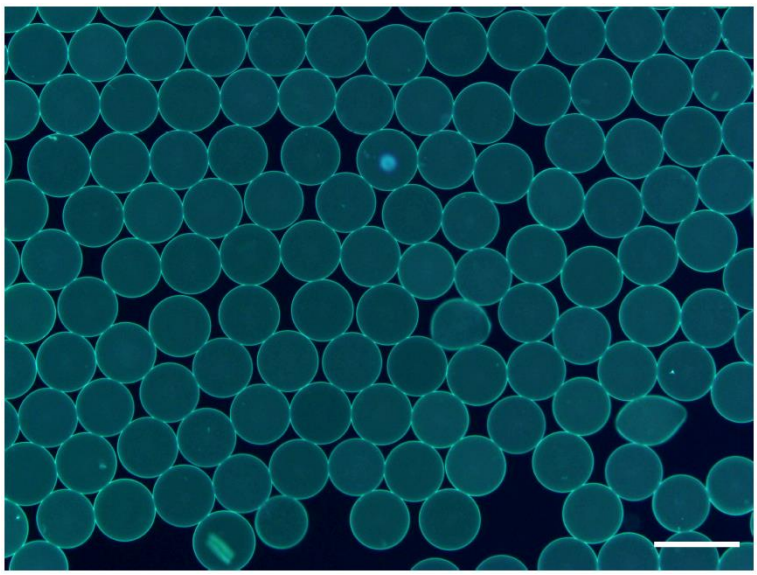

Figure 106. Droplets prepared by microfluidics. Conditions: I_{1TP}: **1TP** 1 mM, milliQ water pH 4-5, flow rate 200 μL/h. I_T : HEPES 50 mM pH 8 as assembly trigger at flow rate of 100 μL/h. I_{oil} as described in the main text, flow rate 500 μL/h. Scale bar denotes 100 μm.

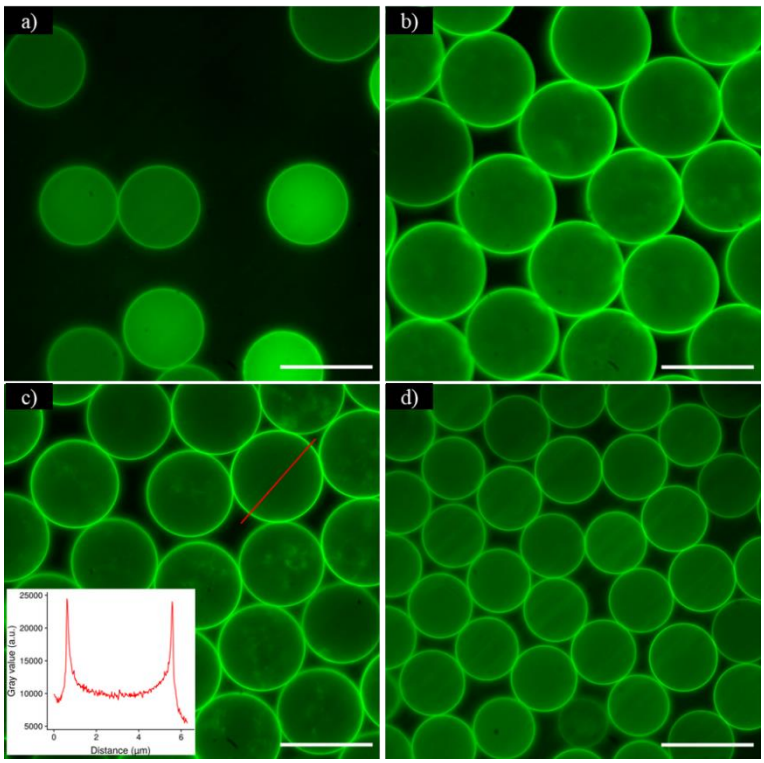

Figure 107. Self-assembly of **1TP** within W/O droplets triggered by pico-injection of NaOH (13 mM). Pico-injections of the following volume were carried out: a) 5; b) 10; c) 20 and d) 30 µL . The insert in c) represents the profile of the droplet. Scale bars are 5 µm. Images are colorized from black and white originals.

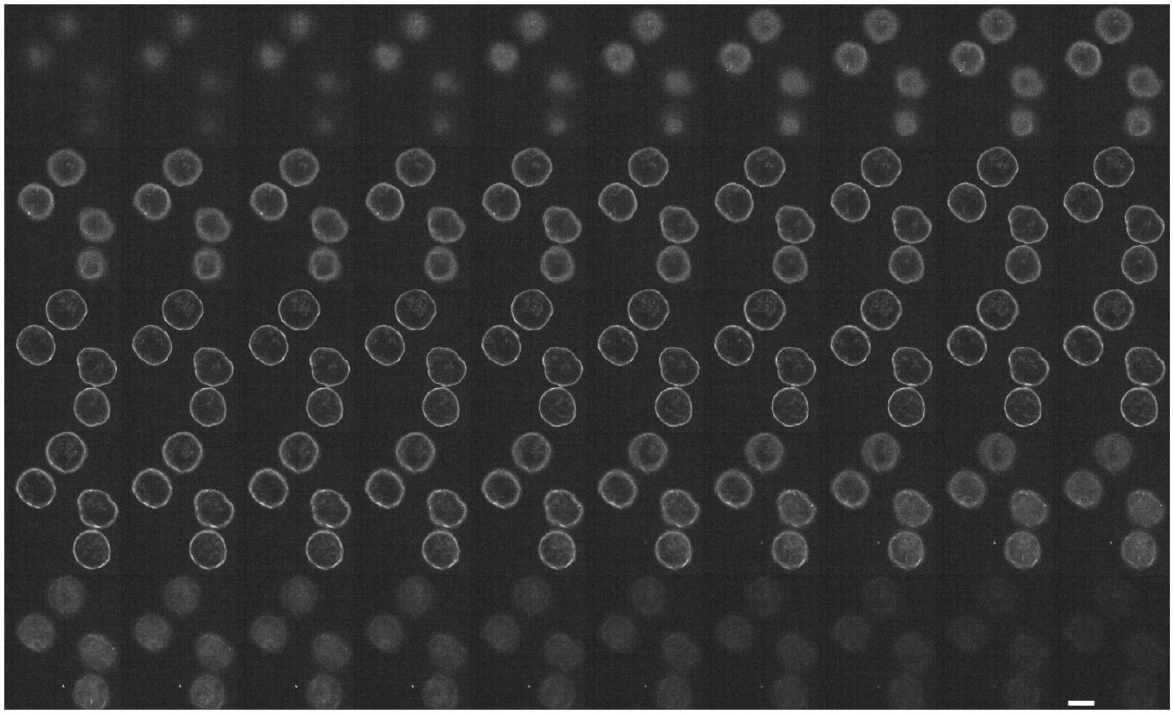

Figure 108. Confocal projections of droplets assembled using **1TP** (1 mM) in I_{1TP} at 200 µL/h and I_T NaOH (3.5 mM) at 100 µL/h. Stack slices are ordered from left to right and from top to bottom. Scale bar is 50 µm.

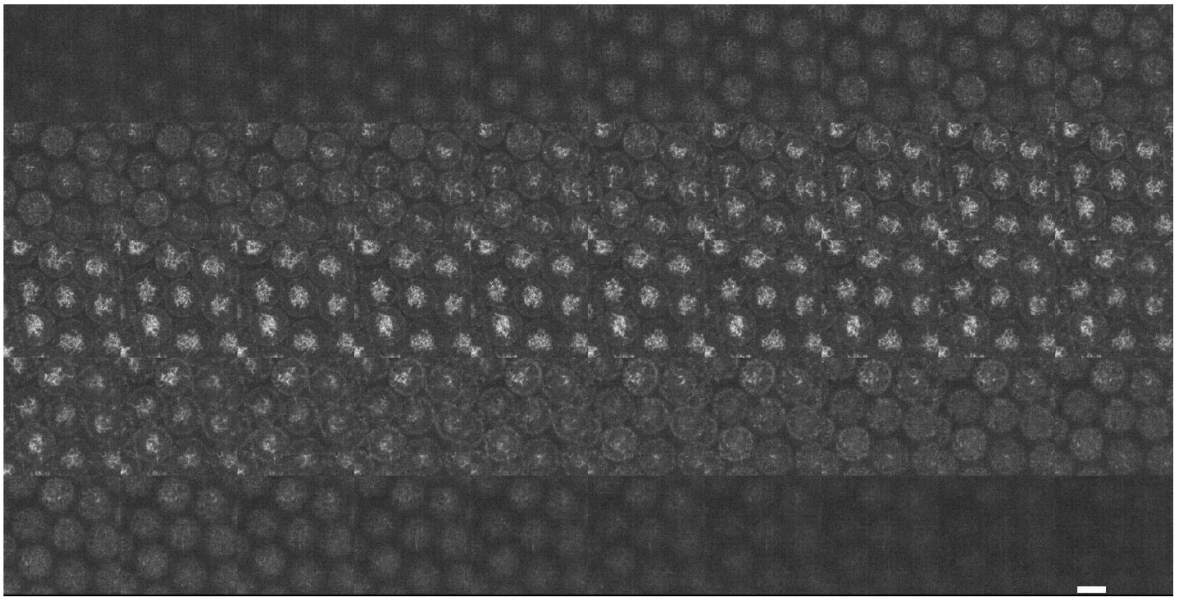

Figure 109. Confocal projections of droplets assembled using **1TP** (1 mM) in I_{1TP} at 150 µL/h and I_T $CaCl_2$ (1 M) at 100 µL/h. Similar results were observed at I_T 75 µL/h. Stack slices are ordered from left to right and from top to bottom. Scale bar is 50 µm.

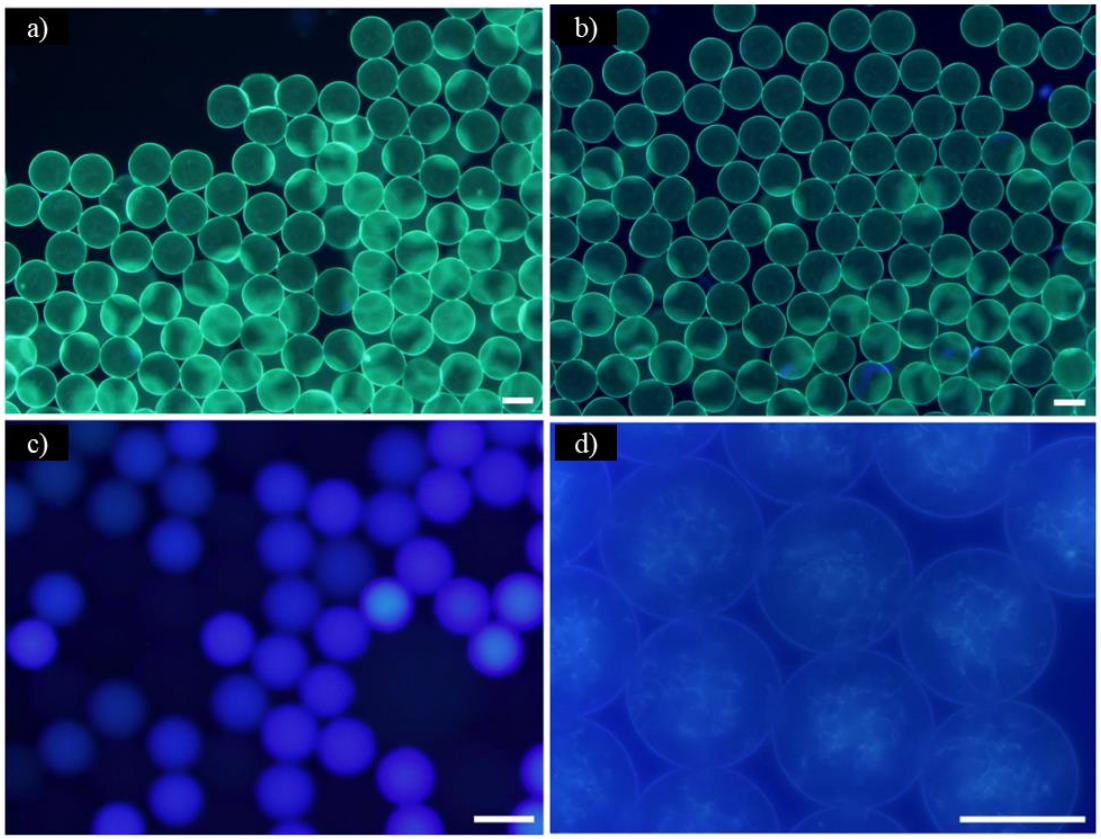

Figure 110. Epifluorescence images of droplets assembled using **1TP** (1 mM) in I_{1TP} and the following conditions: a) 150 µL/h **1TP** and 100 µL/h NaOH (3.5 mM) in I_T ; b) 200 µL/h **1TP** and 100 µL/h NaOH (3.5 mM) in I_T ; c) 150 µL/h **1TP** and 10 µL/h $CaCl_2$ (1 M) in I_T ; d) 150 µL/h **1TP** and 100 µL/h $CaCl_2$ (1 M) in I_T . Scale bars are 50 µm.

3. 2D Assemblies Based On A Tetraphenylethylene *D,L*-Cyclic Peptide Scaffold.

3.1. Characterization

3.1.1. TPE-aldehydes

Compound **TPE$_1$** was prepared as described elsewhere.[492] Compounds **TPE-(CHO)$_4$**, **TPE-(OH)$_4$** and **TPE-(PEG)$_4$**_where prepared and characterized by our collaborator Sebastien Ulrich.[482] All chemical structures can be seen in Figure 111.

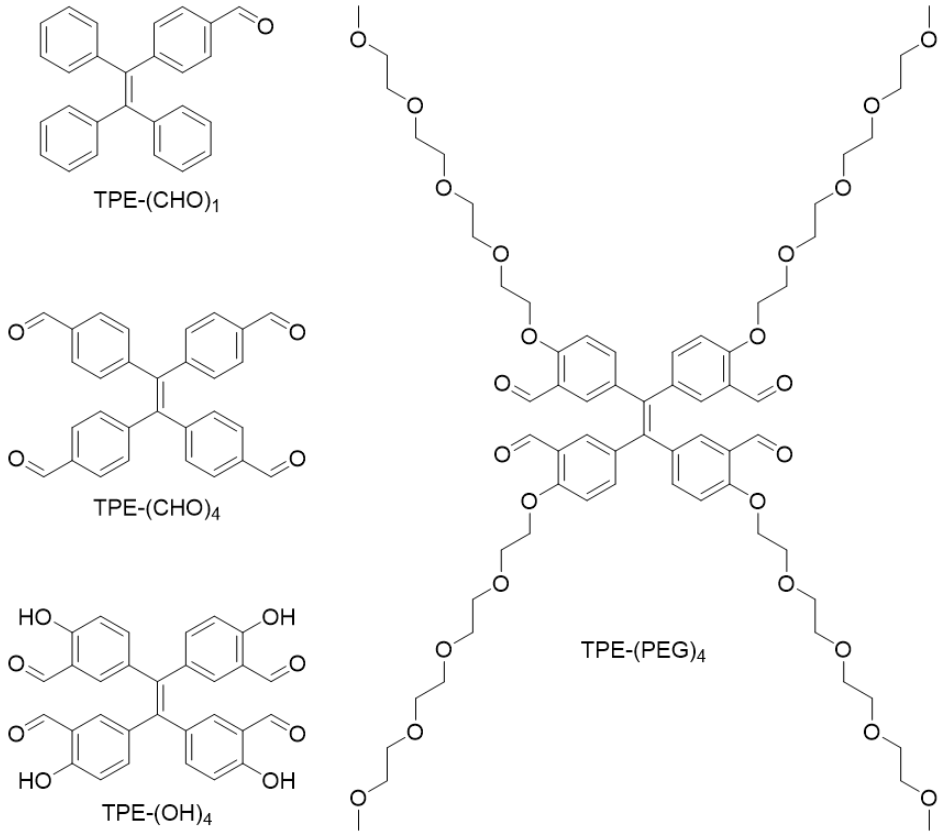

Figure 111. Chemical structures and names of the TPE derivatives.

[492] A. N. Ramya, M. M. Joseph, J. B. Nair, V. Karunakaran, N. Narayanan and K. K. Maiti, *ACS Appl. Mater. Interfaces*, **2016**, *8*, 10220–10225.

3.1.2. Characterization

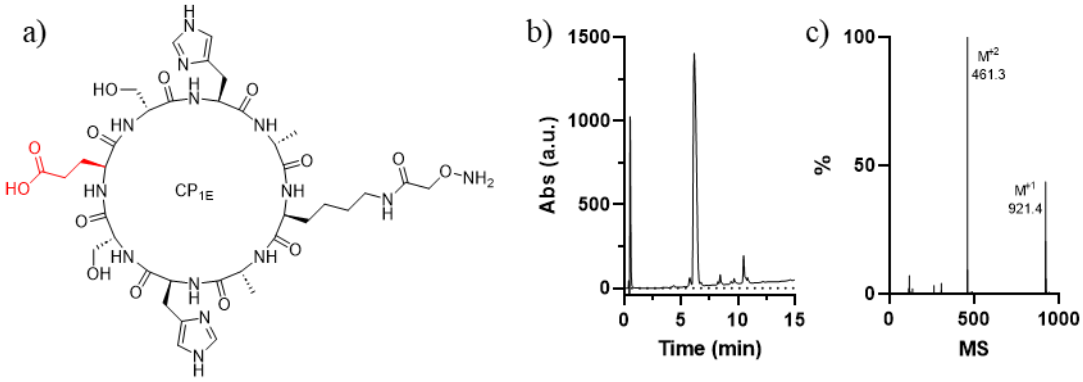

Figure 112. Chemical structure of **CP_{1E}** (modification respect the original structure in red); b) HPLC chromatogram of **CP_{1E}**. Gradient of 0% to 20% ACN (0.1% TFA) in 15 min; and c) MS spectra of the main peak.

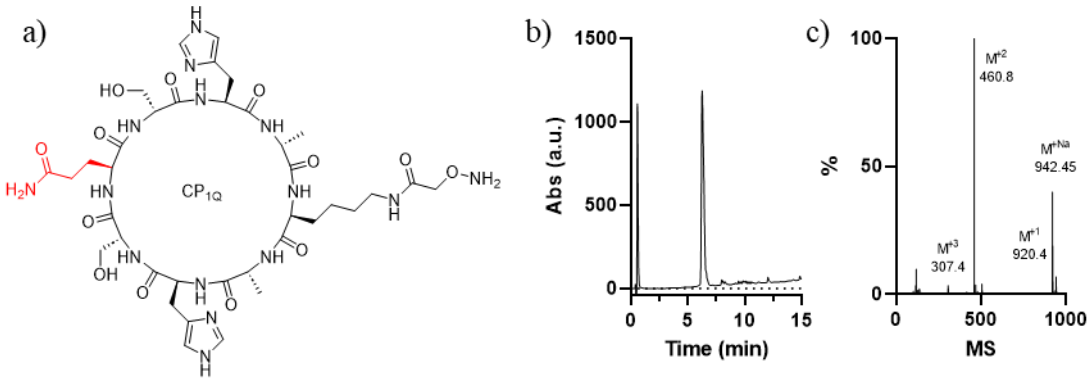

Figure 113. Chemical structure of **CP_{1Q}** (modification respect the original structure in red); b) HPLC chromatogram of **CP_{1Q}**. Gradient of 0% to 20% ACN (0.1% TFA) in 15 min; and c) MS spectra of the main peak.

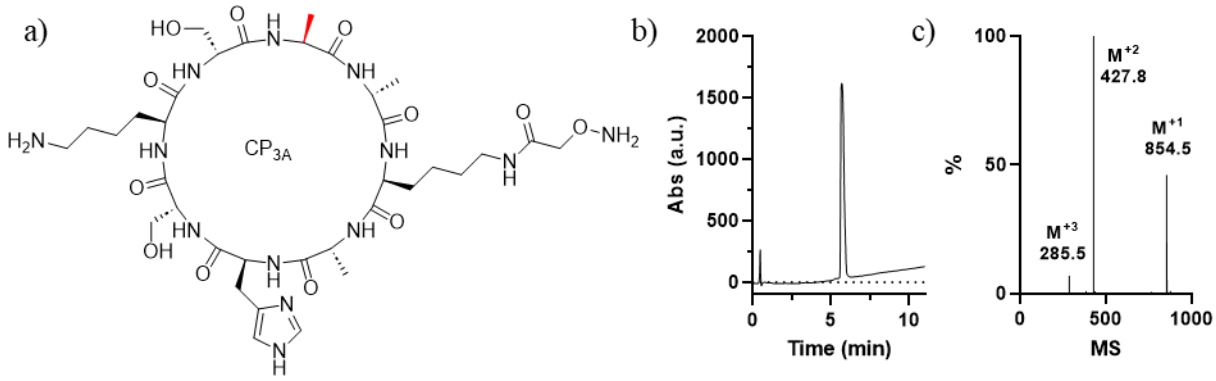

Figure 114. a) Chemical structure of **CP_{3A}** (modification respect the original structure in red); b) HPLC chromatogram of **CP_{3A}**. Gradient of 0% to 20% ACN (0.1% TFA) in 10 min; and c) MS spectra of the main peak.

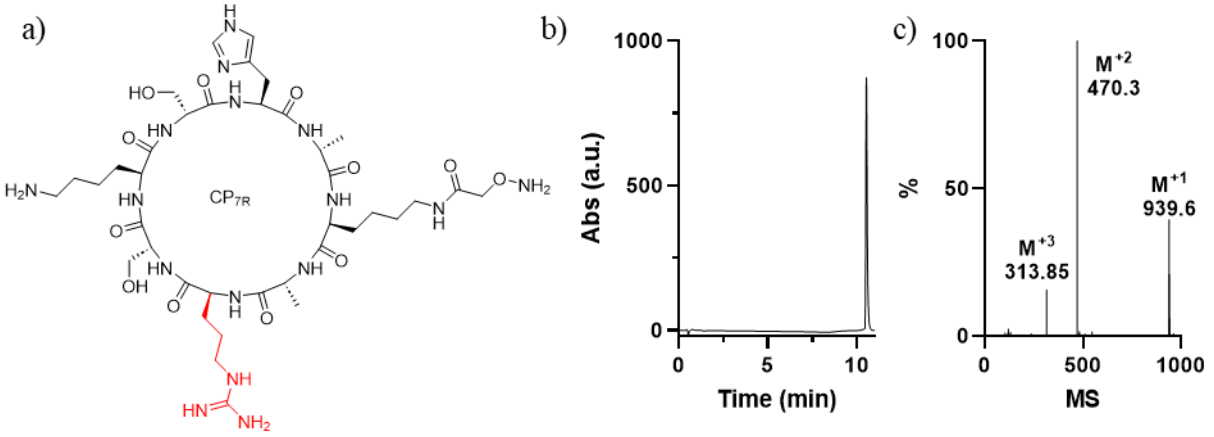

Figure 115. a) Chemical structure of **CP_{7R}** (modification respect the original structure in red). b) HPLC chromatogram of **CP_{7R}**. Gradient of 0% to 20% ACN (0.1% TFA) in 10 min; c) MS spectra of the main peak.

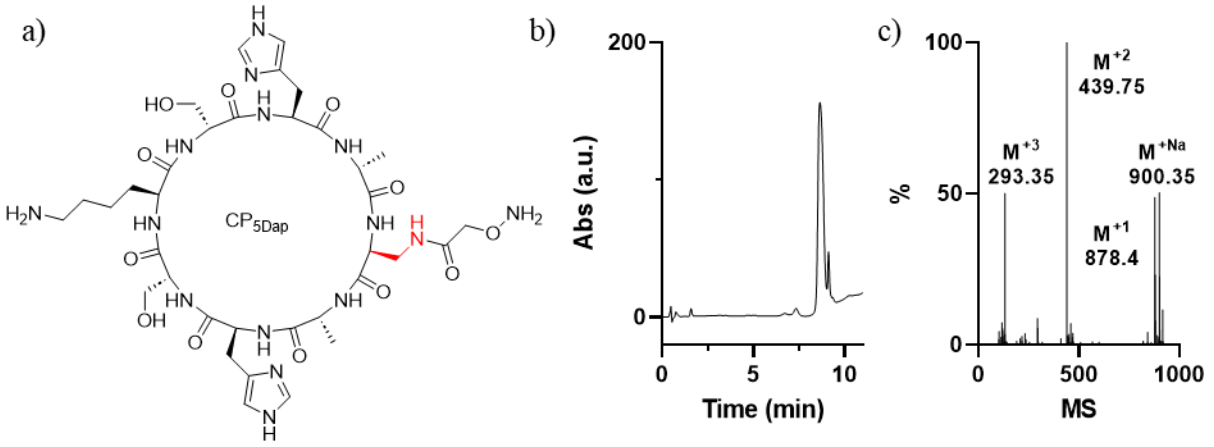

Figure 116. a) Chemical structure of **CP_{5Dap}** (modification respect the original structure in red). b) HPLC chromatogram of **CP_{5Dap}**. Gradient of 0% to 20% ACN (0.1% TFA) in 10 min; c) MS spectra of the main peak.

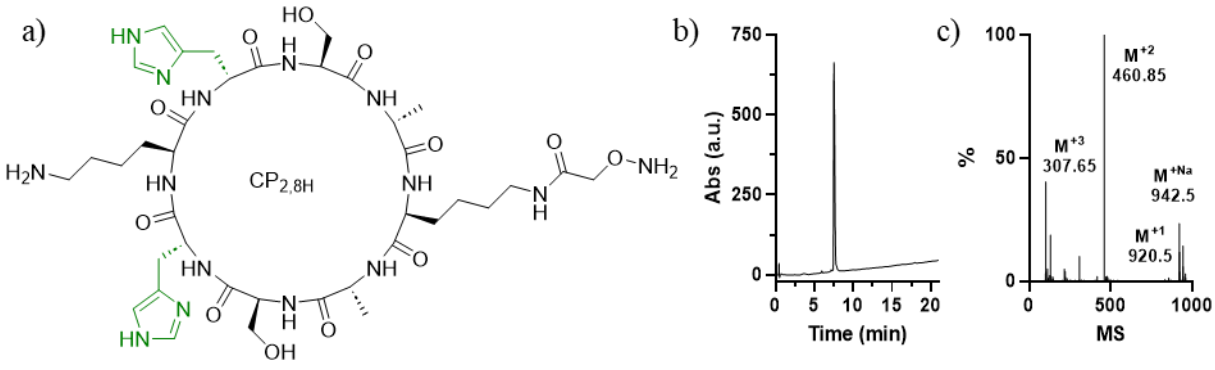

Figure 117. a) Chemical structure of **$CP_{2,8H}$** (green color represents the H movement respect the original structure). b) HPLC chromatogram of **$CP_{2,8H}$**. Gradient of 0% to 20% ACN (0.1% TFA) in 20 min; c) MS spectra of the main peak.

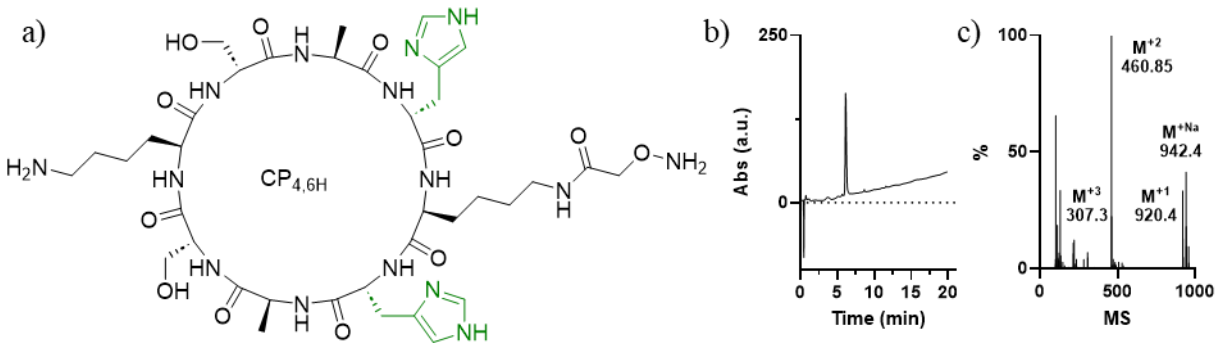

Figure 118. a) Chemical structure of **$CP_{4,6H}$** (green color represents the H movement respect the original structure). b) HPLC chromatogram of **$CP_{4,6H}$**. Gradient of 0% to 20% ACN (0.1% TFA) in 20 min; c) MS spectra of the main peak.

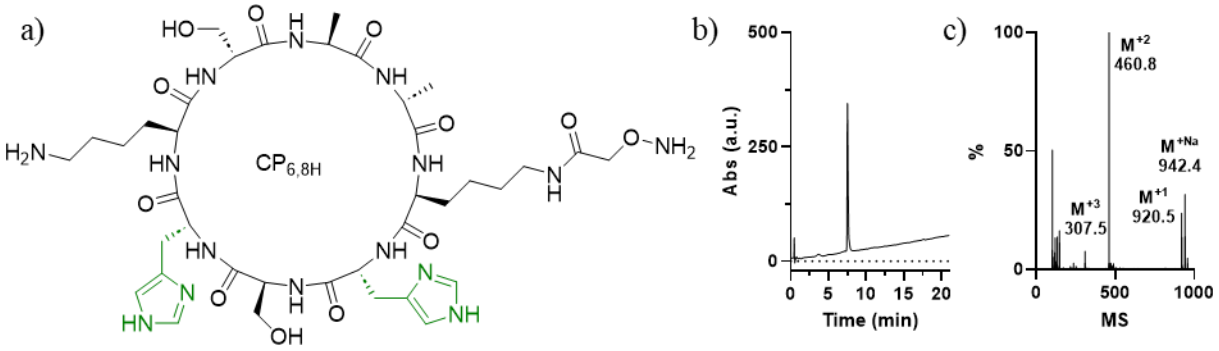

Figure 119. a) Chemical structure of **$CP_{6,8H}$** (green color represents the H movement respect the original structure). b) HPLC chromatogram of **$CP_{6,8H}$**. Gradient of 0% to 20% ACN (0.1% TFA) in 20 min; c) MS spectra of the main peak.

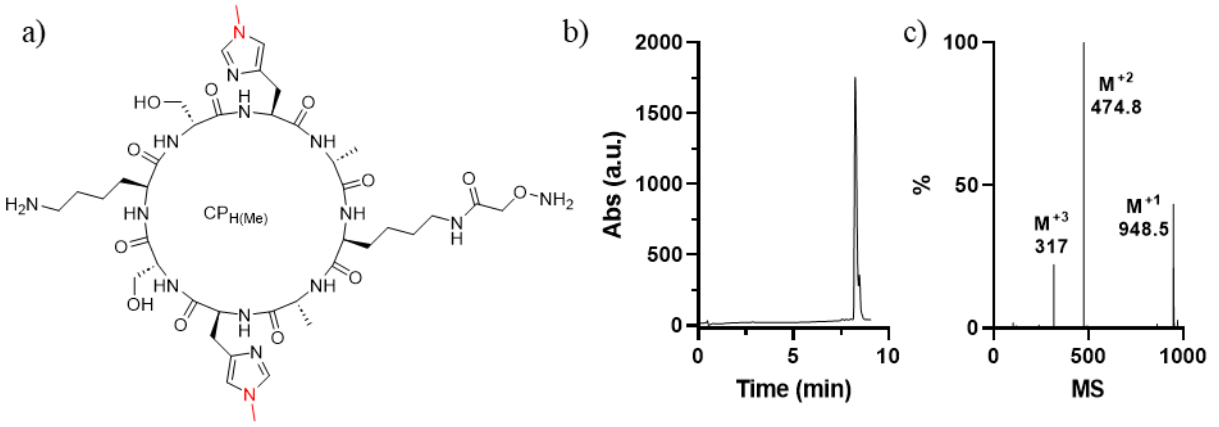

Figure 120. a) Chemical structure of **$CP_{H(Me)}$** (modification respect the original structure in red). b) HPLC chromatogram of **$CP_{H(Me)}$**. Gradient of 0% to 20% ACN (0.1% TFA) in 10 min; c) MS spectra of the main peak.

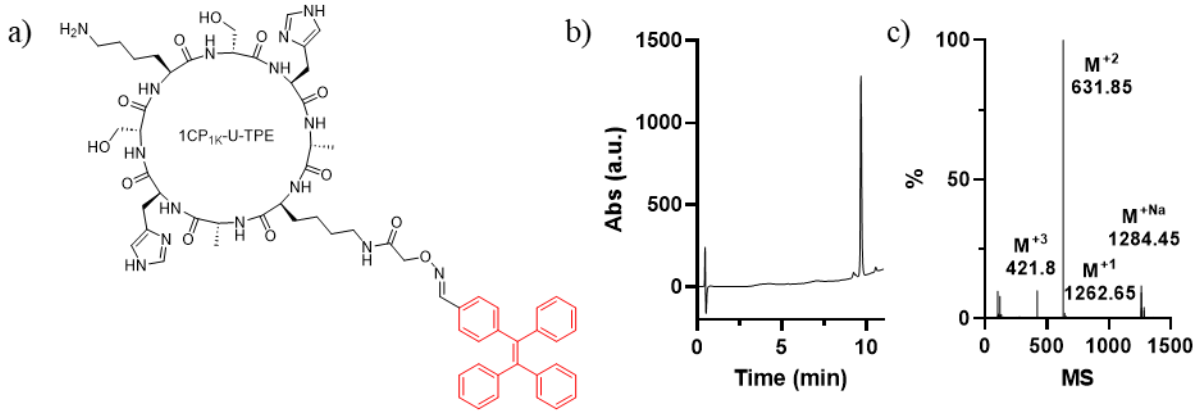

Figure 121. a) Chemical structure of **1CP$_{1K}$-U-TPE** (modification respect the original structure in red). b) HPLC chromatogram of **1CP$_{1K}$-U-TPE**. Gradient of 0% to 75% ACN (0.1% TFA) in 10 min; c) MS spectra of the main peak.

4CP$_{1k}$-U-TPE: ^{1}H NMR (500 MHz, D_2O/H_2O) δ 8.54 (d, J = 7.6 Hz, 1H, a), 8.51 (2s, 2H, b), 8.47 (d, J = 7.6 Hz, 1H, a), 8.34 (d, J = 7.7 Hz, 1H, c), 8.28 (d, J = 6.7 Hz, 1H, d), 8.16 (d, J = 6.5 Hz, 1H, e), 8.13 (s, 1H, f), 8.06 (2d, 2H, d and e), 7.99 (d, J = 7.3 Hz, 1H, c), 7.90 (t, J = 6.1 Hz, 1H, g), 7.45 (s, 2H, h), 7.25 (d, J = 8.0 Hz, 2H, i), 7.19 (s, 1H, j), 7.16 (s, 1H, j), 6.98 (d, J = 7.7 Hz, 2H, k), 4.65 (s, 2H, l), 4.61 – 4.47 (m, 2H, m), 4.38 – 4.31 (m, 2H, n), 4.30 – 4.26 (m, 1H, o), 4.26 – 4.21 (m, 1H, p), 4.21 – 4.16 (m, 1H, p), 4.16 – 4.10 (m, 1H, o), 3.84 – 3.62 (m, 4H, q), 3.27 – 3.18 (m, 2H, r), 3.17 – 3.09 (m, 2H, s), 3.09 – 2.99 (m, 2H, r), 2.88 (s, 2H, t), 1.80 – 1.22 (m, 12H, u), 1.19 (2d, 6H, v). FTIR (neat): 3274, 1659, 1631, 1537, 1433, 1201, 1184, 1132, 1079, 835, 799, 722, 627, 517 cm^{-1}. HRMS calculated for $C_{182}H_{256}N_{60}O_{48}^{+}$: 4050.9469, found: 4050.9398 (extrapolated from the molecular ion M^{+4}: 1013.9904).

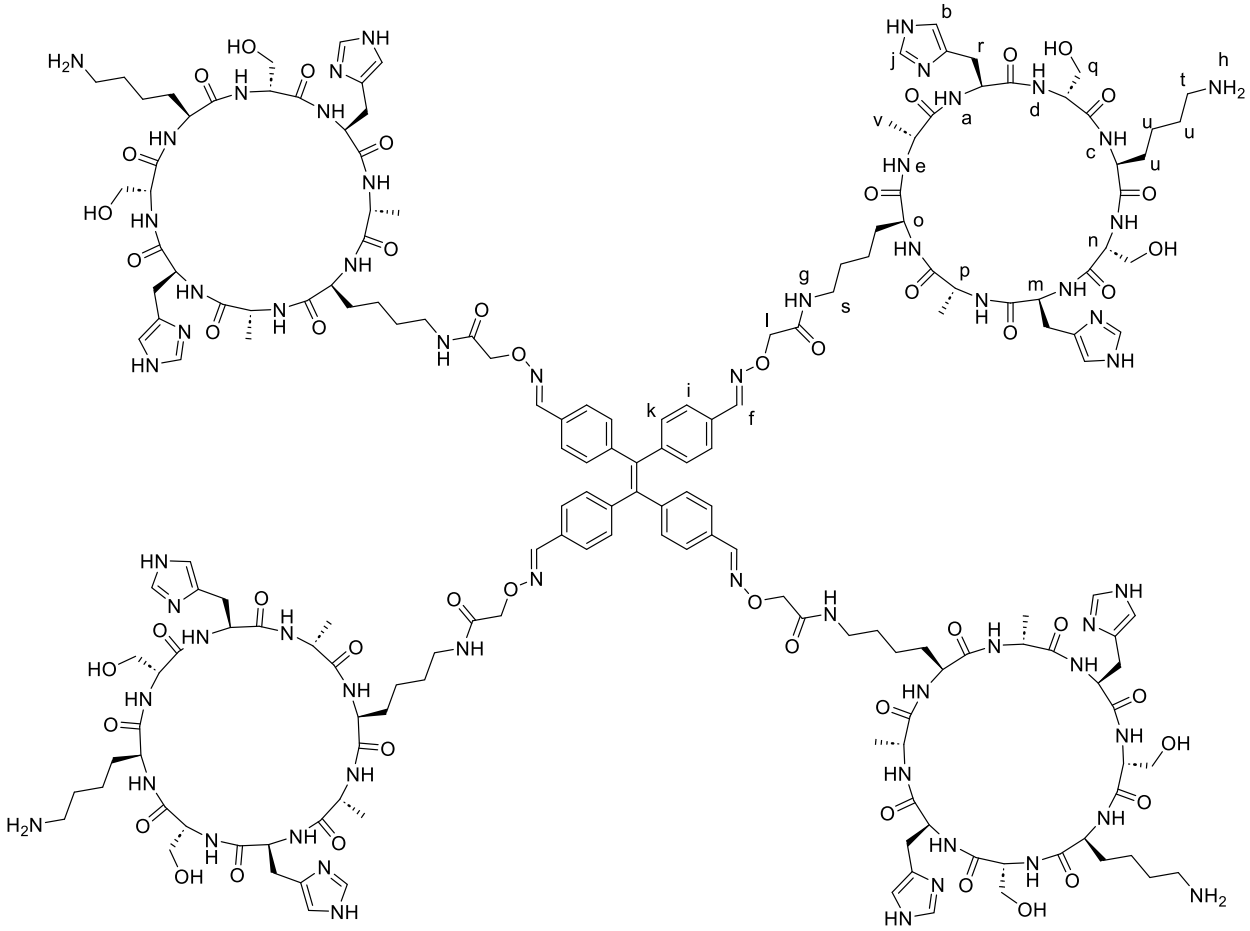

Figure 122. Chemical structure of **4CP$_{1K}$-U-TPE** (letters represent protons of the ^{1}H-NMR).

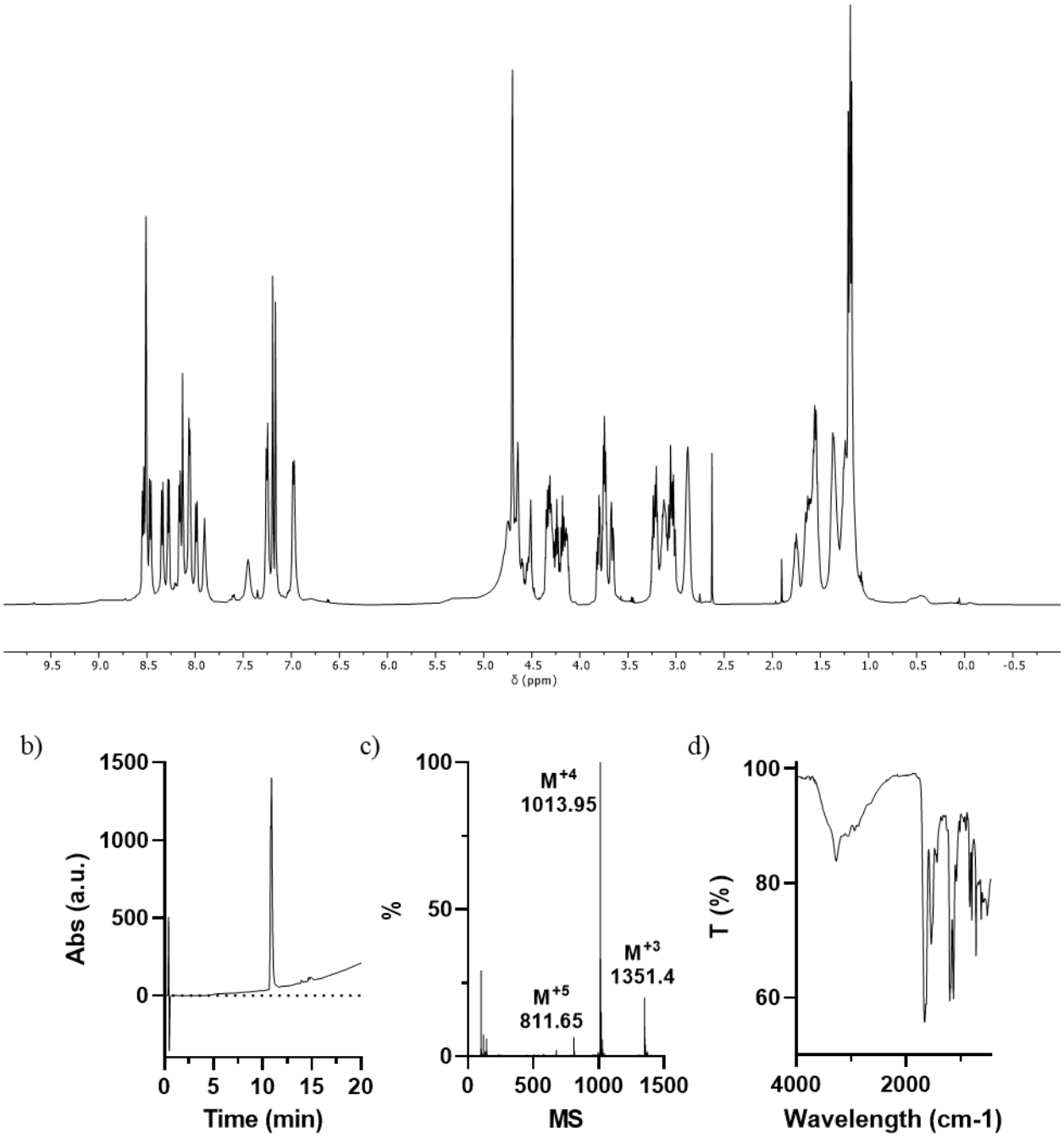

Figure 123. a) ^{1}H NMR spectra (500 MHz, D_2O/H_2O) of **4CP$_{1K}$-U-TPE**; b) HPLC chromatogram of 4**CP$_{1K}$-U-TPE**. Gradient of 0% to 75% ACN (0.1% TFA) in 20 min; c) MS spectra of the main peak; and d) FTIR of 4**CP$_{1K}$-U-TPE**.

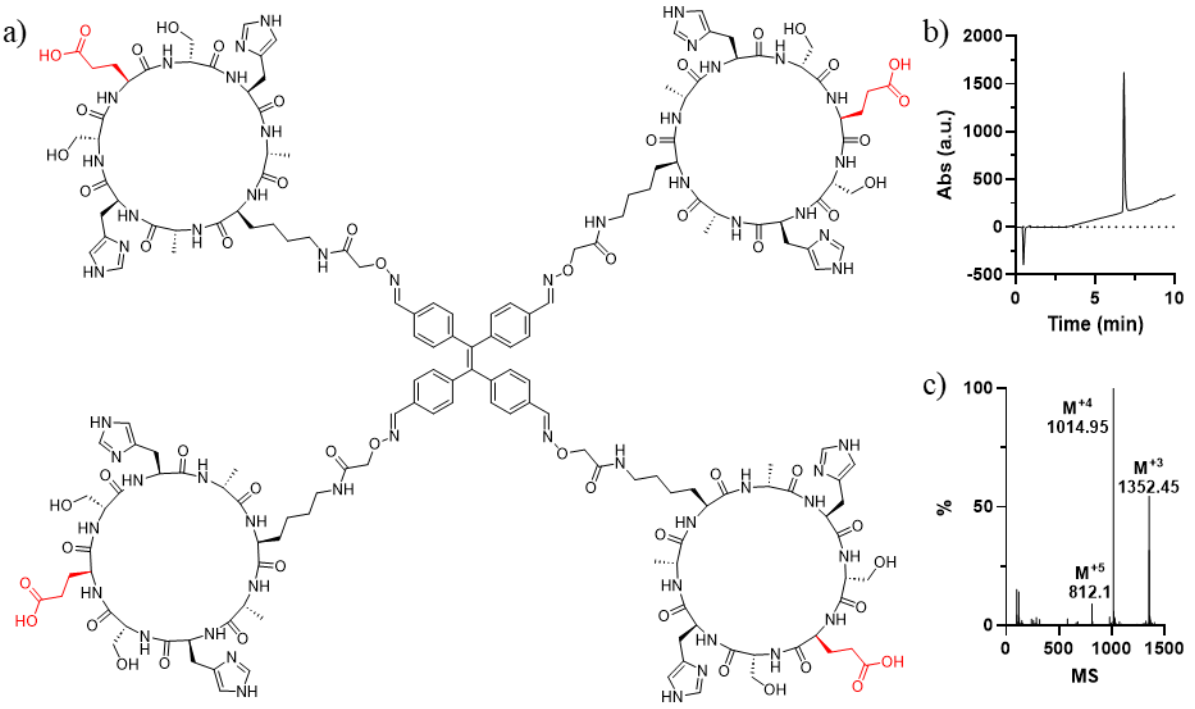

Figure 124. a) Chemical structure of 4**CP$_{1E}$-U-TPE** (modification respect the original structure in red); b) HPLC chromatogram of 4**CP$_{1E}$-U-TPE**. Gradient of 0% to 75% ACN (0.1% TFA) in 10 min; and c) MS spectra of the main peak.

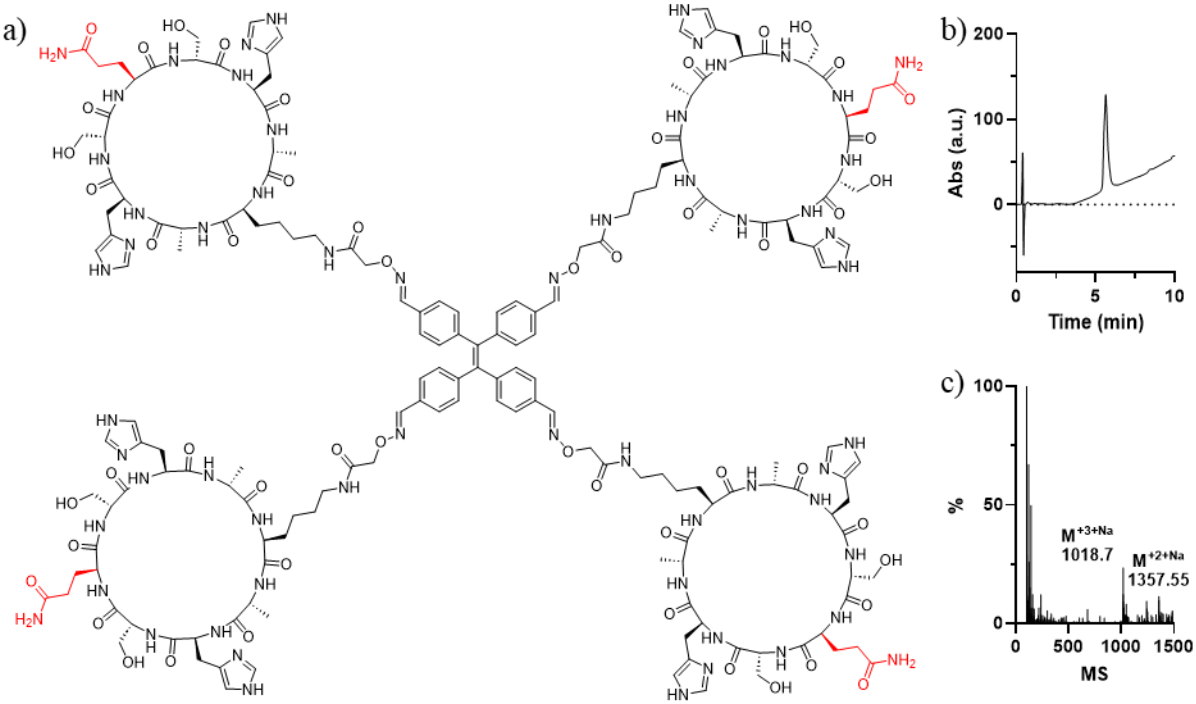

Figure 125. a) Chemical structure of 4**CP$_{1Q}$-U-TPE** (modification respect the original structure in red); b) HPLC chromatogram of 4**CP$_{1Q}$-U-TPE**. Gradient of 0% to 75% ACN (0.1% TFA) in 10 min; and c) MS spectra of the main peak.

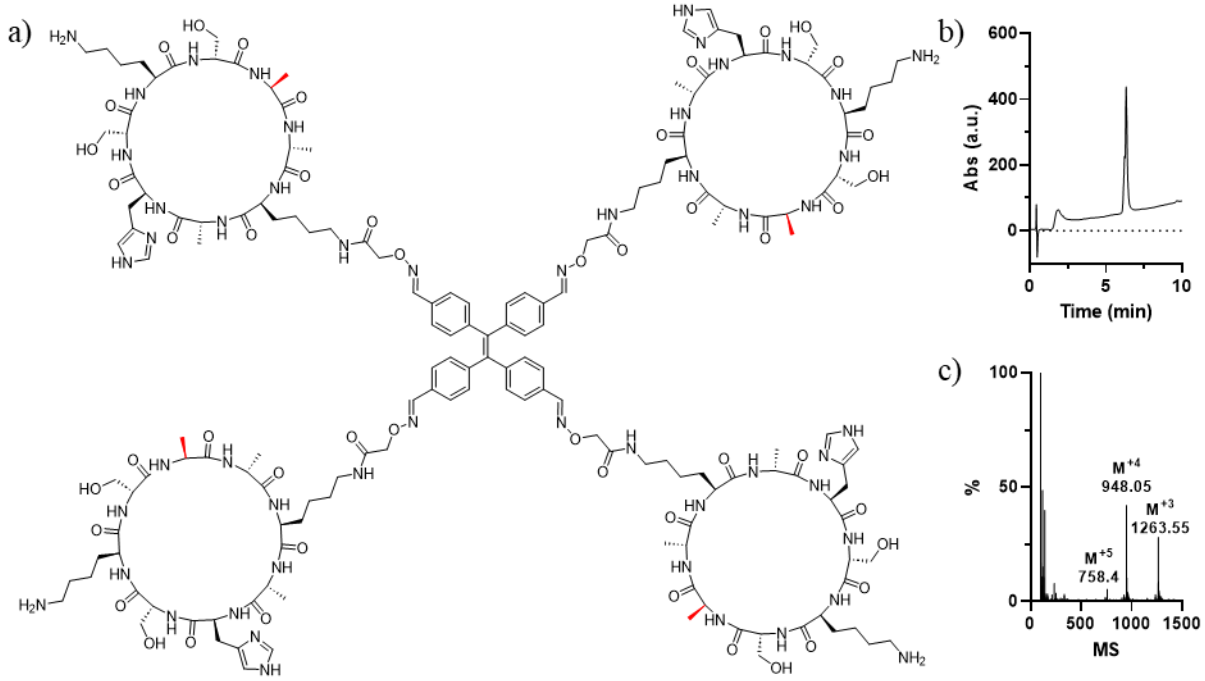

Figure 126. a) Chemical structure of 4**CP$_{3A}$-U-TPE** (modification respect the original structure in red); b) HPLC chromatogram of 4**CP$_{3A}$-U-TPE**. Gradient of 0% to 75% ACN (0.1% TFA) in 10 min; and c) MS spectra of the main peak.

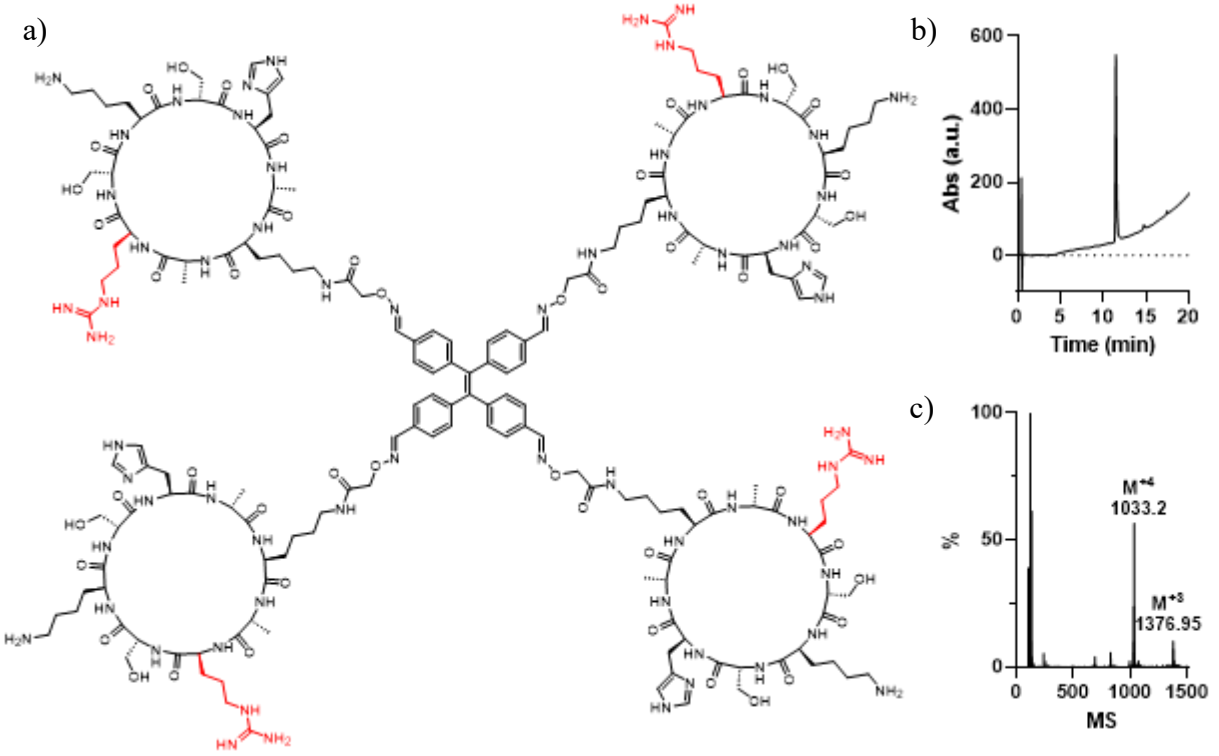

Figure 127. a) Chemical structure of 4**CP$_{7R}$-U-TPE** (modification respect the original structure in red); b) HPLC chromatogram of 4**CP$_{7R}$-U-TPE**. Gradient of 0% to 75% ACN (0.1% TFA) in 20 min; and c) MS spectra of the main peak.

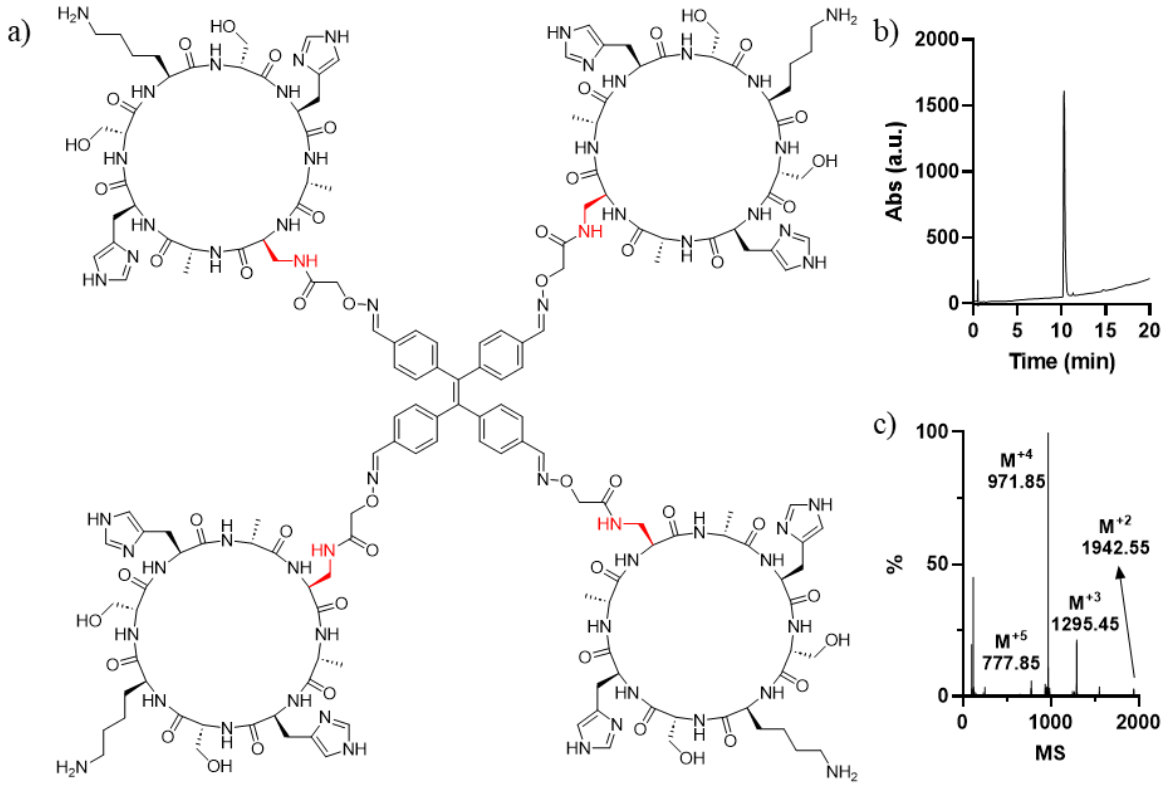

Figure 128. a) Chemical structure of 4**CP$_{5Dap}$-U-TPE** (modification respect the original structure in red); b) HPLC chromatogram of 4**CP$_{5Dap}$-U-TPE**. Gradient of 0% to 75% ACN (0.1% TFA) in 20 min; and c) MS spectra of the main peak.

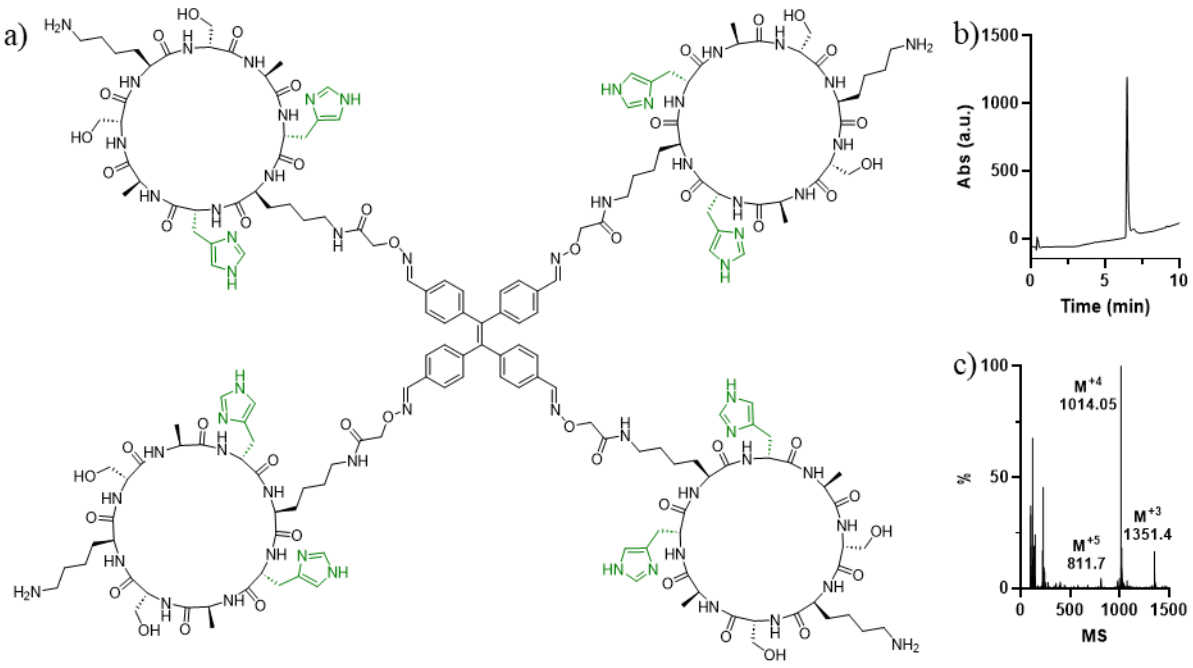

Figure 129. a) Chemical structure of 4**CP$_{4,6H}$-U-TPE** (modification respect the original structure in red); b) HPLC chromatogram of 4**CP$_{4,6H}$-U-TPE**. Gradient of 0% to 75% ACN (0.1% TFA) in 10 min; and c) MS spectra of the main peak.

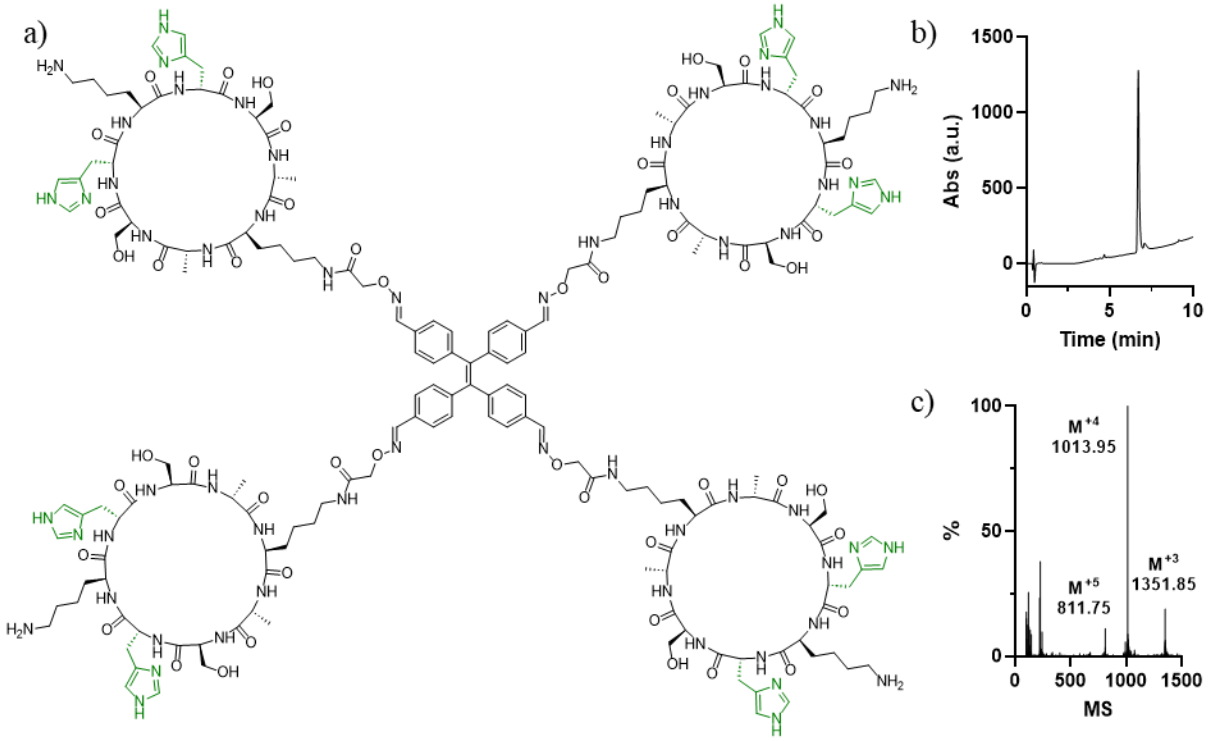

Figure 130. a) Chemical structure of 4**CP$_{2,8H}$-U-TPE** (modification respect the original structure in red); b) HPLC chromatogram of 4**CP$_{2,8H}$-U-TPE**. Gradient of 0% to 75% ACN (0.1% TFA) in 10 min; and c) MS spectra of the main peak.

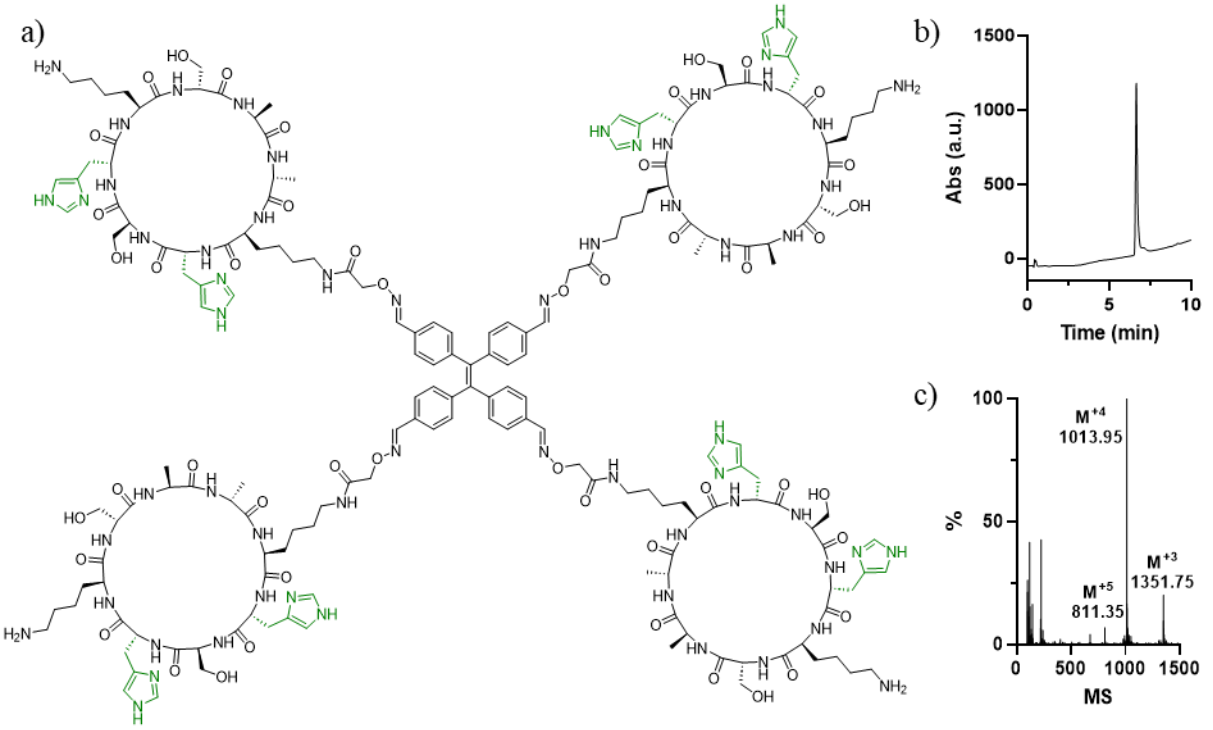

Figure 131. a) Chemical structure of 4**CP$_{6,8H}$-U-TPE** (modification respect the original structure in red); b) HPLC chromatogram of 4**CP$_{6,8H}$-U-TPE**. Gradient of 0% to 75% ACN (0.1% TFA) in 10 min; and c) MS spectra of the main peak.

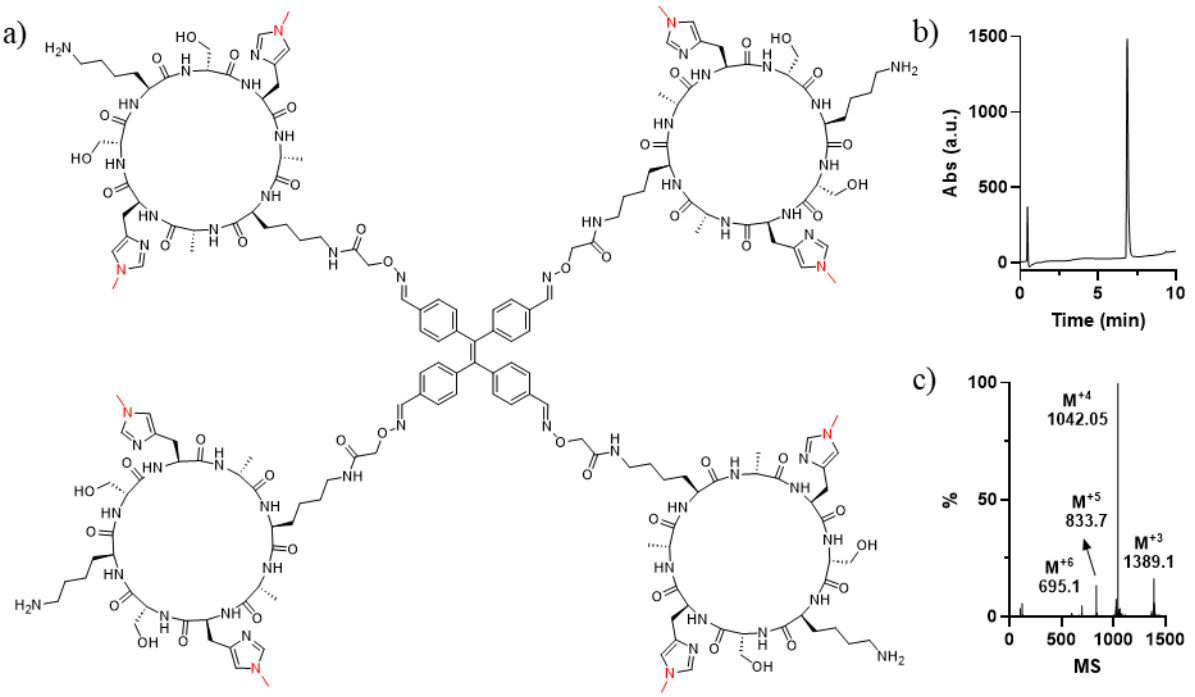

Figure 132. a) Chemical structure of 4**CP$_{H(Me)}$-U-TPE** (modification respect the original structure in red); b) HPLC chromatogram of 4**CP$_{H(Me)}$-U-TPE**. Gradient of 0% to 75% ACN (0.1% TFA) in 10 min; and c) MS spectra of the main peak.

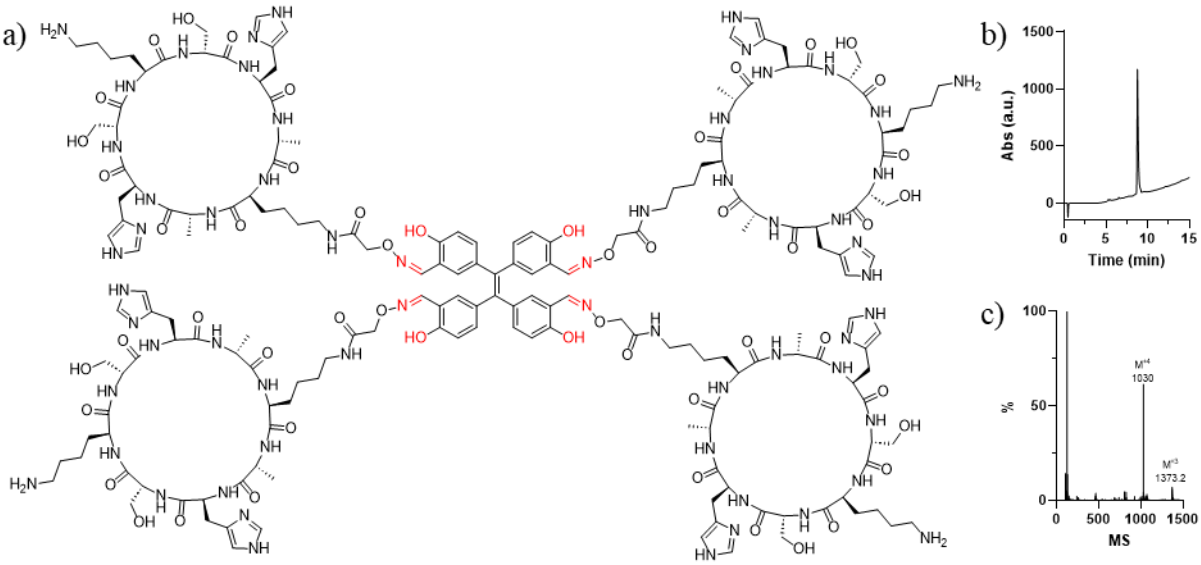

Figure 133. a) Chemical structure of 4**CP$_{1K}$-U-TPE$_{OH}$** (modification respect the original structure in red); b) HPLC chromatogram of 4**CP$_{1K}$-U-TPE$_{OH}$**. Gradient of 0% to 75% ACN (0.1% TFA) in 15 min; and c) MS spectra of the main peak.

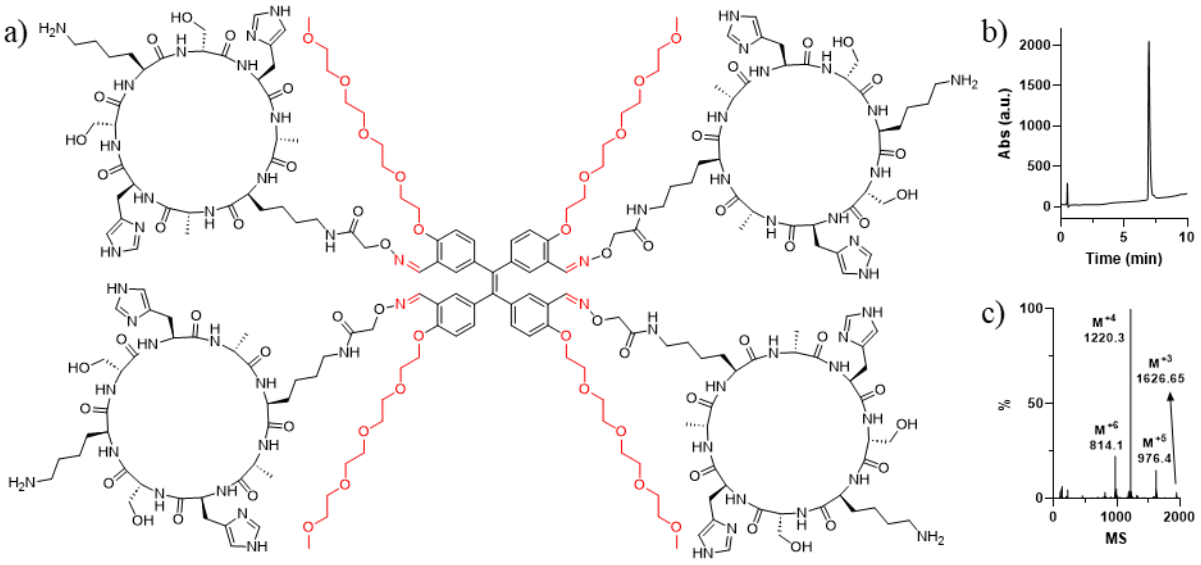

Figure 134. a) Chemical structure of 4**CP$_{1K}$-U-TPE$_{PEG}$** (modification respect the original structure in red); b) HPLC chromatogram of 4**CP$_{1K}$-U-TPE$_{PEG}$**. Gradient of 0% to 75% ACN (0.1% TFA) in 10 min; and c) MS spectra of the main peak.

3.2. Figures

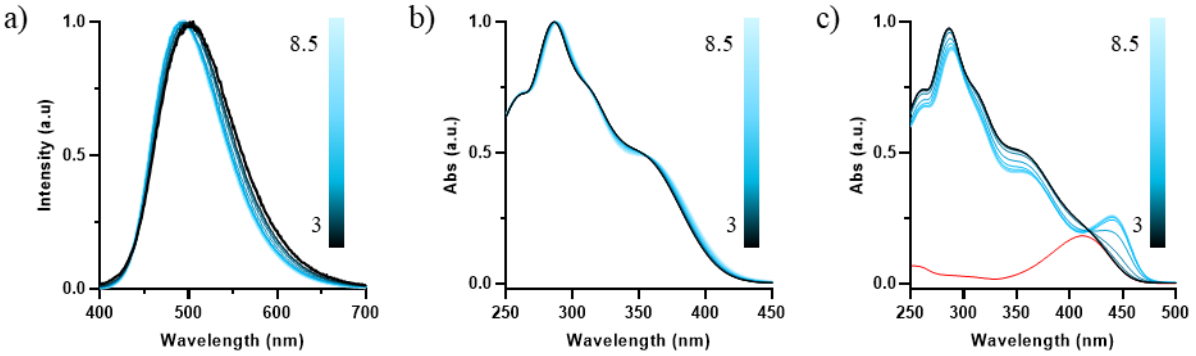

Figure 135. Spectroscopic characterization at different pHs of an aqueous solution of 4**CP$_{1K}$-U-TPE** (50 μM). a) Normalized fluorescence, b) Normalized UV-Vis spectra and c) UV-Vis spectra containing ThT 20 μM (ThT alone is shown in red).

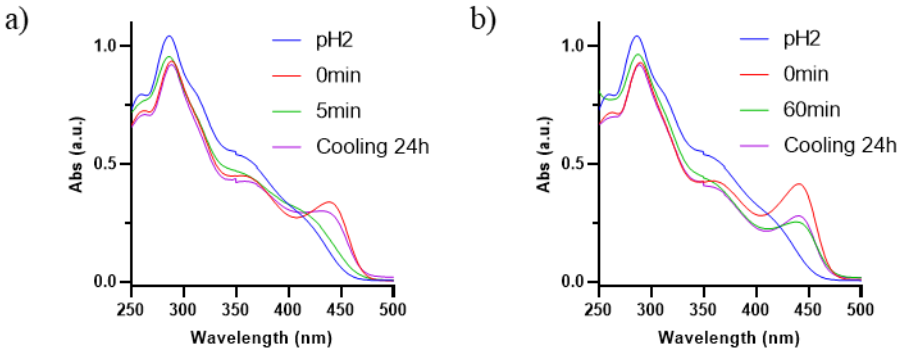

Figure 136. UV-Vis of 4**CP$_{1K}$-U-TPE** (50 μM) containing ThT 10 μM heated to 90ºC at a) pH6 and b) pH8.

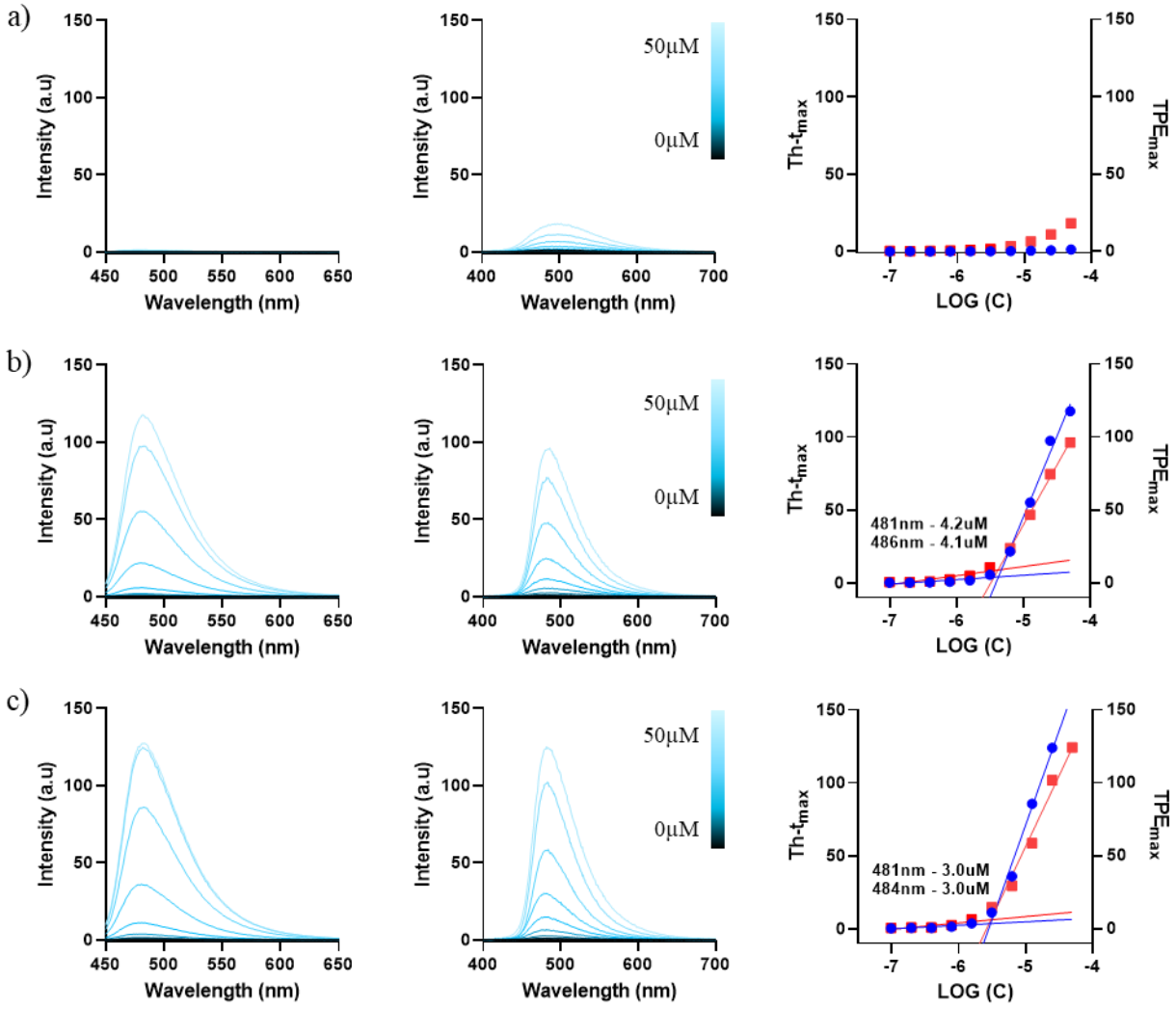

Figure 137. From left to right ThT fluorescence, TPE fluorescence and Imax against Log (C) of 4**CP$_{1K}$-U-TPE** at different concentrations and a constant pH. a) pH2; b) pH5 and c) pH8. The Imax of the ThT is shown in blue and the Imax of the TPE is shown in red.

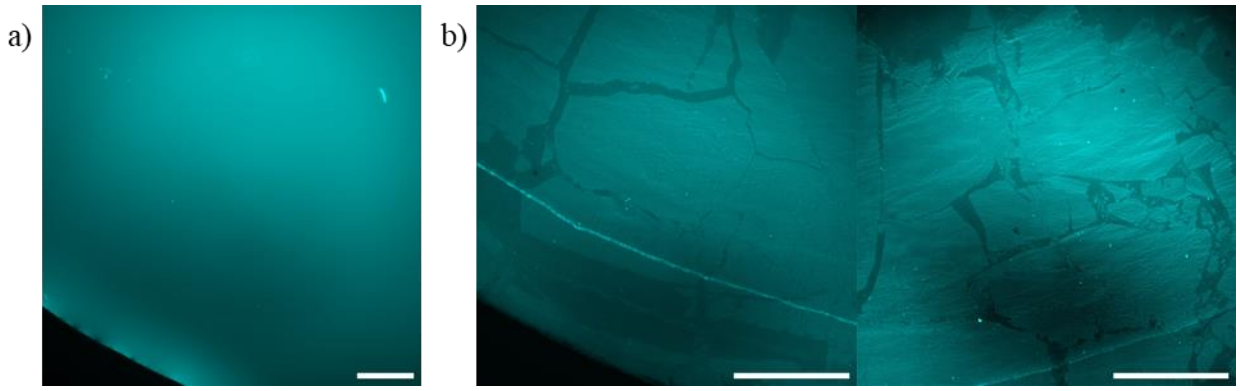

Figure 138. Epifluorescence micrographs of 4**CP$_{1K}$-U-TPE** 20 μM at pH8 (20mM HEPES) a) in solution showing a continuous film and b) deposited showing sheet like structures. Scale bars 200 μm.

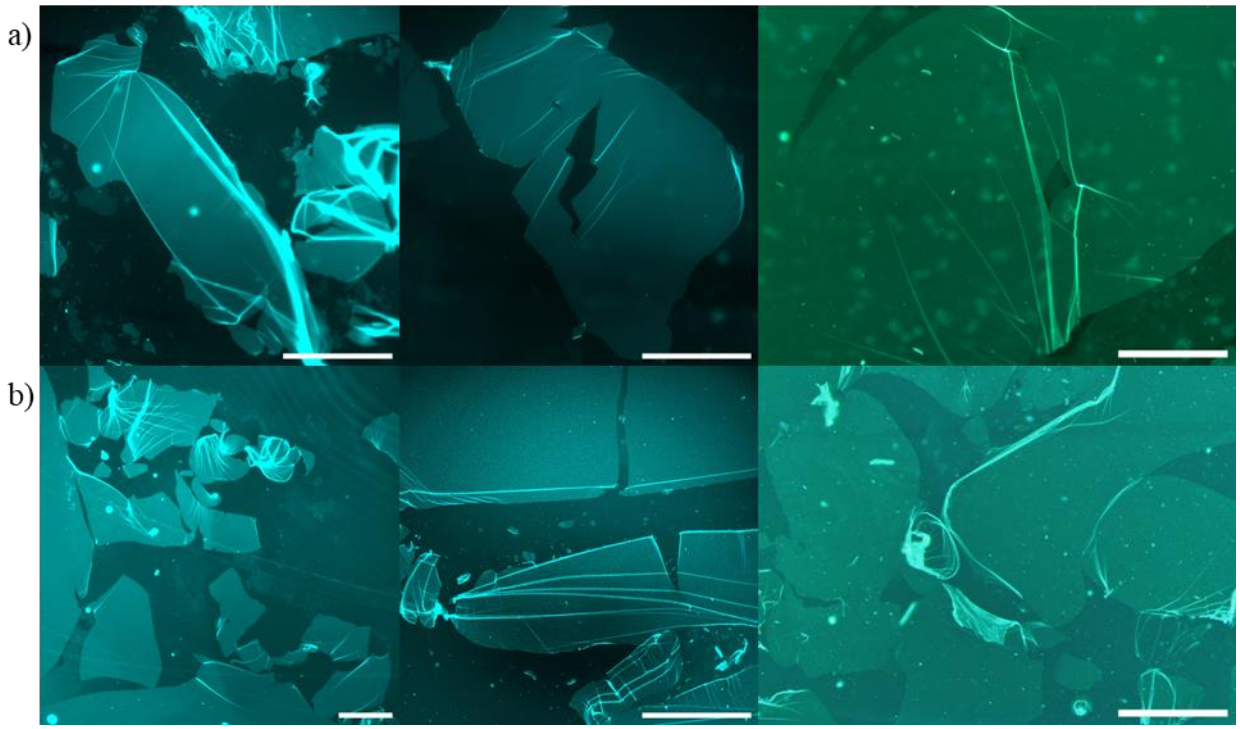

Figure 139. Epifluorescence micrographs of 4**CP$_{1K}$-U-TPE** 20 μM at pH8 (20mM HEPES) showing sheet like structures when a) scratching or b) vigorously agitating the peptide solution on top of the slide. Scale bars 200 μm. Images to the far right are taken in microscope (2).

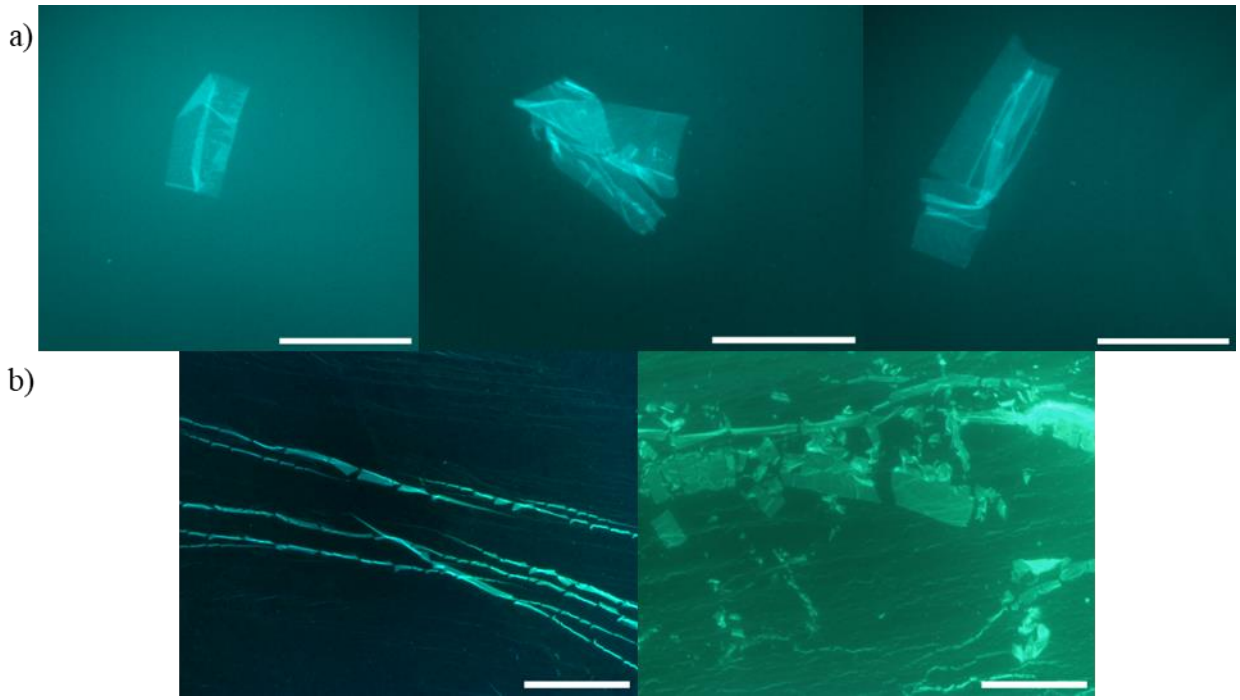

Figure 140. Epifluorescence micrographs of 4**CP$_{1K}$-U-TPE** 20 μM at pH8 (20mM HEPES) showing sheet like structures (scale bar 50μm) a) Microscope (1) and b) Microscope (2).

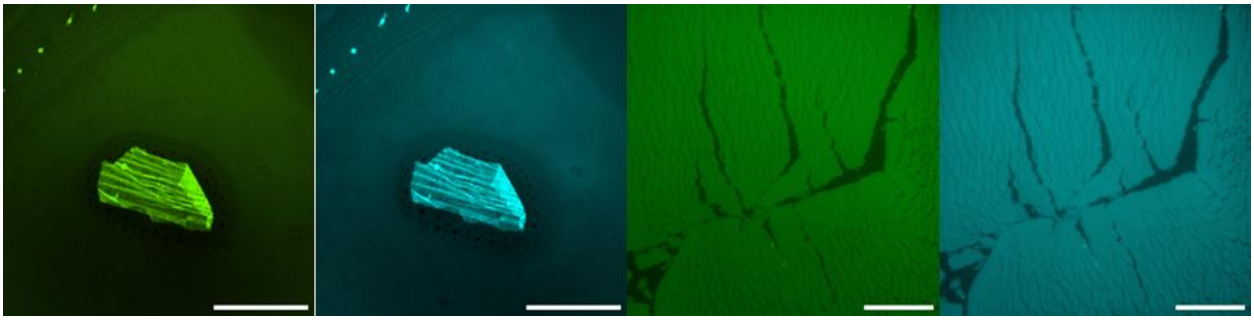

Figure 141. Epifluorescence micrographs of **4CP$_{1K}$-U-TPE** 20 μM at pH8 (20mM HEPES, ThT 10 μM) showing sheet like structures in ThT channel (green) and TPE channel (blue) (scale bar 200 and 50μm respectively).

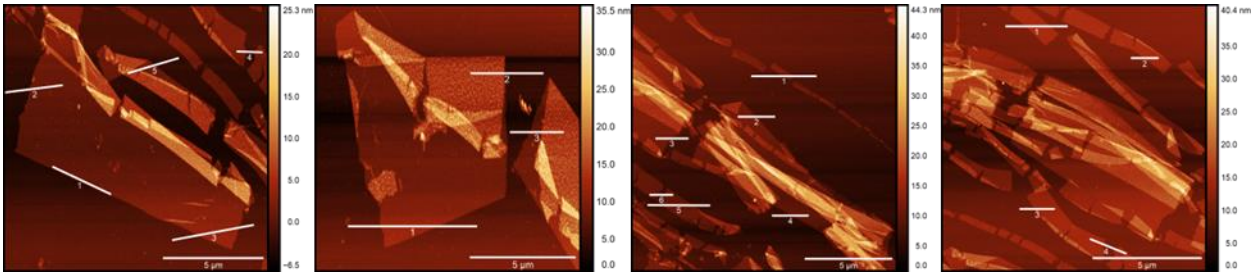

Figure 142. AFM micrographs of **4CP$_{1K}$-U-TPE** 20 μM in a solution at pH 8 (20mM HEPES) demonstrating the presence of sheet-like structures.

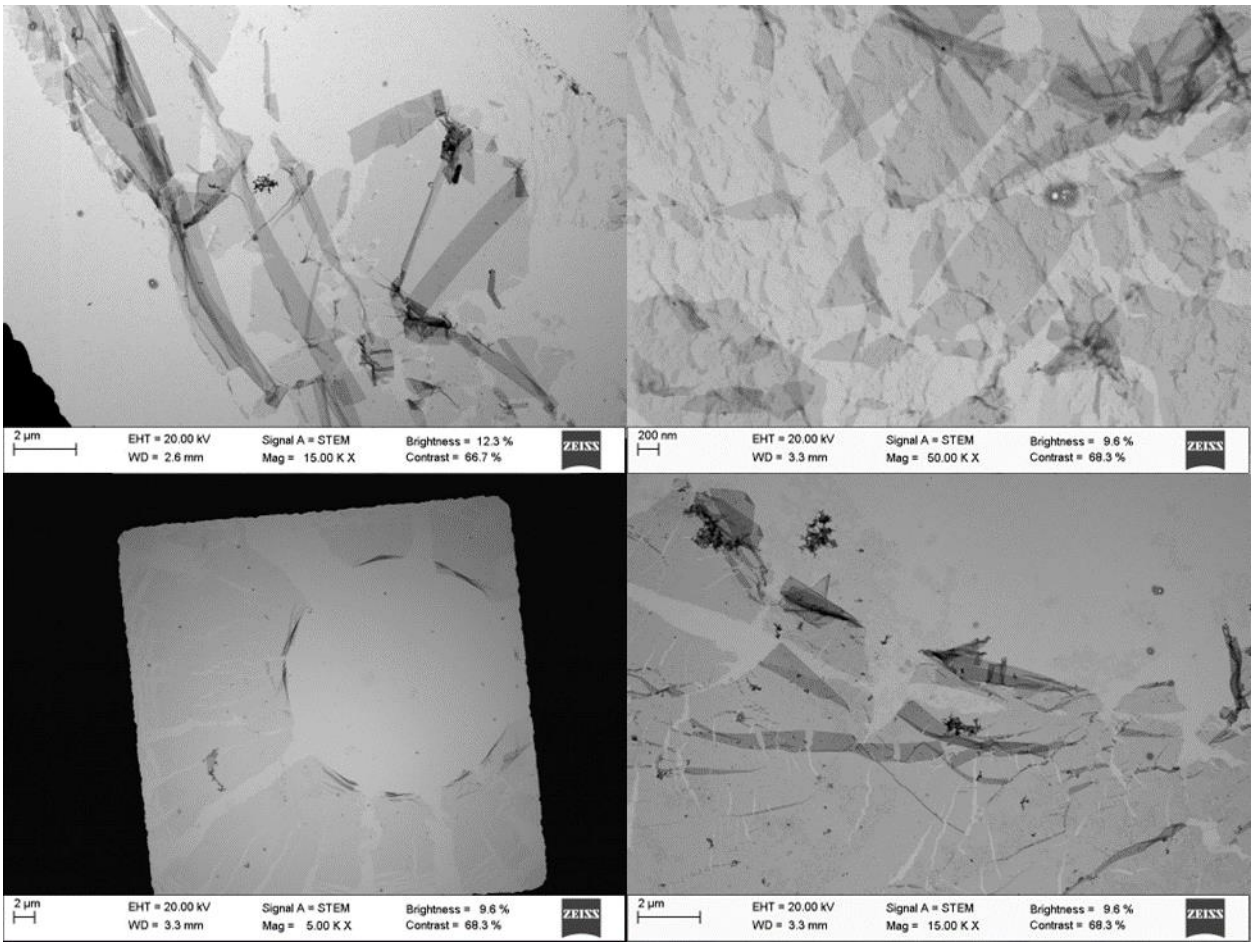

Figure 143. STEM micrographs of **4CP$_{1K}$-U-TPE** 20 µM in a solution at pH 8 (20mM HEPES) demonstrating the presence of sheet-like structures.

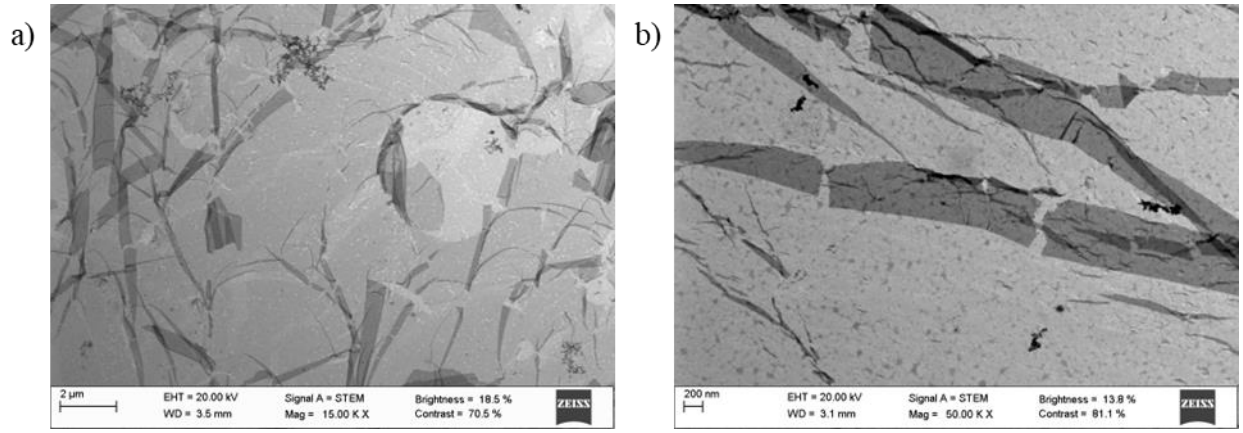

Figure 144. STEM micrographs of **4CP$_{1K}$-U-TPE** 20 µM in a solution at pH 8 (20mM HEPES) demonstrating the presence of sheet-like structures a) at 90ºC and b) at room temperature after cooling.

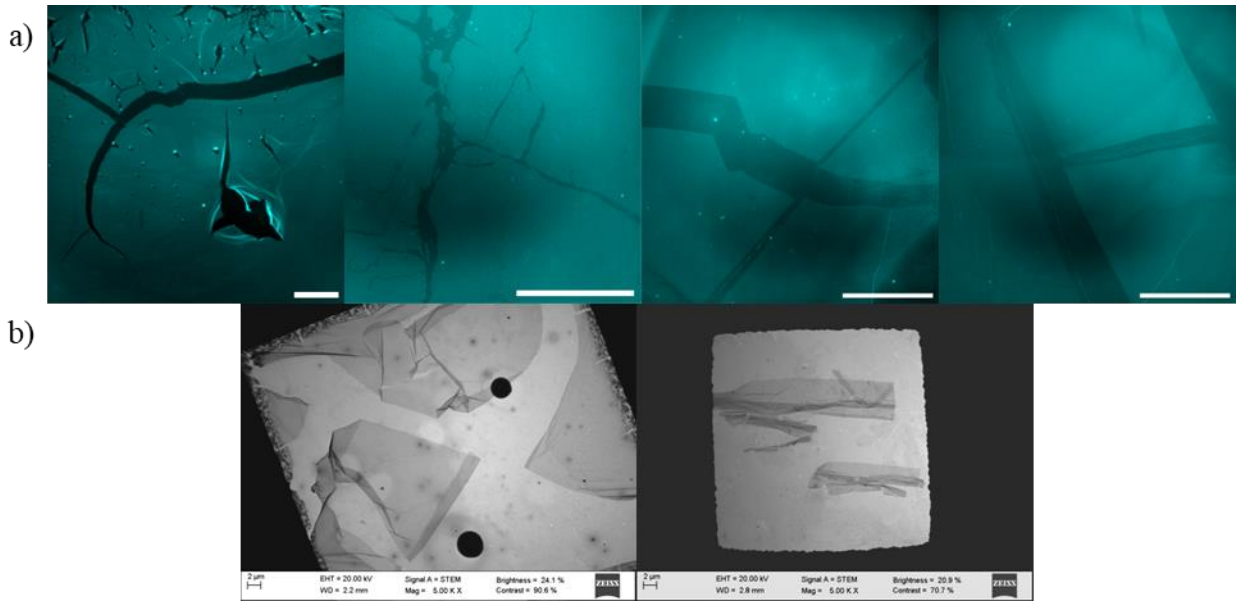

Figure 145. Imaging micrographs of **4CP$_{1K}$-U-TPE** 20 μM in a solution at pH 6 (20mM MES) demonstrating the presence of sheet-like structures by a) epifluorescence microscopy (scale bars 200 μm) and b) STEM.

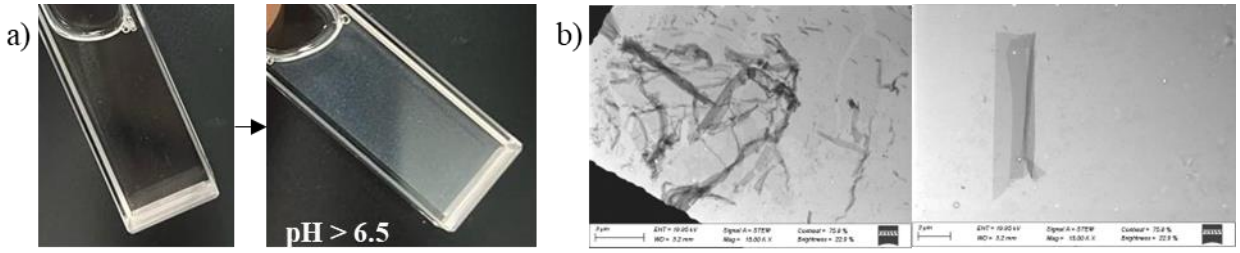

Figure 146. Aqueous solution of **4CP$_{1Q}$-U-TPE** at 50 μM. a) Precipitation of the system when reaching a pH higher than 6.5; and c) STEM images at pH 5.9.

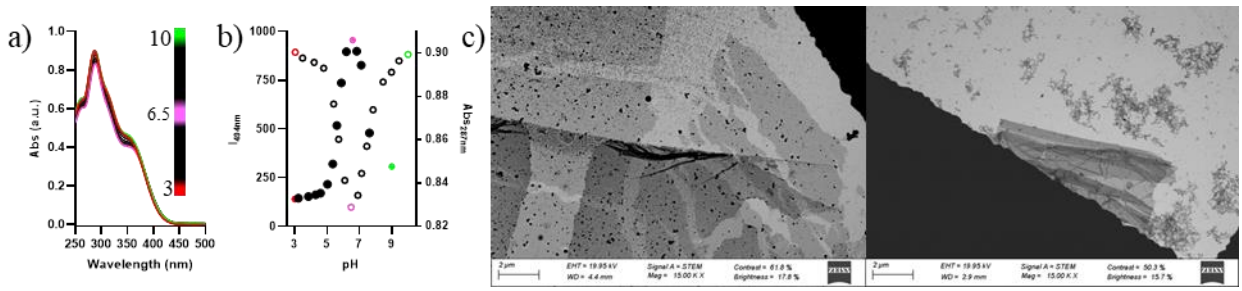

Figure 147. Aqueous solution of **4CP$_{1E}$-U-TPE** 50 μM. a) UV-VIS spectra; b) changes on maximum emission wavelength (dots) and absorbance (circles) with pH; and c) STEM at pH 6.3.

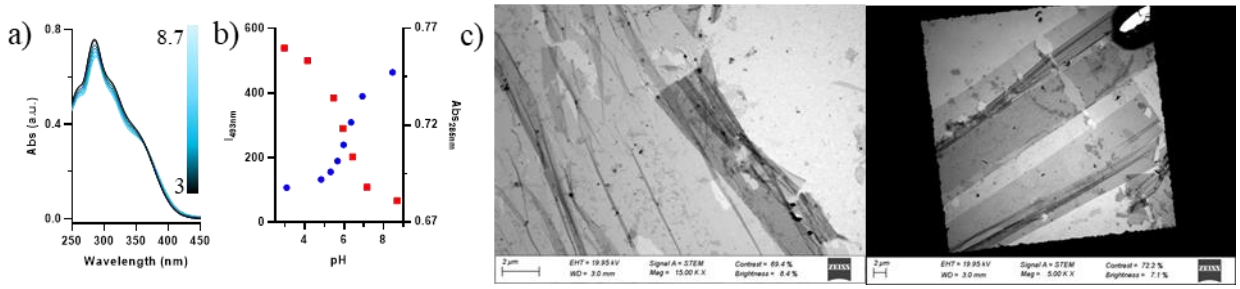

Figure 148. Aqueous solution of **4CP$_{5Dap}$-U-TPE** 50 μM. a) UV-VIS spectra; b) changes on maximum emission wavelength (blue dots) and absorbance (red squares) with pH; and c) STEM at pH 6.9.

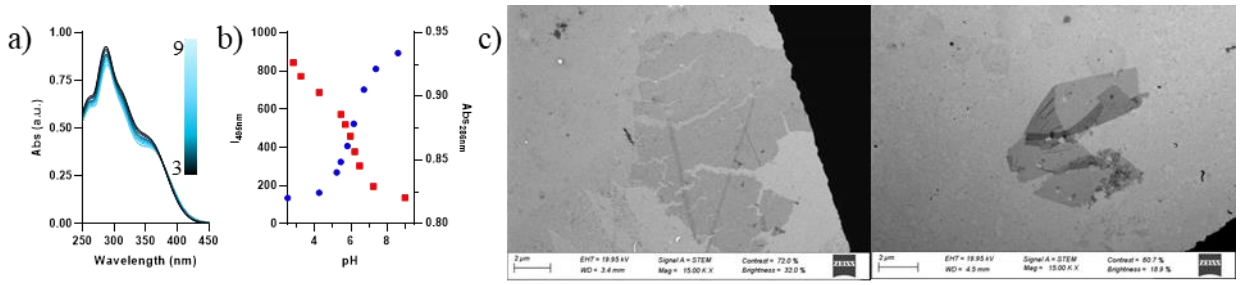

Figure 149. Aqueous solution of **4CP$_{2,8H}$-U-TPE** 50 μM. a) UV-VIS spectra; b) changes on maximum emission wavelength (blue dots) and absorbance (red squares) with pH; and c) STEM at pH 8.1.

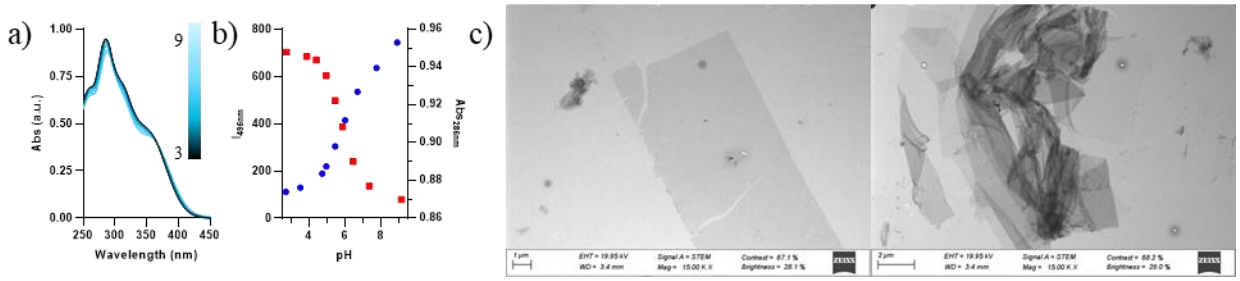

Figure 150. Aqueous solution of **4CP$_{6,8H}$-U-TPE** 50 μM. a) UV-VIS spectra; b) changes on maximum emission wavelength (blue dots) and absorbance (red squares) with pH; and c) STEM at pH 8.3.

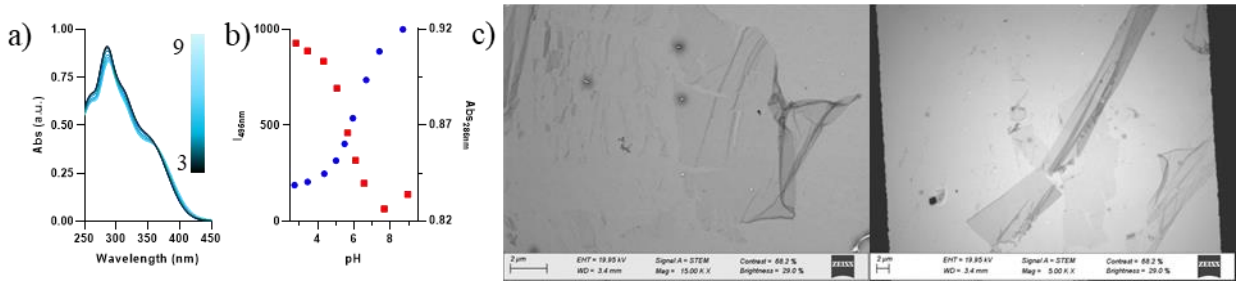

Figure 151. Aqueous solution of **4CP$_{4,6H}$-U-TPE** 50 μM. a) UV-VIS spectra; b) changes on maximum emission wavelength (blue dots) and absorbance (red squares) with pH; and c) STEM at pH 8.1.

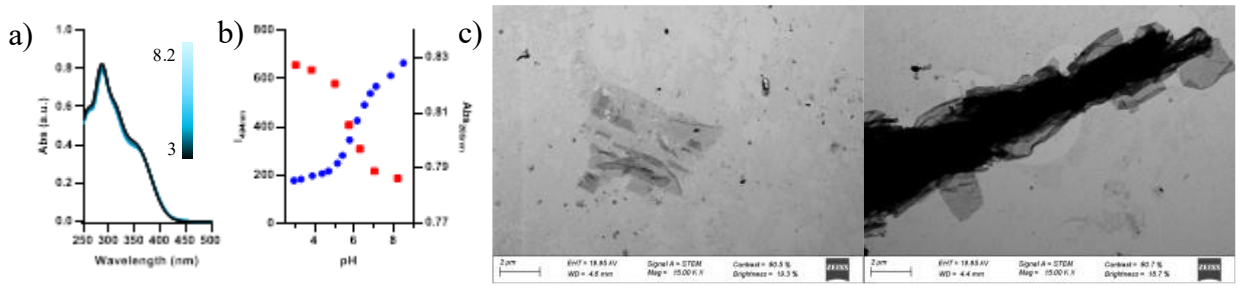

Figure 152. Aqueous solution of **4CP$_{3A}$-U-TPE** 50 μM. a) UV-VIS spectra; b) changes on maximum emission wavelength (blue dots) and absorbance (red squares) with pH; and c) STEM at pH 8.1.

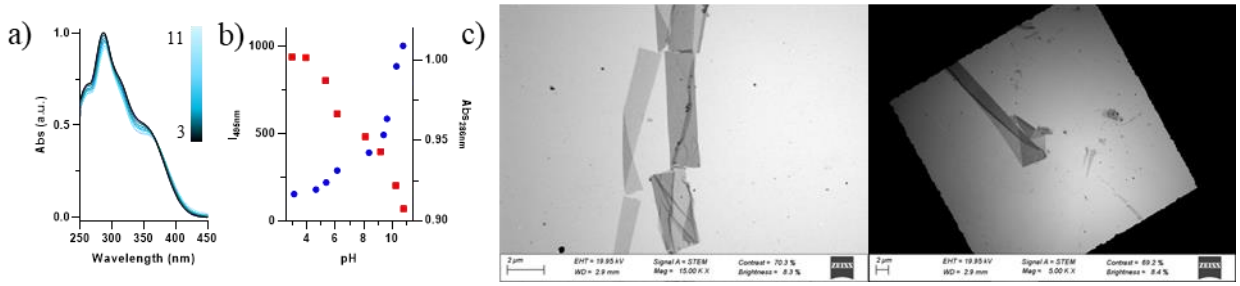

Figure 153. Aqueous solution of **4CP$_{7R}$-U-TPE** 50 μM. a) UV-VIS spectra; b) changes on maximum emission wavelength (blue dots) and absorbance (red squares) with pH; and c) STEM at pH 10 (left) and 11.3 (right).

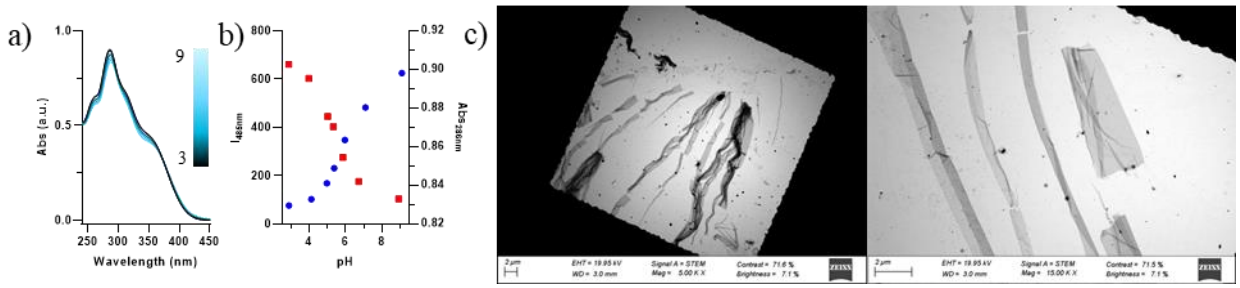

Figure 154. Aqueous solution of **4CP$_{H(Me)}$-U-TPE** 50 μM. a) UV-VIS spectra; b) changes on maximum emission wavelength (blue dots) and absorbance (red squares) with pH; and c) STEM at pH 7.3.

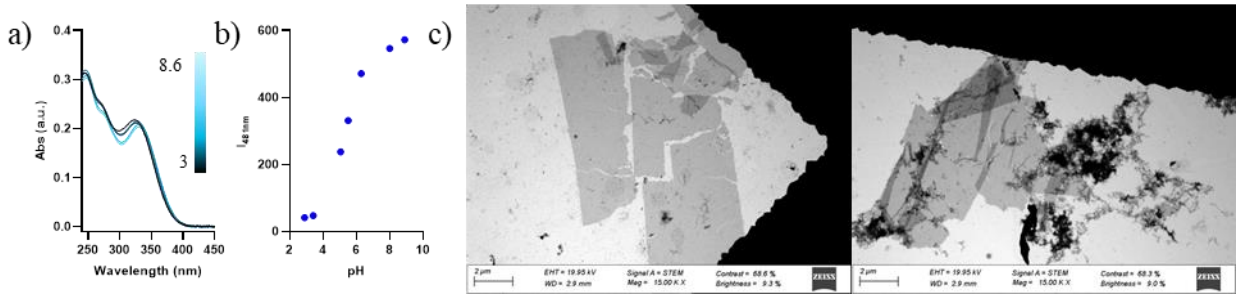

Figure 155. Aqueous solution of **1CP$_{1K}$-U-TPE** 50 μM. a) UV-VIS spectra; b) changes on maximum emission wavelength (blue dots) with pH; and c) STEM at pH 5.8 (left) and 9.0 (right).

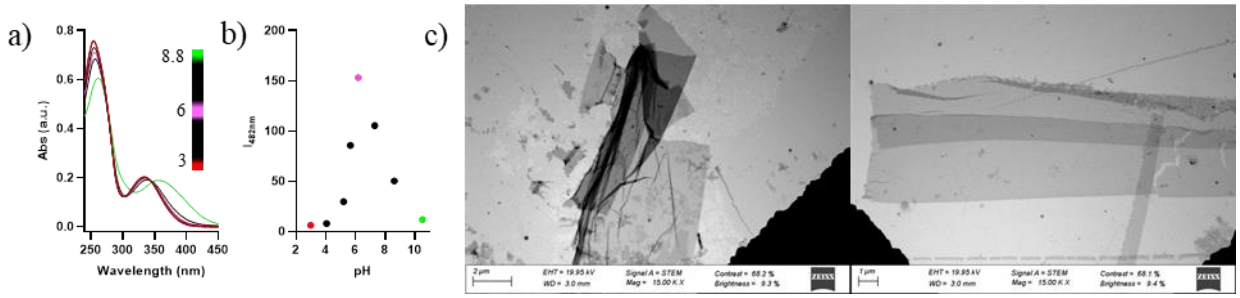

Figure 156. Aqueous solution of **4CP$_{1K}$-U-TPE$_{OH}$** 50 μM. a) UV-VIS spectra; b) changes on maximum emission wavelength (dots) with pH; and c) STEM at pH 6.0.

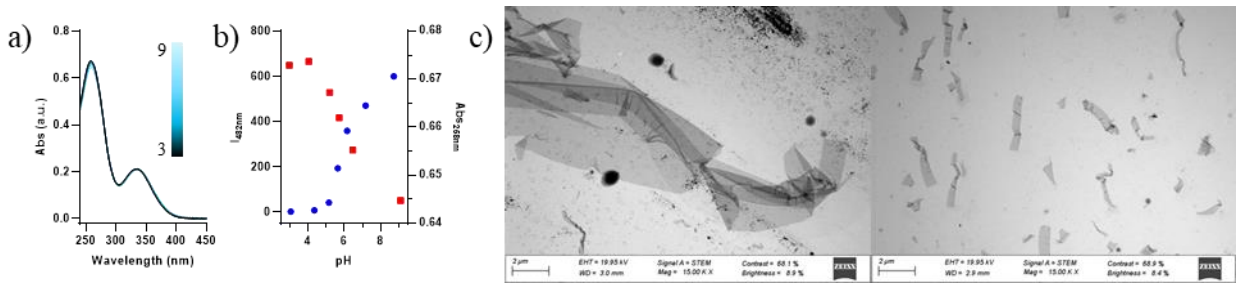

Figure 157. Aqueous solution of **4CP$_{1K}$-U-TPE$_{PEG}$** 50 μM. a) UV-VIS spectra; b) changes on maximum emission wavelength (blue dots) and absorbance (red squares) with pH; and c) STEM at pH 7.3.

APPENDIX

1. RHEOLOGY

Before going into the experimental results of this chapter, some basics on rheology and the most important experiments will be briefly explained. Rheology studies the flow and deformation of matter. It is usually employed to characterize the behavior of complex viscoelastic materials that exhibit properties of both solids and liquids in response to force, deformation, and time.[493]

1.1.Theoretical introduction

Viscoelastic materials behave somewhere in between ideal solids and liquids which obey Hooke's and Newton's laws, respectively. For ideal solids, the deformation is proportional to the applied force and the initial state is recovered upon removal of the force (Hooke's law):[494,495]

$$\tau = G\gamma$$

in which τ is the force per unit area (stress), γ is the relative length change (strain), and G is the proportionality constant (elastic modulus). A great example for this is the stretching of a spring where unless the elastic limit is exceeded, and the deformation is permanent (Figure 158a).[493]

For ideal liquids the behavior is given by Newton's law. It states that an irreversible flow will persist as long as a stress is applied, with a flow rate proportional to stress:[494,495]

$$\tau = \eta\left(\frac{d\gamma}{dt}\right)$$

in which η is the proportionality constant (viscosity). In this sense, a dashpot under an applied force immediately starts to deform at a constant rate until the stress is removed. The energy required for deformation is dissipated within the fluid and the strain is permanent (Figure 158b).[493]

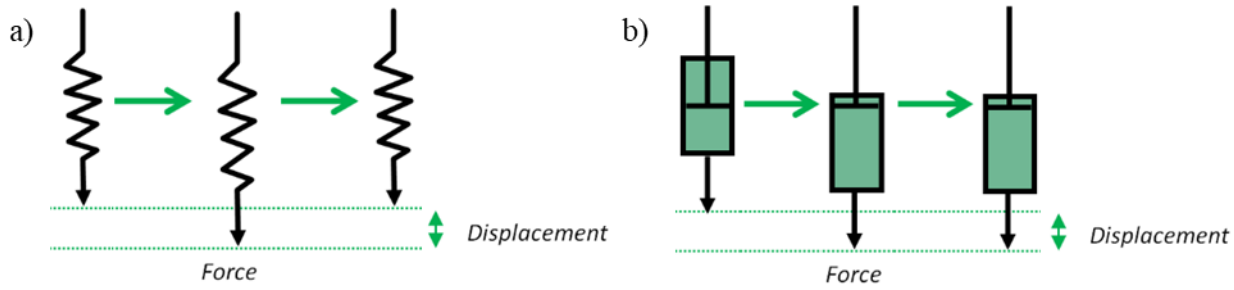

Figure 158. a) and b) Responses of a spring and a dashpot, respectively, to the application and subsequent removal of a strain inducing force. Adapted with permission from Ref.493. Copyright © 2016 Malvern Instruments Limited.

Although there are different kinds of rheometers,[496] here we will discuss only the basics of oscillatory rheometers. To measure the mechanical properties, the sample is loaded between the plates at a known gap. Afterwards, the upper plate oscillates back and forth about its equilibrium position at a given stress or strain and frequency. This movement is described by a sinusoidal curve with an oscillation amplitude equal to the maximum applied stress or strain, and where the

[493] *A Basic Introduction to Rheology*, Malvern Instruments Limited, **2016**.
[494] B. W. Darvell, in *Materials Science for Dentistry*, Woodhead Publishing, Elsevier, 10th edn., **2018**, pp. 92–120.
[495] A. Dawn and H. Kumari, *Chem. Eur. J.*, **2018**, *24*, 762–776.
[496] D. I. Wilson, *Eye*, **2018**, *32*, 179–183.

frequency represents the number of oscillations per second (Figure 159a).[493] The experiments are carried out within linear viscoelastic region, ensuring that the measured hydrogel properties are independent of the magnitude of imposed strain or stress.[497] The rheometer can be strain-controlled where the shear strain applied to the sample and the measured shear stress are given by:[495]

$$\gamma(t) = \gamma_0(\sin \omega t)$$

$$\tau(t) = \tau_0 \sin(\omega t + \delta)$$

in which, ω is the applied angular frequency, δ is the phase difference between the two waves and t represents the time of propagation.

Rheometers also can be stress-controlled where shear stress and shear strain are given by:

$$\tau(t) = \tau_0(\sin \omega t)$$

$$\gamma(t) = \gamma_0 \sin(\omega t + \delta)$$

Moreover, δ values for a pure elastic material is 0º, meaning the strain and stress waves are in phase; while for a pure viscous response both waves are 90º out of phase, thus the viscoelastic materials have a δ value in between (Figure 159b).

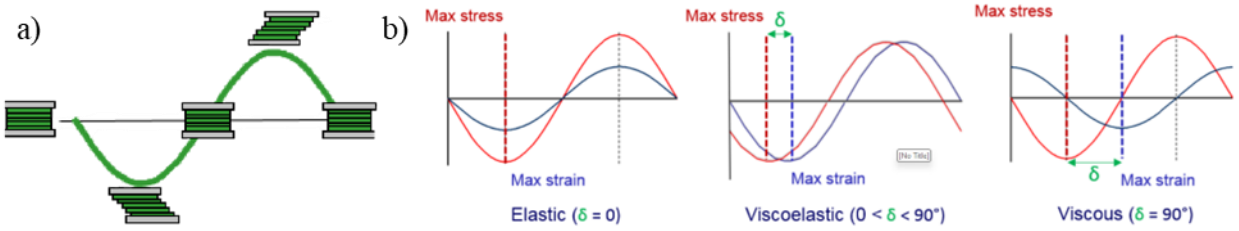

Figure 159. a) Schematic representation of a sample loaded between parallel plates under an oscillatory shear profile; and b) stress and strain waves for elastic, viscoelastic and viscous materials (from left to right). Adapted with permission from Ref.493. Copyright © 2016 Malvern Instruments Limited.

Moreover, if complex notation is used to describe an applied sinusoidal strain, the modulus of the material would be:

$$G^*(\omega) = G'(\omega) + iG''(\omega)$$

in which the real part, G' is the storage or elastic modulus, that measures the stored energy during a strain cycle; and the imaginary part, G'' is the loss or viscous modulus that measures the dissipated energy during a strain cycle. Their relationship G''/G' (tan δ) is known as the loss factor and is indicative of the predominant solid (δ < 1) or viscous (δ > 1) behavior. If necessary, more theoretical information can be found in these books.[494,498]

1.2. Small amplitude oscillatory shear

The most common method for measuring viscoelastic properties using a rotational rheometer is small amplitude oscillatory shear (SAOS). In this case the sample is oscillated about its equilibrium position in a continuous cycle.[493,497] The experiment is carried out at a constant

[497] C. Yan and D. J. Pochan, *Chem. Soc. Rev.*, **2010**, *39*, 3528–3540.
[498] A. Ya. Malkin and A. I. Isayev, *Rheology : concepts, methods, and applications*, ChemTec Publishing, Toronto, 4th edn., **2022**.

frequency with an increasing cyclic level of stress obtaining a typical profile as the seen in Figure 160a. First, a region where the values of both moduli are constant, meaning that the viscoelastic properties are independent of the applied stress, known as the linear viscoelastic behavior. And second, a critical point from which the G'' becomes higher than G', meaning that the material suffered crucial structural alterations that causes the system to flow, known as the yield stress.[495]

1.3. Frequency sweep experiment

Opposite to the previous experiment, during a frequency sweep the measurements are made over a range of oscillation frequencies at a constant oscillation amplitude.[495] In this experiment one can easily observe the behavior of the hydrogel from short to long time scales corresponding to obtained values of G' and G'' at high and low frequencies, respectively ($\omega \approx 1/t$).[493,497]

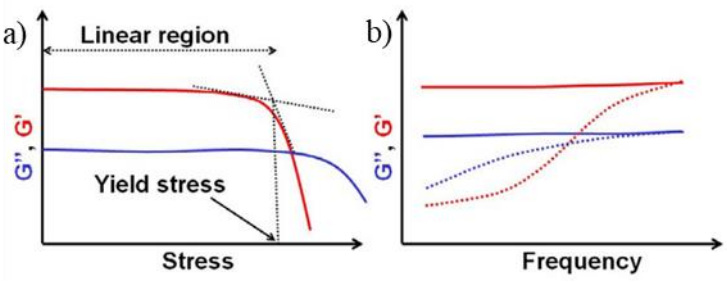

Figure 160. SAOS measurements of a viscoelastic material at a) constant frequency; and b) constant stress. In b) the lines represent a pronounced elastic (solid) or viscous (dotted) behavior. Adapted with permission from Ref.495. Copyright © 2018 WILEY-VCH Verlag GmbH & Co. KGaA, Weinheim.

1.4. Creep test

Creep test experiments involve applying a constant shear stress over a period of time (creep; t_0-t_1) and then remove it (creep recovery; t_0-t_2) while measuring the resultant shear strain.[493] In this regard, ideal materials respond immediately upon the input/output of stress, while viscoelastic materials take more time to respond. Additionally, upon removal of the stress, their recovery is slow and incomplete (Figure 161a).[495] This test allows the elucidation of the recovery properties and efficiency.

1.5. Self-thinning and self-healing

Additionally, there are other two properties important for applications that are the hydrogel recovery after damage (self-healing) and its behavior during flow (shear-thinning). For the first case, the experiment consists on a time dependent evolution of G' and G" to evaluate the mechano-responsive behavior. The experiment starts exposing the sample to a high shear to break the gel integrity and make it flow (G' < G"), followed by a shear release while the recovery of G' and G" are measured (Figure 161b). Recovery of G' to its initial value (or close) within a finite time-scale signifies that the is gel is able to self-heal.[495,497]

For the second case, the viscosity is monitored at different sear rates. Upon increasing the shear rate the is a proportional decrease in viscosity. This zone is usually flanked by high and low constant viscosity zones at low and high shear rates, respectively (Figure 161c).[493] In some rare cases the opposite behavior can be observed, known as shear-thickening.

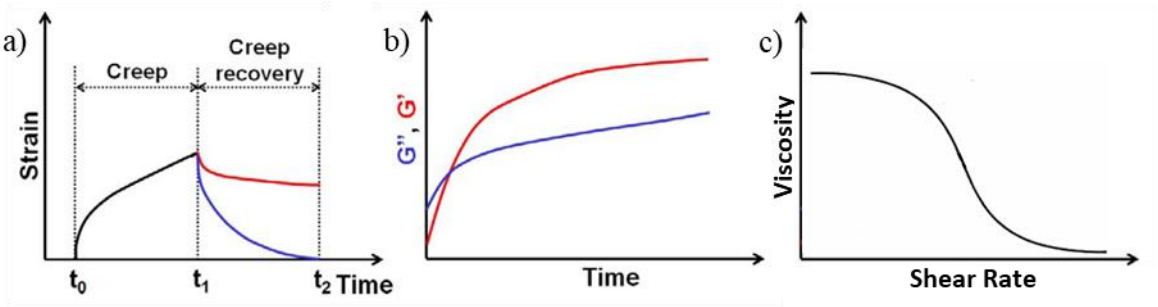

Figure 161. a) Creep test example for viscoelastic (red) and elastic (blue) materials; b) and c) Self-healing and shear-thinning test. Adapted with permission from Ref.495. Copyright © 2018 WILEY-VCH Verlag GmbH & Co. KGaA, Weinheim.

2. List of Publications

2.1. Self-Healing Cyclic Peptide Hydrogels

Quality Indexes

- Impact factor: 7.0 (2022 Journal Citation Reports).
- CiteScore: 11.5 (2022 Scopus).
- SJR: 1.211 (2022 SJR).
- Quartile 1 (Q1) for General Chemistry and Material Science (2022 Scopus).

Specific contribution to the publication

Synthesis and characterization of CPs, spectroscopic behavior of the peptide in dilute solutions and imaging and rheology characterization of the hydrogels.

Authorization from the journal

As it can be read in the following text for thesis and dissertation not permission is required if you are an author of the article as is my case.

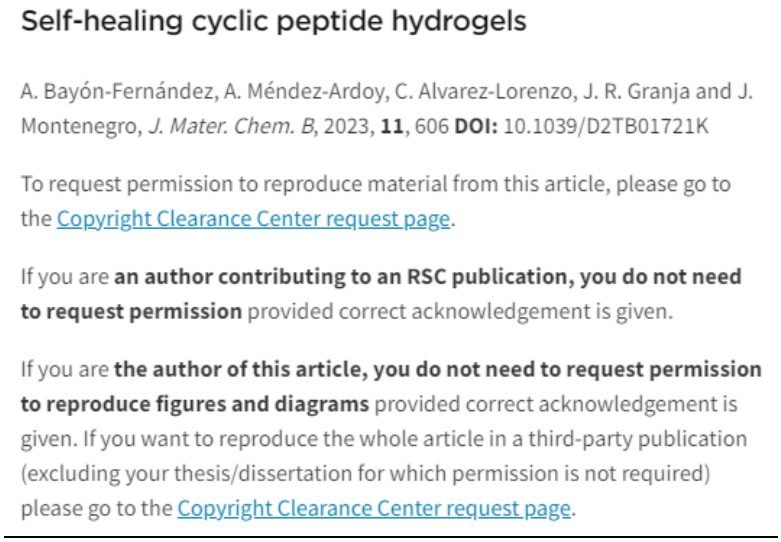

Self-healing cyclic peptide hydrogels

A. Bayón-Fernández, A. Méndez-Ardoy, C. Alvarez-Lorenzo, J. R. Granja and J. Montenegro, *J. Mater. Chem. B*, 2023, **11**, 606 **DOI:** 10.1039/D2TB01721K

To request permission to reproduce material from this article, please go to the Copyright Clearance Center request page.

If you are **an author contributing to an RSC publication, you do not need to request permission** provided correct acknowledgement is given.

If you are **the author of this article, you do not need to request permission to reproduce figures and diagrams** provided correct acknowledgement is given. If you want to reproduce the whole article in a third-party publication (excluding your thesis/dissertation for which permission is not required) please go to the Copyright Clearance Center request page.

2.2. Spatially Controlled Supramolecular Polymerization of Peptide Nanotubes

Quality Indexes

- Impact factor: 16.6 (2022 Journal Citation Reports).
- CiteScore: 26.3 (2022 Scopus).
- SJR: 5.573 (2022 SJR).
- Quartile 1 (Q1) for General Chemistry (2022 Scopus).

Specific contribution to the publication:

Synthesis and characterization of CPs, spectroscopic behavior of the peptide in bulk and microfluidics experiments.

Authorization from the journal

Thank you for your order!

Dear Mr. Alfonso Bayon,

Thank you for placing your order through Copyright Clearance Center's RightsLink® service.

Order Summary

Licensee:	Universidade de Santiago de Compostela
Order Date:	Dec 13, 2023
Order Number:	5687200175264
Publication:	Angewandte Chemie International Edition
Title:	Spatially Controlled Supramolecular Polymerization of Peptide Nanotubes by Microfluidics
Type of Use:	Dissertation/Thesis
Order Ref:	1
Order Total:	0.00 EUR

View or print complete details of your order and the publisher's terms and conditions.

Sincerely,

Copyright Clearance Center

3. Conflict of Interest

The PhD candidate Alfonso Bayón Fernández declares no conflict of interest in relation to the doctoral thesis.

Santiago de Compostela, December 13th 2023.

4. Rights and Permissions of the Images

All ACS images.

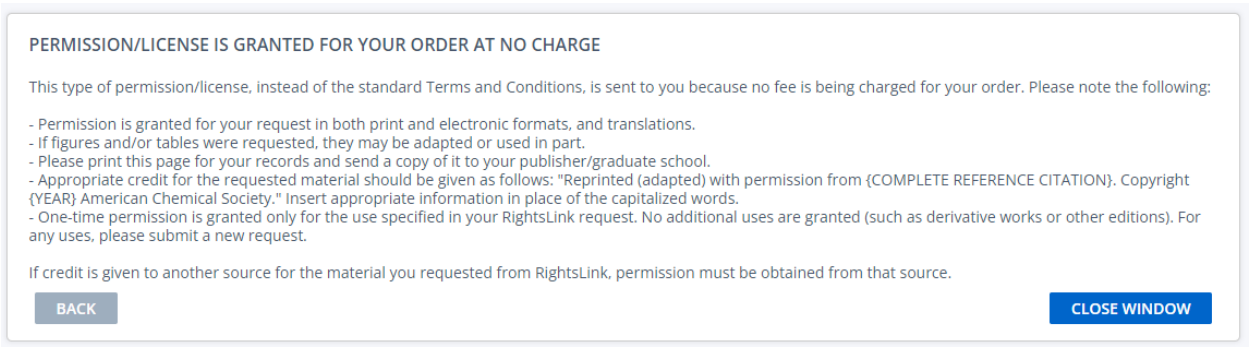

Figure 1

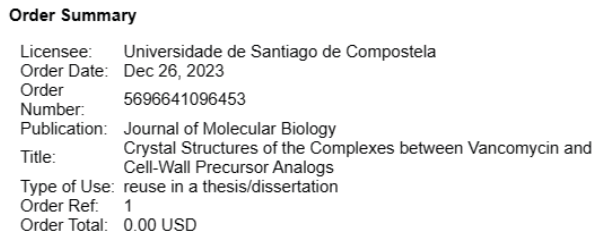

Figure 2

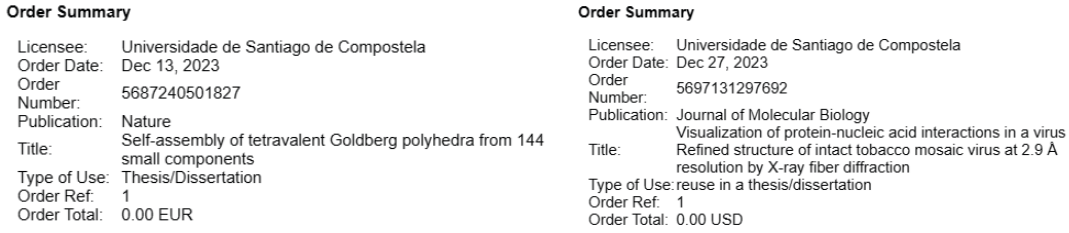

Figure 3

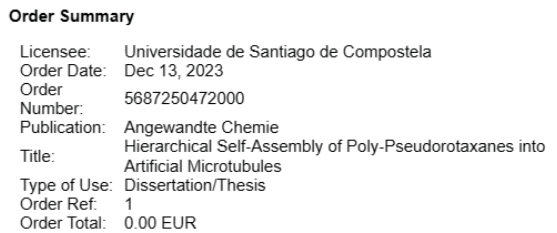

All AAAS images.

Can I use AAAS material in a thesis or dissertation?

Yes, different criteria apply depending upon whether you are the author of the AAAS article being reproduced.

Authors:

If you are the author of the AAAS article being reproduced, please refer to your License to Publish for rules on reproducing your paper in a dissertation or thesis.

Others:

AAAS permits the use of content published in its journals *Science*, *Science Immunology*, *Science Robotics*, *Science Signaling*, and *Science Translational Medicine* to be used in a thesis or dissertation, but only provided the following criteria are met:

1. If you are using figure(s)/table(s), permission is granted for use in print and electronic versions of your dissertation or thesis.
2. A full-text article may be used only in print versions of a dissertation or thesis. AAAS does not permit the reproduction of full-text articles in electronic versions of theses or dissertations.
3. The following credit line must be printed along with the AAAS material: "From [Full Reference Citation]. Reprinted with permission from AAAS."
4. All required credit lines and notices must be visible any time a user accesses any part of the AAAS material and must appear on any printed copies that an authorized user might make.
5. The AAAS material may not be modified or altered, with the exception that figures and tables may be modified with permission from the author. Author permission for any such changes must be secured prior to your use.
6. AAAS must publish the full paper prior to your use of any of its text or figures.
7. If the AAAS material covered by this permission was published in *Science* during the years 1974–1994, you must also obtain permission from the author, who may grant or withhold permission, and who may or may not charge a fee if permission is granted. See original article for author's address. This condition does not apply to news articles.
8. If you are an original author of the AAAS article being reproduced, please refer to your License to Publish for rules on reproducing your paper in a dissertation or thesis.
9. Permission covers the distribution of your dissertation or thesis on demand by a third-party distributor (e.g., ProQuest/UMI), provided the AAAS material covered by this permission remains in situ and is not distributed by that third party outside of the context of your thesis/dissertation.
10. Permission does not apply to figures/photos/artwork or any other content or materials included in your work that are credited to non-AAAS sources. If the requested material is sourced to or references non-AAAS sources, you must obtain authorization from that source as well before using that material. You agree to hold harmless and indemnify AAAS against any claims arising from your use of any content in your work that is credited to non-AAAS sources.
11. By using the AAAS material identified in your request, you agree to abide by all the terms and conditions herein.
12. AAAS makes no representations or warranties as to the accuracy of any information contained in the AAAS material covered by this permission, including any warranties of merchantability or fitness for a particular purpose.

Figure 5

Order Summary

Licensee:	Universidade de Santiago de Compostela
Order Date:	Dec 14, 2023
Order Number:	5687541246655
Publication:	Angewandte Chemie
Title:	A Chemical-Responsive Supramolecular Hydrogel from Modified Cyclodextrins
Type of Use:	Dissertation/Thesis
Order Ref:	1
Order Total:	0.00 EUR

Order Summary:
Order date: 14 Dec 2023
Order number: 1427440
No. of items: 1
Order total: 0,00 EUR
Order license ID link(s): 1427440-1.

Figure 6

Aqueous interfacial gels assembled from small molecule supramolecular polymers

A. S. Groombridge, A. Palma, R. M. Parker, C. Abell and O. A. Scherman, *Chem. Sci.*, 2017, **8**, 1350 **DOI:** 10.1039/C6SC04103E

This article is licensed under a Creative Commons Attribution-NonCommercial 3.0 Unported Licence. **You can use material from this article in other publications, without requesting further permission** from the RSC, provided that the correct acknowledgement is given and it is not used for commercial purposes.

Order Summary

Licensee:	Universidade de Santiago de Compostela
Order Date:	Dec 14, 2023
Order Number:	5687560141480
Publication:	Angewandte Chemie International Edition
Title:	Water-Soluble Supramolecular Polymerization Driven by Multiple Host-Stabilized Charge-Transfer Interactions
Type of Use:	Dissertation/Thesis
Order Ref:	1
Order Total:	0.00 EUR

Figure 7

Order Summary

Licensee:	Universidade de Santiago de Compostela
Order Date:	Dec 14, 2023
Order Number:	5687561086778
Publication:	Nature
Title:	Helical self-assembled polymers from cooperative stacking of hydrogen-bonded pairs
Type of Use:	Thesis/Dissertation
Order Ref:	1
Order Total:	0.00 EUR

Figure 8

Order Summary

Licensee:	Universidade de Santiago de Compostela
Order Date:	Dec 18, 2023
Order Number:	5692011354262
Publication:	Angewandte Chemie International Edition
Title:	Chiral Amplification in the Transcription of Supramolecular Helicity into a Polymer Backbone
Type of Use:	Dissertation/Thesis
Order Ref:	1
Order Total:	0.00 EUR

Figure 10

Order Summary

Licensee:	Universidade de Santiago de Compostela
Order Date:	Dec 18, 2023
Order Number:	5692020764356
Publication:	Angewandte Chemie International Edition
Title:	Superamphiphiles Based on Directional Charge-Transfer Interactions: From Supramolecular Engineering to Well-Defined Nanostructures
Type of Use:	Dissertation/Thesis
Order Ref:	1
Order Total:	0.00 EUR

Figure 9

Order Summary

Licensee:	Universidade de Santiago de Compostela
Order Date:	Dec 18, 2023
Order Number:	5692021448991
Publication:	Angewandte Chemie International Edition
Title:	Selective Synthesis of Single- and Multi-Walled Supramolecular Nanotubes by Using Solvophobic/Solvophilic Controls: Stepwise Radial Growth via "Coil-on-Tube" Intermediates
Type of Use:	Dissertation/Thesis
Order Ref:	1
Order Total:	0.00 EUR

Figure 11

Order Summary

Licensee:	Universidade de Santiago de Compostela
Order Date:	Dec 18, 2023
Order Number:	5692031245730
Publication:	Nature Chemistry
Title:	Tailored self-assembled photocatalytic nanofibres for visible-light-driven hydrogen production
Type of Use:	Thesis/Dissertation
Order Ref:	1
Order Total:	0.00 EUR

Figure 12

Order Summary

Licensee:	Universidade de Santiago de Compostela
Order Date:	Dec 18, 2023
Order Number:	5692040978602
Publication:	Nature Materials
Title:	Free-floating ultrathin two-dimensional crystals from sequence-specific peptoid polymers
Type of Use:	Thesis/Dissertation
Order Ref:	1
Order Total:	0.00 EUR

Figure 14

Order Summary

Licensee:	Universidade de Santiago de Compostela
Order Date:	Dec 22, 2023
Order Number:	5694100297600
Publication:	Nature Chemistry
Title:	Loading and selective release of cargo in DNA nanotubes with longitudinal variation
Type of Use:	Thesis/Dissertation
Order Ref:	1
Order Total:	0.00 EUR

Figure 15

Order Summary

Licensee:	Universidade de Santiago de Compostela
Order Date:	Dec 22, 2023
Order Number:	5694100602043
Publication:	Angewandte Chemie International Edition
Title:	A pH-Triggered, Fast-Responding DNA Hydrogel
Type of Use:	Dissertation/Thesis
Order Ref:	1
Order Total:	0.00 EUR

Order Summary

Licensee:	Universidade de Santiago de Compostela
Order Date:	Dec 22, 2023
Order Number:	5694100778322
Publication:	Advanced Materials
Title:	Self-Assembled DNA Hydrogels with Designable Thermal and Enzymatic Responsiveness
Type of Use:	Dissertation/Thesis
Order Ref:	1
Order Total:	0.00 EUR

Order Summary

Licensee:	Universidade de Santiago de Compostela
Order Date:	Dec 22, 2023
Order Number:	5694100942858
Publication:	Nature
Title:	Folding DNA to create nanoscale shapes and patterns
Type of Use:	Thesis/Dissertation
Order Ref:	1
Order Total:	0.00 EUR

Order Summary

Licensee:	Universidade de Santiago de Compostela
Order Date:	Dec 22, 2023
Order Number:	5694101235881
Publication:	Angewandte Chemie International Edition
Title:	Crystalline Two-Dimensional DNA-Origami Arrays
Type of Use:	Dissertation/Thesis
Order Ref:	1
Order Total:	0.00 EUR

Figure 16

Order Summary

Licensee:	Universidade de Santiago de Compostela
Order Date:	Dec 22, 2023
Order Number:	5694110222979
Publication:	Angewandte Chemie International Edition
Title:	Electrostatic Complementarity Drives Amyloid/Nucleic Acid Co-Assembly
Type of Use:	Dissertation/Thesis
Order Ref:	1
Order Total:	0.00 EUR

Figure 18

Order Summary

Licensee:	Universidade de Santiago de Compostela
Order Date:	Dec 22, 2023
Order Number:	5694111111628
Publication:	Angewandte Chemie International Edition
Title:	Hydrogel Formation upon Photoinduced Covalent Capture of Macrocycle Stacks from Dynamic Combinatorial Libraries
Type of Use:	Dissertation/Thesis
Order Ref:	1
Order Total:	0.00 EUR

Figure 19

Order Summary

Licensee:	Universidade de Santiago de Compostela
Order Date:	Dec 22, 2023
Order Number:	5694120222516
Publication:	Advanced Materials
Title:	Enzyme-Mediated Degradation of Peptide-Amphiphile Nanofiber Networks
Type of Use:	Dissertation/Thesis
Order Ref:	1
Order Total:	0.00 EUR

Order Summary

Licensee:	Universidade de Santiago de Compostela
Order Date:	Dec 22, 2023
Order Number:	5694120375942
Publication:	Nature Materials
Title:	Supramolecular–covalent hybrid polymers for light-activated mechanical actuation
Type of Use:	Thesis/Dissertation
Order Ref:	1
Order Total:	0.00 EUR

Figure 20

Order Summary

Licensee:	Universidade de Santiago de Compostela
Order Date:	Dec 22, 2023
Order Number:	5694120585161
Publication:	Nature Chemistry
Title:	Biocatalytic induction of supramolecular order
Type of Use:	Thesis/Dissertation
Order Ref:	1
Order Total:	0.00 EUR

Order Summary

Licensee:	Universidade de Santiago de Compostela
Order Date:	Dec 22, 2023
Order Number:	5694120585161
Publication:	Nature Chemistry
Title:	Biocatalytic induction of supramolecular order
Type of Use:	Thesis/Dissertation
Order Ref:	1
Order Total:	0.00 EUR

Order Summary

Licensee:	Universidade de Santiago de Compostela
Order Date:	Dec 22, 2023
Order Number:	5694121236216
Publication:	Advanced Materials
Title:	Fmoc-Diphenylalanine Self Assembles to a Hydrogel via a Novel Architecture Based on π–π Interlocked β-Sheets
Type of Use:	Dissertation/Thesis
Order Ref:	1
Order Total:	0.00 EUR

Figure 21

Order Summary

Licensee:	Universidade de Santiago de Compostela
Order Date:	Dec 22, 2023
Order Number:	5694130815165
Publication:	Nature
Title:	Self-assembling organic nanotubes based on a cyclic peptide architecture
Type of Use:	Thesis/Dissertation
Order Ref:	1
Order Total:	0.00 EUR

Order Summary

Licensee:	Universidade de Santiago de Compostela
Order Date:	Dec 22, 2023
Order Number:	5694131068038
Publication:	Helvetica Chimica Acta
Title:	Cyclo-β-peptides: Structure and tubular stacking of cyclic tetramers of 3-aminobutanoic acid as determined from powder diffraction data
Type of Use:	Dissertation/Thesis
Order Ref:	1
Order Total:	0.00 USD

Figure 22

Order Summary

Licensee:	Universidade de Santiago de Compostela
Order Date:	Dec 22, 2023
Order Number:	5694131068038
Publication:	Helvetica Chimica Acta
Title:	Cyclo-β-peptides: Structure and tubular stacking of cyclic tetramers of 3-aminobutanoic acid as determined from powder diffraction data
Type of Use:	Dissertation/Thesis
Order Ref:	1
Order Total:	0.00 USD

Order Summary

Licensee:	Universidade de Santiago de Compostela
Order Date:	Dec 22, 2023
Order Number:	5694130815165
Publication:	Nature
Title:	Self-assembling organic nanotubes based on a cyclic peptide architecture
Type of Use:	Thesis/Dissertation
Order Ref:	1
Order Total:	0.00 EUR

Figure 25

Order Summary

Licensee:	Universidade de Santiago de Compostela
Order Date:	Dec 22, 2023
Order Number:	5694140759978
Publication:	Angewandte Chemie International Edition
Title:	Secondary Self-Assembly of Supramolecular Nanotubes into Tubisomes and Their Activity on Cells
Type of Use:	Dissertation/Thesis
Order Ref:	1
Order Total:	0.00 USD

Figure 26

Order Summary

Licensee:	Universidade de Santiago de Compostela
Order Date:	Dec 22, 2023
Order Number:	5694141033499
Publication:	Chemistry - A European Journal
Title:	Hydrogel and Organogel Formation by Hierarchical Self-Assembly of Cyclic Peptides Nanotubes
Type of Use:	Dissertation/Thesis
Order Ref:	1
Order Total:	0.00 USD

Figure 27

Order Summary

Licensee:	Universidade de Santiago de Compostela
Order Date:	Dec 22, 2023
Order Number:	5694141302197
Publication:	Angewandte Chemie International Edition
Title:	Hierarchical Self-Assembled Photo-Responsive Tubisomes from a Cyclic Peptide-Bridged Amphiphilic Block Copolymer
Type of Use:	Dissertation/Thesis
Order Ref:	1
Order Total:	0.00 USD

Table 4

Order Summary

Licensee:	Universidade de Santiago de Compostela
Order Date:	Dec 22, 2023
Order Number:	5694150732826
Publication:	Biomaterials
Title:	Supramolecular biofunctional materials
Type of Use:	reuse in a thesis/dissertation
Order Ref:	1
Order Total:	0.00 USD

Figure 29

Order Summary

Licensee:	Universidade de Santiago de Compostela
Order Date:	Dec 22, 2023
Order Number:	5694120585161
Publication:	Nature Chemistry
Title:	Biocatalytic induction of supramolecular order
Type of Use:	Thesis/Dissertation
Order Ref:	1
Order Total:	0.00 EUR

Figure 32

Order Summary

Licensee:	Universidade de Santiago de Compostela
Order Date:	Dec 22, 2023
Order Number:	5694151496981
Publication:	Biomaterials
Title:	Bone regeneration mediated by biomimetic mineralization of a nanofiber matrix
Type of Use:	reuse in a thesis/dissertation
Order Ref:	1
Order Total:	0.00 USD

Figure 33

Order Summary

Licensee:	Universidade de Santiago de Compostela
Order Date:	Dec 22, 2023
Order Number:	5694160296752
Publication:	Chem
Title:	Tunable Supramolecular Hydrogels for Selection of Lineage-Guiding Metabolites in Stem Cell Cultures
Type of Use:	reuse in a thesis/dissertation
Order Ref:	1
Order Total:	0.00 USD

Figure 42

Order Summary

Licensee:	Universidade de Santiago de Compostela
Order Date:	Dec 22, 2023
Order Number:	5694161309983
Publication:	Nature
Title:	Cell mechanics and the cytoskeleton
Type of Use:	Thesis/Dissertation
Order Ref:	1
Order Total:	0.00 USD

Figure 44

Order Summary

Licensee:	Universidade de Santiago de Compostela
Order Date:	Dec 22, 2023
Order Number:	5694170269214
Publication:	Nature Cell Biology
Title:	Cell-sized spherical confinement induces the spontaneous formation of contractile actomyosin rings in vitro
Type of Use:	Thesis/Dissertation
Order Ref:	1
Order Total:	0.00 USD

Figure 56

Order Summary

Licensee:	Universidade de Santiago de Compostela
Order Date:	Dec 22, 2023
Order Number:	5694171278222
Publication:	Angewandte Chemie International Edition
Title:	Aggregation-Induced Emission Featured Supramolecular Tubisomes for Imaging-Guided Drug Delivery
Type of Use:	Dissertation/Thesis
Order Ref:	1
Order Total:	0.00 USD

Figure 57

Order Summary

Licensee:	Universidade de Santiago de Compostela
Order Date:	Dec 22, 2023
Order Number:	5694180005452
Publication:	CHEMPLUSCHEM
Title:	Self-Assembly of Tetraphenylethylene-Based Amphiphiles in Aqueous Methanol Solution into Two-Dimensional Chiral Sheets for Enantioselective Sorption
Type of Use:	Dissertation/Thesis
Order Ref:	1
Order Total:	0.00 USD

Figure 160 and Figure 161

Order Summary

Licensee:	Universidade de Santiago de Compostela
Order Date:	Dec 22, 2023
Order Number:	5694180378113
Publication:	Chemistry - A European Journal
Title:	Low Molecular Weight Supramolecular Gels Under Shear: Rheology as the Tool for Elucidating Structure–Function Correlation
Type of Use:	Dissertation/Thesis
Order Ref:	1
Order Total:	0.00 USD

5. DECLARATION OF ALL OTHER IMAGES

All other images in this Doctoral Thesis without the corresponding acknowledgment and proper reproduction have been personally elaborated.

… Y HABLANDO DESDE EL CORAZÓN

Antes de empezar, he de decir que las siguientes personas han sido igual de importantes para mí que las mencionadas en los agradecimientos iniciales. Sin embargo, como la felicidad no tiene precio he respetado el deseo de mi director de tesis de dividir los agradecimientos en científicos y personales. Sin más dilación…

David Lynn, gracias por acogerme en tu grupo con los brazos abiertos en un momento complicado, la "postpandemia". La realización de la estancia predoctoral en la Universidad de Emory me sirvió para crecer científica y personalmente. También me gustaría agradecerles a todos los miembros del grupo Alexis Blake y Alexis Roberson, Ethan, George, Christella, Yihoon, Fernando y Youngsun, su acogida en el grupo. Cambiar de país, lengua y compañeros siempre es difícil, pero vosotros hicisteis que la transición fuese sencilla.

A todo el personal del CIQUS. Mari Carmenes, siempre sacando sonrisas y conversaciones para amenizar los días. Arcadio y Noela, os une el miedo que infundís de primeras sobre la gente, pero también vuestra disposición para solventar los problemas (a veces incluso con una sonrisa). Arcadio, a ti te digo a mayores que eres el pilar más importante del laboratorio, ya que sin tu presencia no tendríamos equipos. Andreita, aún me acuerdo cuando llegaste con una mascarilla y tu famosa frase "yo a ti te conozco". Ese día me asustaste, pero después me di cuenta de que el CiQUS es un sitio más alegre contigo en él. Rebeca Menaya, las células durante estos años no me han tratado bien, pero tú siempre. Gracias por tu ayuda con las células, la electroforesis y los intentos de risa falsa después de un chiste malo. Laura, Mencha, Adrián, María Rey, Elena, Almudena y todas esas personas que día sí y día también resolvéis nuestros problemas, gracias.

A todos los compañeros que me han acompañado durante todos estos años, menos a Marcos que no se lo merece. Tengo el privilegio de deciros a todos que más que compañeros sois amigos.

J. J. Reina, mi arma, siempre trabajando con esa alegría contagiosa que tanto te caracteriza. Gracias a ti aprendí algo de eso que llaman síntesis en disolución con sus columnitas.

Lionel, fuiste la primera persona que conocí del grupo en unas prácticas de Química Orgánica I durante la carrera. Ha sido un placer compartir parte de esta etapa a tu lado.

Juanillo, siempre recordaré el día que nos conocimos como el día del "pajillator". Si hay una cosa que te caracteriza es la felicidad, así que sigue derrochándola allá por donde pases.

Patri Lago, sin ti el grupo se iría a pique. Siempre has estado ahí para resolver cualquier gestión, y lo mejor de todo es que siempre lo nos has atendido con una sonrisa.

Alicia, convencerte a ti para ir al café fue lo más duro del doctorado, aunque al final mi pesadez dio sus frutos. Gracias por regalarnos esas contestaciones que dejaban a Javi sin palabras.

Manuel, lo prometido es deuda. Aquí va una dedicatoria especial a modo de pregunta y espero que ahora me puedas responder. "Una vez escalas el Everest, ¿qué más te queda?"

Yeray, por mi culpa aprendiste que las células a veces mueren y que las cosas no siempre salen en la ciencia. Sin embargo, siempre hay lugar para unas risas sacando fotos en el confocal. No tengo muy claro si debería darte gracias o pedirte perdón, pero me alegra haberte tenido a mi lado durante esta etapa.

Federica Novelli alias Francesca, il terremoto dentro il laboratorio e la calma fuori. Gracias por siempre estar dispuesta para echar un cable o tomarte una cervecita.

Iván, gracias por acogerme con los brazos abiertos recién llegado al grupo. Además, gracias a ti no era el único que se olvidaba la llave del nitrógeno abierta.

Rebe, antes de tu llegada las plantas del laboratorio se morían, tras tu llegada florecían. Gracias por tratarnos como a las flores y hacernos florecer.

Patricia, que decir de ti. Siempre digo que un secreto solo es un secreto cuando solo lo sabe una persona, pero ahora me veo obligado a decir que en ti confío como en mí mismo. Gracias por aparecer en mi vida.

Martita y Álvaro alias mamá y papá, el cariño que os tengo es difícil de poner en palabras. Desde el principio me disteis la mano y os cogí el brazo. Gracias por estar siempre a mi lado, preocuparos por mí y quererme como soy. Y un secreto, quiero un poco más a mamá que a papá.

Lamas, a ti da igual lo que te ponga porque desconectarás mientras lo estés leyendo y te pondrás a hacer otra cosa. Gracias por tener la habilidad de hacernos reír siempre en el laboratorio.

Héctor, my brother from another mother. La distancia y el tiempo hacen que hablemos y nos veamos menos, pero la relación no cambia. Los momentos juntos hablan por sí solos (noches en la terraza de Rua Travesa con las estrellas y los caramelos mentolados, la búsqueda del sol en O Grove, los festivales, LA FOTO en Fisterra, el paseo en moto por Marrakech…). Hay amigos que son para toda la vida.

Jose Mary, la persona más graciosa del laboratorio. Con tu forma de mentir, tu humor, siendo tú, haces que brillen los días negros de tormenta. Sin embargo, Sandrita, te desbanca en el puesto de momento más gracioso (Comida de las Cajales). Hubo un momento en el JAS dominaba los planes del grupo y el gimnasio, ahora JS tendrá que recuperar y asumir toda la responsabilidad.

Evitaaaaaaaaa, que sepas que seguimos siendo amigos a pesar de que no me hayas invitado a la boda. En el bus Pontevedra-Santiago había una que dormía y otro que preparaba los seminarios; pero en el de Santiago-Pontevedra siempre había tiempo para una charlita o una película.

Charlene, una estancia de verano, un máster y el Numaru no consiguieron que te quedases en el grupo, pero sí que yo tenga una gran amiga en Coruña a la que debería visitar más a menudo.

Angelito, la mejor persona que conozco. Siempre dispuesto a mirar por el bien del prójimo por encima del suyo. Aunque jugando el tenis eres de la filosofía de Luis Aragonés "*ganar, ganar, ganar y volver a ganar*".

Mayra, durante tus "vacaciones" iniciales sufriste el humor de Marcos, y el mío. Ya viste que la confianza la cogemos desde el primer día, aunque para cogernos cariño a nosotros se necesita algo más de tiempo. Sigue chambeando todos los días con esa alegría.

Guilia Salluce, mamma dei Gatti. Se dice que la convivencia es difícil, pero nosotros sobrevivimos a compartir laboratorio y piso. Lo que me apena es que, de todas las historias divertidas vividas, probablemente no te acuerdes porque te quedaste dormida.

Iria, mi primera maestra en el laboratorio. No puedo decir mucho más que gracias a la persona que me enseñó a hacer péptidos, mi vida durante los últimos 5 años.

Alfonsito, una dupla mágica hasta que duró la gasolina. Desde un TFM que me preguntó cómo hacer presentaciones, hasta dominar juntos las noches santiaguesas. Poco más se le puede pedir a un compañero.

Hulio, gracias por tener esa habilidad para explicar las cosas difíciles de forma sencilla. Aunque la elastina a mí me odie, yo a ti te tengo un aprecio especial. Nachete, todavía no jugamos la final de Wimbledon, pero si nuestros partidos de tenis se retransmitiesen por la televisión, la gente se quedaría a verlos. Gracias por todos estos años donde en lugar de confeti se tiraban pipas.

Lucía Motomami, no hay persona más lianta ni más liada. Si alguien necesita ayuda, eres la primera en presentarte. Si alguien necesita tomar una cerveza, eres la primera en presentarte. No pierdas esa energía y vitalidad que te caracterizan. Adrián, la cara opuesta. No hay persona menos liada ni con mejores bombas de humo. Eso sí, los pinchos de tortilla a la mañana que no falten.

Lourdes Patricia alias MiniPatri, la alumna que sabe más que cualquier maestro. Lucía Lomba, la campeona gallega de natación desbancada por un aficionado. Ambas estuvisteis poco tiempo en el grupo, pero dejasteis huella.

Amaia, que sepas que no me olvido de que me debes un brownie de chocolate. A pesar de eso gracias por sucumbir a mi pesadez y unirte a jugar a los dardos un día. Después de los cafés de Alicia, esta fue la segunda cosa más dura del doctorado.

Martín Calvelo, desde que te fuiste el stock de Larios en Santiago no hace más que crecer. Gracias por los felpudos, por demostrar que los de computacional son gente normal y por entender que los carnavales de Verín son innegociables.

Marisa y Alberto, la jefa y el payasito. Marisiña, a una persona tan increíble como tú deberían tirarle fuegos artificiales todos los días del año, no solo la noche de su cumpleaños. Siempre sonriente y cariñosa, nunca compartí la idea de que te bajasen 2 pisos. Albertooooo, desde que te fuiste ya no hacemos preguntas difíciles, ni nos cuentan el mismo chiste 30 veces, ni nos hacen acertijos, ni nos enseñan vídeos graciosos. Por la salud mental del laboratorio, plantearos volver.

Victoria, Mary Win, Mary Lose, Vicky G… lo siento, pero tenía que ponerlos. Empezamos juntos y acabamos juntos. El camino ha sido largo, pero contigo y las arrancadas de esa moto ha sido mucho más liviano. Juntos subimos los decibelios del laboratorio, conocimos a Homer en Donostia, paseamos durante el periodo de escritura… Ahora los caminos se separan, pero la amistad seguirá para siempre.

Irene Lostalé, la enciclopedia humana. Durante todos estos años has sido una fuente de conocimiento y ejemplo de compañerismo. Solo puedo darte las gracias por enseñarme tanto y demostrar que el conocimiento no ocupa lugar.

Serginho Serantes, llegaste al laboratorio con mascarilla y pensé que eras guapo. Vaya desilusión me llevé cuando la quitaste. Poco tardaste en captar y encajar en la dinámica del laboratorio. Que sepas que cuando dicen que nuestra personalidad se parece, para mi es un piropo porque tienes una personalidad de oro. No cambies nunca ni dejes que la ciencia te quite la sonrisa.

Manuel, tu igual que Sergio llegaste con mascarilla, pero desde León. Mi brazo agradeció que marchases, pero mi corazón todo lo contrario. En la cruceta contra el secreto ganó la amistad.

Alba, a mi primera alumna siempre le tendré un cariño especial. Tuviste que aguantar a un doctorando poco preparado para la enseñanza ya que nadie nos prepara para eso. Lo hice lo mejor posible y espero que algo te haya enseñado bien. Gracias por aguantarme estos años, pero me temo que ha llegado el momento de dejarte volar. ¡No dudes en "molestar" a Juan ante cualquier duda que ya lo he entrenado yo durante 5 años!

Richard, Ghibom, Geert y Sahnawaz gracias por estar siempre dispuestos a ayudar y encajar tan bien en el grupo. Además, a Richard, gracias por demostrar que los extranjeros también pueden pedir bien una "1009" y que sepas que sin ti, la GRC no hubiese sido lo mismo.

Ezequiel, con el título al mejor nombre completo del laboratorio. La roca, siempre paciente e imposible de picar, hasta que aparece un francés o el camarero del Albaroque. Marcos, el niño tímido que con los años se convirtió en el todopoderoso Javier Fernandez. Siempre con esa sonrisita característica. Aunque a veces hagas llorar a la gente, mantén ese sentido del humor. A los dos os firmo la dedicatoria con un "Desde París con Amor".

Patri Farmacia, de unos experimentos en ortopedia, un grafiti en una bata y varios cafés nació una amistad. ¡Ha sido un placer haber trabajado contigo!

Ce(ci)lia Gitana más conocida por papel de Capitán Dan en los carnavales del 2023. Gracias por no odiarme a pesar de inmortalizar este momento en el que escribo mal tu nombre. Si algo ha quedado claro es que nuestra amistad sobrevive tempestades como la de Forest y su capitán.

Martin Piñeiro alias Sr. ACS catálisis más leído.[499] De la noche que nos conocimos solo se acuerdan tus vecinos y Dani Marcos. A partir de ahí, nos colamos en Tarasca, dimos recitales en el Makumba y descubrimos los bocadillos de chorizo picante. Aunque cuando vamos a correr me odias, es normal que entre hermanos siempre exista esa relación amor-odio.

Natalia, de no saludarme en el ascensor a CASI invitarme a tu piscina. Al final mi pesadez dio como fruto una amistad, para que luego digan que no vale de nada…

David y Ángela, quien me iba a decir que en un tren se podían vivir tantas alegrías. Despertarse a horas intempestivas para subir al tren, salir corriendo para llegar a tiempo… Sin embargo, todos esos momentos valieron la pena porque gracias a eso conocí a dos personas maravillosas. Gracias Team Ourense/Avant.

Javi, un grupo de Facebook y Atlanta consiguieron que nuestros caminos se cruzasen. En dos meses vivimos una vida entera, mientras uno paseaba el otro trabajaba y los findes juntos a viajar. Luego te fuiste y llegó Teresa, y con ella más viajes y aventuras. Gracias a ambos, la estancia no hubiese sido lo mismo sin vosotros.

Eva y Jesu, sois el vivo ejemplo de que a veces los amigos solo te meten en marrones. Gracias por estar dispuestos a solventar los problemas de vuestros amigos con una sonrisa y sin pedir nada a cambio. Sin vosotros esta tesis no hubiese sido posible.

Gracias también a otros compañeros del CIQUS que consiguieron amenizar todas las jornadas laborales: Reza, Roi, Soraya, Bea, Manuela, Enrica, Jacobo, Paula, Gustavo…

[499] M. Piñeiro-Suárez, A. M. Álvarez-Constantino and M. Fañanás-Mastral, *ACS Catal*., **2023**, *13*, 5578–5583.

George Bernard Shaw definió la vida como "*una espléndida antorcha que sostengo en mis manos durante un momento, y quiero que arda con la máxima claridad posible antes de entregarla a futuras generaciones.*" Hablando del doctorado y el laboratorio, a los que aún no habéis acabado, yo mi antorcha os la dejo a vosotros. Espero que mantengáis viva esa llama a través del compañerismo y la pasión por la investigación que siempre han caracterizado a este grupo.

Fuera del laboratorio y centro de trabajo también he disfrutado del apoyo de muchísima gente. A ellos me gustaría agradecerles todas las quejas aguantadas, los ánimos recibidos y experiencias vividas durante estos años.

A mis amigos de la carrera. Especialmente a Irene, Cañizo, Pablito y Rainer. Habéis estado siempre ahí en los buenos y en los malos momentos. Aunque nos vemos poco, en esos momentos, se ve que las cosas no han cambiado. Gracias por hacerme feliz durante los 5 años de farmacia y seguir ahí los 5 de doctorado.

A mis amigos de Ourense de toda la vida Miguel, Ángela, Lucía, Víctor, Suso, Alexis, David, Samu, Iván, Nadir… Siempre que nos vemos aprovechamos cada segundo para pasarlo bien. Miguel, mi mejor amigo desde el instituto y compañero de piso durante la pandemia. Que más se puede decir más que gracias por todo. David, gracias por cruzar EEUU para hacer un miniviaje conmigo. ¡Casi morimos deshidratados el 4 de Julio, pero mereció la pena!

A mis amigos de Verín, Jose, Chantre, Isma, Ana Vigo, Ana Santiago, Alberto, Dani, Iria, Miguel… Gracias por hacer que todos los veranos fuesen inolvidables. Juntarse con vosotros siempre es un remanso de paz mental, aunque el hígado muchas veces sufre.

Marian, mi fisio de confianza. Aún recuerdo el día que intentaste darme clases de baile y casi lo consigo. Dejando eso a parte gracias por todos nuestros paseos junto a Blue y por curarme siempre que lo necesité. Sin ti mi alegría y mi salud estarían por los suelos.

María y Aldara, mis mejores excompañeras de piso que no amigas. Las dos personas que el primer recuerdo que tienen de mi es que era un gilipollas, y sin las cuales a día de hoy no me planteo la vida. Gracias por cambiar vuestra opinión sobre mí, algo merecida en el caso de Aldara.

María Sequeiros, no voy a mentir porque no sé en qué momento empezamos a ser amigos. Pero, sí que sé que no me gusta que rechaces tomar un café conmigo porque estas "estudiando las oposiciones". A pesar de ello, todos los consejos y ánimos que me das me levantan la moral día sí y día también.

Jorge Malingre (y familia), eres el amigo más antiguo que recuerdo. De pequeños no sé dónde pasé más tiempo si en mi casa o en la tuya. Hemos pasado de pasar toda la vida juntos a estar buscando algo de tiempo para vernos, sobreviviendo a una pérdida de contacto. Si no me sale nada en la ciencia estoy seguro de que podré actuar de representarte del mejor preparador físico del mundo.

Giovanna, gracias por hacerme feliz durante gran parte de esta etapa. Durante estos años sufrí momentos malos, tanto personales como laborales, y siempre estuviste ahí para levantarme. Honestamente solo puedo decir cosas buenas sobre ti. Doy gracias por haberte conocido y todo el tiempo y los momentos que pasamos juntos. Ya sabes que haya donde yo esté siempre tendrás un amigo.

Since the beginning of humankind, chemistry has been essential to overcome societal needs and de iciencies. Over the last years, supramolecular materials have shown potential applications in medicine and material science. In this sense, self-assembling cyclic peptide nanotubes stand out as molecular scaffolds since they allow an exquisite bottom-up control over the inal properties. In this work, cyclic peptides functionalized with aromatic moieties are exploited to obtain novel functional materials such as self-healing hydrogels or self-reporting nanosheets. Their characterization demonstrates that functionalization and assembling triggers are key in the hierarchical assembling process. Finally, preliminary studies indicate potential use of these unique materials as cytoskeleton mimicking systems or catalysts.